## Distribution Agreement

In presenting this thesis or dissertation as a partial fulfillment of the requirements for an advanced degree from Emory University, I hereby grant to Emory University and its agents the non-exclusive license to archive, make accessible, and display my thesis or dissertation in whole or in part in all forms of media, now or hereafter known, including display on the world wide web. I understand that I may select some access restrictions as part of the online submission of this thesis or dissertation. I retain all ownership rights to the copyright of the thesis or dissertation. I also retain the right to use in future works (such as articles or books) all or part of this thesis or dissertation.

Signature:

| | |
|---|---|
| Nicholas H. Stair | Date |

# A blessing and a curse of dimensionality: using quantum computers to simulate strongly correlated fermionic systems

By

Nicholas H. Stair
Doctor of Philosophy

Chemistry

---

Francesco Evangelista, Ph.D
Advisor

---

Joel Bowman, Ph.D
Committee Member

---

Michael Heaven, Ph.D
Committee Member

Accepted:

---

Lisa A. Tedesco, Ph.D
Dean of the James T. Laney School of Graduate Studies

---

Date

# A blessing and a curse of dimensionality: using quantum computers to simulate strongly correlated fermionic systems

By

Nicholas H. Stair
B.S. Chemistry, California Polytechnic State University SLO, 2017
B.A. Physics, California Polytechnic State University SLO, 2017

Advisor: Francesco Evangelista, Ph.D

An abstract of
A dissertation submitted to the Faculty of the
James T. Laney School of Graduate Studies of Emory University
in partial fulfillment of the requirements for the degree of
Doctor of Philosophy
in Chemistry
2021

# Abstract

A blessing and a curse of dimensionality: using quantum computers to simulate strongly correlated fermionic systems

By Nicholas H. Stair

In this dissertation, we develop and demonstrate need for novel quantum computational algorithms for simulating molecular systems with strong electronic correlations. First we explore the limitations of classical algorithms for strongly correlated electronic structure problems. To this end, we test the performance of selected configuration interaction (sCI), singular value decomposition full CI (SVD-FCI), and the density matrix renormalization group (DMRG) using a novel set of one, two, and three-dimensional hydrogen models. We find that although a significant reduction in pre-factor can be achieved, a reduction from exponential to polynomial scaling was not observed for any of the three methods in the general case, motivating the development of quantum algorithms for strong correlation. We then introduce a novel quantum Krylov (QK) algorithm, amenable to the simulation of molecular systems. The algorithm uses unitary Hamiltonian time evolution to build a basis of states (stored on a quantum computer) that are equivalent to a classical Krylov basis in a small time-step limit. We apply the QK algorithm, and a selected multi-reference variant (MRSQK) to $H_6$, $H_8$, and $BeH_2$ and find that chemical accuracy can be achieved with a Krylov basis orders of magnitude smaller than that of the full CI (FCI) space. We then introduce another novel quantum simulation algorithm deemed the projective quantum eigensolver (PQE), which is amenable to noisy intermediate-scale quantum (NISQ) hardware. The approach seeks to solve the Schrödinger equation by zeroing its projections onto an orthogonal space of excited determinants. We compare PQE to the variational quantum eigensolver (VQE), both using disentangled unitary coupled cluster ansatz and find that the former is more computationally resource efficient when tested on $H_6$ and $BeH_2$. We also introduce a selected ansatz variant of PQE and show that it compares favorably to classical sCI and DMRG. Finally, we showcase our novel open-source quantum simulation package QFORTE which facilitated the work presented in this dissertation and will be used for future algorithmic developments and comparative studies.

# A blessing and a curse of dimensionality: using quantum computers to simulate strongly correlated fermionic systems

By

Nicholas H. Stair
B.S. Chemistry, California Polytechnic State University SLO, 2017
B.A. Physics, California Polytechnic State University SLO, 2017

Advisor: Francesco Evangelista, Ph.D

A dissertation submitted to the Faculty of the
James T. Laney School of Graduate Studies of Emory University
in partial fulfillment of the requirements for the degree of
Doctor of Philosophy
in Chemistry
2021

# Acknowledgement

There are too many people deserving of thanks and acknowledgment to put down on a single page, but I will do my best. I never would have started down this path without an excellent start from the science department at Paso Robles High School. I will always be grateful to Anthony Overton for pushing me toward chemistry and Cal Poly, to Mike Serpa for teaching me calculus and how to learn things I don't understand right away, to Dave Boicourt for fostering my desire to be an educator (and for many rad surf sessions), and to the many other fantastic PRHS instructors I had the privilege of studying under.

My time at Cal Poly was unforgettable, a period where I learned as much about myself as the natural world. I want to thank Dr. Michael Heying for giving me an great introduction to working on chemical theory, without which I would not have set my sights on graduate school. I also want to thank Dr. Ashley McDonald for her advice to study electronic structure, and for putting me in contact with a talented new professor working on the other side of the country.

On that note, I want to thank my research advisor here at Emory, Dr. Francesco Evangelista. Thank you Francesco for being a model scientist, your passion for new ideas will continue to be an inspiration, and I will always remember that "creativity isn't something you're born with, it is something you have to practice at." Thanks also to my committee members Dr. Joel Bowman, and Dr. Michael Heaven for their help and advice over the last four years. A special thanks to the past and present members of the Evangelista Lab for their camaraderie, and in particular to Dr. Jeff Schriber for many hours of caffeinated (and inebriated) conversations about strong correlation, multi-reference methods, orbital rotations, scientific philosophy, climbing, bike-commuting, beer die, and staying in graduate school.

I once told Francesco that finishing my PhD was a meditative exercise. I think this is still the case, but there are several people in my life who helped me through the parts that were more of an exercise in patience than in meditation. I want to say thanks to the friends I made at emory, and to the many friends I was fortunate enough to stay close with despite a large physical distance. Thank you to my wonderful parents Gary and Penny Stair for whom supporting me has always been first-nature. Thanks mom and dad for listening to me and encouraging fortitude. Thank you Oatly for being my COVID-era desk mate, and for making me go outside every day at lunch. Katie, without you this would have been impossible, you will forever have my thanks and my love. You were here for the best and the worst of things, thank you so much for contributing to my life all of your insightful thoughts, your bad jokes, your good jokes, your patience, and your inspiring capacity for growth.

Finally I want to say a special thanks to Dr. Seth Bush who is a real-life super hero fighting the injustice of public ignorance. You have been an enormous inspiration and I can only aspire to have a career as impactful as yours!

– Nick

# Table of Contents

# List of Figures

# List of Tables

# Chapter 1

# Introduction

*"Nature isn't classical, dammit, and if you want to make a simulation of nature, you'd better make it quantum mechanical, and by golly it's a wonderful problem, because it doesn't look so easy."*

-Richard Feynman

## 1.1 Introduction

It is interesting to consider what the foundational figures of quantum mechanics would find most compelling about the current state of the field. In addition to our continued exploration of fundamental theories, would they be impressed with our progress "making soluble[1]" the equations which bear their names? Could Dirac have predicted after his 1929 statement on the complexity of quantum equations that, only few decades later, elegant mathematical approximations paired with large-scale digital computation would allow theoreticians to predict properties and structures of molecules on-par with experimental studies?[2,3] Would Schrödinger be surprised that nearly 100 years after he reproduced Bohr's results for the Hydrogen spectrum using the now conventional framework of quantum mechanics,[4] quantum computers would be used to study the electronic structure of Hydrogen systems?[5] Perhaps they would be most impressed by the ways in which their ideas, and the colossal body of subsequent work, have changed the everyday lives of nearly every person on the planet through the development of technologies like transistors, integrated circuits,

and lasers.[6]

This dissertation is only a shadow of the colossus, and is concerned with how quantum computers, or computers which rely on quantum bits and quantum logic gates, can be used to determine the properties of quantum systems with many interacting bodies. It has a particular focus on hybrid quantum-classical algorithms well suited to simulate systems for which the interactions between bodies are strong. While much of the work presented in this dissertation is applicable to general many-body systems, the language used and systems studied are conventional in the field of (classical) quantum chemistry. Nature isn't classical dammit,[7] and finally, neither are computers!

## 1.2 The electronic structure problem

In quantum chemistry, one is usually interested in predicting the properties of ground or low-lying electronic states for a molecular system accurately enough to gain scientific insight. In practice this involves the solving the non-relativistic, time-independent, electronic Schrödinger equation

$$\hat{H}\Psi_j = E_j\Psi_j. \tag{1.1}$$

Although simple in print, this equation encapsulates an astoundingly rich physics. The system's eigenstates $\Psi_j$, referred to as wave functions, and its energy eigenvalues $E_j$ correspond to the Hamiltonian operator $\hat{H}$, which incorporates the energetic interactions of the system's constituents. A general (molecular) Hamiltonian includes kinetic energy terms for electrons and nuclei as well as potential energy terms for (i) inter-nucleus interactions, (ii) inter-electron interactions, and (iii) electron-nucleus interactions. However, as pointed out by Born and Oppenheimer, and elaborated upon by Sutcliffe,[8] the tremendous discrepancy between the mass of the electron and the mass of the nuclei allows a critical simplification to the Hamiltonian where one can neglect the nuclear kinetic energy term and the inter-nucleus potential. Under this approximation the electrons interact only in a field of fixed

nuclear potential and the so-called electronic Hamiltonian is given by

$$\hat{H} = -\frac{\hbar^2}{2m_e}\sum_i \nabla_i^2 - \frac{q_e}{4\pi\varepsilon_o}\sum_{iI}\frac{q_I}{r_{iI}} + \frac{q_e^2}{4\pi\varepsilon_o}\sum_{i,j>i}\frac{1}{r_{ij}}, \tag{1.2}$$

where $\hbar$ is Plank's constant divided by $2\pi$, $m_e$ is the electron mass, $q_e$ is the electron charge and $\varepsilon_o$ is the permittivity of free space. In the rest of this dissertation we will use only atomic units in which the aforementioned constants are all equal to one. The indices $i$ and $j$ are over electrons, and the index $I$ is over nuclei such that $r_{iI}$ and denotes the distance between electron $i$ and nucleus $I$ while $r_{ij}$ denotes the distance between electrons $i$ and $j$.

The $n$-electron wave function $\Psi$ for a system with Hamiltonian $\hat{H}$ therefore depends *explicitly* on the real-space coordinates of the electrons $\{\mathbf{r}_i\}$, (i.e. $\Psi = \Psi(\mathbf{r}_1, \mathbf{r}_2, ..., \mathbf{r}_n)$). However, even under the Born-Oppenheimer approximation, $\Psi$ is also *parametrically* a function of the $m$ nuclear coordinates $\{\mathbf{R}_I\}$ because they effect the static field through which the electrons move. Because one integrates over the the electronic coordinates to determine the expectation value of the electronic energy $E_{\text{elec}} = \langle\Psi|\hat{H}|\Psi\rangle$, the total energy of the system $E_{\text{tot}}$ depends only on the nuclear coordinates. It is given by the sum of the electronic energy and and the trivially calculated nuclear-repulsion energy $E_{\text{nuc}}$ as

$$E_{\text{tot}}(\mathbf{R}_1, \mathbf{R}_2, ..., \mathbf{R}_m) = E_{\text{elec}}(\mathbf{R}_1, \mathbf{R}_2, ..., \mathbf{R}_m) + E_{\text{nuc}}(\mathbf{R}_1, \mathbf{R}_2, ..., \mathbf{R}_m). \tag{1.3}$$

It is the total energy as a function of the nuclear coordinates that is of primary interest in quantum chemistry as it is the key to determining the potential energy surface and extracting the wealth of chemical insight it offers.

### 1.2.1 The antisymmetry of fermionic wave functions

It was recognized by early in the history of quantum mechanics by Pauli[9] that that two or more electrons would not occupy the the same quantum state, although surprisingly, rigorous investigation of a proof is still an area of research.[10] His now famous exclusion principle gave at least a heuristic explanation for the structure of the periodic table, and

also suggested the existence of a mysterious "non-classical" quantum number, shortly after determined to be the particle's spin.[11]

The principle has foundational importance to the quantum mechanics of many interacting, but indistinguishable, bodies. To show this, first consider a single-particle state $\phi_p(\mathbf{x}_1)$ defined as

$$\phi_{2a+\delta_\beta^\sigma}(\mathbf{x}_1) = \psi_a(\mathbf{r}_1)\chi_\sigma(\omega_1) \tag{1.4}$$

where $\mathbf{r}_1$ is the spatial coordinate of a particle, $\omega_1$ is the spin coordinate of the particle, $\mathbf{x}_1 = (\mathbf{r}_1, \omega_1)$ is a compound spatial and spin coordinate of the particle. Additionally, $\psi_a$ is a so-called spatial orbital characterized by a unique set of three quantum numbers, and $\chi_\sigma$ is a spin function indexed by $\sigma$ which can indicate either spin up ($\sigma = \alpha$) or spin down ($\sigma = \beta$) (at least if the particle is an electron), and $\delta_\beta^\sigma$ is a Kronecker delta function to stagger the spin to spatial orbital indexing. In the context on indistinguishability, a two-electron wave function $\Psi(\mathbf{x}_1, \mathbf{x}_2)$ *cannot* be written as a simple product of the single-particle states $\phi_p(\mathbf{x}_1)$ and $\phi_q(\mathbf{x}_2)$. Instead, one must consider the wave function as either a symmetric ($+$) or an antisymmetric ($-$) linear combination

$$\Psi(\mathbf{x}_1, \mathbf{x}_2) = \phi_p(\mathbf{x}_1)\phi_q(\mathbf{x}_2) \pm \phi_p(\mathbf{x}_2)\phi_q(\mathbf{x}_1). \tag{1.5}$$

It follows almost from inspection that only the antisymmetric solution satisfies Pauli's exclusion principle. In other words, if $\phi_p = \phi_q$, then then two electrons occupy the same state, and the total wave function

$$\Psi(\mathbf{x}_1, \mathbf{x}_2) = \phi_p(\mathbf{x}_1)\phi_p(\mathbf{x}_2) - \phi_p(\mathbf{x}_2)\phi_p(\mathbf{x}_1) = 0, \tag{1.6}$$

is zero over all space regardless of the electronic coordinates. It is therefore *antisymmetric* wave functions which form the basis for many-body quantum chemistry.

### 1.2.2 Slater determinants as mean-field wave functions

A generalization of the two-electron wave function discussed above was originally proposed by Heisenberg,[12] but it was the subsequent work of Hartree,[13,14] Slater,[15] and Fock[16] which established the determinant

$$\Phi(\mathbf{x}_1,\mathbf{x}_2,...,\mathbf{x}_n) = \frac{1}{\sqrt{n!}}\begin{vmatrix} \phi_1(\mathbf{x}_1) & \phi_1(\mathbf{x}_2) & \dots & \phi_1(\mathbf{x}_n) \\ \phi_2(\mathbf{x}_1) & \phi_2(\mathbf{x}_2) & \dots & \phi_2(\mathbf{x}_n) \\ \vdots & \vdots & \ddots & \vdots \\ \phi_n(\mathbf{x}_1) & \phi_n(\mathbf{x}_2) & \dots & \phi_n(\mathbf{x}_n) \end{vmatrix} \tag{1.7}$$

(which now bears Slater's name), as the basic building block for wave functions in many-electron quantum mechanics. While a single Slater determinant does not exactly solve the electronic Schrödinger equation [Eq. (1.1)], its construction suggests naturally the question: what is the best single determinant, and how could it be determined? The variational principle, at least in the context of quantum mechanics, implies that the energy of *any* trial state is lower bound by the energy of the ground eigenstate $E_0 = \langle\Psi_0|\hat{H}|\Psi_0\rangle$. Early work in this regard was concerned with finding a single determinant (now known as the Hartree-Fock determinant $\Phi_{\text{HF}}$), comprised of a set of single-particle states $\{\phi_p\}$, for which the energy expectation value $E_{\text{HF}} = \langle\Phi_{\text{HF}}|\hat{H}|\Phi_{\text{HF}}\rangle$ was minimized, and therefore closest to the true ground state eigenvalue. The variational flexibility in the determinant arises when the single-particle state $\phi_p(\mathbf{x})$ is given as an expansion of atomic basis functions $\varphi_\mu(\mathbf{x})$ as

$$\phi_p(\mathbf{x}) = \sum_\mu C_{\mu p}\varphi_\mu(\mathbf{x}), \tag{1.8}$$

such that the coefficients $C_{\mu p}$ appearing in the Hartree-Fock determinant are varied to minimize $E_{\text{HF}}$.

The work of Hartree, Fock, and later Roothaan[17] made possible a practical procedure for determining the coefficients $C_{\mu p}$ that minimize $E_{\text{HF}}$ and characterize the so-called Hartree-Fock or mean-field solution. The term mean-field stems from the principle that the optimal single-particle states $\phi_p(\mathbf{x_1})$ which compose the Hartree-Fock determinant [Eq. (1.7)], are found by assuming each electron interacts in the *average* field created by

the other electrons. The iterative Hartree-Fock procedure requires that one compute three initial quantities: (i) the overlap integrals $S_{\mu\nu}$, (ii) the one-electron integrals $\langle\mu|\nu\rangle$, and (iii) the two-electron integrals $\langle\mu\nu|\lambda\sigma\rangle$. The overlap integrals are given simply by

$$S_{\mu\nu} = \int \varphi_\mu^*(\mathbf{x}_1)\varphi_\nu(\mathbf{x}_1)d\mathbf{x}_1. \tag{1.9}$$

The one electron integrals are given by the expectation value of the one electron operator $\hat{h}$ as

$$\langle\mu|\hat{h}|\nu\rangle = \int \varphi_\mu^*(\mathbf{x}_1)\left[-\frac{1}{2}\nabla_{\mathbf{r}_1}^2 - \sum_I \frac{Z_I}{|\mathbf{r}_1 - \mathbf{R}_I|}\right]\varphi_\nu(\mathbf{x}_1)d\mathbf{x}_1, \tag{1.10}$$

where the index $I$ is over the nuclei, $Z_I$ denotes the nuclear charge (in atomic units), and $\mathbf{R}_I$ is the nuclear position. Finally, the two electron integral is given by

$$\langle\mu\nu|\lambda\sigma\rangle = \int\int \varphi_\mu^*(\mathbf{x}_1)\varphi_\nu^*(\mathbf{x}_2)\left[\frac{1}{|\mathbf{r}_1 - \mathbf{r}_2|}\right]\varphi_\lambda(\mathbf{x}_1)\varphi_\sigma(\mathbf{x}_2)d\mathbf{x}_1 d\mathbf{x}_2, \tag{1.11}$$

noting the integration over the (spin and spatial) coordinates of two electrons. Although the details of the iterative Hartree-Fock procedure are an important aspect of quantum chemistry, it is not central to the content of this dissertation and we therefore point the reader to the excellent introductory text by Szabo and Ostlund for farther details.[18] We will, however, return to our discussion about Slater determinants and electron integrals in the following subsection(s).

*Integral transforms*

Because it will be salient future discussions regarding second quantization and quantum simulation algorithms, it is important to point out under certain circumstance one needs to transform the atomic-orbital electron integrals indexed by $\mu,\nu,\lambda,\sigma$ (Eqs. (1.10) and (1.11)) into an alternative basis. For example, if one wants to transform the two-electron integrals to the basis of mean-field molecular orbitals $\phi_p$ [Eq. (1.8)] indexed by $p,q,r,s$ one can perform

$$\langle pq|rs\rangle = \sum_{pqrs}\sum_{\mu\nu\lambda\sigma} C_{\mu p}C_{\nu q}C_{\lambda r}C_{\sigma s}\langle\mu\nu|\lambda\sigma\rangle, \tag{1.12}$$

noting that in practice only a five fold summation with scaling $\left[\mathscr{O}(n^5)\right]$ is necessary rather than the eight fold summation $\left[\mathscr{O}(n^8)\right]$ which is shown for clarity. An analogous transform exists for the one-electron integrals.

### 1.2.3 Second quantization

Thus far, we have considered wave functions as functions of the real-space coordinates of the bodies they represent. These functions are given by projections of a quantum state (vector) onto a position basis. For example, consider the wave function $\psi(x)$ of a particle along a one-dimensional spatial coordinate $x$, given as

$$\psi(x) = \langle x|\psi\rangle = \int \psi(x)\,\langle x|\tilde{x}\rangle\, d\tilde{x}, \tag{1.13}$$

where $|x\rangle$ is a vector with a *continuous* index indicative of a position $x$, and the infinitely large set of vectors $\{|x\rangle\}$ are orthonormal. While wave functions in position space are perhaps the most intuitive way to understand many-body quantum mechanics, it is often more convenient to use the state vector notation ($|\psi\rangle$ in the example above), also referred to as "bra-ket" notation as coined by Dirac. In this way, any general many-body state $|\Psi\rangle$ can be expressed a complex vector in Hilbert (or Fock) space. A single $n$-electron Slater determinant $\Phi$ [Eq. (1.7)] can be represented in this notation as a tensor product of the single-particle states $\left|\phi_p\right\rangle$ given by

$$|\Phi\rangle = |\phi_1\rangle \otimes |\phi_2\rangle \otimes \ldots \otimes |\phi_n\rangle = |\phi_1\phi_2\ldots\phi_n\rangle\,. \tag{1.14}$$

While this notation is powerful and concise, one must also account for the previously discussed (anti)symmetry conditions. In the state vector notation, a determinant for a two electron system for example needs to satisfy:

$$\left|\phi_p\phi_q\right\rangle = \pm\left|\phi_q\phi_p\right\rangle. \tag{1.15}$$

This can be accomplished, as was first done by Dirac and Fock, by introducing a set of

operators that preserve either the bosonic symmetry or fermionic antisymmetry of the state. These operators, known as the creation ($\hat{a}_p^\dagger$) and annihilation operators ($\hat{a}_p$), pertain to single-particle state $\phi_p$. In the case of fermions, which we shall now focus on exclusively, these operators obey the following anti-commutation relationships:

$$\left[\hat{a}_p, \hat{a}_q^\dagger\right]_+ = \hat{a}_p \hat{a}_q^\dagger + \hat{a}_q^\dagger \hat{a}_p = \delta_p^q, \tag{1.16}$$

$$\left[\hat{a}_p, \hat{a}_q\right]_+ = 0, \tag{1.17}$$

and

$$\left[\hat{a}_p^\dagger, \hat{a}_q^\dagger\right]_+ = 0. \tag{1.18}$$

An occupied single-particle state $\left|\phi_p\right\rangle$ can then be constructed, for example, by applying the creation operator $\hat{a}_p^\dagger$ to the vacuum state $|-\rangle$ such that

$$\left|\phi_p\right\rangle = \hat{a}_p^\dagger \left|-\right\rangle. \tag{1.19}$$

Similarly, one can annihilate a particle in state $\left|\phi_p\right\rangle$ to get back the vacuum via

$$\left|-\right\rangle = \hat{a}_p \left|\phi_p\right\rangle. \tag{1.20}$$

A final important aspect of the fermionic operators is that (i) annihilating the vacuum (i.e. $\hat{a}_p \left|-\right\rangle$), or creating a particle in an already occupied state (i.e. $\hat{a}_p^\dagger \left|\phi_p\right\rangle$) zeros the state. This formalism is referred to as second quantization, and allows one to concisely represent both fermionic operators and many-body states. In the following subsections we will use second quantization to describe both the quantum chemistry Hamiltonian and the many-body states that are its eigenvectors.

*The second quantized Hamiltonian*

Armed with the rules of second quantization, one can the re-write the electronic structure Hamiltonian [Eq. (1.2)] using the fermionic operators as

$$\hat{H} = \sum_{pq} \langle p|q\rangle \, \hat{a}_p^\dagger \hat{a}_q + \frac{1}{4} \sum_{pqrs} \langle pq||rs\rangle \, \hat{a}_p^\dagger \hat{a}_q^\dagger \hat{a}_s \hat{a}_r, \tag{1.21}$$

where $\langle p|\hat{h}|q\rangle$ and $\langle pq||rs\rangle = \langle pq|rs\rangle - \langle pq|sr\rangle$ are the one-electron and anti-symmetrized two-electron integrals, respectively. Here we use the indices $p,q,r,s$ to denote the integrals transformed to the Hartree-Fock molecular orbital basis because they are needed as a starting point for most quantum simulation algorithms. We note however that the Hamiltonian is invariant (iso-spectral) to rotations of the orbitals.

*The particle number representation*

It is also important to discuss here, for the sake of future dialog on the representation of states with quantum computers, the so-called particle number (also refered to as occupation number) representation of states. The particle number representation of a state is equivalent to the occupied state representation given in Eq. (1.14), but uses a slightly different notation. Rather than denoting a determinant $|\Phi\rangle$ with an occupied set of $n$ single-particle states $|\phi_1\phi_2...\phi_n\rangle$, one denotes it in terms of the occupations $n_m \in \{1,0\}$ of all $m$ single-particle states as

$$|\Phi\rangle = |\mathbf{n}\rangle = |n_1 n_2 \dots n_m\rangle\,, \tag{1.22}$$

where $\mathbf{n}$ is simply a vector of occupations $(n_1, n_2, \dots, n_n)$. For example, the Hartree-Fock state $|\Phi_{\text{HF}}\rangle$ (comprised of the $n < m$ lowest energy single-particle states $\phi_1, \dots, \phi_n$) is denoted by

$$|\Phi_{\text{HF}}\rangle = |1_1 1_2 \dots 1_n 0_{n+1} 0_{n+2} \dots 0_m\rangle\,, \tag{1.23}$$

where the subscript indices are only shown here for clarity. Analogously, the vacuum $|-\rangle$ is given by a ket of $m$ zeros.

## 1.3 Electron correlation

Thus far we have only described in detail approximate solutions of the $n$-electron Schrödinger equation [Eq. (1.1)] given by a single determinant. Although the mean-field solution usually captures a very large fraction of the total electronic energy, the exact electronic energy is always lower because the motion of the electrons is correlated. To

paraphrase Stanton and Bartlett,[19] "average electronic interactions don't keep electrons as separated as instantaneous interactions do." Incorporating into an approximate theory the flexibility of occupying single-particle states with higher kinetic energy (i.e. in higher energy orbitals), allows one to recover more of the instantaneous interactions. Such an approach gives rise to multi-determinantal wave functions which can capture more (or all) of the electronic correlation effects. In the following subsections we will describe an exact determinantal expansion of the wave function that solves Eq. (1.1), discuss some of the more nuanced aspects of electronic correlation, and review several algorithms which can treat different regimes of correlation.

### 1.3.1 Exact diagonalization and the curse of dimensionality

Here we will attempt to outline the exact solution to the electronic structure problem, that is, the whole enchilada. It is important to note that a *truly exact* solution to Eq. (1.1), that is to say one which would mach a perfect experimental value, would require a *complete* set of basis functions $\{\varphi_\mu\}$ with infinite dimension. Needless to say using an infinite set in practice is impossible, and therefore, any "exact" solution is restricted to a finite set of $m$ basis functions in practical applications. Here and in the remainder of this dissertation usage of a finite basis set is always assumed.

We will begin by considering that the Hartree-Fock procedure produces $m$ mean-field single-particle states $\{\phi_1, \phi_2, ..., \phi_m\}$, but the Hartree-Fock determinant $\Phi_{\text{HF}}$ is comprised of only the $n < m$ lowest energy single-particle states $\{\phi_1, \phi_2, ..., \phi_n\}$. It is completely valid to then construct "excited" determinants from a subset of any $n$ occupied states as

$$|\Phi_I\rangle = |\phi_{i_1}\phi_{i_2}...\phi_{i_n}\rangle \tag{1.24}$$

where $i_i < i_2 < \cdots < i_n$ are the original single-particle state indices and $I = (i_1, i_2, \ldots, i_n)$ is a compound index for a specific determinant. Note also that all determinants constructed in this way are orthonormal such that $\langle\Phi_I|\Phi'_I\rangle = \delta_I^{I'}$ so long as the single-particle states are

as well.

The basic idea of the configuration interaction (CI) method[20] is then to diagonalize the Hamiltonian matrix $\mathbf{H}$ in a basis $\{\Phi_I\}$ of $N_I$ determinants, comprised of the Hartree-Fock determinant and some set of $N_I - 1$ excited determinants. The matrix elements of the Hamiltonian in the basis $\{\Phi_I\}$ are then given by

$$H_{IJ} = \langle \Phi_I | \hat{H} | \Phi_J \rangle , \tag{1.25}$$

and Schrödinger's equation takes the form of a matrix eigenvalue problem $\mathbf{HC} = \vec{E}\mathbf{C}$. The elements ($C_I$) of the eigenvectors $\vec{C}_I$, for example of the ground state ($C_I \in \vec{C}_0 = \mathbf{C}^{(0)}$), give coefficients in a determinantal expansion of the CI wave function. If the set of expansion determinants contains *all* possible $N_{\text{FCI}}$ combinations of $n$ electrons in $m$ states, then the the CI is considered *full* and the basis spans the entire Hilbert space. It follows that the full CI (FCI) state is given by

$$|\Psi_{\text{FCI}}\rangle = \sum_{I}^{N_{\text{FCI}}} C_I |\Phi_I\rangle . \tag{1.26}$$

The variational principal implies that the FCI state is the best possible approximation to the true ground state in a finite basis, capturing the entirety of electronic correlations by allowing for maximum flexibility to account for instantaneous interactions.

Despite the importance of FCI for our theoretical understanding of the electronic structure problem and for benchmarking approximate methods, it is intractable for all but the smallest of molecular systems.[21] The issue, also referred to as the *curse of dimensionality*, is that the dimension of the Hilbert space (and the size $N_{\text{FCI}}$ of the full determinantal basis $\{\Phi_I\}$) scales as a binomial coefficient in $n$ and $m$. Despite a long history of impressive algorithmic improvements[22–24] and the aid of massively parallel subroutine implementations,[25] the largest FCI computation to date only included 22 electrons in 22 (spatial) orbitals.

Such is the objective of modern electronic structure theory: to accurately determine the properties of electronic states at a computational cost somewhere between Hartree-Fock theory and FCI. As we will discuss in the following subsections, the success of approxi-

mate methods is also strongly tied to the degree of electronic correlation, raising important questions about the compactness of classical wave function representations and the usage of quantum computational algorithms.

### 1.3.2 Static and dynamical correlation

As previously mentioned, it is due to electronic correlations that a single determinant is insufficient to exactly describe solutions to Schrödinger's equation. In fact, the difference between the exact FCI energy ($E_0$) and and the Hartree-Fock energy ($E_{\text{HF}}$) is referred to as the correlation energy[26]

$$E_{\text{corr}} = E_0 - E_{\text{HF}}, \tag{1.27}$$

and is the most widely used metric to describe the strength of electronic correlation. It has become common to partition the correlations mainly[19,27] into two classes:[28,29] dynamical (or weak) correlations and static (or strong) correlations, although it is important to note that there exists no rigorous physical distinction.

Dynamical correlation refers to the predominantly local repulsion effects which diminish the value of the wave function when two electrons are near one another, resulting in a reduction in energy. In cases where the total correlation effects are predominantly dynamical, the Hartree-Fock determinant is usually a good approximation to the FCI state. The total correlation energy can be (mostly) recovered by perturbative corrections to the Hartree-Fock state, or by allowing excitations to determinants with only a small number of excited electrons. These approaches characterize the class of *single-reference* electronic structure methods including (but certainly not limited to), 2nd-order Møller–Plesset perturbation theory[30] (MP2), finite-order CI,[20] coupled cluster[31,32] (CC) approaches, or stochastic methods.[33] Many examples, such as ground-state energies for molecular systems at (or near) equilibrium geometries, predominantly exhibit dynamical correlations and are therefore well described by the aforementioned techniques.

Static or "strong" correlation, which is of principal importance to the work in this dis-

sertation, is a phenomenon largely related to orbital degeneracies and is (in general) much more challenging to deal with using approximate theories. In the orbital picture, for example, long-range electronic interactions cause electrons to become localized on atoms when the orbital energies are near-degenerate, such as in bond breaking. This type of correlation is considered to be *strong* or *static*. In such cases the energetic cost of promoting electrons into higher states can become small relative to the local repulsion energies. Analogously, in the condensed matter community, strong correlation is commonly thought of as the regime in which the Hubbard model Hamiltonian[34] has a much larger on-site repulsion coefficient, than site-hopping coefficient.

A consequence of degeneracy and strong correlation, now in the perspective of the many-body state, is that the wave function takes on a pronounced multi determinantal character, such that the Hartree-Fock determinant *is not* a good overall approximation. Figure 1.1 is a graphical illustration of this phenomenon, showing a representation of the FCI coefficients in Eq. (1.26) organized as a matrix for two different geometries of linear $H_{10}$. Specifically, one can see that at the near equilibrium geometry ($r = 1.0$) the wave function is dominated by just a small number of determinants (including the Hartree-Fock determinant), but that once stretched, much of the sparsity is lost and a large number of determinants become important, as indicated by the density of yellow pixels.

The success or failure of single-reference approaches is therefore largely contingent on the degree of degeneracy in the orbitals. A common indicator in particular is the energy gap between the highest occupied molecular orbital (HOMO) and the lowest unoccupied molecular orbital (LUMO). Figure 1.2 simultaneously depicts (top) the increase of orbital degeneracy and vanishing HOMO-LUMO gap, and (bottom) the breakdown of several single-reference methods during the dissociation of linear $H_{10}$, a now paradigmatic model system for strong correlation.[35–38] Despite almost exactly reproducing the FCI energy near equilibrium-geometry, coupled cluster with single, double and perturbative triple excitations[39] [CCSD(T)] (often referred to as the "gold standard" in quantum chemistry)

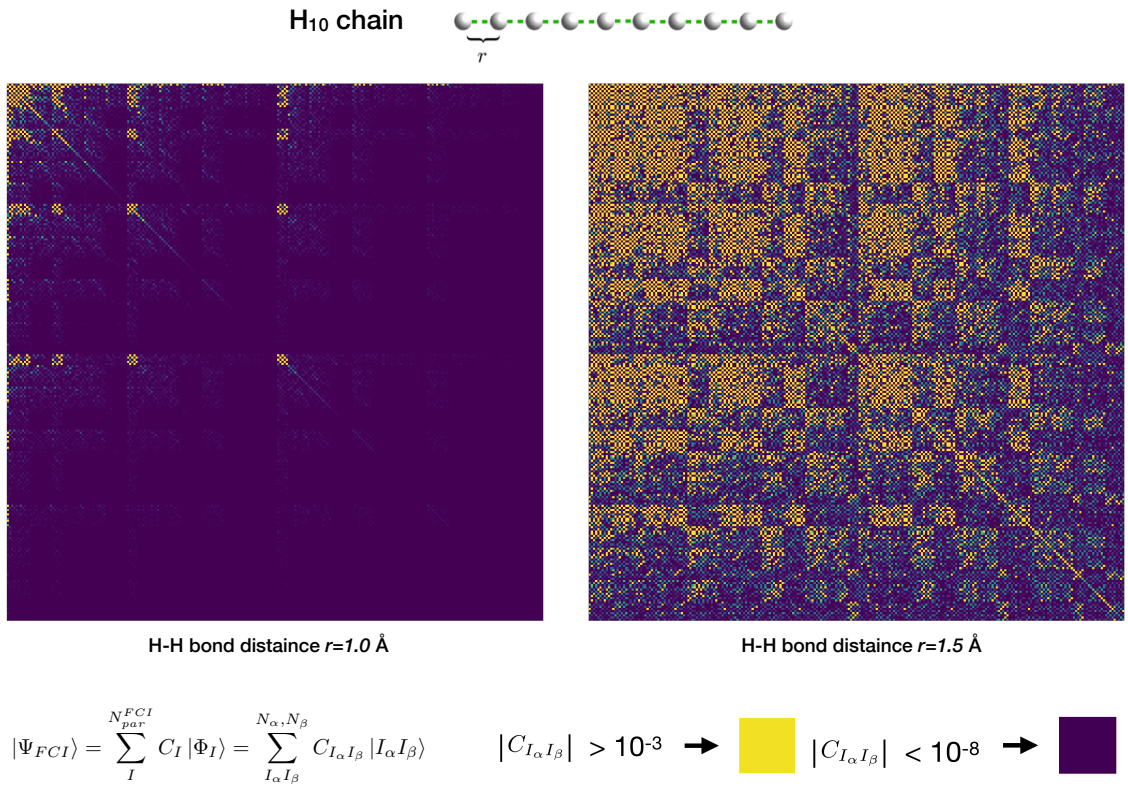


Figure 1.1: Graphical depiction of the FCI wave function coefficients described in Eq. (1.26) for a linear $H_{10}$ chain at $r$=1.0Å (left) and $r$=1.5Å (right). Coefficients are arranged as a matrix indexed by $\alpha$ and $\beta$ spin-orbital occupations. Coefficients with a magnitude greater than $10^{-3}$ are shown by yellow pixels, and coefficients with a magnitude less than $10^{-8}$ are represented by purple pixels. The calculations used to produce the figures utilized a minimal STO-6G basis, resulting in a total of 62,504 coefficients.

fails catastrophically in the strong correlation regime.

### 1.3.3 Classical methods for strong correlation

While the physical principles that give rise to correlation are simple – instantaneous coulombic interactions – the effects of those interactions are very elaborate, and give rise to a myriad of unique physical phenomena and result in complex electronic structures. Computational study of such phenomena and complex states, including bond breaking and photochemical processes,[28,40] molecular magnetism,[41] high-temperature superconductivity,[42] metal-insulator transitions,[43] and others,[44–46] is therefore still an important challenge

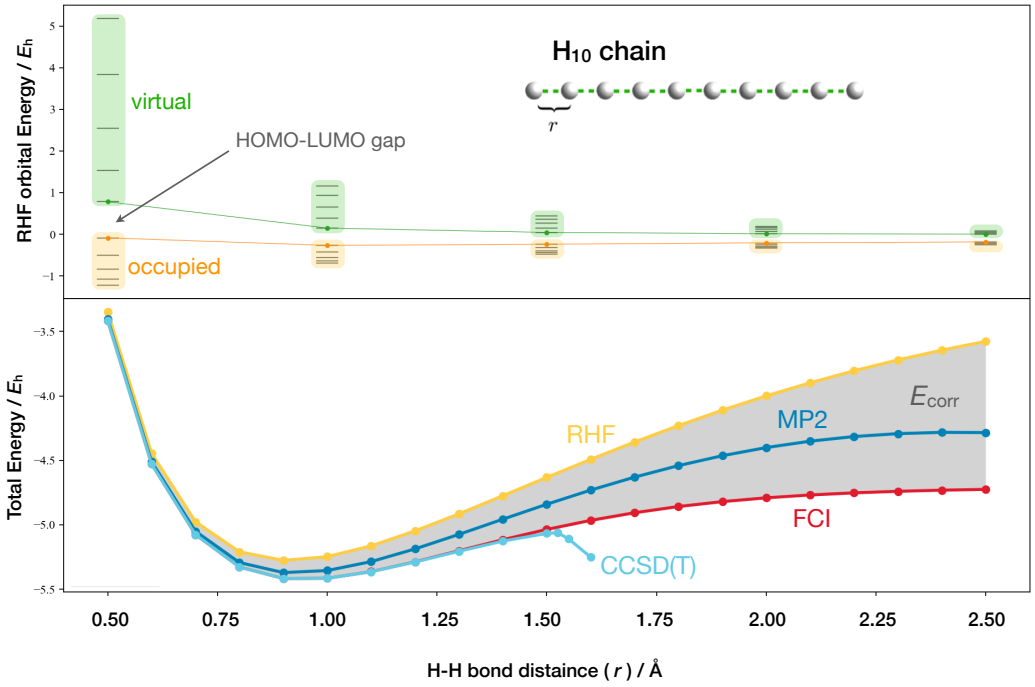


Figure 1.2: Molecular orbital energies from restricted Hartree-Fock (top) and total energy from RHF, MP2, CCSD(T), and FCI (bottom) over the symmetric dissociation of linear $H_{10}$. All calculations employed a STO-6G basis.

in modern computational science.

The last several decades have seen tremendous development of classical computational approaches aimed at treating strong correlation. The first examples the authors are aware of are the works of Ruedenberg[47,48] on the multi-configurational self consistent field (MC-SCF) method, which considered performing CI with excitations containing the valence orbitals paired with a self-consistent orbital reoptimization. Soon after, Roos[49] considered MCSCF which included what he called the active orbitals (rather than strictly valence) and coined the now-conventional term *complete active space* SCF (CASSCF). Unfortunately, CAS methods suffer from the same scaling as FCI, and are limited in practice to calculations with approximately 18 electrons in 18 spatial orbitals (18e, 18o). This limitation has motivated the development of several lower-cost alternatives.

One CAS alternative that is still based on CI theory, is the class of *selected* CI (sCI) methods. Selected CI methods approximate the FCI solution using a subset of the full determinant space but are (generally) not restricted to a fixed excitation order, and mainly differ in how the ideal subset is determined. The earliest examples of sCI,[50–54] some of which predate MCSCF, were originally intend to reduce the cost of CI with only singly and doubly excited determinants rather than to act as an alternative to FCI or CAS methods. In recent years, however, sCI has received renewed attention as an alternative to FCI with new deterministic,[55–66] stochastic,[67–72] and semistochastic[73–76] variants being proposed.

Another family of FCI alternatives, closely related to sCI, is that of determinant-based Monte Carlo methods,[77–84] which generally attempt to sample from the integrated imaginary-time Schrödinger equation. The most notable of these approaches, FCI quantum Monte Carlo (FCIQMC),[77,79] considers a so-called walker formalism where the wave function is approximated from the long-imaginary-time dynamics of the walkers. The success of FCIQMC is in its avoidance of the fermionic sign problem, and its ability to be implemented on massively parallel architectures.[85–91]

Other approaches, which are not explicitly based on a determinantal expansion of the wave function, have also been explored to treat strong correlation. One such method, the variational two-body reduced density matrix[92–96] (V2RDM) algorithm, seeks to determine (as the name implies) the optimized elements of the one and two-body RDM elements, rather than the explicit wave function coefficients. The appeal of these methods is that, in-principle, one is able to recover the exact energy with only the one- and two-body RDMs which scale as $\mathcal{O}(m^2)$ and $\mathcal{O}(m^4)$, where $m$ is the number of spin orbitals, rather than as a binomial coefficient in $n$ and $m$. The challenge for V2RDM methods, however, is enforcing that the optimized RDMs are representable by a physical $n$-electron fermionic wave function, which leads to a constrained semi-definite optimization problem.

A final important class of algorithms able to treat strong correlation, and arguably the most successful, are those which optimize the wave function cast as a tensor network state[97]

(TNS). Conceptually, TNSs are given by the FCI coefficient vector [Eq. (1.26)], decomposed into a product of tensors (ideally chosen to reflect the geometry of a system)[98] that can be truncated to a reduced rank with minimal loss of information. The advantage of TNSs is their ability to maximally exploit locality in quantum systems subject to an entanglement area law,[98,99] such that very low rank tensors can accurately represent even strongly correlated states. In the case that the tensors have three indices (two once a configuration is specified) the wave function is given by a matrix product state[100–102] (MPS), the variational ansatz optimized via the density matrix renormalization group[103] (DMRG) algorithm. DMRG for example, which is ideally suited to optimize MPSs for one dimensional systems, has allowed for very large active space calculations on the order of 100 orbitals for quasi-linear molecular systems.[104–113] Other tensor networks, such as the projected entangled pair states[114] (PEPS), and tree tensor network states[115–117] (TTNS), are in principle well suited to compactly represent the wave functions of two and three-dimensional systems, but in practice are challenging to optimize due to the high computational cost of general tensor contraction.

*A note on the compactness of classical wave function representations*

Despite the impressive theoretical and algorithmic advances highlighted in this subsection, there still exists no general and computationally affordable method to accurately treat strongly correlated systems. It is important to point out that at large enough system sizes (say on the order of $10^3$ or $10^4$ electrons and orbitals) all the methods described here would generally be incapable of even *storing* the parameters (coefficients, cluster amplitudes, RDM or tensor elements) used to characterize the approximate wave function, much less optimizing them. Moreover, as demonstrated in Fig. 1.1, the onset of strong electronic correlations greatly exasperates this problem, as a far greater fraction of the total Hilbert space becomes important. These factors are investigated numerically in Chapter 2 and ultimately motivate the development of quantum algorithms and hardware capable of storing the information pertaining to molecular wave functions.

## 1.4 Quantum computers: the blessing of dimensionality

Although the initial concept of a quantum Turing machine was introduced by Paul Benioff in 1980,[118] Richard Feynman is commonly considered the first to propose usage of such a device to simulate quantum systems.[7] A a so-called *quantum computer* is a device that, like a classical computer, takes in some body of information (an input say with size $n$), performs well-defined manipulations to – or with – that information (via an algorithm), and produces some useful information (an output). The term *computational complexity* can likewise be used for both classical and quantum algorithms, and describes how the required resources for space (related to the number of bits), and for time (related to the number of physical operations) scale with respect to the input size $n$. Concisely put, the crucial difference between a classical and a quantum machine, however, is that a quantum device is able to utilize superpositions of (usually binary) bit states $|1\rangle$ *and* $|0\rangle$, rather than exclusive bit states $|1\rangle$ *or* $|0\rangle$ at a given instant in time. The objective of any quantum computational algorithm is then to solve some problem, for example the determination of low-lying eigenstates and their properties, with significantly lower scaling for space and time requirements than would be required for an optimal classical algorithm.

As discussed in the previous section, (near) exact determination of low-lying eigenstates and their properties is still a problem with *exponential* complexity on classical computers, particularly for systems that exhibit strong correlation effects. The advent of large-scale programmable quantum computers would therefore mark a paradigm shift for the simulation of quantum mechanical systems. Efficient quantum algorithms – those which have only *polynomially* scaling space and time complexity – for determining such properties are of principle interest to chemistry, condensed matter physics, and materials science.[119–122] The potential of quantum computation has motivated rapid development of a wide range of algorithms (including those introduced in this dissertation), and experimental breakthroughs[121,123–127] including the first demonstration of quantum advantage over a classical machine.[128]

In the following subsections we will review the fundamental aspects of quantum computing and quantum simulation, and review of many of the most important algorithmic developments in the field. We hope that the reader finds these overviews illuminating and we will attempt to convey how the advantage of using a quantum device arises, and what the potential challenges may yet be.

### 1.4.1 Quantum bits

Consider first that the most fundamental form of information on a classical machine is a binary bit $b_p$, the state of which can be represented as

$$\left|b_p\right\rangle \in \left\{ \left|0\right\rangle, \left|1\right\rangle \right\}, \tag{1.28}$$

where,

$$\left|0\right\rangle \equiv \begin{pmatrix} 1 \\ 0 \end{pmatrix}, \tag{1.29}$$

and

$$\left|1\right\rangle \equiv \begin{pmatrix} 0 \\ 1 \end{pmatrix} \tag{1.30}$$

are orthonormal basis-vectors. A classical configuration of $m$ bits $\left|\mathbf{B}\right\rangle$ is given by the tensor product

$$\left|\mathbf{B}\right\rangle = \left|b_0\right\rangle \otimes \left|b_1\right\rangle \otimes \cdots \otimes \left|b_{m-1}\right\rangle = \left|b_1 b_2 \ldots b_{m-1}\right\rangle. \tag{1.31}$$

The bit configuration (string) can then be used so store any computational object of interest, for example a double precision number, which would require $m = 64$ classical bits. One may also write (manipulate) values of the bits and/or read the values $b_m$ with essentially 100 percent certainty (which is not the case for quantum bits as we will soon discuss). It also is important here to note that although $\left|\mathbf{B}\right\rangle$ can represent $2^m$ different configurations, it can only represent *one* configuration *at a given instant in time!*

As briefly stated in the previous subsection, a quantum device is able to utilize the phenomena of *superposition* and *entanglement* to store information. This can be expressed by considering the state $\left|q_p\right\rangle$ of a so-called quantum bit (or "qubit") expressed by the super-

position

$$\left|q_p\right\rangle = \alpha\left|0\right\rangle = \beta\left|1\right\rangle, \tag{1.32}$$

where $\alpha$ and $\beta$ are complex normalized probability amplitudes (i.e. $|\alpha|^2 + |\beta|^2 = 1$). A consequence of the superimposed bit states is that, when the value of $\left|q_p\right\rangle$ is read, it is collapses to $|0\rangle$ with probability $|\alpha|^2$ and to $|1\rangle$ with probability $|\beta|^2$.

A general configuration of quantum bits $|\mathbf{Q}\rangle$ can be likewise be represented by a tensor product of individual superimposed qubit states $\left|q_p\right\rangle$ in analogy to Eq. (1.31). However, if more than a single qubit is used ($m > 1$), then $|\mathbf{Q}\rangle$ can also represent *entangled* states, that is, (normalized) states of the form

$$|\mathbf{Q}\rangle = \sum_{\{q_o,\ldots,q_{m-1}\}} C_{q_o,\ldots,q_{m-1}}\left|q_o \ldots q_{m-1}\right\rangle, \tag{1.33}$$

which (in the general case) *cannot* be written as a simple product state. A canonical example of such a state is the Bell state[129] $|\mathbf{Q}_{\text{bell}}\rangle = \frac{1}{\sqrt{2}}|00\rangle + \frac{1}{\sqrt{2}}|11\rangle$, which can't be expressed as a simple product of $|q_0\rangle \otimes |q_1\rangle$. The potential of quantum-computing then lies in the ability to "store" the information content held in the $2^m$ probability amplitudes $C_{q_o,\ldots,q_{m-1}}$ *simultaneously* with only $m$ physical qubits, thus exemplifying a blessing of dimensionality!

### 1.4.2 Quantum circuits

Now that we have outlined the basic principles of storing information using quantum bits, it is appropriate to describe how this information can be manipulated to execute algorithms. In the model of programable quantum computing,[130] this is done via (quantum) circuits constructed from a set of quantum logic gates, analogous to classical logic gates. Because the quantum state $|\mathbf{Q}\rangle$ that exists on the quantum device is a *physical entity*, it must be normalized and, therefore, any quantum circuit used to alter $|\mathbf{Q}\rangle$ must act as a unitary operation $\hat{U}$ (defined such that $\hat{U}^\dagger\hat{U} = 1$). In other words, the action of any quantum circuit

has the form

$$|\mathbf{Q}_{\text{after}}\rangle = \hat{U}\,|\mathbf{Q}_{\text{before}}\rangle\,. \tag{1.34}$$

It is a remarkable result that *any* unitary circuit can be represented by a small universal gate set[131] comprised of operations acting only on one and two-qubits. Some of the most common single-qubit gates, especially in quantum simulation, are the Pauli gates, the Hadamard gate, and the z-rotation gate depicted in Tab 1.1. It is also very common to consider a controlled two-qubit operations [c-$\hat{U}_{\text{target,control}}$], which only applies $\hat{U}$ to configurations of the form $\left|\ldots q_{\text{target}}\ldots 1_{\text{controll}}\ldots\right\rangle$, but leaves configurations $\left|\ldots q_{\text{qtarget}}\ldots 0_{\text{controll}}\ldots\right\rangle$ unchanged. An important example is the controlled application of the Pauli X gate (denoted c-$\hat{X}$ or CNOT), which is the analog of the the classical controlled NOT gate.

Table 1.1: List of common single-qubit quantum gates used in quantum simulation algorithms. Note that these gates will often be subscripted such as $\hat{X}_p$ to denote that the action is on the $p$th qubit.

| gate name | gate symbol | matrix representation |
|---|---|---|
| Pauli X (NOT) | $\hat{X}$ | $\begin{pmatrix} 0 & 1 \\ 1 & 0 \end{pmatrix}$ |
| Pauli Y | $\hat{Y}$ | $\begin{pmatrix} 0 & i \\ -i & 0 \end{pmatrix}$ |
| Pauli Z | $\hat{Z}$ | $\begin{pmatrix} 1 & 0 \\ 0 & -1 \end{pmatrix}$ |
| Hadamard | $\hat{H}$ | $\frac{1}{\sqrt{2}}\begin{pmatrix} 1 & 1 \\ 1 & -1 \end{pmatrix}$ |
| Z Rotation | $\hat{R}_z(\theta)$ | $\begin{pmatrix} e^{\frac{-i\theta}{2}} & 0 \\ 0 & e^{\frac{i\theta}{2}} \end{pmatrix}$ |

Any product the quantum gates described here gives a unitary circuit, and one can construct entangled states from unentangled states via their application. For example, consider how one could construct the Bell state $|\mathbf{Q}_{\text{bell}}\rangle$ with a two-qubit quantum computer initial-

ized to the state $|00\rangle$ by applying

$$\text{c-}\hat{X}_{1,0}\hat{H}_0\,|00\rangle = \frac{1}{\sqrt{2}}\,|00\rangle + \frac{1}{\sqrt{2}}\,|11\rangle\,. \tag{1.35}$$

As a supplement to mathematical formulas, circuit diagrams often provide a convenient graphical representation of their execution order and gate composition. A diagram for the above construction of the bell state via application of a Hadamard gate, followed by a CNOT is given in Fig. 1.3. Circuit diagrams depict the execution of the gates from left to

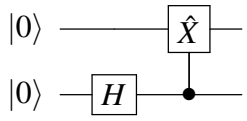


Figure 1.3: Circuit diagram for the construction of the bell state from the vacuum $|00\rangle$. Note the use of the vertical line with a dot connected to the control qubit to denote the c-$\hat{X}_{1,0}$ (CNOT) gate.

right, and gates that can be executed in parallel are often drawn in a single column.

The one and two-qubit gates described here are directly executable as physical operations on quantum hardware, for example, they can be applied as timed microwave pulses which drive the rotation of qubit states. The total runtime for the execution of a quantum circuit (i.e. how long it takes) is linearly proportional to the *depth* of the circuit, given by the number of non-parallel operations (elementary gates) it requires. The challenge in practice then becomes to construct algorithmically useful circuits with shallow depths, or with depths that scale favorably with input size.

### 1.4.3 Determination of expectation values

The final aspect which merits discussion before an overview quantum simulation can be given, is how to numerically determine expectation values $\lambda$ of some operator $\hat{O}$ with respect to the state of the quantum computer $|\mathbf{Q}\rangle$ given by

$$\lambda = \langle \mathbf{Q}|\hat{O}|\mathbf{Q}\rangle\,. \tag{1.36}$$

In practice one can only measure expectation values in the basis $\{|0\rangle, |1\rangle\}$ (often referred to as the computational basis), which are the eigenvectors of the Pauli Z gate. As a consequence, any operator $\hat{O}$ comprised of anything other than a product of $\hat{Z}$ operators, must be transformed into the computational basis as

$$\hat{O} = \hat{V}^{\dagger} \hat{O}_z \hat{V}, \tag{1.37}$$

where $\hat{O}_z$ is a product of $\hat{Z}$ operators corresponding to unique qubits, and $\hat{V}$ is a unitary operator that performs the similarity transformation.

The number of individual measurements $M$ required to determine $\lambda$ is related to the variance of the operator

$$\mathrm{Var}[\hat{O}] = \langle \mathbf{Q} | \hat{O}^2 | \mathbf{Q} \rangle - \Big( \langle \mathbf{Q} | \hat{O} | \mathbf{Q} \rangle \Big)^2, \tag{1.38}$$

which is zero in the case that $|\mathbf{Q}\rangle$ is an eigenvector of $\hat{O}$. The exact relationship is given by

$$M = \frac{\mathrm{Var}[\hat{O}]}{\varepsilon^2}, \tag{1.39}$$

where $\varepsilon$ is the precision to which one wants to numerically determine $\lambda$.

So far we have only considered operators $\hat{O}$ with only a single term, but commonly in quantum simulation, one wants to determine the expectation value for an operator $\hat{O}$ given by a sum of individual operators $\hat{P}_\ell$, each comprised of a product of Pauli operators $\hat{\sigma}_k$ such that

$$\hat{O} = \sum_\ell \hat{P}_\ell = \sum_\ell \left( \prod_k \hat{\sigma}_k^{(\ell)} \right) \tag{1.40}$$

and,

$$\langle \mathbf{Q} | \hat{O} | \mathbf{Q} \rangle = \sum_\ell \langle \mathbf{Q} | \hat{P}_\ell | \mathbf{Q} \rangle = \sum_\ell \left( \prod_k \langle \mathbf{Q} | \hat{V}_k^{(\ell)\dagger} \hat{Z}_k^{(\ell)} \hat{V}_k^{(\ell)} | \mathbf{Q} \rangle \right). \tag{1.41}$$

In this case, $k = (p, [X, Y, \text{ or } Z])$ is a compound index over the products in a term $\hat{P}_\ell$ and denotes both the qubit ($p$) and specific Pauli gate. The transformation unitary $\hat{V}_k^{(\ell)}$ is a one qubit gate that transforms $\hat{X}$ or $\hat{Y}$ into $\hat{Z}$.

### 1.4.4 The fermionic encoding problem

As described in is Sec. 1.2.3, many-body quantum mechanics is often written using the language of second quantization. In the case of quantum chemistry, this implies heavy usage of the Fermionic annihilation and creation operators. If one is interested in quantum computational algorithms for the simulation of electronic systems, there then exists the challenge of representing fermionic operators with quantum gates. This problem is referred to as the fermionic encoding or fermionic mapping problem, and arises due to the need to preserve the anti-symmetry conditions of fermionic wave functions, and the properties of changing state occupation numbers.

The most commonly employed strategy, and the one employed in works presented in this dissertation, was actually outlined by Pascal Jordan and Eugene Wigner almost a century ago.[132] In the aptly-named Jordan-Wigner transformation, the fermionic annihilation ($\hat{a}_p$) and creation ($\hat{a}_p^\dagger$) operators are represented by strings of operators as

$$\hat{a}_p = \frac{1}{2}\left(\hat{X}_p + i\hat{Y}_p\right)\hat{Z}_{p-1}\ldots\hat{Z}_0, \tag{1.42}$$

and,

$$\hat{a}_p^\dagger = \frac{1}{2}\left(\hat{X}_p - i\hat{Y}_p\right)\hat{Z}_{p-1}\ldots\hat{Z}_0, \tag{1.43}$$

where $\hat{X}_p$, $\hat{Y}_p$, and $\hat{Z}_p$ are the Pauli operators (acting on the $p$th qubit) discussed in the previous subsections. A convenient feature of the Jordan-Wigner encoding is that, for an $m$ spin-orbital system with determinants given in the occupation number representation [Sec. 1.2.3] $|\Phi_I\rangle = |\mathbf{n}\rangle = |n_o\ldots n_m\rangle$, the determinants map directly to $m$-qubit quantum basis states $|\mathbf{q}\rangle = |q_o\ldots q_m\rangle$. Conceptually, one can then think of the $(\hat{X}_p + i\hat{Y}_p)$ term as an operator that changes the occupation of spin-orbital $\phi_p$ (now represented by a single-qubit state 0 or 1), and the product $\hat{Z}_{p-1}\ldots\hat{Z}_0$ as an operator that keeps track of the fermionic sign changes. The $\hat{Z}$ product term also has two significant consequences: (i) it breaks the locality of the fermionic operation on only spin-orbital $p$, and (ii) it implies that the number of elementary gates needed to implement a single fermionic operation for a system

of $m$ spin orbitals scales (at worst) as $\mathcal{O}(m)$. As a result, many algorithms that utilize the Jordan-Wigner transformation have an additional factor of $m$ in their scaling.

Developing alternative fermionic encodings that reduce quantum computational overhead is very much an active area of research. The most promising alternatives include the so-called parity encoding,[133] Bravyi-Kitaev[134] (BK) encoding (as well as several of its more-recent variants),[135–137] and other techniques which employ auxiliary qubits.[138,139] In brief, the BK family of encodings attempts to represent information of both the occupation and parity locally, resulting in an elementary gate scaling of $\mathcal{O}(\log(m))$.

### 1.4.5 Operators in the qubit basis

With the simple expressions given by Eqs. (1.42) and (1.43) (or any of the alternative encodings), one can represent a large variety of states on a quantum device built from second quantized operators. Here we will clarify some of the notation often used in the quantum simulation literature as it will be used throughout the rest of this dissertation.

Firstly, it is important to note that the the second quantized Hamiltonian [Eq. (1.44)] can be written as a sum of products $\hat{P}_\ell = \prod_k^{n_\ell} \hat{\sigma}_k^{(\ell)}$ of the Pauli operators ($\hat{X}$, $\hat{Y}$, or $\hat{Z}$). The so-called "qubit" Hamiltonian is then given by

$$\hat{H} = \sum_\ell^{N_\ell} \theta_\ell \hat{P}_\ell, \tag{1.44}$$

where $\theta_\ell$ is a one or two-electron integral (multiplied by a fraction), and $N_\ell$ is the number of terms (scaling as $\mathcal{O}(m^4)$). As will be described in future sections, other operators such as the coupled cluster $\hat{T}$ operator[140] may be expressed in a very similar fashion.

Importantly, it is very common in quantum algorithms to consider the application of quantum circuits that represent terms of the form

$$e^{i\theta_\ell \hat{P}_\ell} = \left(\prod_k^{n_\ell} \hat{V}_k^{(\ell)}\right)^\dagger \left(\prod_k^{n_\ell - 1} \text{c-}\hat{X}_{k,k+1}^{(\ell)}\right)^\dagger \hat{R}_z(2\theta_\ell) \left(\prod_k^{n_\ell - 1} \text{c-}\hat{X}_{k,k+1}^{(\ell)}\right) \left(\prod_k^{n_\ell} \hat{V}_k^{(\ell)}\right), \tag{1.45}$$

where $n_\ell$ is the number of qubits the term $\hat{P}_\ell$ acts on, and where we use similar notation

to that used in Eq. (1.41). In brief, the three components of the circuit–the $\hat{V}_k^{(\ell)}$ terms, the CNOT gates, and the rotation gate–are respectively rationalized by: (i) the need to transform any $\hat{X}$ and $\hat{Y}$ Pauli's to the computational basis, (ii) the need to keep track of the parity from multiple $\hat{Z}$ actions, and (iii) the need to rotate by a parametric amount. A circuit for the exponential given in Eq. (1.45) is shown in Fig. 1.4.

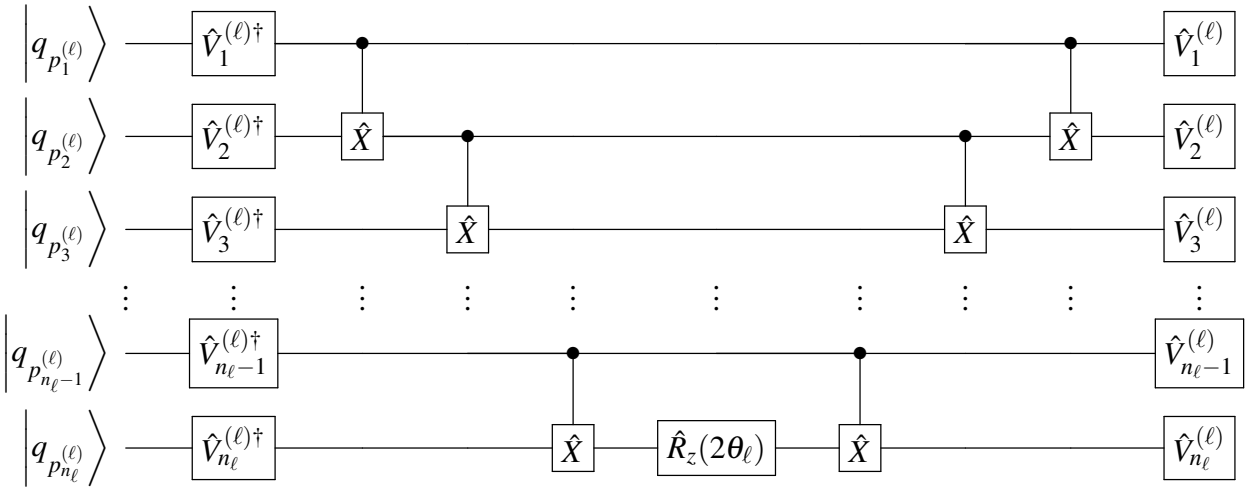


Figure 1.4: Circuit diagram for a unitary of the form $e^{i\theta_\ell \hat{P}_\ell}$, commonly used in many quantum simulation algorithms.

## 1.5 Quantum algorithms for electronic structure

As discussed in Sec. 1.2, the primary challenge of the electronic structure problem is to determine the eigenvalues and properties (usually) of the low-lying states of a quantum system. In this section we present an overview of the two primary classes of quantum algorithms amenable to solving the electronic structure problem: (i) those based on Hamiltonian dynamics, and (ii) those based on variational minimization. While both classes of algorithm will play a central role in the present and future of quantum simulation, it is important to note that today's quantum computers, often referred to as noisy intermediate-scale quantum[141] (NISQ) devices, are in their infancy and are largely relegated to the latter category. Additionally, because strong correlation effects are likewise an important aspect

of this dissertation, particular focus will be given to quantum algorithms amenable to thier treatment.

### 1.5.1 Algorithms based on Hamiltonian dynamics

The first class of algorithms we will discuss are those which rely, at least as a critical subroutine, on application of the time evolution operator $e^{-it\hat{H}}$ for a Hamiltonian $\hat{H}$, noting that this operation has exponential complexity on a classical device. This operation acts as the critical subroutine in the majority of state-of-the-art quantum algorithms including quantum phase estimation,[142,143] quantum Krylov diagonalization,[144–147] and quantum imaginary time evolution[148,149] (in an approximate way).

Due to the central importance of efficient Hamiltonian dynamics to quantum phase estimation, the past two decades have seen great improvements reducing the circuit depths required for the application of the time evolution operator. The earliest and most common strategy for writing the time evolution operator as a quantum circuit is to approximate the exponential sum as a product formula.[150] The Trotter-Suzuki decomposition[151,152] of the operator (with $r$ Trotter steps) has become a mainstay in this regard, and is given by

$$e^{-it\hat{H}} = e^{-it\sum_\ell \theta_\ell \hat{P}_\ell} \approx \left( \prod_\ell e^{\frac{-it\theta_\ell \hat{P}_\ell}{r}} \right)^r + \mathscr{O}\left(\frac{t^2}{r}\right), \tag{1.46}$$

noting the use of the Hamiltonian written in terms its Pauli operator form [Eq. (1.44)]. The circuit for the so-called Trotter operator product can be obtained via Eq. (1.45). It is obvious from Eq. (1.46) that the accuracy of the Trotter approximation is controlled by the variable $r$, which is commonly referred to as the Trotter number, or the number of Trotter steps.

There are then two components which contribute to the total circuit-depth scaling in Trotter based approximations: primitive depth and repetition-depth. These come respectively from (i) the number of terms in the two-body Hamiltonian and, (ii) the required number $(r)$ of repeated time-evolutions necessary to keep the so-called Trotter error at

fixed precision. The need to preserve the fermionic anti-commutation relations in a qubit representation [as discussed in Sec. 1.4.4] adds an additional scaling factor of $\mathcal{O}(m)$ using the Jordan-Wigner transformation[132] or $\mathcal{O}(\log(m))$ using the Bravyi-Kitaev transformation[134] generally be added to the primitive depth. The primitive depth unitary is then given by the most approximate case where $r = 1$. Here we show the first-order Trotter approximation for simplicity, but the second-order approximation is used more commonly and is generally agreed to offer the best trade off between depth and error mitigation for small time steps.

In recent years, attempts to reduce the scaling of the primitive depth circuits have included exploitation of local orbital structure,[153] leverage of low-rank[154] or sparse[155,156] representations of the Hamiltonian, optimally reordering the Hamiltonian terms,[157] and utilization of plane-wave[158] or discontinuous Galerkin[159] basis sets. On the front of reducing the repetition depth, less progress has been made, and is largely relegated to analysis demonstrating tighter bounds, or arguing based on empirical results that current bounds are a significant overestimation.[160] Table 1.2 gives an overview of some of the most significant advances in Trotterized time evolution approaches.

Table 1.2: A variety of recent quantum algorithms that rely on Trotterization. Algorithms are reported with primitive ($d_o$), repetition ($r$), and total circuit depth scaling with number of single-particle states (spin-orbitals) $m$ and number of particles $n$. The notation $\mathcal{O}$ denotes a rigorous upper bound, $\Theta$ denotes an upper bound specific to the algorithmic implementation (restricted to operators of a particular rank), and $\Omega$ represents a lower bound. A tilde over a bound [$\tilde{\mathcal{O}}$] indicates suppression of poly-logarithmic factors, and the approximate symbol inside a bound [$\mathcal{O}(\approx)$] indicates that the scaling was obtained only empirically.

| Reference | Representation | Algorithm | Primitive depth $d_o$ | Repetitions $r$ | Total |
|---|---|---|---|---|---|
| Aspuru-Guzik *et al.*[120] | JW Gaussian | Trotter QPE | $\mathcal{O}$(poly(m)) | $\mathcal{O}$(poly($m$)) | $\mathcal{O}$(poly(m)) |
| Kassal *et al.*[161] | Real space | Trotter QPE | $\mathcal{O}$(poly(m)) | $\mathcal{O}$(poly(m)) | $\mathcal{O}$(poly(m)) |
| Whitfield *et al.*[162] | JW Gaussian | Trotter QPE | $\Theta(m^5)$ | $\mathcal{O}$(poly(m)) | $\mathcal{O}$(poly(m)) |
| Seeley *et al.*[133] | BK Gaussian | Trotter QPE | $\tilde{\Theta}(m^4)$ | $\mathcal{O}$(poly(m)) | $\mathcal{O}$(poly(m)) |
| Wecker *et al.*[163] | JW Gaussian | Trotter QPE | $\Theta(m^5)$ | $\mathcal{O}(m^5)$ | $\mathcal{O}(m^{10})$ |
| Hastings *et al.*[164] | JW Gaussian | Trotter QPE | $\Theta(m^4)$ | $\mathcal{O}(m^4)$ | $\mathcal{O}(m^8)$ |
| Poulin *et al.*[165] | JW Gaussian | TrotterQPE | $\Theta(m^4)$ | $\mathcal{O}(\approx m^2)$ | $\mathcal{O}(\approx m^6)$ |
| McClean *et al.*[153] | BK Gaussian | Trotter QPE | $\tilde{\Theta}(m^2)$ | $\mathcal{O}(m^4)$ | $\tilde{\mathcal{O}}(m^6)$ |
| Babbush *et al.*[160] | JW Gaussian | Trotter QPE | $\Theta(m^4)$ | $\mathcal{O}(\approx m)$ | $\mathcal{O}(\approx m^5)$ |
| Babbush *et al.*[158] | JW Plane wave | Trotter QPE | $\Theta(m)$ | $\mathcal{O}(n^{1.83}m^{0.67})$ | $\mathcal{O}(n^{1.83}m^{1.67})$ |

Advancements for reduced scaling have also been achieved by considering Taylor se-

ries expansions of the time evolution operator,[166,167] or via a strategy know as qubitization,[168–170] at the cost of increasing the number of ancilla qubits required for the linear combination of unitiaries[171] subroutine. Although these non-product-formula strategies are not considered heavily in this dissertation, it should be noted that they do represent the current state-of-the-art in terms of time complexity for Hamiltonian time evolution. Of particular note is the very recent work of Lee *et. al.*,[172] who have combined the techniques of tensor hyper-contraction[173] with qubitizaiton, allowing for an (estimated) simulation time of large transition-metal complexes on the order of days.

*Quantum phase estimation*

In the late 1990's, Abrams and Lloyd[142,143] used Kitaev's quantum phase estimation (QPE) algorithm[174] in conjunction with Hamiltonian time evolution to demonstrate the first polynomially scaling algorithm for eigenvalue determination. In the quantum simulation literature, the combined approach is (somewhat confusingly) also referred to as quantum phase estimation, although Kitaev's article describes a general approach for estimating eigenvalues as global phases.

The quantum phase estimation algorithm can be separated into three distinct subroutines: (i) preparation of the trial state, (ii) controlled time evolution of the Hamiltonian, and (iii) application of the inverse quantum Fourier transform.[175,176] Figure 1.5 shows a schematic of the QPE algorithm where the top wire represents the main register and the three $|0\rangle$ states represent ancillary (ancialla) qubits. QPE has been realized experimentally and is largely believed to be the algorithm which could be used to demonstrate quantum supremacy for simulation of quantum many-body systems.[177] Preparation of the trial state $|\Phi\rangle$ can be accomplished via adiabatic techniques,[178,179] or variational methods,[180,181] such that some preparation unitary $\hat{U}_{\text{prep}}$ acts on an unentangled state $|\bar{0}\rangle$ to produce $|\Phi\rangle = \hat{U}_{\text{prep}}|\bar{0}\rangle$. The primary purpose of the state preparation step is to find $|\Phi\rangle$ such that its overlap with a true eigenstate $|\Psi_j\rangle$ is close to unity, i.e. $|\langle\Phi|\Psi_j\rangle|^2 \approx 1$. If, for example, the trial state is a good approximation to the ground state $|\Psi_0\rangle$, one can consider

it written as a linear expansion of eigenstates $|\Phi\rangle = \sum_j C_j |\Psi_j\rangle$ with $|C_0|^2 \approx 1$.

While efficient preparation of the trial states is an ongoing area of research,[182,183] the most costly subroutine of QPE is by far the (controlled) Hamiltonian time evolution. Time evolving the the trial state gives

$$e^{-it\hat{H}}|\Phi\rangle = |\Phi(t)\rangle = e^{-it\hat{H}}\left(\sum_j C_j |\Psi_j\rangle\right) = \sum_i C_j e^{-itE_j}|\Psi_j\rangle. \tag{1.47}$$

In the case where the trial state is an exact eigenstate, information about the eigenvalue $E_j$ is then encoded in the global phase, the binary representation (within modulo $2\pi$) can then be read out using the inverse quantum Fourier transform. In the case that the trial state is not an exact eigenstate, the QPE procedure will result in the binary readout of $E_j$ with a success probability proportional to the expansion coefficient $C_j$.

*Quantum Imaginary time evolution*

An alternative algorithm to QPE that likewise utilizes Hamiltonian time evolution is the quantum imaginary time evolution (QITE) algorithm.[148,149] The quantum imaginary time evolution algorithm is based on the principle that the ground state can be found by evolving a trial state $|\Phi\rangle$ with the imaginary time evolution operator $e^{-\beta\hat{H}}$ in the infinite time-step limit, such that a factor of $1/\sqrt{c(\beta)} = 1/\sqrt{\langle\Phi_0|e^{-2\beta\hat{H}}|\Phi\rangle}$ normalizes the evolved state. The imaginary time evolution operator is non-unitary, making it impractical for implemen-

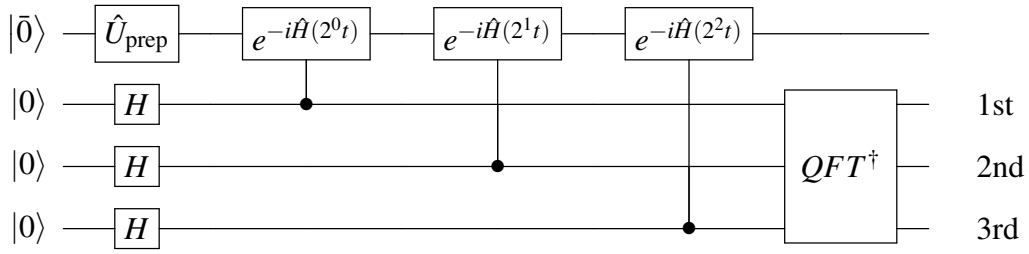


Figure 1.5: A schematic of the QPE algorithm using three ancilla qubits, corresponding to three binary digits of eigenvalue readout. The ancialla qubits are first initialized to a superposition with a Hadamard gate. After the inverse quantum Fourier transform, the ancialla register readout gives the binary decimal representation of the phase $\varphi_j$, such that the energy eigenvalue is computed by $E_j = -(2\pi/t)\varphi_j = -(2\pi/t)0.z_1z_2z_3...$, were $z_i$ is the measured state (0 or 1) of the $i$th ancilla qubit.

tation on quantum computers. However, one may approximate the action of the imaginary time evolution operator with time step $\beta$ using a unitary operation of the form

$$c(\beta)^{-1/2} e^{-\beta \hat{H}} |\Phi\rangle \approx |\psi(\beta)\rangle \equiv e^{-i\beta \hat{A}} |\Phi\rangle , \tag{1.48}$$

where $\hat{A}$ is Hermitian. Approximating both sides to first order and left multiplying by $\hat{A}^\dagger$ and $\langle\Phi|$, respectively, gives

$$c(\beta)^{-1/2} \langle\Phi| \hat{A}^\dagger \hat{H} |\Phi\rangle \approx -i \langle\Phi| \hat{A}^\dagger \hat{A} |\Phi\rangle , \tag{1.49}$$

the principal equation of QITE. The Hermitian operator $\hat{A}$ can be written as a linear expansion of Pauli operator products $\hat{\rho}_\mu = \prod_l \hat{\sigma}_{\mu_l}^{(l)}$ such that $\hat{A} = \sum_{\mu \in \mathscr{P}} \alpha_\mu \hat{\rho}_\mu$. Here, $\mathscr{P}$ is a subset with dimension $M$ of all possible $4^{N_{\text{qb}}}$ Pauli operator products $\mathscr{Q}$, $\mu \equiv (\mu_1, \mu_2, .., \mu_{N_{\text{qb}}})$ is a multi-index describing a unique Pauli operator product, and $\mu_l \in \{I, X, Y, Z\}$. Inserting the above from of $\hat{A}$ into Eq. (5.29) gives

$$c(\beta)^{-1/2} \langle\Phi| \sum_{\mu \in \mathscr{P}} \alpha_\mu \hat{\rho}_\mu^\dagger \hat{H} |\Phi\rangle \approx -i \langle\Phi| \sum_{\mu,\nu \in \mathscr{P}} \alpha_\mu \alpha_\nu \hat{\rho}_\mu^\dagger \hat{\rho}_\nu |\Phi\rangle , \tag{1.50}$$

from which one seeks to solve the $M$ dimensional linear system $\mathbf{S}\boldsymbol{\alpha} = \mathbf{b}$. The elements of $\mathbf{S}$, and $\mathbf{b}$, as well as the value of $c(\beta)$ can be determined via measurement of symmetric expectation values such that

$$S_{\mu\nu} = \langle\Phi| \hat{\rho}_\mu^\dagger \hat{\rho}_\nu |\Phi\rangle , \tag{1.51}$$

$$b_\mu = \frac{-i}{\sqrt{c(\beta)}} \langle\Phi| \hat{\rho}_\mu^\dagger \hat{H} |\Phi\rangle , \tag{1.52}$$

and,

$$c(\beta) \approx 1 - 2\beta \langle\Phi| \hat{H} |\Phi\rangle . \tag{1.53}$$

The QITE formalism has also recently been extended[184] to non-local Hamiltonians using a fermionic basis.

Another important extension to QITE, also discussed in the original article,[148] is the so-called Lanczos variant, or quantum Lanczos (QL). In QL, one wants utilize

the QITE subroutine to determine the matrix elements $S_{mn} = \langle\psi(\beta_m)|\psi(\beta_n)\rangle$ and $H_{mn} = \langle\psi(\beta_m)|\hat{H}|\psi(\beta_n)\rangle$ of a generalized eigenvalue problem $\mathbf{Hc} = \mathbf{Sc}E$, where $\beta_m = m\Delta\beta$ are different integer $m$ durations of imaginary time evolution. A convenient feature of QL is that the matrix elements can be (approximately) evaluated in terms of the normalization coefficients $c$, such that

$$S_{mn} \approx \langle\Phi| e^{-m\Delta\beta\hat{A}} e^{-n\Delta\beta\hat{A}} |\Phi\rangle = \frac{c(\beta_m)c(\beta_n)}{c^2(\beta_k)} \tag{1.54}$$

and,

$$H_{mn} \approx \langle\Phi| e^{-m\Delta\beta\hat{A}} \hat{H} e^{-n\Delta\beta\hat{A}} |\Phi\rangle = \frac{c(\beta_m)c(\beta_n)}{c^2(\beta_k)} \langle\psi(\beta_k)|\hat{H}|\psi(\beta_k)\rangle \tag{1.55}$$

where $2k = m+n$. This is significant because it implies that all of the quantities needed for QL can be determined *without* ancilla qubits, making its implementation on NISQ devices a possibility.

*Quantum Krylov diagonalization*

Quantum Krylov diagonalization (QKD) techniques are another recently developed family of algorithms that relies on Hamiltonian time evolution.[144–147] Chapter 3 in fact introduces the first (concurrently with Parrish and McMahon[144]) example of this type of method, which is largely inspired by the quantum Lanczos[148] method described above, but where real time evolution is used instead of imaginary. In QKD, a general state is written as a linear combination of the basis $\{\psi_n\}$ generated from Hamiltonian evolutions of time $t_n = n\Delta t$ as

$$|\Psi\rangle = \sum_n c_n |\psi_n\rangle = \sum_{n=0}^{s} c_n e^{-it_n\hat{H}} |\Phi\rangle . \tag{1.56}$$

Variational minimization of the energy for state $\Psi$ leads to a generalized eigenvalue problem $\mathbf{Hc} = \mathbf{Sc}E$, where the elements of the overlap matrix ($\mathbf{S}$) and Hamiltonian ($\mathbf{H}$) are given by $S_{mn} = \langle\psi_m|\psi_n\rangle$ and $H_{mn} = \langle\psi_m|\hat{H}|\psi_n\rangle$, respectively. The quantum circuits used to evaluate $\mathbf{S}$ and $\mathbf{H}$ are a variant of the now-commonplace Hadamard Test.[185] The basis of states $\mathscr{K}_s(\psi_n)$ generated by real-time evolution spans a classical Krylov space. Consider a linear combination of the elements of $\mathscr{K}_s(\psi_n)$ and expand the exponential into a Taylor

series keeping terms up to order $(\Delta t)^s$

$$\begin{aligned} |\Psi\rangle &= \sum_{n=0}^{s} c_n e^{-in\Delta t\hat{H}} |\Phi\rangle \\ &= \sum_{k=0}^{s} \left( \sum_{n=0}^{s} \frac{(-in\Delta t)^k}{k!} c_n \right) \hat{H}^k |\Phi\rangle + \mathscr{O}(\Delta t^{s+1}) \\ &= \sum_{k=0}^{s} \left( \sum_{n=0}^{s} M_{kn} c_n \right) \hat{H}^k |\Phi\rangle + \mathscr{O}(\Delta t^{s+1}) \end{aligned} \tag{1.57}$$

The square matrix $\mathbf{M}$ is invertible, and therefore, the coefficients $c_n$ may be chosen to represent any combination of the classical Krylov basis $\{\hat{H}^k |\Phi\rangle\}$ with $k = 0, \ldots, s$, up to higher-order terms. This observation has resulted in very recent work farther expanding on the formalism.[186] It has also recently been pointed out in subsequent work by Klymko *et al.*[147] that a linear combination of time-evolved states [Eq. (1.56)] can cancel the phases of unwanted eigenstates, implying that the method should in principle work even beyond the short time-step limit.

### 1.5.2 Quantum variational optimization algorithms

Largely due to the prospect of using NISQ devices in a meaningful way[121,123,124,126,127] (to perform simulation of non-trivial systems), the past decade has seen the emergence of low-depth variational quantum algorithms[187] (VQA). The most prolific subclass of VQAs is the variational quantum eigensolver (VQE),[180,181] which is primarily used to simulate ground states of quantum systems, but has been extended to treat excited-states as well.[188–191] The VQE approach is considered a hybrid quantum-classical algorithm, and is characterized by an iterative three phase procedure: (i) preparation of a trial state using a parameterized unitary ansatz, (ii) measurement of the expectation value of the Hamiltonian (and optionally the energy gradients), and (iii) updating of the parameters using a classical optimization algorithm. Below we will describe each of these steps in detail as well as advances in the literature.

In the first phase of VQE, one considers a unitary circuit $\hat{U}(\boldsymbol{\theta})$ characterized by the vector of classical parameters $\boldsymbol{\theta}$. This unitary (often referred to as an ansatz) is used to

rotate an easily prepared reference state $|\Phi_0\rangle$ (such as the Hartree-Fock state) into the entangled VQE state

$$|\Psi_{\mathrm{VQE}}\rangle = \hat{U}(\boldsymbol{\theta})\,|\Phi_0\rangle\,. \tag{1.58}$$

The specific form used for the ansatz is, on its own, the subject of a large body of work. Notable examples include ansatz based on unitary coupled cluster (UCC) theory theory[192–196] (discussed in more detail in Sec. 1.5.2), but more recently have included so-called hardware-efficient[121] and qubit-space[197] UCC variants as well. The so-called variational Hamiltonian ansatz,[198–200] which attempts to approximate adiabatic state relaxation to the ground state, and ansatz inspired by tensor networks[201–203] have also recently been considered.

The second step of VQE is the determination of the Hamiltonian expectation value given by

$$E(\boldsymbol{\theta}) = \langle\Phi|\,\hat{U}^{\dagger}(\boldsymbol{\theta})\hat{H}\hat{U}(\boldsymbol{\theta})\,|\Phi\rangle\,. \tag{1.59}$$

This is usually accomplished by the process of operator averaging[181] [see Sec. 1.4.3], for which the bound on number of measurements $M$ scales inherently as $\mathscr{O}(\Gamma/\varepsilon^2)$, where $\Gamma$ is the norm of the Hamiltonian and and $\varepsilon$ is the desired precision in the expectation value. As such a large body of work has been concerned with improving measurement efficiency in VQE, either by grouping commuting Pauli operators,[121,181,204,205] or employing alternative bases.[158,159] One may also wish to evaluate the energy gradients

$$g_\mu = \frac{\partial E_{\mathrm{VQE}}}{\partial \theta_\mu}, \tag{1.60}$$

with respect to a specific parameter $\theta_\mu$. Evaluation of the gradients on a quantum device can be accomplished with[206] or without[207,208] ancilla qubits, but is still rather costly in either case. This observation in part has motivated our development of the projective quantum eigensolver introduced in Chapter 4, which does not require determination of the gradients to optimize the wave function.

The final step in VQE is to update the parameter vector by using a classical (usu-

ally non-linear) optimization algorithm. Several optimization strategies have found popularity in preliminary studies including the Broyden–Fletcher–Goldfarb–Shannon algorithm,[209–212] or its limited-memory variant.[213] However, due to the many sources of noise present during the first two steps of VQE, it has also become favorable to employ stochastic gradient decent methods[214,215] or gradient free approaches such as the simultaneous perturbation stochastic approximation algorithm.[216]

Although the primary applications of VQAs has been the simulation of physical systems, it is important to note that their application encompass more general optimization problems.[217] Notable examples include application of quantum approximate optimization algorithm[218] to the combinatorial constraint satisfaction,[219] and max-cut[220] problems, but many additional applications for mathematical problems such as linear systems,[221,222] integer factorization[223] and others have also been proposed.

*VQE ansatz inspired by UCC*

The original,[180] and still most widely used ansatz in VQE is based on the cluster operator[140] $\hat{T}$ defined as

$$\hat{T} = \sum_{\mu} t_{\mu} \hat{\tau}_{\mu} = \sum_{ij\cdots \in \mathrm{occ}} \sum_{ab\cdots \in \mathrm{vir}} t_{ij\ldots}^{ab\cdots} \hat{a}_a^\dagger \hat{a}_b^\dagger \ldots \hat{a}_j \hat{a}_i, \tag{1.61}$$

assuming the reference state is an easily-prepared single determinant $|\Phi_0\rangle = |\phi_1 \phi_2 \cdots\rangle$ (such as the Hartree-Fock determinant) specified by occupied spin orbitals $\{\phi_i\}$ and unoccupied (virtual) spin orbitals $\{\phi_a\}$. Note that the operator $\hat{\tau}_{\mu} \equiv \hat{\tau}_{ij\ldots}^{ab\cdots} = \hat{a}_a^\dagger \hat{a}_b^\dagger \cdots \hat{a}_j \hat{a}_i$ is a particle-hole excitation operator who's action turns the reference determinant $|\Phi_0\rangle$ into the excited determinant $\left|\Phi_{\mu}\right\rangle$. In traditional coupled cluster theory,[31,32] the exponential of the cluster operator $e^{\hat{T}}$ is employed. However, it is the *unitary* variant of coupled cluster theory,[192–196] that is of interest in the context of VQE, because the operator

$$\hat{U}_{\mathrm{UCC}}(\mathbf{t}) = e^{\hat{T} - \hat{T}^\dagger} = e^{\sum_{\mu} t_{\mu} \hat{\kappa}_{\mu}}, \tag{1.62}$$

where the operators $\hat{\kappa}_\mu = \hat{\tau}_\mu - \hat{\tau}_\mu^\dagger$ are anti-Hermitian, is implementable on a quantum device.

In principle it is possible to construct a circuit that exactly implements the action of the UCC operator defined in Eq. (1.62), but in practice it is common to use a unitary with a simpler, and shallower, circuit. This is frequently accomplished using a factorized (or disentangled) form of the UCC ansatz (dUCC)

$$\hat{U}_{\mathrm{dUCC}}(\mathbf{t}) = \prod_\mu e^{t_\mu \hat{\kappa}_\mu}. \tag{1.63}$$

We note that the disentangled treatment is equivalent to utilizing a single-step first order Trotter approximation [see Eq. (1.46)] of $\hat{U}_{\mathrm{UCC}}$, but that recent analysis[224] suggests that $\hat{U}_{\mathrm{dUCC}}(\mathbf{t})$ should be viewed as an entirely separate ansatz rather than simply a Trotter approximation to $\hat{U}_{\mathrm{UCC}}$.

In recent years, the UCC formalism (as used with VQE) has been investigated with generalized operators,[225] strategies for optimizing the compilation of fermionic operators,[154,226,227] and the usage of exclusively qubit operators (deemed qubit CC [QCC]) which omit antisymmetry constraints.[197]

*Adaptive VQE ansatz*

A subclass of VQE algorithms of particular importance to this dissertation is that of *adaptive* ansatz algorithms, because of their suitability for the treatment of strong correlation. Generally speaking, these approaches incorporate an additional iterative layer of "macro-iterations" in which the VQE unitary [Eq. (1.58)] is appended at each iteration $k$. Adaptive procedures are often capable of constructing a compact unitaries (both in terms of circuit-depth and number of classical parameters) that can systematically approach a rotation of $|\Phi_0\rangle$ into an exact eigenstate.

The first and most prominent of these adaptive approaches is the *adaptive derivative assembled pseudo-trotterized* (ADAPT)-VQE.[228] In ADAPT-VQE, the unitary ansatz at

macro-iteration $k$ is defined as

$$\hat{U}^{(k)}_{\text{ADAPT}}(\mathbf{t}) = \prod_{\nu}^{k} e^{t_\nu^{(k)} \hat{\kappa}_\nu^{(k)}}, \tag{1.64}$$

where $\nu$ is likewise a compound index corresponding to unique operators $\hat{\kappa}_\nu$ in a pool $\mathscr{P}$ of generalized single and double excitation/de-excitation operators (although as the authors discuss it is possible to construct $\mathscr{P}$ in a variety of ways). Note that the parameters $t_\nu^{(k)}$ are re-optimized at each macro-iteration. New operators are determined from the pool by computing the energy gradient

$$g_\nu = \langle \Psi_{\text{VQE}} | \left[ \hat{H}, \hat{\kappa}_\nu \right] | \Psi_{\text{VQE}} \rangle, \tag{1.65}$$

with respect to $t_\nu$ of each operator in $\mathscr{P}$ and selecting the operator with the largest gradient magnitude to place at the end of the ansatz in the next iteration. The ADAPT-VQE algorithm has been shown, as we will discuss in more detail in Chapter 4, to be capable of producing accurate trial states with low-depth circuits. The success of ADAPT has additionally inspired a variety of subsequent algorithms such as the iterative qubit CC (iQCC),[229] its own qubit operator variant.[230]

## 1.6 Prospectus

In Chapter 2 we provide a detailed analysis of the performance of various classical electronic structure methods in the regime of strong electronic correlation using a benchmark set of multi-dimensional hydrogen lattices. Each of the employed classical algorithms is able to systematically approach the FCI solution using an increasing number of variational parameters. The study motivates the need for quantum (or hybrid quantum-classical) algorithms which are able to treat strong correlation using a tractable number of classical parameters. In Chapter 3 we introduce our novel quantum Krylov algorithm, which solves the Schrödinger equation in a non-orthogonal many-body basis generated by integer time evolutions of a reference state. We apply this method to a group of small molecular sys-

tems in the regime of strong correlation and compare it to ADAPT-VQE.[228] In Chapter 3 we demonstrate the usage of a novel projective quantum eigensolver (PQE) as an alternative to VQE for optimizing disentangled unitary coupled cluster wave functions. We compare our PQE method to VQE optimized with analytical gradients and the BFGS optimization algorithm. We also introduce a selected variant of PQE and test its performance relative to classical algorithms using the same strongly correlated benchmark models introduced in Chapter 2. In Chapter 5, we discuss the quantum computer simulator and algorithms library QFORTE, which we developed to facilitate the work presented in this dissertation and beyond. Finally, in Chapter 6 we discuss the conclusions of our studies and briefly consider directions of future work.

# Bibliography

[1] P. A. M. Dirac. "Quantum mechanics of many-electron systems." *Proceedings of the Royal Society of London. Series A, Containing Papers of a Mathematical and Physical Character* **123**, 714 (1929).

[2] H. F. Schaefer. "Methylene: A paradigm for computational quantum chemistry." *Science* **231**, 1100 (1986).

[3] H. Kroto. "The first predictions in the Buckminsterfullerene crystal ball." *Fullerenes, Nanotubes, and Carbon Nanostructures* **2**, 333 (1994).

[4] E. Schrödinger. "Quantisierung als eigenwertproblem." *Annalen der physik* **385**, 437 (1926).

[5] G. A. Quantum *et al.*. "Hartree-Fock on a superconducting qubit quantum computer." *Science* **369**, 1084 (2020).

[6] R. P. Feynman, R. B. Leighton, and M. Sands. *The Feynman lectures on physics, Vol. I: The new millennium edition: mainly mechanics, radiation, and heat*, volume 1. Basic books (2011).

[7] R. P. Feynman. "Simulating physics with computers." *Int. J. Theor. Phys* **21** (1982).

[8] B. Sutcliffe. "Fundamentals of computational quantum chemistry." In "Computational Techniques in Quantum Chemistry and Molecular Physics," 1–105. Springer (1975).

[9] W. Pauli. "Über den Zusammenhang des Abschlusses der Elektronengruppen im Atom mit der Komplexstruktur der Spektren." *Zeitschrift für Physik* **31**, 765 (1925).

[10] I. Kaplan. "The Pauli exclusion principle. Can it be proved?" *Foundations of Physics* **43**, 1233 (2013).

[11] G. E. Uhlenbeck and S. Goudsmit. "Ersetzung der Hypothese vom unmechanischen Zwang durch eine Forderung bezüglich des inneren Verhaltens jedes einzelnen Elektrons." *Naturwissenschaften* **13**, 953 (1925).

[12] W. Heisenberg. "Mehrkörperproblem und Resonanz in der Quantenmechanik." *Zeitschrift für Physik* **38**, 411 (1926).

[13] D. R. Hartree. "The wave mechanics of an atom with a non-Coulomb central field. Part I. Theory and methods." (1928).

[14] D. R. Hartree. "The wave mechanics of an atom with a non-coulomb central field. Part II. Some results and discussion." In "Mathematical Proceedings of the Cambridge Philosophical Society," volume 24, 111–132. Cambridge University Press (1928).

[15] J. C. Slater. "The theory of complex spectra." *Physical Review* **34**, 1293 (1929).

[16] V. Fock. "Näherungsmethode zur Lösung des quantenmechanischen Mehrkörperproblems." *Zeitschrift für Physik* **61**, 126 (1930).

[17] C. Roothaan. "Self-consistent field theory for open shells of electronic systems." *Rev. Mod. Phys.* **32**, 179 (1960).

[18] A. Szabo and N. S. Ostlund. *Modern Quantum Chemistry: Introduction to Advanced Electronic Structure Theory*. Courier Corporation (2012).

[19] R. J. Bartlett and J. F. Stanton. "Reviews in Computational Chemistry: Applications of Post-Hartree—Fock Methods: A Tutorial." 65–169. Wiley Online Library (1994).

[20] C. D. Sherrill and H. F. Schaefer. "The Configuration Interaction Method: Advances in Highly Correlated Approaches." volume 34 of *Advances in Quantum Chemistry*, 143 – 269. Academic Press (1999).

[21] R. Laughlin and D. Pines. "The Theory of Everything." *Proc. Natl. Acad. Sci. U.S.A* **97**, 28 (2000).

[22] N. C. Handy. "Multi-root configuration interaction calculations." *Chem. Phys. Lett.* **74**, 280 (1980).

[23] M. L. Leininger, C. D. Sherrill, W. D. Allen, and H. F. Schaefer. "Systematic study of selected diagonalization methods for configuration interaction matrices." *J. Comp. Chem.* **22**, 1574 (2001).

[24] D. Zuev, E. Vecharynski, C. Yang, N. Orms, and A. I. Krylov. "New algorithms for iterative matrix-free eigensolvers in quantum chemistry." *Journal of computational chemistry* **36**, 273 (2015).

[25] K. D. Vogiatzis, D. Ma, J. Olsen, L. Gagliardi, and W. A. De Jong. "Pushing configuration-interaction to the limit: Towards massively parallel MCSCF calculations." *J. Chem. Phys.* **147**, 184111 (2017).

[26] P.-O. Löwdin. "Correlation Problem in Many-Electron Quantum Mechanics I. Review of Different Approaches and Discussion of Some Current Ideas." *Adv. Chem. Phys.* **2**, 207 (1958).

[27] D. P. Tew, W. Klopper, and T. Helgaker. "Electron correlation: The many-body problem at the heart of chemistry." *J. Comput. Chem.* **28**, 1307 (2007).

[28] D. K. Mok, R. Neumann, and N. C. Handy. "Dynamical and nondynamical correlation." *J. Phys. Chem.* **100**, 6225 (1996).

[29] F. A. Evangelista. "Perspective: Multireference coupled cluster theories of dynamical electron correlation." *The Journal of chemical physics* **149**, 030901 (2018).

[30] C. Møller and M. S. Plesset. "Note on an approximation treatment for many-electron systems." *Physical review* **46**, 618 (1934).

[31] F. Coester and H. Kümmel. "Short-range correlations in nuclear wave functions." *Nuclear Physics* **17**, 477 (1960).

[32] J. Čížek. "On the correlation problem in atomic and molecular systems. Calculation of wavefunction components in Ursell-type expansion using quantum-field theoretical methods." *The Journal of Chemical Physics* **45**, 4256 (1966).

[33] J. B. Anderson. "A random-walk simulation of the Schrödinger equation: H+ 3." *The Journal of Chemical Physics* **63**, 1499 (1975).

[34] M. Cyrot. "The Hubbard hamiltonian." *Physica B+ C* **91**, 141 (1977).

[35] A. V. Sinitskiy, L. Greenman, and D. A. Mazziotti. "Strong correlation in hydrogen chains and lattices using the variational two-electron reduced density matrix method." *J. Chem. Phys.* **133**, 014104 (2010).

[36] M. Motta, D. M. Ceperley, G. K.-L. Chan, J. A. Gomez, E. Gull, S. Guo, C. A. Jiménez-Hoyos, T. N. Lan, J. Li, F. Ma, *et al.*. "Towards the solution of the many-electron problem in real materials: equation of state of the hydrogen chain with state-of-the-art many-body methods." *Phys. Rev. X* **7**, 031059 (2017).

[37] A. Biborski, A. P. Kadzielawa, and J. Spałek. "Metallization of solid molecular hydrogen in two dimensions: Mott-Hubbard-type transition." *Phys. Rev. B* **96**, 085101 (2017).

[38] M. Motta, C. Genovese, F. Ma, Z.-H. Cui, R. Sawaya, G. K.-L. Chan, N. Chepiga, P. Helms, C. Jiménez-Hoyos, A. J. Millis, *et al.*. "Ground-state properties of the hydrogen chain: dimerization, insulator-to-metal transition, and magnetic phases." *Physical Review X* **10**, 031058 (2020).

[39] K. Raghavachari, G. W. Trucks, J. A. Pople, and M. Head-Gordon. "A fifth-order perturbation comparison of electron correlation theories." *Chem. Phys. Lett.* **157**, 479 (1989).

[40] D. Roca-Sanjuán, F. Aquilante, and R. Lindh. "Multiconfiguration second-order perturbation theory approach to strong electron correlation in chemistry and photochemistry." *Wiley Interdiscip. Rev. Comput. Mol. Sci.* **2**, 585 (2012).

[41] J. P. Malrieu, R. Caballol, C. J. Calzado, C. de Graaf, and N. Guihery. "Magnetic interactions in molecules and highly correlated materials: physical content, analytical derivation, and rigorous extraction of magnetic Hamiltonians." *Chem. Rev.* **114**, 429 (2014).

[42] P. A. Lee. "From high temperature superconductivity to quantum spin liquid: progress in strong correlation physics." *Rep. Prog. Phys.* **71**, 012501 (2007).

[43] M. Imada, A. Fujimori, and Y. Tokura. "Metal-insulator transitions." *Rev. Mod. Phys.* **70**, 1039 (1998).

[44] M. B. Salamon and M. Jaime. "The physics of manganites: Structure and transport." *Rev. Mod. Phys.* **73**, 583 (2001).

[45] Y. Tokura. "Critical features of colossal magnetoresistive manganites." *Rep. Prog. Phys.* **69**, 797 (2006).

[46] G. Murthy and R. Shankar. "Hamiltonian theories of the fractional quantum Hall effect." *Rev. Mod. Phys.* **75**, 1101 (2003).

[47] K. Ruedenberg and K. R. Sundberg. "MCSCF studies of chemical reactions: natural reaction orbitals and localized reaction orbitals." In "Quantum Science," 505–515. Springer (1976).

[48] K. Ruedenberg, L. Cheung, and S. Elbert. "MCSCF optimization through combined use of natural orbitals and the Brillouin–Levy–Berthier theorem." *International Journal of Quantum Chemistry* **16**, 1069 (1979).

[49] B. O. Roos. "The complete active space SCF method in a fock-matrix-based super-CI formulation." *International Journal of Quantum Chemistry* **18**, 175 (1980).

[50] M. J. M. Bernal and S. F. Boys. "Electronic Wave Functions. VIII. A Calculation of the Ground States NaFormula, Ne and FFormula." *Philosophical Transactions of the Royal Society A: Mathematical, Physical and Engineering Sciences* **245**, 139 (1952).

[51] B. Huron, J.-P. Malrieu, and P. Rancurel. "Iterative perturbation calculations of ground and excited state energies from multiconfigurational zerothâĂŘorder wavefunctions." *J. Chem. Phys.* **58**, 5745 (1973).

[52] R. J. Buenker and S. D. Peyerimhoff. "Individualized configuration selection in CI calculations with subsequent energy extrapolation." *Theor. Chim. Acta* **35**, 33 (1974). ISSN 1432-2234.

[53] R. J. Buenker and S. D. Peyerimhoff. "Energy extrapolation in CI calculations." *Theor. Chim. Acta* **39**, 217 (1975). ISSN 1432-2234.

[54] S. Evangelisti, J.-P. Daudey, and J.-P. Malrieu. "Convergence of an improved CIPSI algorithm." *Chem. Phys.* **75**, 91 (1983). ISSN 0301-0104.

[55] V. García, O. Castell, R. Caballol, and J.-P. Malrieu. "An iterative difference-dedicated configuration interaction. Proposal and test studies." *Chem. Phys. Lett.* **238**, 222 (1995). ISSN 0009-2614.

[56] F. Neese. "A spectroscopy oriented configuration interaction procedure." *J. Chem. Phys.* **119**, 9428 (2003).

[57] H. Nakatsuji and M. Ehara. "Iterative CI general singles and doubles (ICIGSD) method for calculating the exact wave functions of the ground and excited states of molecules." *J. Chem. Phys.* **122**, 194108 (2005).

[58] M. L. Abrams and C. D. Sherrill. "Important configurations in configuration interaction and coupled-cluster wave functions." *Chem. Phys. Lett.* **412**, 121 (2005). ISSN 0009-2614.

[59] L. Bytautas and K. Ruedenberg. "A priori identification of configurational deadwood." *Chem. Phys.* **356**, 64 (2009). ISSN 0301-0104.

[60] R. Roth. "Importance truncation for large-scale configuration interaction approaches." *Phys. Rev. C* **79**, 064324 (2009).

[61] F. A. Evangelista. "Adaptive multiconfigurational wave functions." **140**, 054109 (2014).

[62] P. J. Knowles. "Compressive sampling in configuration interaction wavefunctions." *Mol. Phys.* **113**, 1655 (2015).

[63] W. Liu and M. R. Hoffmann. "iCI: Iterative CI toward full CI." *J. Chem. Theor. Comput.* **12**, 1169 (2016).

[64] J. B. Schriber and F. A. Evangelista. "Communication: An adaptive configuration interaction approach for strongly correlated electrons with tunable accuracy." *J. Chem. Phys.* **144**, 161106 (2016).

[65] A. A. Holmes, N. M. Tubman, and C. J. Umrigar. "Heat-Bath Configuration Interaction: An Efficient Selected Configuration Interaction Algorithm Inspired by Heat-Bath Sampling." *J. Chem. Theory Comput.* **12**, 3674 (2016).

[66] J. B. Schriber and F. A. Evangelista. "Adaptive Configuration Interaction for Computing Challenging Electronic Excited States with Tunable Accuracy." *J. Chem. Theory Comput.* **13**, 5354 (2017).

[67] J. C. Greer. "Estimating full configuration interaction limits from a Monte Carlo selection of the expansion space." *J. Chem. Phys.* **103**, 1821 (1995).

[68] J. C. Greer. "Monte Carlo Configuration Interaction." *J. Comput. Phys.* **146**, 181 (1998). ISSN 0021-9991.

[69] J. Coe, P. Murphy, and M. Paterson. "Applying Monte Carlo configuration interaction to transition metal dimers: Exploring the balance between static and dynamic correlation." *Chem. Phys. Lett.* **604**, 46 (2014). ISSN 0009-2614.

[70] J. P. Coe and M. J. Paterson. "State-averaged Monte Carlo configuration interaction applied to electronically excited states." *J. Chem. Phys.* **139**, 154103 (2013).

[71] J. P. Coe and M. J. Paterson. "Development of Monte Carlo configuration interaction: Natural orbitals and second-order perturbation theory." *J. Chem. Phys.* **137**, 204108 (2012).

[72] W. Győrffy, R. J. Bartlett, and J. C. Greer. "Monte Carlo configuration interaction predictions for the electronic spectra of Ne, CH2, C2, N2, and H2O compared to full configuration interaction calculations." *J. Chem. Phys.* **129**, 064103 (2008).

[73] S. Sharma, A. A. Holmes, G. Jeanmairet, A. Alavi, and C. J. Umrigar. "Semistochastic Heat-Bath Configuration Interaction Method: Selected Configuration Interaction with Semistochastic Perturbation Theory." *J. Chem. Theory Comput.* **13**, 1595 (2017).

[74] A. A. Holmes, C. J. Umrigar, and S. Sharma. "Excited states using semistochastic heat-bath configuration interaction." *J. Chem. Phys.* **147**, 164111 (2017).

[75] A. D. Chien, A. A. Holmes, M. Otten, C. J. Umrigar, S. Sharma, and P. M. Zimmerman. "Excited States of Methylene, Polyenes, and Ozone from Heat-Bath Configuration Interaction." *J. Phys. Chem. A* **122**, 2714 (2018).

[76] J. Li, M. Otten, A. A. Holmes, S. Sharma, and C. J. Umrigar. "Fast semistochastic heat-bath configuration interaction." *J. Chem. Phys.* **149**, 214110 (2018).

[77] G. H. Booth, A. J. W. Thom, and A. Alavi. "Fermion Monte Carlo without fixed nodes: A game of life, death, and annihilation in Slater determinant space." *J. Chem. Phys.* **131**, 054106 (2009).

[78] D. Cleland, G. H. Booth, and A. Alavi. "Communications: Survival of the fittest: Accelerating convergence in full configuration-interaction quantum Monte Carlo." *J. Chem. Phys.* **132**, 041103 (2010).

[79] G. H. Booth, D. Cleland, A. J. W. Thom, and A. Alavi. "Breaking the carbon dimer: The challenges of multiple bond dissociation with full configuration interaction quantum Monte Carlo methods." *J. Chem. Phys.* **135**, 084104 (2011).

[80] D. Cleland, G. H. Booth, and A. Alavi. "A study of electron affinities using the initiator approach to full configuration interaction quantum Monte Carlo." *J. Chem. Phys.* **134**, 024112 (2011).

[81] D. Cleland, G. H. Booth, C. Overy, and A. Alavi. "Taming the First-Row Diatomics: A Full Configuration Interaction Quantum Monte Carlo Study." *J. Chem. Theory Comput.* **8**, 4138 (2012).

[82] R. E. Thomas, C. Overy, G. H. Booth, and A. Alavi. "Symmetry Breaking and Broken Ergodicity in Full Configuration Interaction Quantum Monte Carlo." *J. Chem. Theory Comput.* **10**, 1915 (2014).

[83] G. H. Booth, S. D. Smart, and A. Alavi. "Linear-scaling and parallelisable algorithms for stochastic quantum chemistry." *Mol. Phys.* **112**, 1855 (2014).

[84] G. Li Manni, S. D. Smart, and A. Alavi. "Combining the complete active space self-consistent field method and the full configuration interaction quantum Monte Carlo within a super-CI framework, with application to challenging metal-porphyrins." *J. Chem. Theory Comput.* **12**, 1245 (2016).

[85] W. Purwanto, S. Zhang, and H. Krakauer. "Excited state calculations using phaseless auxiliary-field quantum Monte Carlo: Potential energy curves of low-lying C2 singlet states." *J. Chem. Phys.* **130**, 094107 (2009).

[86] E. Giner, A. Scemama, and M. Caffarel. "Using perturbatively selected configuration interaction in quantum Monte Carlo calculations." *Can. J. Chem.* **91**, 879 (2013).

[87] F. R. Petruzielo, A. A. Holmes, H. J. Changlani, M. P. Nightingale, and C. J. Umrigar. "Semistochastic projector Monte Carlo method." *Phys. Rev. Lett.* **109**, 230201 (2012).

[88] S. Ten-no. "Stochastic determination of effective Hamiltonian for the full configuration interaction solution of quasi-degenerate electronic states." *J. Chem. Phys.* **138**, 164126 (2013).

[89] N. S. Blunt, A. Alavi, and G. H. Booth. "Krylov-projected quantum Monte Carlo method." *Phys. Rev. Lett.* **115**, 050603 (2015).

[90] G. Li Manni, S. D. Smart, and A. Alavi. "Combining the complete active space self-consistent field method and the full configuration interaction quantum monte carlo within a super-CI framework, with application to challenging metal-porphyrins." *J. Chem. Theor. Comput.* **12**, 1245 (2016).

[91] E. Giner, R. Assaraf, and J. Toulouse. "Quantum Monte Carlo with reoptimised perturbatively selected configuration-interaction wave functions." *Mol. Phys.* **114**, 910 (2016).

[92] F. Colmenero and C. Valdemoro. "Approximating q-order reduced density matrices in terms of the lower-order ones. II. Applications." *Phys. Rev. A* **47**, 979 (1993).

[93] H. Nakatsuji and K. Yasuda. "Direct determination of the quantum-mechanical density matrix using the density equation." *Phys. Rev. Lett.* **76**, 1039 (1996).

[94] D. A. Mazziotti. "Contracted Schrödinger equation: Determining quantum energies and two-particle density matrices without wave functions." *Phys. Rev. A* **57**, 4219 (1998).

[95] D. A. Mazziotti. "Two-electron reduced density matrix as the basic variable in many-electron quantum chemistry and physics." *Chem. Rev.* **112**, 244 (2011).

[96] J. Fosso-Tande, T.-S. Nguyen, G. Gidofalvi, and A. E. DePrince III. "Large-scale variational two-electron reduced-density-matrix-driven complete active space self-consistent field methods." *J. Chem. Theory Comput.* **12**, 2260 (2016).

[97] H.-H. Zhao, Z.-Y. Xie, Q. N. Chen, Z.-C. Wei, J. W. Cai, and T. Xiang. "Renormalization of tensor-network states." *Physical Review B* **81**, 174411 (2010).

[98] G. Evenbly and G. Vidal. "Tensor Network States and Geometry." *J. Stat. Phys.* **145**, 891 (2011). ISSN 1572-9613.

[99] J. Eisert, M. Cramer, and M. Plenio. "Area laws for the entanglement entropy—a review, 2009." *Rev. Mod. Phys* **20**, 30 (2009).

[100] S. Östlund and S. Rommer. "Thermodynamic limit of density matrix renormalization." *Phys. Rev. Lett.* **75**, 3537 (1995).

[101] J. Dukelsky, M. A. Martín-Delgado, T. Nishino, and G. Sierra. "Equivalence of the variational matrix product method and the density matrix renormalization group applied to spin chains." *EPL* **43**, 457 (1998).

[102] U. Schollwöck. "The density-matrix renormalization group in the age of matrix product states." *Ann. Phys. (N. Y.)* **326**, 96 (2011).

[103] S. R. White. "Density matrix formulation for quantum renormalization groups." *Phys. Rev. Lett.* **69**, 2863 (1992).

[104] G. K.-L. Chan and M. Head-Gordon. "Highly correlated calculations with a polynomial cost algorithm: A study of the density matrix renormalization group." *J. Chem. Phys.* **116**, 4462 (2002).

[105] J. Hachmann, W. Cardoen, and G. K.-L. Chan. "Multireference correlation in long molecules with the quadratic scaling density matrix renormalization group." *J. Chem. Phys.* **125**, 144101 (2006).

[106] A. O. Mitrushchenkov, G. Fano, R. Linguerri, and P. Palmieri. "On the importance of orbital localization in QC-DMRG calculations." *Int. J. Quantum Chem.* **112**, 1606 (2012).

[107] S. Wouters, P. A. Limacher, D. Van Neck, and P. W. Ayers. "Longitudinal static optical properties of hydrogen chains: Finite field extrapolations of matrix product state calculations." *J. Chem. Phys.* **136**, 134110 (2012).

[108] Y. Ma and H. Ma. "Assessment of various natural orbitals as the basis of large active space density-matrix renormalization group calculations." *J. Chem. Phys.* **138**, 224105 (2013).

[109] J. Hachmann, J. J. Dorando, M. Avilés, and G. K.-L. Chan. "The radical character of the acenes: A density matrix renormalization group study." *J. Chem. Phys.* **127**, 134309 (2007).

[110] C. Raghu, Y. A. Pati, and S. Ramasesha. "Structural and electronic instabilities in polyacenes: Density-matrix renormalization group study of a long-range interacting model." *Phys. Rev. B* **65**, 155204 (2002).

[111] C. Raghu, Y. Anusooya Pati, and S. Ramasesha. "Density-matrix renormalization-group study of low-lying excitations of polyacene within a Pariser-Parr-Pople model." *Phys. Rev. B* **66**, 035116 (2002).

[112] Y. Kurashige, G. K.-L. Chan, and T. Yanai. "Entangled quantum electronic wavefunctions of the Mn4CaO5 cluster in photosystem II." *Nat. Chem.* **5**, 660 (2013).

[113] S. Sharma, K. Sivalingam, F. Neese, and G. K.-L. Chan. "Low-energy spectrum of iron-sulfur clusters directly from many-particle quantum mechanics." *Nat. Chem.* **6**, 927 (2014).

[114] F. Verstraete and J. I. Cirac. "Renormalization algorithms for quantum-many body systems in two and higher dimensions." *arXiv preprint cond-mat/0407066* (2004).

[115] V. Murg, F. Verstraete, O. Legeza, and R. M. Noack. "Simulating strongly correlated quantum systems with tree tensor networks." *Phys. Rev. B* **82**, 205105 (2010).

[116] N. Nakatani and G. K.-L. Chan. "Efficient tree tensor network states (TTNS) for quantum chemistry: Generalizations of the density matrix renormalization group algorithm." *J. Chem. Phys.* **138**, 134113 (2013).

[117] V. Murg, F. Verstraete, R. Schneider, P. R. Nagy, and O. Legeza. "Tree tensor network state with variable tensor order: An efficient multireference method for strongly correlated systems." *J. Chem. Theory Comput.* **11**, 1027 (2015).

[118] P. Benioff. "The computer as a physical system: A microscopic quantum mechanical Hamiltonian model of computers as represented by Turing machines." *Journal of statistical physics* **22**, 563 (1980).

[119] S. Lloyd. "Universal Quantum Simulators." *Science* **273**, 1073 (1996).

[120] A. Aspuru-Guzik, A. D. Dutoi, P. J. Love, and M. Head-Gordon. "Simulated quantum computation of molecular energies." *Science* **309**, 1704 (2005).

[121] A. Kandala, A. Mezzacapo, K. Temme, M. Takita, M. Brink, J. M. Chow, and J. M. Gambetta. "Hardware-efficient variational quantum eigensolver for small molecules and quantum magnets." *Nature* **549**, 242 (2017).

[122] A. Kandala, K. Temme, A. D. Córcoles, A. Mezzacapo, J. M. Chow, and J. M. Gambetta. "Error mitigation extends the computational reach of a noisy quantum processor." *Nature* **567**, 491 (2019).

[123] P. J. J. O'Malley, R. Babbush, I. D. Kivlichan, J. Romero, J. R. McClean, R. Barends, J. Kelly, P. Roushan, A. Tranter, N. Ding, B. Campbell, Y. Chen, Z. Chen, B. Chiaro, A. Dunsworth, A. G. Fowler, E. Jeffrey, E. Lucero, A. Megrant, J. Y. Mutus, M. Neeley, C. Neill, C. Quintana, D. Sank, A. Vainsencher, J. Wenner, T. C. White, P. V. Coveney, P. J. Love, H. Neven, A. Aspuru-Guzik, and J. M. Martinis. "Scalable Quantum Simulation of Molecular Energies." *Phys. Rev. X* **6**, 031007 (2016).

[124] J. I. Colless, V. V. Ramasesh, D. Dahlen, M. S. Blok, M. Kimchi-Schwartz, J. McClean, J. Carter, W. De Jong, and I. Siddiqi. "Computation of molecular spectra on a quantum processor with an error-resilient algorithm." *Physical Review X* **8**, 011021 (2018).

[125] Y. Shen, X. Zhang, S. Zhang, J.-N. Zhang, M.-H. Yung, and K. Kim. "Quantum implementation of the unitary coupled cluster for simulating molecular electronic structure." *Physical Review A* **95**, 020501 (2017).

[126] C. Hempel, C. Maier, J. Romero, J. McClean, T. Monz, H. Shen, P. Jurcevic, B. P. Lanyon, P. Love, R. Babbush, *et al.*. "Quantum chemistry calculations on a trapped-ion quantum simulator." *Physical Review X* **8**, 031022 (2018).

[127] Y. Nam, J.-S. Chen, N. C. Pisenti, K. Wright, C. Delaney, D. Maslov, K. R. Brown, S. Allen, J. M. Amini, J. Apisdorf, *et al.*. "Ground-state energy estimation of the water molecule on a trapped-ion quantum computer." *npj Quantum Information* **6**, 1 (2020).

[128] F. Arute, K. Arya, R. Babbush, D. Bacon, J. C. Bardin, R. Barends, R. Biswas, S. Boixo, F. G. Brandao, D. A. Buell, *et al.*. "Quantum supremacy using a programmable superconducting processor." *Nature* **574**, 505 (2019).

[129] D. Sych and G. Leuchs. "A complete basis of generalized Bell states." *New Journal of Physics* **11**, 013006 (2009).

[130] M. A. Nielsen and I. L. Chuang. "Programmable quantum gate arrays." *Physical Review Letters* **79**, 321 (1997).

[131] D. E. Deutsch, A. Barenco, and A. Ekert. "Universality in quantum computation." *Proceedings of the Royal Society of London. Series A: Mathematical and Physical Sciences* **449**, 669 (1995).

[132] P. Jordan and E. P. Wigner. "über das paulische äquivalenzverbot." In "The Collected Works of Eugene Paul Wigner," 109–129. Springer (1993).

[133] J. T. Seeley, M. J. Richard, and P. J. Love. "The Bravyi-Kitaev transformation for quantum computation of electronic structure." *The Journal of chemical physics* **137**, 224109 (2012).

[134] S. B. Bravyi and A. Y. Kitaev. "Fermionic quantum computation." *Annals of Physics* **298**, 210 (2002).

[135] V. Havlíček, M. Troyer, and J. D. Whitfield. "Operator locality in the quantum simulation of fermionic models." *Physical Review A* **95**, 032332 (2017).

[136] K. Setia and J. D. Whitfield. "Bravyi-Kitaev Superfast simulation of electronic structure on a quantum computer." *The Journal of chemical physics* **148**, 164104 (2018).

[137] K. Setia, S. Bravyi, A. Mezzacapo, and J. D. Whitfield. "Superfast encodings for fermionic quantum simulation." *Physical Review Research* **1**, 033033 (2019).

[138] R. Ball. "Fermions without fermion fields." *Physical review letters* **95**, 176407 (2005).

[139] F. Verstraete and J. I. Cirac. "Mapping local Hamiltonians of fermions to local Hamiltonians of spins." *Journal of Statistical Mechanics: Theory and Experiment* **2005**, P09012 (2005).

[140] T. D. Crawford and H. F. Schaefer. *An Introduction to Coupled Cluster Theory for Computational Chemists*, volume 45 of *Lipkowitz/Reviews*. John Wiley & Sons, Ltd, Hoboken, NJ, USA (2007).

[141] J. Preskill. "Quantum Computing in the NISQ era and beyond." *Quantum* **2**, 79 (2018).

[142] D. S. Abrams and S. Lloyd. "Simulation of Many-Body Fermi Systems on a Universal Quantum Computer." *Phys. Rev. Lett.* **79**, 2586 (1997).

[143] D. S. Abrams and S. Lloyd. "Quantum algorithm providing exponential speed increase for finding eigenvalues and eigenvectors." *Phys. Rev. Lett.* **83**, 5162 (1999).

[144] R. M. Parrish and P. L. McMahon. "Quantum Filter Diagonalization: Quantum Eigendecomposition without Full Quantum Phase Estimation." *e-print arXiv:1909.08925 [quant-ph]* (2019).

[145] N. H. Stair, R. Huang, and F. A. Evangelista. "A Multireference Quantum Krylov Algorithm for Strongly Correlated Electrons." *J. Chem. Theory Comput.* **16**, 2236 (2020). ISSN 1549-9626.

[146] K. Seki and S. Yunoki. "Quantum power method by a superposition of time-evolved states." *Phys. Rev. X Quantum* **2**, 010333 (2021).

[147] K. Klymko, C. Mejuto-Zaera, S. J. Cotton, F. Wudarski, M. Urbanek, D. Hait, M. Head-Gordon, K. B. Whaley, J. Moussa, N. Wiebe, *et al.*. "Real time evolution for ultracompact Hamiltonian eigenstates on quantum hardware." *arXiv preprint arXiv:2103.08563* (2021).

[148] M. Motta, C. Sun, A. T. Tan, M. J. O'Rourke, E. Ye, A. J. Minnich, F. G. Brandão, and G. K.-L. Chan. "Determining eigenstates and thermal states on a quantum computer using quantum imaginary time evolution." *Nat. Phys.* **16**, 1 (2019).

[149] S.-N. Sun, M. Motta, R. N. Tazhigulov, A. T. Tan, G. K.-L. Chan, and A. J. Minnich. "Quantum Computation of Finite-Temperature Static and Dynamical Properties of Spin Systems Using Quantum Imaginary Time Evolution." *PRX Quantum* **2**, 010317 (2021).

[150] A. M. Childs, Y. Su, M. C. Tran, N. Wiebe, and S. Zhu. "Theory of trotter error with commutator scaling." *Physical Review X* **11**, 011020 (2021).

[151] H. F. Trotter. "On the product of semi-groups of operators." *Proceedings of the American Mathematical Society* **10**, 545 (1959).

[152] M. Suzuki. "Improved Trotter-like formula." *Physics Letters A* **180**, 232 (1993).

[153] J. R. McClean, R. Babbush, P. J. Love, and A. Aspuru-Guzik. "Exploiting locality in quantum computation for quantum chemistry." *The journal of physical chemistry letters* **5**, 4368 (2014).

[154] M. Motta, E. Ye, J. R. McClean, Z. Li, A. J. Minnich, R. Babbush, and G. K. Chan. "Low rank representations for quantum simulation of electronic structure." *arXiv preprint arXiv:1808.02625* (2018).

[155] E. Campbell. "Random compiler for fast Hamiltonian simulation." *Physical review letters* **123**, 070503 (2019).

[156] Y. Ouyang, D. R. White, and E. T. Campbell. "Compilation by stochastic Hamiltonian sparsification." *Quantum* **4**, 235 (2020).

[157] A. Tranter, P. J. Love, F. Mintert, N. Wiebe, and P. V. Coveney. "Ordering of trotterization: Impact on errors in quantum simulation of electronic structure." *Entropy* **21**, 1218 (2019).

[158] R. Babbush, N. Wiebe, J. McClean, J. McClain, H. Neven, and G. K.-L. Chan. "Low-depth quantum simulation of materials." *Physical Review X* **8**, 011044 (2018).

[159] J. R. McClean, F. M. Faulstich, Q. Zhu, B. O'Gorman, Y. Qiu, S. R. White, R. Babbush, and L. Lin. "Discontinuous Galerkin discretization for quantum simulation of chemistry." *New Journal of Physics* **22**, 093015 (2020).

[160] R. Babbush, J. McClean, D. Wecker, A. Aspuru-Guzik, and N. Wiebe. "Chemical basis of Trotter-Suzuki errors in quantum chemistry simulation." *Physical Review A* **91**, 022311 (2015).

[161] I. Kassal, S. P. Jordan, P. J. Love, M. Mohseni, and A. Aspuru-Guzik. "Polynomial-time quantum algorithm for the simulation of chemical dynamics." *Proceedings of the National Academy of Sciences* **105**, 18681 (2008).

[162] J. D. Whitfield, J. Biamonte, and A. Aspuru-Guzik. "Simulation of electronic structure Hamiltonians using quantum computers." *Molecular Physics* **109**, 735 (2011).

[163] D. Wecker, B. Bauer, B. K. Clark, M. B. Hastings, and M. Troyer. "Gate-count estimates for performing quantum chemistry on small quantum computers." *Physical Review A* **90**, 022305 (2014).

[164] M. B. Hastings, D. Wecker, B. Bauer, and M. Troyer. "Improving quantum algorithms for quantum chemistry." *arXiv preprint arXiv:1403.1539* (2014).

[165] D. Poulin, M. B. Hastings, D. Wecker, N. Wiebe, A. C. Doherty, and M. Troyer. "The Trotter step size required for accurate quantum simulation of quantum chemistry." *arXiv preprint arXiv:1406.4920* (2014).

[166] D. W. Berry, A. M. Childs, R. Cleve, R. Kothari, and R. D. Somma. "Simulating Hamiltonian dynamics with a truncated Taylor series." *Physical review letters* **114**, 090502 (2015).

[167] R. Babbush, D. W. Berry, I. D. Kivlichan, A. Y. Wei, P. J. Love, and A. Aspuru-Guzik. "Exponentially more precise quantum simulation of fermions in second quantization." *New Journal of Physics* **18**, 033032 (2016).

[168] G. H. Low and I. L. Chuang. "Hamiltonian simulation by qubitization." *Quantum* **3**, 163 (2019).

[169] D. W. Berry, C. Gidney, M. Motta, J. McClean, and R. Babbush. "Qubitization of arbitrary basis quantum chemistry by low rank factorization." *arXiv preprint arXiv:1902.02134* (2019).

[170] D. W. Berry, C. Gidney, M. Motta, J. R. McClean, and R. Babbush. "Qubitization of arbitrary basis quantum chemistry leveraging sparsity and low rank factorization." *Quantum* **3**, 208 (2019).

[171] A. M. Childs and N. Wiebe. "Hamiltonian simulation using linear combinations of unitary operations." *arXiv preprint arXiv:1202.5822* (2012).

[172] J. Lee, D. Berry, C. Gidney, W. J. Huggins, J. R. McClean, N. Wiebe, and R. Babbush. "Even more efficient quantum computations of chemistry through tensor hypercontraction." *arXiv preprint arXiv:2011.03494* (2020).

[173] E. G. Hohenstein, R. M. Parrish, and T. J. Martínez. "Tensor hypercontraction density fitting. I. Quartic scaling second-and third-order Møller-Plesset perturbation theory." *J. Chem. Phys.* **137**, 044103 (2012).

[174] A. Y. Kitaev. "Quantum measurements and the Abelian stabilizer problem." *e-print arXiv:9511026 [quant-ph]* (1995).

[175] A. Ekert and R. Jozsa. "Quantum computation and Shor's factoring algorithm." *Reviews of Modern Physics* **68**, 733 (1996).

[176] R. Jozsa. "Quantum algorithms and the Fourier transform." *Proceedings of the Royal Society of London. Series A: Mathematical, Physical and Engineering Sciences* **454**, 323 (1998).

[177] V. E. Elfving, B. W. Broer, M. Webber, J. Gavartin, M. D. Halls, K. P. Lorton, and A. Bochevarov. "How will quantum computers provide an industrially relevant computational advantage in quantum chemistry?" *arXiv preprint arXiv:2009.12472* (2020).

[178] E. Farhi, J. Goldstone, S. Gutmann, and M. Sipser. "Quantum computation by adiabatic evolution." *arXiv preprint quant-ph/0001106* (2000).

[179] R. Babbush, P. J. Love, and A. Aspuru-Guzik. "Adiabatic quantum simulation of quantum chemistry." *Scientific reports* **4**, 1 (2014).

[180] A. Peruzzo, J. McClean, P. Shadbolt, M.-H. Yung, X.-Q. Zhou, P. J. Love, A. Aspuru-Guzik, and J. L. O'Brien. "A variational eigenvalue solver on a photonic quantum processor." *Nat. Commun.* **5**, 4213 (2014).

[181] J. R. McClean, J. Romero, R. Babbush, and A. Aspuru-Guzik. "The theory of variational hybrid quantum-classical algorithms." *New J. Phys.* **18**, 023023 (2016).

[182] Y. Ge, J. Tura, and J. I. Cirac. "Faster ground state preparation and high-precision ground energy estimation with fewer qubits." *Journal of Mathematical Physics* **60**, 022202 (2019).

[183] L. Lin and Y. Tong. "Near-optimal ground state preparation." *Quantum* **4**, 372 (2020).

[184] N. Gomes, F. Zhang, N. F. Berthusen, C.-Z. Wang, K.-M. Ho, P. P. Orth, and Y. Yao. "Efficient step-merged quantum imaginary time evolution algorithm for quantum chemistry." *J. Chem. Theory Comput.* **16**, 6256 (2020).

[185] D. Aharonov, V. Jones, and Z. Landau. "A polynomial quantum algorithm for approximating the Jones polynomial." *Algorithmica* **55**, 395 (2009).

[186] K. Seki and S. Yunoki. "Quantum power method by a superposition of time-evolved states." *arXiv preprint arXiv:2008.03661* (2020).

[187] M. Cerezo, A. Arrasmith, R. Babbush, S. C. Benjamin, S. Endo, K. Fujii, J. R. McClean, K. Mitarai, X. Yuan, L. Cincio, *et al.*. "Variational quantum algorithms." *arXiv preprint arXiv:2012.09265* (2020).

[188] O. Higgott, D. Wang, and S. Brierley. "Variational quantum computation of excited states." *Quantum* **3**, 156 (2019).

[189] T. Jones, S. Endo, S. McArdle, X. Yuan, and S. C. Benjamin. "Variational quantum algorithms for discovering hamiltonian spectra." *Physical Review A* **99**, 062304 (2019).

[190] R. M. Parrish, E. G. Hohenstein, P. L. McMahon, and T. J. Martínez. "Quantum computation of electronic transitions using a variational quantum eigensolver." *Physical review letters* **122**, 230401 (2019).

[191] P. J. Ollitrault, A. Kandala, C.-F. Chen, P. K. Barkoutsos, A. Mezzacapo, M. Pistoia, S. Sheldon, S. Woerner, J. M. Gambetta, and I. Tavernelli. "Quantum equation of motion for computing molecular excitation energies on a noisy quantum processor." *Physical Review Research* **2**, 043140 (2020).

[192] P. G. Szalay, M. Nooijen, and R. J. Bartlett. "Alternative ansätze in single reference coupled-cluster theory. III. A critical analysis of different methods." *The Journal of chemical physics* **103**, 281 (1995).

[193] A. G. Taube and R. J. Bartlett. "New perspectives on unitary coupled-cluster theory." *International journal of quantum chemistry* **106**, 3393 (2006).

[194] B. Cooper and P. J. Knowles. "Benchmark studies of variational, unitary and extended coupled cluster methods." *The Journal of chemical physics* **133**, 234102 (2010).

[195] F. A. Evangelista. "Alternative single-reference coupled cluster approaches for multireference problems: The simpler, the better." *J. Chem. Phys.* **134**, 224102 (2011).

[196] G. Harsha, T. Shiozaki, and G. E. Scuseria. "On the difference between variational and unitary coupled cluster theories." *The Journal of chemical physics* **148**, 044107 (2018).

[197] I. G. Ryabinkin, T.-C. Yen, S. N. Genin, and A. F. Izmaylov. "Qubit Coupled Cluster Method: A Systematic Approach to Quantum Chemistry on a Quantum Computer." *J. Chem. Theory Comput.* **14**, 6317 (2018).

[198] D. Wecker, M. B. Hastings, and M. Troyer. "Progress towards practical quantum variational algorithms." *Phys. Rev. A* **92**, 042303 (2015).

[199] W. W. Ho and T. H. Hsieh. "Efficient variational simulation of non-trivial quantum states." *SciPost Phys* **6**, 29 (2019).

[200] R. Wiersema, C. Zhou, Y. de Sereville, J. F. Carrasquilla, Y. B. Kim, and H. Yuen. "Exploring entanglement and optimization within the Hamiltonian Variational Ansatz." *PRX Quantum* **1**, 020319 (2020).

[201] J.-G. Liu, Y.-H. Zhang, Y. Wan, and L. Wang. "Variational quantum eigensolver with fewer qubits." *Physical Review Research* **1**, 023025 (2019).

[202] F. Barratt, J. Dborin, M. Bal, V. Stojevic, F. Pollmann, and A. G. Green. "Parallel quantum simulation of large systems on small quantum computers." *arXiv preprint arXiv:2003.12087* (2020).

[203] X. Yuan, J. Sun, J. Liu, Q. Zhao, and Y. Zhou. "Quantum simulation with hybrid tensor networks." *arXiv preprint arXiv:2007.00958* (2020).

[204] T.-C. Yen, V. Verteletskyi, and A. F. Izmaylov. "Measuring all compatible operators in one series of single-qubit measurements using unitary transformations." *Journal of Chemical Theory and Computation* **16**, 2400 (2020).

[205] V. Verteletskyi, T.-C. Yen, and A. F. Izmaylov. "Measurement optimization in the variational quantum eigensolver using a minimum clique cover." *The Journal of Chemical Physics* **152**, 124114 (2020).

[206] J. Romero, R. Babbush, J. R. McClean, C. Hempel, P. J. Love, and A. Aspuru-Guzik. "Strategies for quantum computing molecular energies using the unitary coupled cluster ansatz." *Quantum Sci. Technol.* **4**, 014008 (2019).

[207] M. Schuld, V. Bergholm, C. Gogolin, J. Izaac, and N. Killoran. "Evaluating analytic gradients on quantum hardware." *Physical Review A* **99**, 032331 (2019).

[208] J. S. Kottmann, A. Anand, and A. Aspuru-Guzik. "A Feasible Approach for Automatically Differentiable Unitary Coupled-Cluster on Quantum Computers." *arXiv preprint arXiv:2011.05938* (2020).

[209] C. G. Broyden. "The convergence of a class of double-rank minimization algorithms 1. general considerations." *IMA Journal of Applied Mathematics* **6**, 76 (1970).

[210] R. Fletcher. "A new approach to variable metric algorithms." *The computer journal* **13**, 317 (1970).

[211] D. Goldfarb. "A family of variable-metric methods derived by variational means." *Mathematics of computation* **24**, 23 (1970).

[212] D. F. Shanno. "Conditioning of quasi-Newton methods for function minimization." *Mathematics of computation* **24**, 647 (1970).

[213] R. H. Byrd, P. Lu, J. Nocedal, and C. Zhu. "A limited memory algorithm for bound constrained optimization." *SIAM Journal on scientific computing* **16**, 1190 (1995).

[214] D. P. Kingma and J. Ba. "Adam: A method for stochastic optimization." *arXiv preprint arXiv:1412.6980* (2014).

[215] J. M. Kübler, A. Arrasmith, L. Cincio, and P. J. Coles. "An adaptive optimizer for measurement-frugal variational algorithms." *Quantum* **4**, 263 (2020).

[216] J. C. Spall *et al.*. "Multivariate stochastic approximation using a simultaneous perturbation gradient approximation." *IEEE transactions on automatic control* **37**, 332 (1992).

[217] N. Moll, P. Barkoutsos, L. S. Bishop, J. M. Chow, A. Cross, D. J. Egger, S. Filipp, A. Fuhrer, J. M. Gambetta, M. Ganzhorn, *et al.*. "Quantum optimization using variational algorithms on near-term quantum devices." *Quantum Science and Technology* **3**, 030503 (2018).

[218] E. Farhi, J. Goldstone, and S. Gutmann. "A quantum approximate optimization algorithm." *arXiv preprint arXiv:1411.4028* (2014).

[219] C. Y.-Y. Lin and Y. Zhu. "Performance of QAOA on typical instances of constraint satisfaction problems with bounded degree." *arXiv preprint arXiv:1601.01744* (2016).

[220] Z. Wang, S. Hadfield, Z. Jiang, and E. G. Rieffel. "Quantum approximate optimization algorithm for maxcut: A fermionic view." *Physical Review A* **97**, 022304 (2018).

[221] C. Bravo-Prieto, R. LaRose, M. Cerezo, Y. Subasi, L. Cincio, and P. J. Coles. "Variational quantum linear solver." *arXiv preprint arXiv:1909.05820* (2019).

[222] H.-Y. Huang, K. Bharti, and P. Rebentrost. "Near-term quantum algorithms for linear systems of equations." *arXiv preprint arXiv:1909.07344* (2019).

[223] E. Anschuetz, J. Olson, A. Aspuru-Guzik, and Y. Cao. "Variational quantum factoring." In "International Workshop on Quantum Technology and Optimization Problems," 74–85. Springer (2019).

[224] F. A. Evangelista, G. K.-L. Chan, and G. E. Scuseria. "Exact parameterization of fermionic wave functions via unitary coupled cluster theory." *The Journal of Chemical Physics* **151**, 244112 (2019).

[225] J. Lee, W. J. Huggins, M. Head-Gordon, and K. B. Whaley. "Generalized unitary coupled cluster wave functions for quantum computation." *Journal of chemical theory and computation* **15**, 311 (2018).

[226] Y. Matsuzawa and Y. Kurashige. "Jastrow-type decomposition in quantum chemistry for low-depth quantum circuits." *Journal of chemical theory and computation* **16**, 944 (2020).

[227] I. D. Kivlichan, J. McClean, N. Wiebe, C. Gidney, A. Aspuru-Guzik, G. K.-L. Chan, and R. Babbush. "Quantum simulation of electronic structure with linear depth and connectivity." *Physical review letters* **120**, 110501 (2018).

[228] H. R. Grimsley, S. E. Economou, E. Barnes, and N. J. Mayhall. "An adaptive variational algorithm for exact molecular simulations on a quantum computer." *Nat. Commun.* **10**, 1 (2019).

[229] I. G. Ryabinkin, R. A. Lang, S. N. Genin, and A. F. Izmaylov. "Iterative Qubit Coupled Cluster approach with efficient screening of generators." *Journal of Chemical Theory and Computation* **16**, 1055 (2020).

[230] H. L. Tang, V. Shkolnykov, G. Barron, H. Grimsley, N. Mayhall, E. Barnes, and S. Economou. "qubit-ADAPT-VQE: An adaptive algorithm for constructing hardware-efficient ansätze on a quantum processor." *Bulletin of the American Physical Society* (2021).

# Chapter 2

# Exploring Hilbert space on a budget

## 2.1 Introduction

An outstanding challenge in modern electronic structure theory is solving the many-body Schrödinger equation for strongly correlated electrons. The availability of accurate computational methods for strongly correlated systems is imperative to study a myriad of important phenomena such as bond breaking and photochemical processes,[1,2] molecular magnetism,[3] high-temperature superconductivity,[4] and many others.[5–8] In brief, strong correlation arises when the cost of promoting electrons to higher energy orbitals is small in comparison to the electron pairing energy (Coulombic repulsion). Consequently, strongly correlated electrons cannot be qualitatively described by a mean-field picture because the wave function may contain nontrivial contributions from many Slater determinants.[9,10] In this situation, electronic structure methods that build upon a mean-field reference cannot effectively approximate the wave function with a polynomial number of parameters and, therefore, often yield inaccurate energies and molecular properties.

The full configuration interaction (FCI) expansion captures all correlation effects for $N$ electrons in $L$ spatial orbitals. Restricting FCI to a complete active space (CAS), with (CASSCF)[11] or without (CASCI) orbital optimization is also a common strategy when strong correlation effects are limited to few orbitals. However, the size of the FCI (or CASSCF) determinant space scales like a binomial coefficient in $N$ and $L$, making these

methods intractable for most systems of chemical interest[12] containing more than approximately 18 electrons in 18 orbitals (18e,18o)—although massively-parallel computations have recently managed to push this figure to (22e,22o).[13]

Fortunately, for many ground and low-lying states, the complexity of the wave function is reduced by symmetry restrictions, sparsity bread by non-interacting determinants, and regular structure resulting from the local nature of Coulombic correlation. Much work has thus been devoted to the development of methods that can exploit sparsity or use decomposition techniques to compactly approximate the wave function. However, it is not generally known what approaches are the most efficient (i.e., which ones can reach a target accuracy using the fewest parameters) given the physical dimension of the system, the degree of correlation strength, and choice of molecular orbitals.

Understanding the degree to which different wave functions may be compressed is important to guide future development of both classical and quantum computational methods.[14] In particular, there is a growing need for benchmark sets that may be used to compare classical and new quantum algorithms in various regimes of electron correlation. Since many classes of emerging quantum algorithms—such as variational quantum eigensolvers[15–18] and quantum subspace diagonalization techniques[19–22]—use parameterized ansätze, one way to compare them to classical algorithms is to quantify their efficiency in terms of classical resources needed to achieve a target energy accuracy. Such characterization is also useful in answering whether or not a quantum algorithm has an advantage over a purely classical approach.

The goal of this work is to examine how to best compress the FCI wave function of strongly correlated systems using classical methods. To this end, we introduce a benchmark set and a simple metric to analyze the performance of a method. We consider three families of deterministic methods that systematically approach FCI in a near-continuous fashion: i) selected CI (sCI),[23–26] ii) singular value decomposition FCI (SVD-FCI) (related to the methods discussed in Refs. 27–29), and iii) the density matrix renormalization group

(DMRG).[30] These exemplify different strategies to approximate the exact wave function; however, they all converge to the exact energy in the limit of no truncation, and their accuracy can be controlled by a single parameter.

Selected CI schemes approximate the FCI solution using a subset of the full determinant space. Therefore, they are most efficient when the exact wave function has a sparse structure. Contrary to other forms of truncated CI, selected CI methods identify an optimal determinant basis using an iterative selection procedure that gradually expands the determinant space. Although selected CI[23–26] was proposed decades ago, in recent years it has received renewed attention with new deterministic,[31–42] stochastic,[43–48] and semistochastic[49–52] variants being proposed. The closely related family of determinant-based Monte Carlo methods[53–60] has also been explored.

The singular value decomposition finds use in several areas of quantum chemistry as a way to achieve low-loss compression of data.[61–68] The SVD can be applied to compress the FCI state once the coefficient vector is reshaped as a matrix, a representation naturally suggested by string-based CI algorithms.[69] Taylor has proposed to reduce the memory requirements of FCI by performing a SVD decomposition at each iteration of the Davidson procedure.[28] Another method that employs a compressed representation of the FCI vector is rank-reduced FCI (RR-FCI), originally proposed by Koch[27] and recently extended by Fales and co-workers.[29] RR-FCI approximates the FCI solution with a polar decomposition of the FCI vector (represented as a matrix) combined with variational minimization of the energy. We note that both Taylor's "gzip" approach and RR-FCI approaches cannot be justified on the basis of a symmetry or a physical principle, although a variant of RR-FCI that exploits locality has been proposed (see Ref. 70).

Tensor network states (TNSs) represent a broad family of methods that approximate the FCI coefficients (viewed as a tensor) with a collection of tensors connected by contractions. The simplest type of TNS is a matrix product state (MPS), the underlying ansatz[71–73] of the density matrix renormalization group (DMRG).[30] MPSs are able to maximally exploit local

orbital entanglement, that is, for states that satisfy an area law for the entanglement entropy, MPSs can yield near-exact results in 1D and quasi-1D systems.[74,75] The generalization of the MPS ansatz to two- (2D) and three-dimensional (3D) TNS using high-order tensor factorizations is also an active area of research.[75–77] In practice, the variational optimization of TNSs suffers from very high scaling and is less efficient relative to MPSs. DMRG (as applied to quantum chemistry),[78–82] has been tremendously successful in describing the ground states of quasi-linear molecular systems. For example, DMRG has enabled the investigation of long hydrogen chains,[78,83–86] oligoacenes,[87–89] and large biochemically-relevant transition metal complexes with up to 100 orbitals.[90,91]

To test the performance of electronic structure theories in the strongly correlated regime, we have introduced a benchmark set of one, two, and three-dimensional (3D) hydrogen systems. These systems model strongly correlated electrons in significantly different regimes and dimensionalities, and allow us to explore the physics of Mott insulators and spin frustrated systems in 2- and 3D. 1D hydrogen systems have recently been the subject of comprehensive benchmark studies aimed at treating strong correlation in real materials.[92–94] Hydrogen lattices with localized spins are also related to the more fundamental Heisenberg and Hubbard models, exhibiting similar spin correlation patterns and band structures. Our benchmark set contains four $H_{10}$ models: the well-investigated 1D chain and ring, as well as a 2D triangular lattice (referred to as "sheet" throughout the paper), and a 3D close-packed pyramid. For each model, we consider both the effect of the H–H distance on the strength of correlation, and the use of different molecular orbital bases (delocalized/localized). We characterize these models by computing various metrics of correlation, including the norm of the two-body cumulant, the total quantum information, and spin-spin correlation functions. Additionally, to investigate the compression efficiency as a function of system size, we also consider $H_{12}$, $H_{14}$ , and $H_{16}$ analogs of the four models.

Since the methods considered here play an important role as substitutes for FCI in

multireference treatments of electron correlation,[95–100] we are particularly interested in assessing their performance when applied only to valence orbitals. To simulate this scenario, our computations employ a minimal basis set. Note, that this treatment may be considered equivalent to diagonalizing a valence effective Hamiltonian[101] with interactions modified by dynamical correlation effects. It is important to point out that since we only consider zero-temperature quantum chemistry approaches, we focus in particular on regimes of electron correlation that range from weak to medium/strong. We intentionally avoid the limit of infinite H–H separation, because all the models considered here develop a massively degenerate ground state containing $2^{10}$ states. At large separation, it is ludicrous to characterize a ground state, and one should instead seek to compute thermal averages employing a finite-temperature approach.[102–104]

To compare the performance of each method, we evaluate the error in the energy and the two-body density cumulant as a function of the number of variational parameters. These errors measure how well electronic correlation effects are preserved in the compression, and therefore can indicate the quality of an approximate wave function and its properties. From this information, we extract a single metric, the *accuracy volume*, which measures the number of variational parameters necessary to achieve a target energy error. Although the accuracy volume does not take into account the actual cost of a computation, this metric serves as a proxy for the computational resources required by each method, independently of implementation details. We also compare the energy errors produced with Hartree–Fock theory, second-order Møller–Plesset many-body perturbation theory (MP2), coupled cluster theory with singles and doubles (CCSD),[105] CCSD with perturbative triples [CCSD(T)],[106] the completely renormalized CC approach with perturbative triples [CR-CC(2,3)],[107] and the variational two-particle reduced density matrix (V2RDM) method.[108–112] We have collected the data generated in this study in an online repository[113] in the hope that it will be useful in future studies.

The remainder of this article is organized as follows: Sec. 4.2 defines the accuracy

volume, summarizes the three methods compared in this study, and defines the metrics used to assess correlation strength in the hydrogen model systems. Section 2.3 provides the computational details of our study. Numerical results are reported in Sec. 4.3, and Sec. 4.4 summarizes our findings and discusses their relevance in the context of classical and quantum algorithms for strongly correlated systems.

## 2.2 Theory

### 2.2.1 Definition of the accuracy volume

For a systematically improvable method $X$ we indicate the energy computed using $N_{\text{par}}$ parameters as $E_X(N_{\text{par}})$. We then define the accuracy volume, $\mathscr{V}_X(\alpha)$, to be the smallest number of parameters such that the error per electron with respect to the FCI energy ($E_{\text{FCI}}$) is less than or equal to $10^{-\alpha}$:

$$\mathscr{V}_X(\alpha) = N_{\text{par}} : \frac{|E_X(N_{\text{par}}) - E_{\text{FCI}}|}{N} \leq 10^{-\alpha}\, E_{\text{h}}. \tag{2.1}$$

For convenience, in the rest of the paper we always assume the target energy error is 1 m$E_{\text{h}}$ for the $H_{10}$ systems, which corresponds to a 0.1 m$E_{\text{h}}$ error per electron ($\alpha = 4$) and use the more compact symbol $\mathscr{V}_X$ instead. For methods that exploit the sparsity of the FCI wave function (e.g., selected CI), the accuracy volume is a measure of the number of Slater determinants or configuration state functions (equal to the number of parameters). This literal interpretation of the accuracy volume does not extend to approximation schemes based on tensor decomposition, in which case it only reflects the total number of parameters employed. We intend the accuracy volume to be used as a performance metric of a method, since it approximately measures the computational resources (memory and CPU) necessary to achieve a target accuracy. Because the accuracy volume can be equally applied to purely classical and hybrid quantum-classical methods, it provides a straightforward way to compare the two on more equal footing. Our definition of $\mathscr{V}_X$ [Eq. (2.1)] considers the energy error per electron to allow the comparison of systems with different numbers of

electrons. This approach is consistent with the fact that approximate methods that are size consistent, when applied to noninteracting fragments, give an error that is additive in the error of each fragment. We also choose to define $\mathscr{V}_X$ as the absolute number of parameters, as opposed to the fraction of the total Hilbert space, since the former is proportional to the computational resources required by a method. In contrast, a comparison based on the fraction of Hilbert space parameters employed by a method would be dependent on the exploitable symmetries for the orbitals that are chosen (e.g. symmetry adapted delocalized vs. localized orbitals) making comparisons of different computations less indicative of actual computational resources.

### 2.2.2 Overview of the computational methods

Given a basis of $K$ spin orbitals $\{\psi_p\}$ with $p = 1,\ldots,K$, we indicate a generic $N$-electron determinant $|\psi_{i_1}\cdots\psi_{i_N}\rangle$ using the notation $|\Phi_I\rangle$ where the multindex $I = (i_1,\ldots,i_N)$ represents an ordered list of indices ($i_1 < i_2 < \ldots < i_N$). The set of $N$-electron determinants ($\mathscr{H}_N$) forms a Hilbert space of dimension $|\mathscr{H}_N| = N_{\mathscr{H}}$. Using this notation, the FCI wave function is written as a linear combination of determinants, each parameterized by a coefficient ($C_{i_1,\ldots,i_N} \equiv C_I$)

$$|\Psi_{\mathrm{FCI}}\rangle = \sum_{i_1<i_2<\ldots<i_N}^{K} C_{i_1\cdots i_N}\,|\Phi_{i_1\cdots i_N}\rangle = \sum_{I}^{N_{\mathscr{H}}} C_I\,|\Phi_I\rangle\,. \tag{2.2}$$

An equivalent way to express the FCI wave function employs occupation vectors. In this representation, each determinant $|\Phi_I\rangle$ is associated with a vector of length $K$, $|\mathbf{n}\rangle = |n_1,n_2,\ldots,n_K\rangle$, where $n_i \in \{0,1\}$ is the occupation number of spin orbital $\psi_i$. The FCI wave function represented in the occupation vector form is given by

$$|\Psi_{\mathrm{FCI}}\rangle = \sum_{\{n_i\}} C_{n_1\ldots n_K}\,|n_1\ldots n_K\rangle = \sum_{\mathbf{n}} C_{\mathbf{n}}\,|\mathbf{n}\rangle \tag{2.3}$$

where the sum over all occupation vectors ($\{n_i\} \equiv \mathbf{n}$) is restricted to $N$-electron determinants ($\sum_i n_j = N$) of given spin and spatial symmetry.

*Selected CI*

Selected CI methods approximate the FCI wave function using a subset $\mathscr{M}$ (model space) of the full determinant space

$$|\Psi_{\text{sCI}}\rangle = \sum_{I \in \mathscr{M}} \tilde{C}_I |\Phi_I\rangle . \tag{2.4}$$

All flavors of selected CI aim to approximate the FCI vector with the smallest number of elements and differ primarily in the way they determine the set $\mathscr{M}$. For sCI methods, we report $N_{\text{par}}$ as the size of the space $\mathscr{M}$ (or equivalently, the size of the vector $\tilde{C}_I$).

The first approach we consider consists of an *a posteriori* selected CI (ap-sCI) compression of the exact FCI wave function. This compressed representation is obtained by sorting the determinants according to their weight $w_I = |C_I|^2$, and discarding elements with the smallest weight while satisfying the condition

$$\sum_{I \notin \mathscr{M}} |C_I|^2 < \tau_{\text{sCI}}. \tag{2.5}$$

The compressed ap-sCI vector $\tilde{C}_I$ is then normalized and the energy is computed as the expectation value of the Hamiltonian. Even though this compression scheme does not yield a variationally optimal solution, the error in the ap-sCI energy is quadratic in the wave function error. Still, this ideal (albeit impractical) version of selected CI is useful in assessing the error introduced by the different selection schemes used in practical sCI approaches.

The second approach we consider, the adaptive configuration interaction (ACI),[40,42] identifies the space $\mathscr{M}$ via an iterative procedure that seeks to control the energy error. ACI is unique in the regime of selected CI methods as it aims to approximate the FCI energy within a user-specified error tolerance $\sigma$

$$E_{\text{ACI}}(\sigma) - E_{\text{FCI}} \approx \sigma, \tag{2.6}$$

where $E_{\text{ACI}}(\sigma)$ is the ACI energy. In ACI, the model space is divided into two spaces

$\mathscr{M} = \mathscr{P} \cup \mathscr{Q}$, where $\mathscr{P}$ contains the most important determinants and $\mathscr{Q}$ contains singly and doubly excited determinants spawned from $\mathscr{P}$. New candidate determinants ($\Phi_A$) for the model space are selected from the singly and doubly excited determinants generated from the current $\mathscr{P}$ space. Each candidate determinant is ranked by its energy contribution, $\varepsilon(\Phi_A)$, a quantity estimated by diagonalizing the Hamiltonian in the basis of the ACI wave function at the current iteration and $\Phi_A$. To determine an improved model space, the candidate determinants are sorted according to $|\varepsilon(\Phi_A)|$ and unimportant elements are removed until the sum of their estimated energy is less than or equal to $\sigma$

$$\sum_{\Phi_I \notin \mathscr{M}} |\varepsilon(\Phi_I)| \leq \sigma. \tag{2.7}$$

Optionally, additional determinants are included in $\mathscr{M}$ at each iteration to ensure spin completeness.

After adding these determinants, the Hamiltonian is diagonalized and a new $\mathscr{P}$ space is formed by coarse graining $\mathscr{M}$ according to their weight using a cumulative metric similar to Eq. (2.7). The course graining step increases the overall efficiency of the procedure and reduces the dependency of the final solution on the initial guess (usually the HF determinant or a small CASCI).

The final ACI energy is computed by diagonalization of the Hamiltonian in the model space basis. However, during the selection process it is possible to accumulate the estimate of the energy contributions from the discarded determinants ($E_{\text{PT2}}$) and this quantity can be added to the ACI energy to obtain an improved energy ($E_{\text{ACI+PT2}}$).

*Singular value decomposition FCI*

In this work we consider an *a posteriori* rank reduction of the FCI tensor obtained via a singular value decomposition (SVD-FCI). Our approach is essentially identical to the "gzip" treatment used by Taylor (Ref. 28) with the caveat that we only perform SVD of the final converged wave function rather than at each FCI iteration. The SVD-FCI approach is also inspired by the the rank-reduced FCI method (RR-FCI).[27,29] However, because we do

not variationally optimize the SVD-FCI wave function, RR-FCI would yield lower energies than SVD-FCI for a specified rank (particularly at low ranks).

SVD-FCI starts from a string-based representation of the FCI wave function,[114] in which each determinant is labeled by separate multi-indices (strings) for alpha and beta electrons ($I_\alpha$ and $I_\beta$), and the determinant $|\Phi_I\rangle = \left|\Phi_{I_\alpha}\Phi_{I_\beta}\right\rangle$ factorizes into products of alpha ($\Phi_{I_\alpha}$) and beta ($\Phi_{I_\beta}$) spin orbitals. Consequently, the FCI vector $C_I$ is represented as a matrix indexed by string configurations ($I_\alpha/I_\beta$), $(\mathbf{C})_{I_\alpha I_\beta} = C_{I_\alpha I_\beta}$, and the wave function is written as

$$|\Psi_{\text{FCI}}\rangle = \sum_{I_\alpha}^{N_\alpha}\sum_{I_\beta}^{N_\beta} C_{I_\alpha I_\beta}\left|\Phi_{I_\alpha}\Phi_{I_\beta}\right\rangle, \tag{2.8}$$

where $N_\alpha$ and $N_\beta$ are the number of alpha and beta strings, respectively. While the original RR-FCI algorithm is based on variational minimization of the energy, in this work we consider only an *a posteriori* compression. To this end we perform the singular value decomposition of the FCI coefficient matrix, $\mathbf{C} = \mathbf{USV}$, where we assume that the entries of $\mathbf{C}$ are real. To find the most compact reduced-rank approximations of $\mathbf{C}$ we reconstruct an approximate matrix $\widetilde{\mathbf{C}}^{\text{SVD}}$ defined as

$$\widetilde{\mathbf{C}}^{\text{SVD}} = \mathbf{U}\widetilde{\mathbf{S}}\mathbf{V}, \tag{2.9}$$

where $\widetilde{\mathbf{S}}$ is a truncated version of $\mathbf{S}$. Assuming the singular values $s_i = S_{ii}$ are sorted in decreasing order, we keep in $\widetilde{\mathbf{S}}$ the diagonals $s_1, \ldots, s_R$ such that the sum of the square of the elements excluded is less than a user-provided threshold ($\tau_{\text{SVD}}$)

$$\sum_{i=R+1} s_i^2 < \tau_{\text{SVD}}. \tag{2.10}$$

Therefore, $R$ represents the rank of $\widetilde{\mathbf{C}}^{\text{SVD}}$ and the error in the FCI wave function is given by

$$\|\mathbf{C} - \widetilde{\mathbf{C}}^{\text{SVD}}\|_{\text{F}} < \sqrt{\tau_{\text{SVD}}}, \tag{2.11}$$

where $\|\cdot\|_{\mathrm{F}}$ is the Frobenius norm. The SVD-FCI energy is computed as

$$E^{\text{SVD-FCI}} = (\widetilde{\mathbf{C}}^{\text{SVD}})^{\dagger}\mathbf{H}\widetilde{\mathbf{C}}^{\text{SVD}}, \tag{2.12}$$

and although it does not correspond to the optimal energy for a wave function of rank $R$, this estimate deviates from the variational energy by a quadratic term. For SVD-FCI, we calculate the number of parameters as $N_{\text{par}} = R(N_\alpha + N_\beta)$, where we have assumed that the singular values $\widetilde{\mathbf{S}}$ are folded into either $\mathbf{U}$ or $\mathbf{V}$. Note that with no truncation, the SVD-FCI requires twice the number of parameters as the size of the Hilbert space. We also point out that since the FCI wave function is invariant with respect to unitary rotations of the orbitals, the rank $R$ SVD approximation yields the same approximate wave function in any orbital basis. However, the number of parameters may differ from one orbital basis to another if symmetry is employed and the SVD is applied only to the non-zero blocks of $\mathbf{C}$.

*Density-matrix renormalization group*

The matrix product state representation at the basis of the DMRG is a conceptually different form of compression that aims to exploit the local character of entanglement. A MPS decomposition of the FCI tensor in the occupation number representation is given by

$$C_{n_1\ldots n_K} \approx C^{\text{DMRG}}_{n_1\ldots n_K} = \mathbf{A}_1^{n_1}\mathbf{A}_2^{n_2}\cdots\mathbf{A}_K^{n_K}, \tag{2.13}$$

where, for a given value of the occupation number $n_j$, a generic term $\mathbf{A}_j^{n_j}$ is a $M \times M$ matrix, except for the first and last terms which are a row and a column vector of size $M$, respectively. Given an occupation number pattern ($\mathbf{n}$), the corresponding tensor element $C_{n_1\ldots n_K}$ is approximated by the product of all the $\mathbf{A}_j^{n_j}$ matrices. Quantum chemistry implementations of DMRG exploit the symmetry group of the Hamiltonian (particle number, spin, point group) to induce a block-sparse structure in the MPS tensors $\mathbf{A}_j^{n_j}$, with consequent reduction in computational and storage costs. We calculate $N_{\text{par}}$ for DMRG as the sum of the number of parameters in each site tensor $\mathbf{A}_j^{n_j}$ in the converged MPS, taking into account the block structure induced by symmetries (assuming at most abelian point groups).

Formally, the MPS representation can be derived by performing a series of successive SVDs on the FCI tensor (appropriately reshaped), at each step retaining only $M$ terms. Therefore, it is exact in the limit of $M \to N_{\mathscr{H}}$. In practice, the DMRG method directly builds the MPS representations via a sweep algorithm using a fixed value of $M$ specified by the user. For chemical applications, the quality of the MPS as a function of $M$ is controlled by two choices: the type (localized vs. delocalized) and ordering of the orbitals. These aspects present a challenge for practical calculations since different orbital types and orderings can dramatically affect the final outcome of a calculation. Although there are rules of thumb for specific cases—such as choosing localized orbitals ordered to be spatially adjacent for elongated molecules[115]—the choice of these parameters is generally a non-trivial problem beyond 1D. Various approaches to ordering delocalized orbitals have also been explored.[116–119]

### 2.2.3 Metrics of strong electronic correlation

*Metrics based on mean-field and coupled cluster wave functions*

In computational quantum chemistry, the prevailing measure of electronic correlation is the correlation energy. This metric dates back to the work of Löwdin[120] and is defined as the difference between the FCI and mean-field ($E_{\mathrm{MF}}$) energy

$$E_{\mathrm{corr}} = E_{\mathrm{FCI}} - E_{\mathrm{MF}}. \tag{2.14}$$

The correlation energy may be further partitioned into dynamical and non-dynamical contributions, as proposed by Sinanoğlu and others.[121,122]

One can similarly estimate correlation effects from the magnitude of the overlap of the Hartree–Fock determinant with the *normalized* FCI wave function, $|C_{\mathrm{HF}}| = |\langle \Phi_{\mathrm{HF}} | \Psi \rangle|$. This metric has been discussed as a diagnostic tool for determining the quality of single-reference electron correlation methods.[123] However, for infinite systems $|C_{\mathrm{HF}}| \to 0$, so this metric is probably suited only for comparing systems with the same number of electrons.

In the context of coupled cluster theory, several diagnostics have been introduced. The

$D_1$ diagnostic captures deficiencies in the reference, and is defined as the 2-norm of the matrix of singles cluster amplitudes $(\mathbf{T})_{ia} = t_i^a$, where the indices $i$ and $a$ span the occupied and virtual orbitals, respectively. This metric is defined as

$$D_1 = \|\mathbf{T}\|_2 = \sqrt{\lambda_{\max}(\mathbf{T}\mathbf{T}^T)}, \tag{2.15}$$

where $\lambda_{\max}(\mathbf{T}\mathbf{T}^T)$ indicates the largest eigenvalue of the matrix $\mathbf{T}\mathbf{T}^T$. The $D_2$ diagnostic is a measure of correlation, and it is similarly defined using doubles amplitudes ($t_{ij}^{ab}$) with the above equation modified to make this metric orbital invariant.[124]

*Measures based on the two-body density cumulant*

The norm of the two-body cumulant ($\boldsymbol{\lambda}_2$) has become a well established metric of correlation.[125–129] This quantity is the portion of the two-body density matrix $\boldsymbol{\gamma}_2$ that is not separable into one-body contributions, and it is defined as

$$\lambda_{pq}^{rs} = \gamma_{pq}^{rs} - \gamma_p^r \gamma_q^s + \gamma_p^r \gamma_s^q, \tag{2.16}$$

where $\gamma_q^p$ and $\gamma_{pq}^{rs}$ are the one- and two-body reduced density matrices:

$$\gamma_q^p = \langle \Psi | \, a_p^\dagger a_q \, | \Psi \rangle \,, \quad \gamma_{rs}^{pq} = \langle \Psi | \, a_p^\dagger a_q^\dagger a_s a_r \, | \Psi \rangle \,. \tag{2.17}$$

The information contained in $\boldsymbol{\lambda}_2$ can be distilled down to a single value metric via its Frobenius norm:

$$\|\boldsymbol{\lambda}_2\|_{\mathrm{F}} = \sqrt{\sum_{pqrs} |\lambda_{pq}^{rs}|^2}, \tag{2.18}$$

which captures both spin entanglement and Coulombic correlation effects,[127,129] and is null for a single determinant. The two-body density cumulant also has a direct connection to the number of effectively unpaired electrons, which itself has been used as a metric of correlation.[130–132] For two non-interacting fragments A and B with no interfragment spin entanglement, the *square* Frobenius norm is additive,[127,129] that is $\|\boldsymbol{\lambda}_2(\mathrm{A})\|_{\mathrm{F}}^2 + \|\boldsymbol{\lambda}_2(\mathrm{B})\|_{\mathrm{F}}^2 = \|\boldsymbol{\lambda}_2(\mathrm{A}\cdots\mathrm{B})\|_{\mathrm{F}}^2$, where "$\mathrm{A}\cdots\mathrm{B}$" indicates A and B at infinite separation. Therefore, in our comparison of the models we report the square Frobenius norm.

Moreover, the two body cumulant is directly related to the definition of the intrinsic correlation energy (ICE) proposed by Kutzelnigg.[10] By expressing the energy in terms of 1- and 2-RDMs and expanding the latter in terms of the two-body cumulants, one may rewrite the two-body contribution to the total energy as a sum of Coulombic, exchange, and correlation contributions, $E_2 = E_{\text{Coul}} + E_{\text{ex}} + E_{\text{ICE}}$. Here, $E_{\text{ICE}}$ is a pure two-body potential energy term which may be expressed using the two-body cumulant represented in coordinate space $[\lambda_2(1,2;1,2)]$ as

$$E_{\text{ICE}} = \frac{1}{4}\sum_{pqrs}\lambda_{rs}^{pq}\langle rs\|pq\rangle = \frac{1}{2}\int\frac{\lambda_2(1,2;1,2)}{r_{12}}d\tau_1 d\tau_2. \tag{2.19}$$

This intrinsic correlation energy has the advantage of being defined irrespective of a reference mean-field wave function.

*Spin correlation metrics*

We also characterize electronic states using various metrics based on the spin-spin correlation function as they are helpful n diagnosing spin frustration. The spin-spin correlation function ($A_{ij}$), defined as

$$A_{ij} = \langle\hat{\mathbf{S}}_i\cdot\hat{\mathbf{S}}_j\rangle - \langle\hat{\mathbf{S}}_i\rangle\cdot\langle\hat{\mathbf{S}}_j\rangle, \tag{2.20}$$

measures the irreducible correlation of total spin ($\hat{\mathbf{S}}_i$) for two localized spatial orbitals $\phi_i$ and $\phi_j$. In this work we employ Pipek–Mezey localized orbitals[133] to define spin-spin correlation metrics. We also compute the spin-spin correlation density $A_i(\mathbf{r})$, which can be used to graphically represent the spatial correlations of spin with respect to a localized orbital $\phi_i$. For well localized atomic orbitals, $A_i(\mathbf{r})$ can be approximated as

$$A_i(\mathbf{r}) = \langle\hat{\mathbf{S}}_i\cdot\hat{\mathbf{S}}(\mathbf{r})\rangle - \langle\hat{\mathbf{S}}_i\rangle\cdot\langle\hat{\mathbf{S}}(\mathbf{r})\rangle \approx \sum_j A_{ij}|\phi_j(r)|^2, \tag{2.21}$$

where $\hat{\mathbf{S}}(\mathbf{r})$ is the total spin operator in real space, $|\phi_j(r)|^2$ is the spatial density of the $j$-th orbital, and $A_{ij}$ are elements of the spin-spin correlation function.

Additionally, we consider three scalar metrics introduced in previous molecular spin

frustration studies: i) the sum of the absolute value of the spin-spin correlations $\langle S^2 \rangle_{\text{abs}}$,[134]

$$\langle S^2 \rangle_{\text{abs}} = \sum_{ij} |\langle \hat{\mathbf{S}}_i \cdot \hat{\mathbf{S}}_j \rangle|, \tag{2.22}$$

ii) the sum of the absolute value of the long range spin-spin correlations $\langle S^2 \rangle_{\text{abs,lr}}$,

$$\langle S^2 \rangle_{\text{abs,lr}} = \langle S^2 \rangle_{\text{abs}} - \sum_{i} |\langle \hat{\mathbf{S}}_i \cdot \hat{\mathbf{S}}_i \rangle| - 2 \sum_{\langle kl \rangle} |\langle \hat{\mathbf{S}}_k \cdot \hat{\mathbf{S}}_l \rangle|, \tag{2.23}$$

and iii) the sum of the nearest-neighbor spin-spin interactions $\langle S^2 \rangle_{\text{nn}}$,

$$\langle S^2 \rangle_{\text{nn}} = \sum_{\langle kl \rangle} \langle \hat{\mathbf{S}}_k \cdot \hat{\mathbf{S}}_l \rangle, \tag{2.24}$$

where $i$ and $j$ index all orbital sites, and $\langle kl \rangle$ is a double sum over nearest neighbor orbital sites.

*Metrics based on quantum information theory*

Metrics inspired by quantum information theory have also been recently used to investigate various phenomena related to strong correlation and entanglement,[135] and find several applications in computational chemistry.[118,119,136–138]

We consider two quantities, the single-orbital entanglement entropy (SOEE) and the total quantum information ($I_{\text{tot}}$), both of which can be derived from the 1- and 2-RDMs. The SOEE describes the entanglement of a spatial orbital $\phi_i$ with the remaining *bath* orbitals. For a given spatial orbital $\phi_i$, we can write four occupation patterns for the corresponding $\alpha$ and $\beta$ spin orbitals $|p\rangle \equiv \left| n_{i_\alpha} n_{i_\beta} \right\rangle \in \{|00\rangle, |01\rangle, |10\rangle, |11\rangle\}$, which we label with the index $p = 1,2,3,4$. The reduced density matrix $\rho^i_{pq} = \text{Tr}_{\text{bath}}[\langle p|\Psi\rangle\langle\Psi|q\rangle]$ is computed by projecting the wave function onto single-orbital configurations $|q\rangle$ and $|p\rangle$ of orbital $\phi_i$ and tracing out all other degrees of freedom. For states with fixed number of electrons, this

matrix is diagonal with elements given by

$$\rho^i_{11} = 1 - \gamma^{i^\alpha}_{i^\alpha} - \gamma^{i^\beta}_{i^\beta} + \gamma^{i^\alpha i^\beta}_{i^\alpha i^\beta}, \tag{2.25}$$

$$\rho^i_{22} = \gamma^{i^\alpha}_{i^\alpha} - \gamma^{i^\alpha i^\beta}_{i^\alpha i^\beta}, \tag{2.26}$$

$$\rho^i_{33} = \gamma^{i^\beta}_{i^\beta} - \gamma^{i^\alpha i^\beta}_{i^\alpha i^\beta}, \tag{2.27}$$

$$\rho^i_{44} = \gamma^{i^\alpha i^\beta}_{i^\alpha i^\beta}. \tag{2.28}$$

The SOEE of orbital $\phi_i$ is then computed as the Shannon entropy with respect to the four occupations

$$S_i = -\sum_{p=1}^{4} \rho^i_{pp} \ln\left(\rho^i_{pp}\right). \tag{2.29}$$

The total quantum information ($I_{\text{tot}}$) is given as the sum of the SOEEs for all spatial orbitals

$$I_{\text{tot}} = \sum_{i=1}^{L} S_i. \tag{2.30}$$

Large values of $I_{\text{tot}}$ indicate departure from integer orbital occupations and are associated with strong correlation effects.[139] We note, however, that the value of $I_{\text{tot}}$ is not invariant with respect to unitary rotations of the orbitals, and therefore, will depend on the type of orbital basis employed in a computation.

## 2.3 Computational details

The ground-state singlet energies and two-body density cumulants of the model systems were calculated using FCI, ACI, and DMRG. The ap-sCI and SVD-FCI wave functions were obtained from FCI wave functions as described in Sec. 2.2.2. All computations employed self consistent field (SCF) orbitals obtained with the open-source quantum chemistry package Psi4[140,141] and used a STO-6G basis set.[142] Canonical (delocalized) orbitals were computed using restricted Hartree–Fock (RHF). Localized orbitals were obtained by first performing a restricted open-shell Hartree-Fock (ROHF) computation using maximum multiplicity (e.g., $S = 5$ for $H_{10}$) and then localizing the orbitals with the Pipek–Mezey

(PM)[133] procedure (allowing rotations among all orbitals).

Computations based on canonical RHF orbitals were run in $D_{2h}$ symmetry for the $H_{10}$ chain, ring, and sheet and in $C_{2v}$ symmetry for the $H_{10}$ pyramid. The $H_{12}$, $H_{14}$, and $H_{16}$ analogs of the four systems were run with the same symmetry as their $H_{10}$ counterparts with the exception of the $H_{14}$ pyramid, which used $D_{2h}$ symmetry. All computations using localized orbitals were performed in $C_1$ symmetry.

MP2, CCSD, and CCSD(T) computations were performed using the PSI4, while V2RDM calculations employed the open source V2RDM-CASSCF plugin.[112] CR-CC(2,3) computations were performed using GAMESS.[143] FCI and ACI computations were performed using our open-source code FORTE.[144] All ACI computations included additional determinants to ensure spin completeness of the $\mathscr{P}$ and $\mathscr{Q}$ spaces. The rank-reduction procedure used for SVD-FCI and the *a posteriori* determinant screening procedure for ap-sCI were implemented in a development version of FORTE.

Density matrix renormalization group calculations were performed with CHEMPS2.[145] DMRG calculations associated with a particular final value of $M$ were preceded by three preliminary computations with smaller bond dimension and added noise. This procedure has been shown to make the overall DMRG calculation converge more rapidly and produce more accurate results.[78,146] In the first two preliminary computations $M$ is set to 150, 500, 500, and 500 (for $H_{10}$, $H_{12}$, $H_{14}$, and $H_{16}$ respectively) to build an initialization for the last two instructions with a larger value of $M$. In cases where the final value of $M$ is less than the values specified above, the same value of $M$ is used for the three preliminary calculations and for the final calculation. As mentioned already, due to the block structure of the DMRG tensors induced by symmetries, the final MPS in general does not correspond to a set of dense matrices of dimension $M^2$. For DMRG calculations using a localized basis, orbitals for the 1D chain and ring were ordered to be spatially consecutive. Localized orbitals for the 2D sheet and 3D pyramid systems used a Fiedler vector ordering derived from the two electron integrals to account fo physical proximity and orbital overlap.[82]

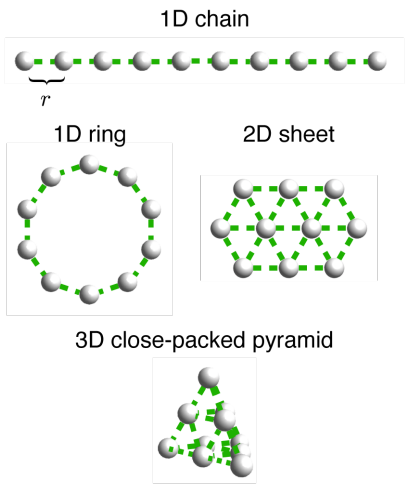


Figure 2.1: Structure of the $H_{10}$ model systems studied in this work. Geometries are parameterized by the nearest-neighbor H–H distance ($r$), indicated by green dashed lines.

For canonical MOs, orbitals were grouped into blocks by irreducible representation and (within each irreducible representation) ordered energetically. For calculations using $D_{2h}$ symmetry, the irreducible representation blocks were ordered as $A_g$, $B_{1u}$, $B_{3u}$, $B_{2g}$, $B_{2u}$, $B_{3g}$, $B_{1g}$, $A_u$ such that blocks corresponding to bonding and anti-bonding orbitals were adjacent on the DMRG lattice. This strategy has been shown to be successful for several DMRG studies[81,147–149] and is rationalized by quantum information principles.[119] For calculations using symmetries other than $D_{2h}$, the ordering of the irreducible representations followed Cotton's ordering.

## 2.4 Results

In this section we analyze the results of our study for the $H_{10}$ models. Fig. 2.1 shows the structure of the four $H_{10}$ model systems. The geometry of each model is controlled by a parameter $r$ which determines the nearest neighbor H–H distance (in Å). The geometries of all models, raw data for the potential energy curves, and energy errors are collected in a GitHub repository.[113]

The $r$ values considered here (0.75–2.0 Å) cover both the weak and strong electron correlation regimes of each model. This point can be quantified by estimating the $U/t$ ratio

Table 2.1: Properties of the singlet ground state of the four $H_{10}$ systems at different values of the H–H distance ($r$). Summary of correlation metrics: correlation energy ($E_{\text{corr}}$), the squared Frobenius norm of the two-body density cumulant ($\|\boldsymbol{\lambda}_2\|_{\text{F}}^2$), coupled-cluster amplitude diagnostics ($D_1$ and $D_2$), magnitude of the Hartree Fock coefficient in the normalized FCI expansion ($|C_{\text{HF}}|$), and total quantum information in a RHF canonical basis ($I_{\text{tot}}^{\text{d}}$) and a localized basis ($I_{\text{tot}}^{\text{l}}$). For the $H_{10}$ pyramid at $r = 2.0$ Å, the data reported correspond to an excited state adiabatically connected to the ground state at smaller values of $r$.

| System | $r$ / Å | $E_{\text{FCI}}$ / $E_{\text{h}}$ | $E_{\text{corr}}$ / $E_{\text{h}}$ | $E_{\text{ICE}}$ / $E_{\text{h}}$ | $\|\boldsymbol{\lambda}_2\|_{\text{F}}^2$ | $D_1$ | $D_2$ | $\|C_{\text{HF}}\|$ | $I_{\text{tot}}^{\text{d}}$ | $I_{\text{tot}}^{\text{l}}$ |
|---|---|---|---|---|---|---|---|---|---|---|
| $H_{10}$ 1D Chain | 0.75 | −5.228560 | −0.1082 | −0.2628 | 0.61 | 0.018 | 0.202 | 0.96 | 1.24 | 13.74 |
| | 1.00 | −5.415393 | −0.1678 | −0.4351 | 1.46 | 0.015 | 0.302 | 0.91 | 2.57 | 13.52 |
| | 1.50 | −5.036293 | −0.4038 | −1.0662 | 6.11 | 0.010 | 0.696 | 0.67 | 7.42 | 11.99 |
| | 2.00 | −4.790989 | −0.7912 | −1.6754 | 13.27 | - | - | 0.37 | 11.78 | 9.22 |
| $H_{10}$ 1D Ring | 0.75 | −5.151378 | −0.1026 | −0.2323 | 0.43 | 0.000 | 0.122 | 0.97 | 1.01 | 13.81 |
| | 1.00 | −5.422958 | −0.1475 | −0.3650 | 1.02 | 0.000 | 0.189 | 0.94 | 2.05 | 13.67 |
| | 1.50 | −5.048052 | −0.3616 | −1.0197 | 5.96 | 0.000 | 0.643 | 0.67 | 7.28 | 12.24 |
| | 2.00 | −4.794398 | −0.7678 | −1.6659 | 13.64 | - | - | 0.32 | 11.87 | 9.35 |
| $H_{10}$ 2D Sheet | 0.75 | −3.917633 | −0.1040 | −0.2325 | 0.35 | 0.008 | 0.107 | 0.98 | 0.85 | 13.65 |
| | 1.00 | −4.891538 | −0.1393 | −0.3262 | 0.71 | 0.014 | 0.159 | 0.95 | 1.58 | 13.56 |
| | 1.50 | −4.903192 | −0.2868 | −0.7820 | 2.85 | 0.038 | 0.337 | 0.79 | 5.47 | 12.92 |
| | 2.00 | −4.739235 | −0.6886 | −1.6949 | 9.22 | - | - | 0.21 | 12.36 | 9.44 |
| $H_{10}$ 3D Pyramid | 0.75 | −2.853673 | −0.1737 | −0.4151 | 1.13 | 0.015 | 0.320 | 0.93 | 1.77 | 13.54 |
| | 1.00 | −4.269379 | −0.2397 | −0.5811 | 2.28 | 0.031 | 0.486 | 0.84 | 3.13 | 13.40 |
| | 1.50 | −4.733459 | −0.4051 | −0.9765 | 3.54 | 0.067 | 0.635 | 0.62 | 6.88 | 12.67 |
| | 2.00* | −4.694062 | −0.7480 | −1.7252 | 3.59 | 0.093 | 0.685 | 0.25 | 12.62 | 9.48 |

of the Hubbard Hamiltonian:

$$\hat{H} = -t \sum_{i,\sigma} \left( \hat{a}_{i,\sigma}^{\dagger} \hat{a}_{i+1,\sigma} + \hat{a}_{i+1,\sigma}^{\dagger} \hat{a}_{i,\sigma} \right) + U \sum_{i} \hat{n}_{i\uparrow} \hat{n}_{i\downarrow}, \tag{2.31}$$

where $t$ and $U$ are obtained by fitting the excitations energies (for singlet and triplet states) of the Hubbard dimer to those of the $H_2$ molecule with bond length $r$. Using this approach, we find that $U/t$ ranges from about 0.94 at $r = 0.75$ Å to 8.55 at $r = 2.0$ Å.

### 2.4.1 Ground and low-lying electronic states

We have found a variety of interesting characteristics in the ground and low lying excited states of the $H_{10}$ model systems. Metrics of correlation for the ground state of the four $H_{10}$ systems as a function of the $r$ are reported in Tab. 2.1. As expected, the numbers show an increase in correlation as $r$ increases across all four systems. However, when comparing different systems, there are interesting discrepancies between the metrics. For example, at $r = 1.5$ Å the 1D chain has the second largest absolute value of $E_{\text{corr}}$ (0.4038 $E_{\text{h}}$), the

largest absolute value of intrinsic correlation energy (1.066 $E_\mathrm{h}$), a high $\|\boldsymbol{\lambda}_2\|_F^2$ value (6.11), and the largest $D_2$ value (0.70); however, this system unexpectedly displays a relatively large weight of the Hartree–Fock determinant ($|C_\mathrm{HF}| = 0.67$). A comparison of the ring with the chain, shows that the former is slightly less correlated than the latter. In the case of the 2D sheet at $r = 1.5$ Å, all metrics of correlation indicate that this system has the smallest degree of electron correlation. In contrast, the 3D pyramid displays the strongest correlation effects, yielding the largest absolute value of $E_\mathrm{corr}$ (0.4051 $E_\mathrm{h}$), a large intrinsic correlation energy (0.9765 $E_\mathrm{h}$), and the smallest HF determinant weight ( $|C_\mathrm{HF}| = 0.62$). However, strong correlation in the 3D system is not reflected in the value of $\|\boldsymbol{\lambda}_2\|_F^2$ (3.54), which is smaller than that of both 1D systems ($\approx 6$). The quantum information metric (in a delocalized basis) $I_\mathrm{tot}^\mathrm{d}$ paints a similar picture: the pyramid total information lies in between that of the 1D systems and the less correlated 2D system. However, in a localized basis, the same metric $I_\mathrm{tot}^\mathrm{l}$ decreases for all systems as a function of $r$. This behavior is interesting as it suggests that quantum information metrics could potentially be useful for choosing orbitals to use with various approximate methods. As discussed in more detail in Sec. 2.4.2, the low value of $\|\boldsymbol{\lambda}_2\|_F^2$ observed for the 3D pyramid is likely a consequence of spin frustration, which results in a rapid decay of spin correlation functions. We also note that after $r = 1.5$ Å the ground state of the 3D pyramid crosses several low-lying singlet states and by $r = 2.0$ Å it corresponds to the third excited state of $A_g$ symmetry.

The small discrepancies observed in the various metrics can be owed to the fact that they measure different aspects of correlation. While $E_\mathrm{corr}$ and $|C_\mathrm{HF}|$ quantify the deficiency of the mean-field treatment (measured in both energetic and wave function terms), quantities like $\|\boldsymbol{\lambda}_2\|_F^2$ and $I_\mathrm{tot}$ capture only statistical aspects of correlation. The intrinsic correlation energy ($E_\mathrm{ICE}$) appears to offer a good compromise between the mean-field and statical measures of correlation; nevertheless, its value is significantly larger than the $E_\mathrm{corr}$ values and captures contributions due to Coulomb repulsion (i.e., absent Coulomb repulsion, $E_\mathrm{ICE}$ is zero even for a correlated state). The $D_1$ and $D_2$ metrics measure the importance of orbital

rotations ($D_1$) and correlation effects ($D_2$) in the CCSD wave function. In particular, since $D_1$ is not directly related to electron correlation, its behavior is very different from that of $D_2$, with the latter growing with $r$ in all models. In contrast, $D_1$ decreases in the 1D chain, it is identically zero in the 1D ring due to the different symmetry of singly excited determinants, and it grows with $r$ in the 2D and 3D models.

Another common approach to diagnose the onset of strong correlation is symmetry breaking of the Hartree–Fock solution. The Coulson–Fischer point (here defined in terms of the restricted $\rightarrow$ unrestricted symmetry breaking) of the chain and ring models is found at $r = 0.85$ Å and 1.05 Å, respectively. Consistent with the lower degree of correlation in the 2D sheet, the corresponding UHF solution exhibits spin-contamination at a point farther out in the dissociation curve (1.35 Å). Instead, the 3D pyramid exhibits symmetry breaking at the smallest distance (0.70 Å) compared to the other three systems.

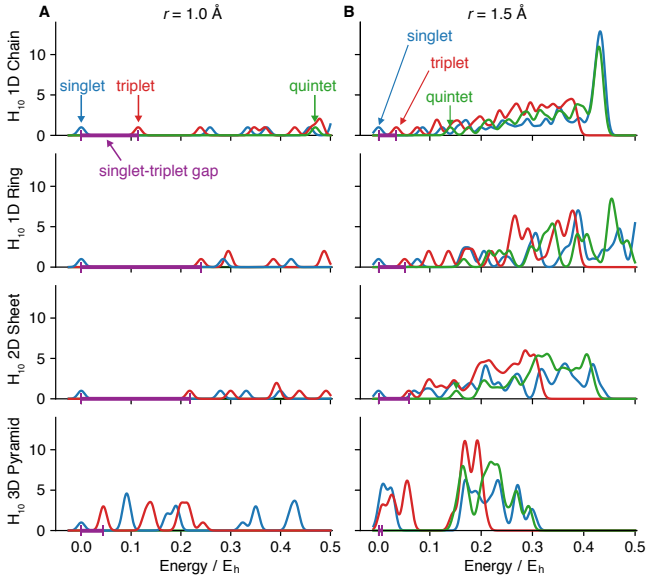


Figure 2.2: Density of states with fixed electron number convoluted with a Gaussian function [$D_g(E)$, defined in Eq. (2.32)] computed from the 50 lowest singlet, triplet, and quintet states of the $H_{10}$ systems at an H–H distance (A) $r$ = 1 Å and (B) $r$ = 1.5 Å. The density of states was convoluted with a Gaussian function of exponent $\alpha = 10^5\ E_h^{-2}$.

Lastly, we characterize the strength of correlations by computing the density of states (DOS) with fixed particle number [$D(E)$]. For convenience, we convolute the density of

states with a Gaussian function of exponent $\alpha$ and shift the energies by the ground state energy ($E_0$). This convoluted DOS is expressed in terms of excitation energies $\Delta E_i = E_i - E_0$, where $E_i$ are energies of singlet, triplet, and quintet electronic excited states, and it is given by

$$D_g(E) = \sum_i \exp\left(-\alpha(\Delta E_i - E)^2\right). \tag{2.32}$$

Note that this quantity is different from the DOS computed for electron attached/detached states.

Figure 2.2 shows the energy spectra in the range 0–0.5 $E_\mathrm{h}$ (0–13.6 eV) relative to the ground state from computations of the lowest 50 singlet, triplet, and quintet states of the $H_{10}$ systems. At shorter bond lengths ($r = 1.0$ Å), the 1D and 2D systems show large gaps between the ground state and the lowest triplet state. However, this gap closes significantly in the 3D pyramid to ca. 0.044 $E_\mathrm{h}$. At longer bond lengths ($r = 1.5$ Å), the singlet-triplet gap decreases for all systems. Interestingly, the 3D pyramid shows an almost zero gap (ca. 0.007 $E_\mathrm{h}$) and several singlet near-degenerate states accumulate near the ground state.

### 2.4.2 Spin correlation and frustration

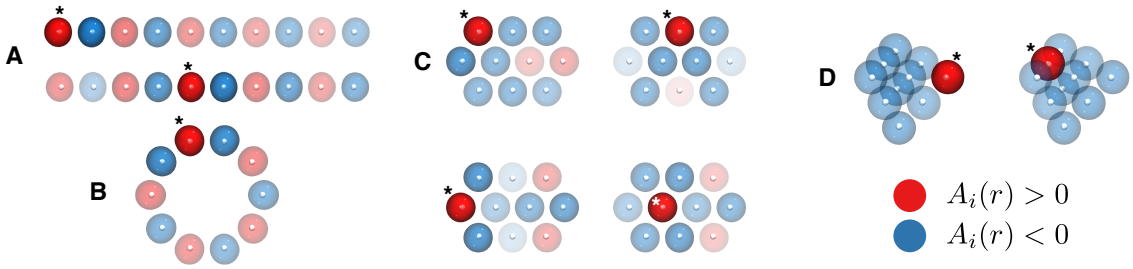


Figure 2.3: Spin correlation density $A_i(\mathbf{r})$ of the $H_{10}$ models at an H–H distance $r = 1.25$ Å plotted for (A) the edge and central localized MO sites of the hydrogen chain, (B) the symmetry unique site of the hydrogen ring, (C) the four symmetry unique sites of the $H_{10}$ sheet, and (D) the two symmetry unique sites of the $H_{10}$ pyramid. Positive and negative values of $A_i(\mathbf{r})$ are indicated in red and blue, respectively, and in each plot the localized orbital $\phi_i$ is denoted by an asterisk.

We have found that there are signs of spin frustration in the 2D sheet and 3D pyramid models. Frustration is indicated by the inability to satisfy antiferromagnetic interactions—

a condition which is not mathematically rigorous but that has, nonetheless, been used to define systems as spin frustrated[150]—and the lack of long range antiferromagnetic ordering beyond nearest-neighbor interactions.

The spin-spin correlation densities shown in Fig. 2.3 A and B indicate clear antiferromagnetic ordering beyond nearest neighbors in the 1D chain and ring. Each localized spin is anti-correlated with its nearest neighbor, as depicted by the adjacent red and blue shading. Fig. 2.3 C shows spin-spin correlation density for the four symmetry unique sites in the 2D sheet. In contrast to the 1D models, it can be seen that there is no way to simultaneously satisfy all antiferromagnetic interactions for the 2D sheet, and consequentially, spin correlations decay more rapidly. This is also the case for the 3D pyramid (see Fig. 2.3 D), for which each site is anti-correlated with all other sites, suggesting no antiferromagnetic ordering beyond nearest neighbors. Tab. 2.2 summarizes spin correlation properties for the $H_{10}$, $H_{12}$, and $H_{14}$ systems at $r = 1.5$ Å. As is the case with the 2-body cumulant norm, the $H_{10}$ 1D chain and ring systems have larger absolute spin correlation $\langle S^2 \rangle_{\text{abs}}$ (17.42 and 18.66, respectively) than the 2D or 3D systems (11.55 and 10.86, respectively). The short-range nature of spin correlation of the 2D and 3D $H_{10}$ systems is also indicated by their smaller value of $\langle S^2 \rangle_{\text{abs,lr}}$ (2.46 and 3.04), compared to the 1D systems (5.25 and 6.51, for the chain and ring respectively). These results are consistent with the spin correlation density analysis in Figs. 2.3. We note that the scaling of $\langle S^2 \rangle_{\text{abs}}$ and $\langle S^2 \rangle_{\text{abs,lr}}$ with $n$ for the sheet and pyramid systems is (in most cases) linear or super-linear, which is not expected for systems absent of long range spin ordering. However, this is likely because the lattice sizes considered are still relatively small, and the addition of two hydrogens at a time does not extend the lattices in a completely uniform manner, thus altering (possibly greatly) the frustrated character. It is also possible to observe a lack of long-range correlation and ordering for the 2D sheet and 3D pyramid by considering the radial distribution of spin-spin correlations and absolute spin-spin correlations.

It is evident from the various metrics of correlation, the DOS plots, and our analysis of

Table 2.2: Ground-state of the four $H_n$ systems at an H–H distance $r = 1.50$ Å. Sum of the absolute value of the spin-spin correlations ($\langle S^2 \rangle_{\text{abs}}$), the sum of the absolute value of the long range spin-spin correlations ($\langle S^2 \rangle_{\text{abs,lr}}$), and the sum of the nearest neighbor spin-spin interactions ($\langle S^2 \rangle_{\text{nn}}$). See Eqs. (2.22)–(2.24) for the definition of these metrics.

| System | $n$ | $\langle S^2 \rangle_{\text{abs}}$ | $\langle S^2 \rangle_{\text{abs,lr}}$ | $\langle S^2 \rangle_{\text{nn}}$ |
|---|---|---|---|---|
| | 10 | 17.42 | 5.25 | −3.10 |
| $H_n$ Chain | 12 | 21.77 | 7.18 | −3.72 |
| | 14 | 26.29 | 9.27 | −4.35 |
| | 10 | 18.66 | 6.51 | −3.16 |
| $H_n$ Ring | 12 | 24.13 | 9.39 | −3.84 |
| | 14 | 28.95 | 11.91 | −4.42 |
| | 10 | 11.55 | 2.46 | −1.94 |
| $H_n$ Sheet | 12 | 14.31 | 2.59 | −2.66 |
| | 14 | 17.16 | 3.63 | −3.06 |
| | 10 | 10.86 | 3.04 | −1.19 |
| $H_n$ Pyramid | 12 | 18.06 | 4.02 | −3.63 |
| | 14 | 18.30 | 5.94 | −2.40 |

spin correlation, that the $H_{10}$ lattices display a broad range of correlation regimes. Therefore, we believe it is important to consider the 2D and 3D models in future benchmarks of electronic structure methods because they capture some aspect of the physics of spin frustration that are not displayed by 1D hydrogen models.

### 2.4.3 Performance of sCI, SVD-FCI, and DMRG

Having characterized the nature of the ground state of the $H_{10}$ models we now proceed to analyze the efficiency with which sCI, SVD-FCI, and DMRG approximate the wave functions of these systems.

In Fig. 2.4 we plot the energy error $[E_X(N_{\text{par}}) - E_{\text{FCI}}]$ as a function of the number of variational parameters for the $H_{10}$ systems in the regime of strong electron correlation ($r = 1.5$ Å). The accuracy volume may be obtained from these plots by finding the number of parameters corresponding to a 1 m$E_{\text{h}}$ error. When using canonical orbitals, we see that DMRG affords the most compact representation, although $\mathscr{V}_{\text{ap-sCI}}$ and $\mathscr{V}_{\text{ACI+PT2}}$ are within a factor of 1.5–2 of $\mathscr{V}_{\text{DMRG}}$. ACI without the PT2 correction always requires more variational parameters to match the accuracy of ap-sCI and ACI+PT2, and $\mathscr{V}_{\text{ACI}}$ is 2–3 times $\mathscr{V}_{\text{DMRG}}$.

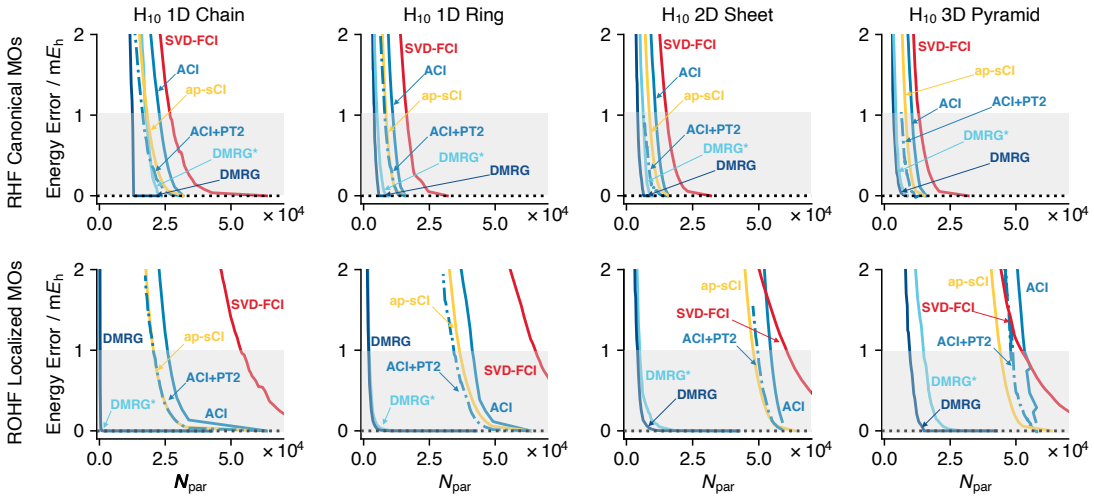


Figure 2.4: Ground-state of the four $H_{10}$ models at an H–H distance $r = 1.5$ Å. Energy error with respect to FCI vs. number of parameters ($N_{\text{par}}$) of approximate methods. The gray shaded region represents chemically accurate energies (error less than $1\text{m}E_{\text{h}}$).

For all four $H_{10}$ systems, SVD-FCI exhibits the worst efficiency, although only by a small margin, such that $\mathscr{V}_{\text{SVD-FCI}}$ is 2–4 times greater than $\mathscr{V}_{\text{DMRG}}$. Note that we include two sets of results for DMRG: the lowest energy eigenvalue found during all DMRG sweep optimizations (labeled DMRG, see Ref. 145 for details), and the energy obtained from the reduced density matrices of the final MPS (indicated with DMRG*). When a large bond number $M$ is used, the two energy values are nearly identical, but for smaller values of $M$, the DMRG* value may be slightly higher than the DMRG one.

When using localized orbitals, we see that DMRG again produces the most compact representation and by a much larger margin for all four $H_{10}$ systems. In particular, for the 1D chain $\mathscr{V}_{\text{DMRG}}$ is two orders of magnitude lower than all other methods. Comparing the accuracy volume of DMRG with different orbital bases, one notices that the localized basis is more efficient in the 1D systems, while the delocalized basis leads to smaller $\mathscr{V}_{\text{DMRG}}$ for the 3D model. For the 2D model, the localized and canonical basis yield comparable $\mathscr{V}_{\text{DMRG}}$ values. The advantage of using canonical orbitals is inconsistent with previous findings,[82] and it is likely due to the size of the systems considered here. In this case, the compression afforded by using a localized basis is outweighed by the advantages of using

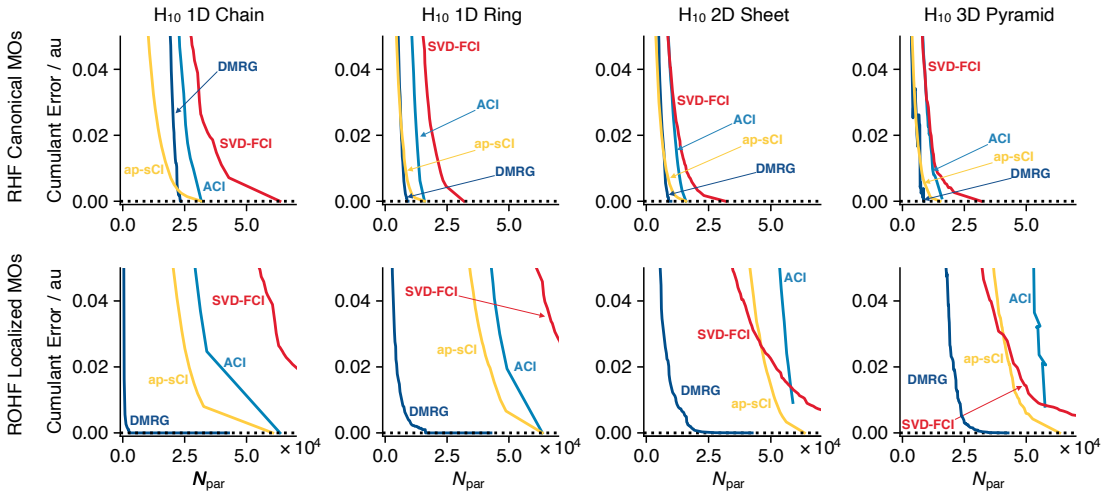


Figure 2.5: Ground-state of the four $H_{10}$ models at an H–H distance $r = 1.5$ Å. Density cumulant error $\|\Delta\boldsymbol{\lambda}_2\|_F$ with respect to FCI vs. number of parameters ($N_{\text{par}}$) of approximate methods.

point group symmetry. When comparing results across canonical and localized orbitals for the other methods, we find that the accuracy volume is always smaller in the delocalized basis, so there is no advantage to orbital localization. This is in agreement with past observations[100] that localization is beneficial for sCI methods only after a certain system size is reached. It is interesting to observe that the accuracy volume for DMRG and sCI mirrors the behavior of the total quantum information for both delocalized and localized bases (see Tab. 2.1), suggesting that this metric may be useful for determining the best orbital basis to use at a given geometry.

We note that for the sheet and pyramid, there are a few values of $\sigma$ for which the ACI results do not converge monotonically and lead to small bumps. We have also encountered cases where the iterative ACI algorithm finds the first excited state due to near-degeneracies, an issue that may be resolved using a state-averaged version of the method.[42] These incorrect energies were not included in Fig. 2.4.

Fig. 2.5 shows plots of $N_{\text{par}}$ vs. the two-body cumulant error $\|\Delta\boldsymbol{\lambda}_2\|_F$ for the four $H_{10}$ systems at $r = 1.5$ Å. These plots do not include ACI+PT2 results since second-order corrections to the ACI 1- and 2-RDMs were not available. We find similar trends for the

Table 2.3: Accuracy volume ($\mathscr{V}_X$) computed for the ground state of the $H_{10}$ models for various methods. Values are reported for both localized and delocalized molecular orbital bases. The Hilbert space size ($|\mathscr{H}_N|$) for all models in $C_1$ symmetry is 63504. Hilbert space sizes with the largest abelian symmetry exploited in the computations are reported in the table. ACI+PT2 values with a $<$ sign indicate that the energy error with the reported number of parameters is significantly lower than 1.0 m$E_h$. Finding more precise values of $\mathscr{V}_X$ for ACI+PT2 is challenging as the energy error is not monotonic as a function of $\sigma$.

| | | | Delocalized (RHF Canonical) | | | | | Localized (Pipek–Mezey) | | | | |
|---|---|---|---|---|---|---|---|---|---|---|---|---|
| System | $\lvert\mathscr{H}_N\rvert$ | $r$ / Å | ap-sCI | ACI | ACI+PT2 | SVD-FCI | DMRG | ap-sCI | ACI | ACI+PT2 | SVD-FCI | DMRG |
| 1D Chain | 31752 ($D_{2h}$) | 0.75 | 1491 | 2066 | <335 | 5292 | 2600 | 41872 | 46882 | 45052 | 10584 | 468 |
| | | 1.00 | 5122 | 6978 | <2156 | 10584 | 4896 | 35962 | 42332 | 39510 | 21168 | 388 |
| | | 1.25 | 11201 | 14231 | 7347 | 17136 | 9598 | 29148 | 35306 | 30732 | 34272 | 376 |
| | | 1.50 | 18176 | 22989 | 16356 | 26964 | 12674 | 20424 | 26008 | 20564 | 53928 | 176 |
| 1D Ring | 15912 ($D_{2h}$) | 0.75 | 577 | 873 | <181 | 2784 | 740 | 53358 | 56244 | 53448 | 11088 | 3359 |
| | | 1.00 | 2019 | 2803 | 663 | 5328 | 1522 | 49982 | 53364 | 50084 | 21168 | 3164 |
| | | 1.25 | 4791 | 6384 | 2701 | 9492 | 2663 | 45452 | 49537 | 43486 | 37800 | 2688 |
| | | 1.50 | 8520 | 11056 | 7895 | 16296 | 4034 | 36450 | 41254 | 34134 | 65016 | 1884 |
| 2D Sheet | 15912 ($D_{2h}$) | 0.75 | 766 | 1102 | <218 | 2532 | 1117 | 53252 | 59470 | 58050 | 10080 | 4649 |
| | | 1.00 | 1899 | 2809 | <718 | 4296 | 1853 | 51822 | 58256 | 56252 | 17136 | 4071 |
| | | 1.25 | 4139 | 5283 | 3478 | 7848 | 2626 | 50318 | 57036 | 53852 | 31248 | 4113 |
| | | 1.50 | 8667 | 11122 | 6468 | 15156 | 4218 | 47916 | 54466 | 49540 | 60480 | 4192 |
| 3D Pyramid | 15912 ($C_{2v}$) | 0.75 | 1478 | 2115 | <787 | 4044 | 1630 | 44062 | 56232 | 55452 | 16128 | 10832 |
| | | 1.00 | 2755 | 3605 | <1607 | 7056 | 2250 | 45812 | 55986 | 55078 | 28224 | 12556 |
| | | 1.25 | 4997 | 6530 | 2869 | 9864 | 2927 | 45844 | 56348 | 52728 | 39312 | 10998 |
| | | 1.50 | 8097 | 10519 | 6457 | 13152 | 3495 | 43932 | 53280 | 48580 | 52416 | 9489 |

efficiency to represent $\boldsymbol{\lambda}_2$ as we do for the energy, with the caveat that in a canonical basis, ap-sCI generally gives the best compression efficiency. It can be seen that with canonical orbitals, ap-sCI actually preserves the accuracy of the two-body density cumulant after compression better than DMRG does for the 1D chain, and similarly to DMRG for the other three systems. There is also a larger disparity in the performance of ap-sCI and ACI for cumulant compression performance, which can be attributed to two reasons. First, ACI adds additional determinants at each iteration to ensure spin completeness (the compressed ap-sCI wave function is not guaranteed to be an eigenfunction of spin). Second, ACI selects determinants according to their energetic contribution, and not explicitly their contribution to the wave function. SVD-FCI is the least efficient in compressing the wave function for the 1D systems, but does nearly as well as ACI for the 2D sheet and 3D pyramid. However, it possible that if variational optimization is used for SVD-FCI the cumulant error may increase, similarly to the behavior observed for ACI. When using localized orbitals, it can

be seen that DMRG likewise shows the best compression efficiency with respect to $\|\Delta\boldsymbol{\lambda}_2\|_{\mathrm{F}}$, especially for the 1D chain and ring systems.

As shown in Tab. 2.1 of Sec. 2.4.1, the degree of correlation for all models increases as the H–H distance $r$ becomes larger. In Tab. 2.3 we can see that in a delocalized basis the complexity of the wave function, as gauged by $\mathscr{V}_X$, also increases as $r$ becomes larger, such that all methods require a larger number of parameters to achieve chemical accuracy. In a localized basis $\mathscr{V}_{\mathrm{DMRG}}$, $\mathscr{V}_{\text{ap-sCI}}$, and $\mathscr{V}_{\mathrm{ACI}}$ decrease with increasing $r$, suggesting that these methods can exploit the local character of correlation, although in most cases not enough to outweigh the benefits of symmetry-adapted delocalized orbitals. In a delocalized basis, we note that for small values of $r$ the ACI+PT2 produces very accurate results with very few parameters, outperforming DMRG using just a few hundred determinants. It is interesting to note that compression efficiency for SVD-FCI decreases dramatically as $r$ increases, suggesting that the method is not able to take advantage of local correlation. Additionally, it can be seen that at more contracted geometries (smaller values of $r$), there is less of a disparity between the compression performance of the various approaches.

### 2.4.4 Comparison with other electronic structure methods

It is interesting to use the $\mathrm{H}_{10}$ models to benchmark the robustness and accuracy of conventional methods that employ a fixed number of parameters. Fig. 2.6 compares the energy errors relative to FCI for RHF, MP2, CCSD, CCSD(T), CR-CC(2,3), V2RDM with the two-body positive-semidefinite P, Q, and G conditions (V2RDM-PQG), and V2RDM-PQG with additional three-body positive semidefinite $\mathrm{T}_2$ conditions (V2RDM-PQGT2). RHF deviates significantly from FCI for all four systems, even near the $\mathrm{H}_2$ equilibrium geometry ($r_e = 0.74$ Å), where it gives errors of approximately 80–100 m$E_{\mathrm{h}}$. MP2 reduces the energy error near $r_e$ to about 10 m$E_{\mathrm{h}}$. While the RHF and MP2 energies do not diverge, they do not capture the dissociation of the $\mathrm{H}_{10}$ systems even qualitatively, giving energy errors well over 100–200 m$E_{\mathrm{h}}$ for $r \geq 1.6$ Å.

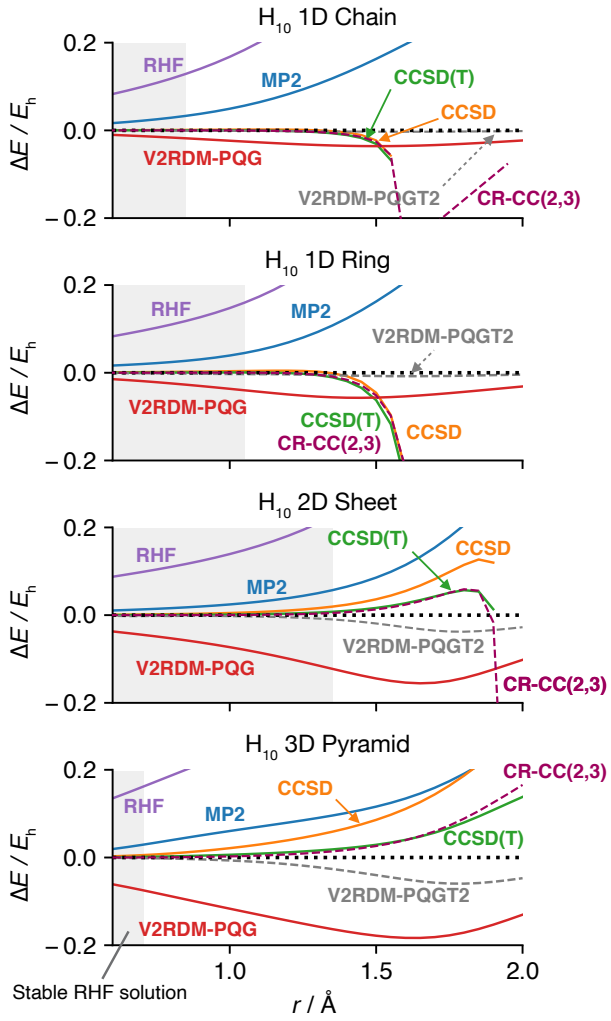


Figure 2.6: Ground-state potential energy curves of the four $H_{10}$ models. Energy error ($\Delta E$) with respect to FCI for various electronic structure methods as a function of the H–H distance ($r$). The gray shaded region indicates the range of $r$ for which the restricted Hartree–Fock solution is stable.

The three coupled cluster variants—CCSD, CCSD(T), and CR-CC(2,3)— achieve chemical accuracy for the 1D chain and ring systems for $r \leq 1.0$ Å, and diverge beginning around $r \geq 1.5$ Å, past the Coulson–Fisher point. Performance for CCSD, CCSD(T), and CR-CC(2,3) is slightly worse for the 2D sheet and 3D pyramid, where chemical accuracy is only achieved for $r \leq 0.75$ Å, and divergence is seen once again at larger values of $r$. For all four systems, when $r > 1.25$ Å, the magnitude of the HF coefficient $|C_{\text{HF}}|$ in the FCI wave function is less (or significantly less) than 0.9. It is worth mentioning here, however, that a handful of hydrogen systems have been investigated with variants of CC

that provide stable results relative to the examples in Fig. 2.6. Namely, the paired coupled cluster doubles (pCCD)[151] and the singlet pCCD (CCD0).[152]

The V2RDM approaches achieve the best descriptions of the potential energy surfaces compared to the other methods used in this section. Enforcing the PQG conditions during the optimization gives a good qualitative description of the dissociations, but still produces large quantitative errors in the range of 10–50 m$E_\mathrm{h}$ for the 1D chain and ring systems and 50–200 m$E_\mathrm{h}$ errors for the 2D sheet and 3D pyramid. Enforcing the additional T2 condition improves the V2RDM results significantly, such that energy errors for the chain and ring systems at $r = 1.50$ Å are 3.0 m$E_\mathrm{h}$ and 7.4 m$E_\mathrm{h}$, respectively. It can be seen, however, that for the 2D sheet and 3D pyramid, V2RDM-PQGT2 fails to produce chemically accurate results by a large margin, with errors of the order of 10–50 m$E_\mathrm{h}$ at stretched geometries. Interestingly, the performance of V2RDM is far less sensitive to $r$ than RHF, MP2, or CC as indicated by smaller values of nonparallelism error (the maximum error minus the minimum error over the entire range of $r$). Additionally, the error for V2RDM has a maximum in the re-coupling region ($r \approx 1.5$ Å), while all other methods generally decrease in accuracy with increasing $r$.

## 2.5 Scaling of the accuracy volume and size consistency

In this section we discuss some of the formal properties of the methods and present numerical results concerning scaling of the accuracy volume and size consistency. We begin by comparing the scaling with respect to system size. sCI may be considered a zero-dimensional ansatz, in the sense that it is particularly efficient in the description of few electrons in many virtual orbitals, especially due to the PT2 correction. If one demands that the sCI energy is size consistent for a set non-interacting fragments $A \cdots B \cdots C \cdots$, one concludes that the number of parameters grows as $N_A N_B N_C \ldots$. In other words, the sCI accuracy volume (per electron) grows exponentially with the number of electrons $N$ (albeit with a smaller prefactor than FCI), $\mathcal{V}_\mathrm{sCI} \propto \exp(N)$. In practice we find this to be the

case for ACI using localized orbitals. To achieve an accuracy of approximately $10^{-4}$ $E_\mathrm{h}$ per electron for a system of five non-interacting $H_2$ molecules requires 2380 parameters, rather than the 20 parameters required by a product state built from solutions for each $H_2$ molecule.

Our analysis also suggests that the SVD-FCI approach suffers from exponential growth of the accuracy volume (independently from dimensionality), although, to the best of our knowledge a formal analysis has not been reported. Even in the best case scenario, the number of parameters for a rank 1 SVD-FCI approximation scales as $N_{\text{SVD-FCI}} \propto 2\sqrt{N_{\mathscr{H}}}$, which implies $\mathscr{V}_{\text{SVD-FCI}} \geq 2\sqrt{N_{\mathscr{H}}}$. We likewise observe that for the same system of dissociated hydrogens, SVD-FCI requires 14616 parameters to achieve approximately $10^{-4}$ $E_\mathrm{h}$ per electron. Like the result for sCI, this indicates that SVD-FCI with a fixed number of parameters is not size consistent.

In the case of a DMRG, a MPS with bond dimension $M$ can describe a system with entanglement entropy $S$ bound by the condition $S \leq \log_2 M$,[75] or equivalently, $\exp(S) \leq CM$, with $C$ a constant. For gapped systems of dimensionality $D$ that satisfy an area law, the entanglement entropy is expected to scale as $S \propto L^{D-1}$ (plus logarithmic corrections for non-gapped systems), where $L$ is the length scale of the system.[153] Therefore, in DMRG the bond dimension $M$ scales at most as $\exp\left(\gamma L^{D-1}\right) \propto \exp\left(\gamma N^{(D-1)/D}\right)$. Similarly, we estimate that the accuracy volume of DMRG scales as $\mathscr{V}_{\text{DMRG}} \propto NM^2 = N\exp\left(2\gamma N^{(D-1)/D}\right)$. For one dimensional systems ($D = 1$) $\mathscr{V}_{\text{DMRG}}$ is independent of system size and the ground state can be well approximated by a finite bond dimension. Beyond one dimension, this analysis suggests that the DMRG bond dimension grows exponentially. However, for $D = 2$, DMRG is already exponentially more efficient than sCI since $\mathscr{V}_{\text{DMRG}} \propto N\exp\left(2\gamma N^{1/2}\right)$. This in practice implies that DMRG is still applicable without exponential cost to both one-dimensional and "thin" two-dimensional problems.[154]

DMRG is formally size consistent, giving additively separable energies for non-interacting fragments $A \cdots B$, so long as the orbitals are localized on either $A$ or $B$.[79,115]

If the orbitals in the DMRG lattice are ordered by subsystem ($[A \cdots B]$) then the wave function for noninteracting fragments becomes a product state of the MPS on $A$ and $B$. Then a MPS obtained by concatenating the MPS of $A$ and $B$ with a bond of dimension one ($M = 1$) is sufficient to represent the product state and satisfy size consistency. This implies that the $\mathcal{V}_{\mathrm{DMRG}}^{A+B}$ for a system of non-interacting fragments is approximately equal to $\mathcal{V}_{\mathrm{DMRG}}^{A} + \mathcal{V}_{\mathrm{DMRG}}^{B}$. In practice we have found this to be nearly true, a product state for a system of five non-interacting $H_2$ molecules has 20 parameters, and DMRG can reproduce the FCI energy exactly with a bond dimension as small as $M = 3$ (with 60 parameters). In principle DMRG should be able to achieve this result already with $M = 2$, but we find that instead it converges to a local minimum rather than the FCI energy.

Finally, we present numerical results for the scaling with system size of the accuracy volume for analogous of our four model systems with upt to up to sixteen hydrogens. In Fig. 2.7, we plot the accuracy volume for $n$ = 10, 12, 14, 16 at $r = 1.5$ Å, corresponding to absolute energy errors of 1.0, 1.2, 1.4, and 1.6 m$E_{\mathrm{h}}$, respectively. For comparison, we have also included the size of the FCI space (in $C_1$ symmetry) and a curve with $n^4$ scaling, which is proportional to the number of Hamiltonian matrix elements. We note that the ground states of the $H_{12}$ ring, $H_{16}$ ring, and $H_{16}$ sheet have symmetries ($B_{1\mathrm{g}}$), ($B_{1\mathrm{g}}$), and ($B_{3\mathrm{u}}$), respectivly, different from that of all other systems ($A_{\mathrm{g}}$). Additionally, we note a small dip in the curve for the 3D systems at 14 hydrogens, which we attribute to the different symmetry used for that lattice, $D_{2\mathrm{h}}$ as opposed to $C_{2\mathrm{v}}$. It can be seen that DMRG again provides the best compression of the wave function as measured by the accuracy of the energy for different systems sizes. In a localized basis, a polynomial fit of $\mathcal{V}_{\mathrm{DMRG}}$ as a function of the number of hydrogens ($n$) gives a scaling proportional to $n^{2.1}$ for the chain and $n^{3.3}$ for the ring, demonstrating the advantage of this methods for one-dimensional systems. It is also worth pointing out that for the larger systems ($H_{12}$–$H_{16}$), it is advantageous (though still exponentially scaling) to use localized orbitals with DMRG even for the 2D systems. This result is consistent with other DMRG studies comparing

localized vs. canonical orbitals for finite 2D arene systems.[82] For all the other methods, $\mathscr{V}_X$ in a delocalized basis appears to scale exponentially with a prefactor smaller than that of FCI.

It may be helpful to the reader to note that for all the systems considered here we find that in many cases the FCI computations are still faster than ACI and DMRG even up to 16 electrons. On a single node, FCI computations run in about 1 second up to 3 hours for the $H_{10}$–$H_{16}$ systems, whereas the implementation of DMRG used in this work can take up to 1–2 days on a single node for the more challenging 2D and 3D systems. We observe the most striking difference in the case of DMRG applied to the 1D systems, where even a very accurate computation in a localized basis can take on the order of 1 second even for $H_{16}$.

## 2.6 Conclusions and future work

This work accomplishes two main goals. Firstly, we propose a series of benchmark hydrogen models with a tunable degree of correlation that cover a wide range of electronic structures. These include 1D hydrogen chains and rings with antiferromagnetic ground states, a 2D triangular lattice (sheet) with spin frustrated interactions, and a 3D pyramid system that displays both spin frustration and a vanishing energy gap (dense manifold of near-degenerate states). We analyze these systems with various correlation metrics and by computing their low-energy spectra and spin-spin correlation functions. The models are found to have drastically different electronic structures depending on the physical dimension. In particular, since 2D and 3D systems exhibit some of the fingerprints of spin frustration and they are not efficiently approximated with MPS, they nicely complement benchmark sets based on 1D lattices. Our comparison of different metrics of correlation also highlights the importance of using multiple descriptors to characterize electronic states, as our results clearly show that they measure different aspects of correlation.

Secondly, using the hydrogen models, we compare the performance of selected CI,

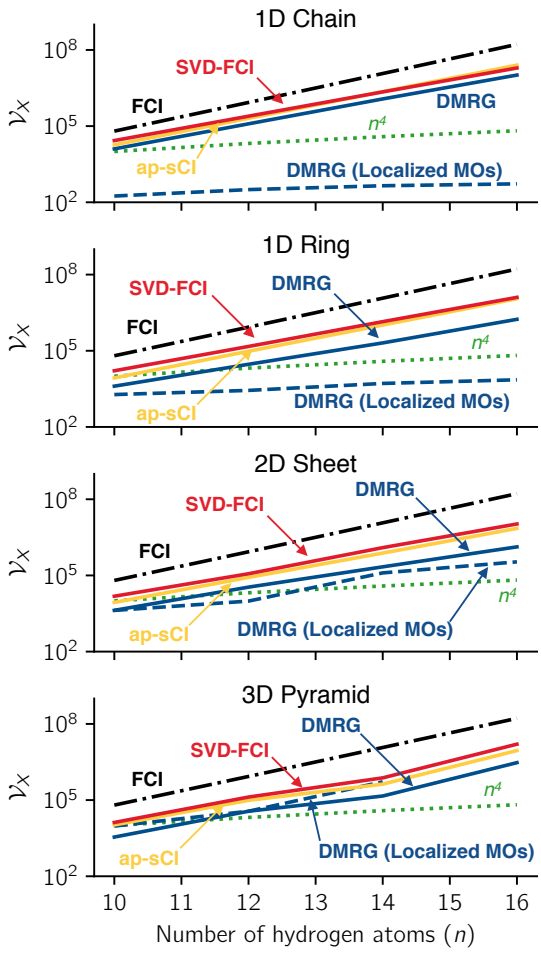


Figure 2.7: Accuracy volume ($\mathcal{V}_X$) for various approximate methods as a function of the number of number of hydrogen atoms ($n$) for the four $H_n$ models. For comparison we also report the number of FCI determinants (in $C_1$ symmetry) and the curve $n^4$. The 12, 14, and 16 hydrogen chains, rings, sheets, and pyramids are extensions of the $H_{10}$ models in that the additional hydrogens are placed within the same lattice structure. Unless otherwise noted, all results employ canonical RHF orbitals.

SVD-FCI, and DMRG in various regimes of strong electron correlation. We focus in particular on determining the ability of each method to efficiently compress the information content of the FCI wave function. To quantify this property, we introduce a new metric, the accuracy volume ($\mathcal{V}_X$), which corresponds to the minimum number of variational parameters necessary to achieve a target energy error (in our case, defined as $1\text{m}E_\text{h}$). As expected, DMRG affords the most efficient representation for the 1D $H_{10}$ chain and ring, using at least an order of magnitude fewer parameters to achieve the same level of energy

or two-body cumulant accuracy compared to the other methods. Nevertheless, this efficiency is gradually lost when going from 1D to higher-dimensional systems. In contrast, all flavors of sCI perform best in a delocalized basis but are generally less efficient than DMRG. The SVD-FCI, which we use as a proxy for rank-reduced FCI, is generally found to be the most inefficient approach to approximate the $H_{10}$ wave functions. However, as mentioned previously in Sec. 2.2.2, the variational optimization in RR-FCI would yield lower accuracy volumes than SVD-FCI, likely making RR-FCI more competitive with sCI and DMRG. We have similarly analyzed the ability of each method to accurately represent electron distributions, namely the cumulant of the two-body density matrix. In this case, the trends are similar to those observed for the energy, with the difference that sCI shows better performance for the 2D and 3D systems in a delocalized basis.

In analyzing the compressibility of the wave functions for $H_{12}$, $H_{14}$, and $H_{16}$ analogs of the four $H_{10}$ models, we have determined that DMRG consistently shows the smallest accuracy volume, and that the performance of SVD-FCI is more on par with that of ap-sCI for the larger systems, suggesting that future developments of RR-FCI methods such as those in Refs. 27 and 29 are certainly worthwhile, especially for systems larger than those considered in this study. Despite the significant reduction in the number of parameters relative to the FCI wave function afforded by selected CI, SVD-FCI, and DMRG, none of these methods bring a reduction in scaling from exponential to polynomial in the general case. Alternative methods, such as higher-dimensional tensor network states, quantum Monte Carlo, and quantum computational algorithms, may be required to circumvent storage cost of an exponentially scaling wave function.

We note that while the accuracy volume is a generally applicable metric for determining the performance of a method, the benchmark set considered here uses a minimal basis, is restricted to small systems amenable to FCI computations, and does not include atoms with more complex electronic structures. Therefore, one should be cautious in extrapolating the relative performance of the methods in the case of more complex systems. In future

studies it might be also interesting to investigate the advantages of employing other orbitals bases, like natural orbitals and split-localized orbitals. In addition, our work has focused only two tensor decomposition methods. It would be interesting to examine the accuracy volume of projected entangled-pair states,[155] the multi-scale entanglement renormalization ansatz,[156] tree tensor network states,[76,77,139] and other more general tensor network states. With appropriate modifications, the accuracy volume is also applicable to stochastic methods,[157,158] both in real and determinant space, and could provide a way to compare these approaches to deterministic methods like the ones considered in this work.

Our work does raise a few important questions as we (potentially) approach an era of quantum advantage for molecular computations. Although quantum computational algorithms are able to avoid the explicit storage of the wave function, they still suffer from non-trivial classical computational overhead. For example, the quantum phase estimation[159,160] (QPE) algorithm relies on time evolution of the Hamiltonian, which implies a computational scaling and storage costs (ignoring the cost of state preparation) at least proportional to $K^4$ in a delocalized basis, although more efficient representations have been recently proposed.[161,162] For the purpose of comparing the resource cost of classical and quantum algorithms, in Fig. 2.7 we have also reported an estimate of the resources needed by quantum algorithms computed as $n^4$, where $n$ is the number of hydrogen atoms (equal to the number of spatial orbitals). This plot shows that classical compression approaches use more than $n^4$ parameters even with systems as small as 12 electrons. While this prefatory comparison highlights the importance of quantum algorithm development even for modestly sized systems, it also suggests a threshold for the maximum number of classical parameters a quantum algorithm should employ. In other words, a successful quantum algorithm should achieve a $\mathscr{V}_X$ smaller (and with lower $n$-scaling) than state-of-the art classical methods such as selected CI and DMRG for a given level of accuracy. The competitiveness of any quantum algorithm could be tested for various regimes of correlation by comparing the computational resources (classical variational parameters) required to achieve a 1 m$E_\mathrm{h}$

energy error with those reported in Table 2.3.

In summary, this study has explored the limits of classical state-of-the-art electronic structure methodologies as applied to strongly correlated electrons. The hydrogen benchmark set and the accuracy volume metric are two new tools that will be useful in guiding the development of the next generation of classical and hybrid quantum-classical methods for strongly correlated systems. An important open problem in electronic structure theory is identifying the practical limits of classical methods and knowing under what circumstances quantum algorithms can overcome these limits. This work approaches this problem from a computational perspective and sheds some light on the first aspect; in future work we plan to investigate the ability of various quantum algorithms to go beyond the limits of classical methods.

# Bibliography

[1] D. K. Mok, R. Neumann, and N. C. Handy. "Dynamical and nondynamical correlation." *J. Phys. Chem.* **100**, 6225 (1996).

[2] D. Roca-Sanjuán, F. Aquilante, and R. Lindh. "Multiconfiguration second-order perturbation theory approach to strong electron correlation in chemistry and photochemistry." *Wiley Interdiscip. Rev. Comput. Mol. Sci.* **2**, 585 (2012).

[3] J. P. Malrieu, R. Caballol, C. J. Calzado, C. de Graaf, and N. Guihery. "Magnetic interactions in molecules and highly correlated materials: physical content, analytical derivation, and rigorous extraction of magnetic Hamiltonians." *Chem. Rev.* **114**, 429 (2014).

[4] P. A. Lee. "From high temperature superconductivity to quantum spin liquid: progress in strong correlation physics." *Rep. Prog. Phys.* **71**, 012501 (2007).

[5] M. Imada, A. Fujimori, and Y. Tokura. "Metal-insulator transitions." *Rev. Mod. Phys.* **70**, 1039 (1998).

[6] M. B. Salamon and M. Jaime. "The physics of manganites: Structure and transport." *Rev. Mod. Phys.* **73**, 583 (2001).

[7] Y. Tokura. "Critical features of colossal magnetoresistive manganites." *Rep. Prog. Phys.* **69**, 797 (2006).

[8] G. Murthy and R. Shankar. "Hamiltonian theories of the fractional quantum Hall effect." *Rev. Mod. Phys.* **75**, 1101 (2003).

[9] D. P. Tew, W. Klopper, and T. Helgaker. "Electron correlation: The many-body problem at the heart of chemistry." *J. Comput. Chem.* **28**, 1307 (2007).

[10] W. Kutzelnigg. "Theory of electron correlation." In J. Rychlewski, editor, "Explicitly Correlated Wave Functions in Chemistry and Physics," 3–90. Springer (2003).

[11] B. O. Roos, P. R. Taylor, and P. E. M. Siegbahn. "A complete active space SCF method (CASSCF) using a density matrix formulated super-CI approach." *Chem. Phys.* **48**, 157 (1980).

[12] R. Laughlin and D. Pines. "The Theory of Everything." *Proc. Natl. Acad. Sci. U.S.A* **97**, 28 (2000).

[13] K. D. Vogiatzis, D. Ma, J. Olsen, L. Gagliardi, and W. A. De Jong. "Pushing configuration-interaction to the limit: Towards massively parallel MCSCF calculations." *J. Chem. Phys.* **147**, 184111 (2017).

[14] S. McArdle, S. Endo, A. Aspuru-Guzik, S. C. Benjamin, and X. Yuan. "Quantum computational chemistry." *Rev. Mod. Phys.* **92**, 015003 (2020).

[15] A. Peruzzo, J. McClean, P. Shadbolt, M.-H. Yung, X.-Q. Zhou, P. J. Love, A. Aspuru-Guzik, and J. L. O'Brien. "A variational eigenvalue solver on a photonic quantum processor." *Nat. Commun.* **5**, 4213 (2014).

[16] M.-H. Yung, J. Casanova, A. Mezzacapo, J. Mcclean, L. Lamata, A. Aspuru-Guzik, and E. Solano. "From transistor to trapped-ion computers for quantum chemistry." *Sci. Rep.* **4**, 3589 (2014).

[17] J. R. McClean, J. Romero, R. Babbush, and A. Aspuru-Guzik. "The theory of variational hybrid quantum-classical algorithms." *New J. Phys.* **18**, 023023 (2016).

[18] H. R. Grimsley, S. E. Economou, E. Barnes, and N. J. Mayhall. "An adaptive variational algorithm for exact molecular simulations on a quantum computer." *Nat. Commun.* **10**, 1 (2019).

[19] J. R. McClean, M. E. Kimchi-Schwartz, J. Carter, and W. A. de Jong. "Hybrid quantum-classical hierarchy for mitigation of decoherence and determination of excited states." *Phys. Rev. A* **95**, 042308 (2017).

[20] M. Motta, C. Sun, A. T. Tan, M. J. O'Rourke, E. Ye, A. J. Minnich, F. G. Brandão, and G. K.-L. Chan. "Determining eigenstates and thermal states on a quantum computer using quantum imaginary time evolution." *Nat. Phys.* **16**, 1 (2019).

[21] R. M. Parrish and P. L. McMahon. "Quantum Filter Diagonalization: Quantum Eigendecomposition without Full Quantum Phase Estimation." *e-print arXiv:1909.08925 [quant-ph]* (2019).

[22] N. H. Stair, R. Huang, and F. A. Evangelista. "A Multireference Quantum Krylov Algorithm for Strongly Correlated Electrons." *J. Chem. Theory Comput.* **16**, 2236 (2020). ISSN 1549-9626.

[23] B. Huron, J.-P. Malrieu, and P. Rancurel. "Iterative perturbation calculations of ground and excited state energies from multiconfigurational zerothâĂŘorder wavefunctions." *J. Chem. Phys.* **58**, 5745 (1973).

[24] R. J. Buenker and S. D. Peyerimhoff. "Individualized configuration selection in CI calculations with subsequent energy extrapolation." *Theor. Chim. Acta* **35**, 33 (1974). ISSN 1432-2234.

[25] R. J. Buenker and S. D. Peyerimhoff. "Energy extrapolation in CI calculations." *Theor. Chim. Acta* **39**, 217 (1975). ISSN 1432-2234.

[26] S. Evangelisti, J.-P. Daudey, and J.-P. Malrieu. "Convergence of an improved CIPSI algorithm." *Chem. Phys.* **75**, 91 (1983). ISSN 0301-0104.

[27] H. Koch and E. Dalgaard. "A variational matrix decomposition applied to full configuration-interaction calculations." *Chem. Phys. Lett.* **198**, 51 (1992). ISSN 0009-2614.

[28] P. R. Taylor. "Lossless compression of wave function information using matrix factorization: A "gzip" for quantum chemistry." *J. Chem. Phys.* **139**, 074113 (2013).

[29] B. S. Fales, S. Seritan, N. F. Settje, B. G. Levine, H. Koch, and T. J. Martínez. "Large-Scale Electron Correlation Calculations: Rank-Reduced Full Configuration Interaction." *J. Chem. Theory Comput.* **14**, 4139 (2018).

[30] S. R. White. "Density matrix formulation for quantum renormalization groups." *Phys. Rev. Lett.* **69**, 2863 (1992).

[31] V. García, O. Castell, R. Caballol, and J.-P. Malrieu. "An iterative difference-dedicated configuration interaction. Proposal and test studies." *Chem. Phys. Lett.* **238**, 222 (1995). ISSN 0009-2614.

[32] F. Neese. "A spectroscopy oriented configuration interaction procedure." *J. Chem. Phys.* **119**, 9428 (2003).

[33] H. Nakatsuji and M. Ehara. "Iterative CI general singles and doubles (ICIGSD) method for calculating the exact wave functions of the ground and excited states of molecules." *J. Chem. Phys.* **122**, 194108 (2005).

[34] M. L. Abrams and C. D. Sherrill. "Important configurations in configuration interaction and coupled-cluster wave functions." *Chem. Phys. Lett.* **412**, 121 (2005). ISSN 0009-2614.

[35] L. Bytautas and K. Ruedenberg. "A priori identification of configurational deadwood." *Chem. Phys.* **356**, 64 (2009). ISSN 0301-0104.

[36] R. Roth. "Importance truncation for large-scale configuration interaction approaches." *Phys. Rev. C* **79**, 064324 (2009).

[37] F. A. Evangelista. "Adaptive multiconfigurational wave functions." *J. Chem. Phys.* **140**, 124114 (2014).

[38] P. J. Knowles. "Compressive sampling in configuration interaction wavefunctions." *Mol. Phys.* **113**, 1655 (2015).

[39] W. Liu and M. R. Hoffmann. "iCI: Iterative CI toward full CI." *J. Chem. Theory Comput.* **12**, 1169 (2016).

[40] J. B. Schriber and F. A. Evangelista. "Communication: An adaptive configuration interaction approach for strongly correlated electrons with tunable accuracy." *J. Chem. Phys.* **144**, 161106 (2016).

[41] A. A. Holmes, N. M. Tubman, and C. J. Umrigar. "Heat-Bath Configuration Interaction: An Efficient Selected Configuration Interaction Algorithm Inspired by Heat-Bath Sampling." *J. Chem. Theory Comput.* **12**, 3674 (2016).

[42] J. B. Schriber and F. A. Evangelista. "Adaptive Configuration Interaction for Computing Challenging Electronic Excited States with Tunable Accuracy." *J. Chem. Theory Comput.* **13**, 5354 (2017).

[43] J. C. Greer. "Estimating full configuration interaction limits from a Monte Carlo selection of the expansion space." *J. Chem. Phys.* **103**, 1821 (1995).

[44] J. C. Greer. "Monte Carlo Configuration Interaction." *J. Comput. Phys.* **146**, 181 (1998). ISSN 0021-9991.

[45] J. Coe, P. Murphy, and M. Paterson. "Applying Monte Carlo configuration interaction to transition metal dimers: Exploring the balance between static and dynamic correlation." *Chem. Phys. Lett.* **604**, 46 (2014). ISSN 0009-2614.

[46] J. P. Coe and M. J. Paterson. "State-averaged Monte Carlo configuration interaction applied to electronically excited states." *J. Chem. Phys.* **139**, 154103 (2013).

[47] J. P. Coe and M. J. Paterson. "Development of Monte Carlo configuration interaction: Natural orbitals and second-order perturbation theory." *J. Chem. Phys.* **137**, 204108 (2012).

[48] W. Győrffy, R. J. Bartlett, and J. C. Greer. "Monte Carlo configuration interaction predictions for the electronic spectra of Ne, CH2, C2, N2, and H2O compared to full configuration interaction calculations." *J. Chem. Phys.* **129**, 064103 (2008).

[49] S. Sharma, A. A. Holmes, G. Jeanmairet, A. Alavi, and C. J. Umrigar. "Semistochastic Heat-Bath Configuration Interaction Method: Selected Configuration Interaction with Semistochastic Perturbation Theory." *J. Chem. Theory Comput.* **13**, 1595 (2017).

[50] A. A. Holmes, C. J. Umrigar, and S. Sharma. "Excited states using semistochastic heat-bath configuration interaction." *J. Chem. Phys.* **147**, 164111 (2017).

[51] A. D. Chien, A. A. Holmes, M. Otten, C. J. Umrigar, S. Sharma, and P. M. Zimmerman. "Excited States of Methylene, Polyenes, and Ozone from Heat-Bath Configuration Interaction." *J. Phys. Chem. A* **122**, 2714 (2018).

[52] J. Li, M. Otten, A. A. Holmes, S. Sharma, and C. J. Umrigar. "Fast semistochastic heat-bath configuration interaction." *J. Chem. Phys.* **149**, 214110 (2018).

[53] G. H. Booth, A. J. W. Thom, and A. Alavi. "Fermion Monte Carlo without fixed nodes: A game of life, death, and annihilation in Slater determinant space." *J. Chem. Phys.* **131**, 054106 (2009).

[54] D. Cleland, G. H. Booth, and A. Alavi. "Communications: Survival of the fittest: Accelerating convergence in full configuration-interaction quantum Monte Carlo." *J. Chem. Phys.* **132**, 041103 (2010).

[55] G. H. Booth, D. Cleland, A. J. W. Thom, and A. Alavi. "Breaking the carbon dimer: The challenges of multiple bond dissociation with full configuration interaction quantum Monte Carlo methods." *J. Chem. Phys.* **135**, 084104 (2011).

[56] D. Cleland, G. H. Booth, and A. Alavi. "A study of electron affinities using the initiator approach to full configuration interaction quantum Monte Carlo." *J. Chem. Phys.* **134**, 024112 (2011).

[57] D. Cleland, G. H. Booth, C. Overy, and A. Alavi. "Taming the First-Row Diatomics: A Full Configuration Interaction Quantum Monte Carlo Study." *J. Chem. Theory Comput.* **8**, 4138 (2012).

[58] R. E. Thomas, C. Overy, G. H. Booth, and A. Alavi. "Symmetry Breaking and Broken Ergodicity in Full Configuration Interaction Quantum Monte Carlo." *J. Chem. Theory Comput.* **10**, 1915 (2014).

[59] G. H. Booth, S. D. Smart, and A. Alavi. "Linear-scaling and parallelisable algorithms for stochastic quantum chemistry." *Mol. Phys.* **112**, 1855 (2014).

[60] G. Li Manni, S. D. Smart, and A. Alavi. "Combining the complete active space self-consistent field method and the full configuration interaction quantum Monte Carlo within a super-CI framework, with application to challenging metal-porphyrins." *J. Chem. Theory Comput.* **12**, 1245 (2016).

[61] T. Kinoshita, O. Hino, and R. J. Bartlett. "Singular value decomposition approach for the approximate coupled-cluster method." *J. Chem. Phys.* **119**, 7756 (2003).

[62] O. Hino, T. Kinoshita, and R. J. Bartlett. "Singular value decomposition applied to the compression of T3 amplitude for the coupled cluster method." *J. Chem. Phys.* **121**, 1206 (2004).

[63] C. A. Lewis, J. A. Calvin, and E. F. Valeev. "Clustered Low-Rank Tensor Format: Introduction and Application to Fast Construction of Hartree–Fock Exchange." *J. Chem. Theory Comput.* **12**, 5868 (2016).

[64] P.-O. Löwdin and H. Shull. "Natural Orbitals in the Quantum Theory of Two-Electron Systems." *Phys. Rev.* **101**, 1730 (1956).

[65] F. A. Bischoff and E. F. Valeev. "Low-order tensor approximations for electronic wave functions: Hartree–Fock method with guaranteed precision." *J. Chem. Phys.* **134**, 104104 (2011).

[66] P. Å. Malmqvist and V. Veryazov. "The binatural orbitals of electronic transitions." *Mol. Phys.* **110**, 2455 (2012).

[67] G. J. O. Beran and M. Head-Gordon. "Extracting dominant pair correlations from many-body wave functions." *J. Chem. Phys.* **121**, 78 (2004).

[68] I. Mayer. "Using singular value decomposition for a compact presentation and improved interpretation of the CIS wave functions." *Chem. Phys. Lett.* **437**, 284 (2007). ISSN 0009-2614.

[69] P. J. Knowles and N. C. Handy. "A New Determinant-Based Full Configuration-Interaction Method." *Chem. Phys. Lett.* **111**, 315 (1984).

[70] M. Weinstein, A. Auerbach, and V. R. Chandra. "Reducing memory cost of exact diagonalization using singular value decomposition." *Phys. Rev. E* **84**, 056701 (2011).

[71] S. Östlund and S. Rommer. "Thermodynamic limit of density matrix renormalization." *Phys. Rev. Lett.* **75**, 3537 (1995).

[72] J. Dukelsky, M. A. Martín-Delgado, T. Nishino, and G. Sierra. "Equivalence of the variational matrix product method and the density matrix renormalization group applied to spin chains." *EPL* **43**, 457 (1998).

[73] U. Schollwöck. "The density-matrix renormalization group in the age of matrix product states." *Ann. Phys. (N. Y.)* **326**, 96 (2011).

[74] J. Eisert, M. Cramer, and M. Plenio. "Area laws for the entanglement entropy—a review, 2009." *Rev. Mod. Phys* **20**, 30 (2009).

[75] G. Evenbly and G. Vidal. "Tensor Network States and Geometry." *J. Stat. Phys.* **145**, 891 (2011). ISSN 1572-9613.

[76] V. Murg, F. Verstraete, O. Legeza, and R. M. Noack. "Simulating strongly correlated quantum systems with tree tensor networks." *Phys. Rev. B* **82**, 205105 (2010).

[77] N. Nakatani and G. K.-L. Chan. "Efficient tree tensor network states (TTNS) for quantum chemistry: Generalizations of the density matrix renormalization group algorithm." *J. Chem. Phys.* **138**, 134113 (2013).

[78] G. K.-L. Chan and M. Head-Gordon. "Highly correlated calculations with a polynomial cost algorithm: A study of the density matrix renormalization group." *J. Chem. Phys.* **116**, 4462 (2002).

[79] G. K.-L. Chan and S. Sharma. "The density matrix renormalization group in quantum chemistry." *Annu. Rev. Phys. Chem.* **62**, 465 (2011).

[80] G. Moritz, A. Wolf, and M. Reiher. "Relativistic DMRG calculations on the curve crossing of cesium hydride." *J. Chem. Phys.* **123**, 184105 (2005).

[81] Y. Kurashige and T. Yanai. "High-performance ab initio density matrix renormalization group method: Applicability to large-scale multireference problems for metal compounds." *J. Chem. Phys.* **130**, 234114 (2009).

[82] R. Olivares-Amaya, W. Hu, N. Nakatani, S. Sharma, J. Yang, and G. K.-L. Chan. "The ab-initio density matrix renormalization group in practice." *J. Chem. Phys.* **142**, 034102 (2015).

[83] J. Hachmann, W. Cardoen, and G. K.-L. Chan. "Multireference correlation in long molecules with the quadratic scaling density matrix renormalization group." *J. Chem. Phys.* **125**, 144101 (2006).

[84] A. O. Mitrushchenkov, G. Fano, R. Linguerri, and P. Palmieri. "On the importance of orbital localization in QC-DMRG calculations." *Int. J. Quantum Chem.* **112**, 1606 (2012).

[85] S. Wouters, P. A. Limacher, D. Van Neck, and P. W. Ayers. "Longitudinal static optical properties of hydrogen chains: Finite field extrapolations of matrix product state calculations." *J. Chem. Phys.* **136**, 134110 (2012).

[86] Y. Ma and H. Ma. "Assessment of various natural orbitals as the basis of large active space density-matrix renormalization group calculations." *J. Chem. Phys.* **138**, 224105 (2013).

[87] J. Hachmann, J. J. Dorando, M. Avilés, and G. K.-L. Chan. "The radical character of the acenes: A density matrix renormalization group study." *J. Chem. Phys.* **127**, 134309 (2007).

[88] C. Raghu, Y. A. Pati, and S. Ramasesha. "Structural and electronic instabilities in polyacenes: Density-matrix renormalization group study of a long-range interacting model." *Phys. Rev. B* **65**, 155204 (2002).

[89] C. Raghu, Y. Anusooya Pati, and S. Ramasesha. "Density-matrix renormalization-group study of low-lying excitations of polyacene within a Pariser-Parr-Pople model." *Phys. Rev. B* **66**, 035116 (2002).

[90] Y. Kurashige, G. K.-L. Chan, and T. Yanai. "Entangled quantum electronic wavefunctions of the Mn4CaO5 cluster in photosystem II." *Nat. Chem.* **5**, 660 (2013).

[91] S. Sharma, K. Sivalingam, F. Neese, and G. K.-L. Chan. "Low-energy spectrum of iron-sulfur clusters directly from many-particle quantum mechanics." *Nat. Chem.* **6**, 927 (2014).

[92] A. V. Sinitskiy, L. Greenman, and D. A. Mazziotti. "Strong correlation in hydrogen chains and lattices using the variational two-electron reduced density matrix method." *J. Chem. Phys.* **133**, 014104 (2010).

[93] M. Motta, D. M. Ceperley, G. K.-L. Chan, J. A. Gomez, E. Gull, S. Guo, C. A. Jiménez-Hoyos, T. N. Lan, J. Li, F. Ma, *et al.*. "Towards the solution of the many-electron problem in real materials: equation of state of the hydrogen chain with state-of-the-art many-body methods." *Phys. Rev. X* **7**, 031059 (2017).

[94] M. Motta, C. Genovese, F. Ma, Z.-H. Cui, R. Sawaya, G. K. Chan, N. Chepiga, P. Helms, C. Jimenez-Hoyos, A. J. Millis, *et al.*. "Ground-state properties of the hydrogen chain: insulator-to-metal transition, dimerization, and magnetic phases." *e-print arXiv:1911.01618 [quant-ph]* (2019).

[95] T. Yanai, Y. Kurashige, E. Neuscamman, and G. K.-L. Chan. "Multireference quantum chemistry through a joint density matrix renormalization group and canonical transformation theory." *J. Chem. Phys.* **132**, 024105 (2010).

[96] M. Saitow, Y. Kurashige, and T. Yanai. "Multireference configuration interaction theory using cumulant reconstruction with internal contraction of density matrix renormalization group wave function." *J. Chem. Phys.* **139**, 044118 (2013).

[97] Y. Kurashige, J. Chalupský, T. N. Lan, and T. Yanai. "Complete active space second-order perturbation theory with cumulant approximation for extended active-space wavefunction from density matrix renormalization group." *J. Chem. Phys.* **141**, 174111 (2014).

[98] S. Guo, M. A. Watson, W. Hu, Q. Sun, and G. K.-L. Chan. "N-Electron Valence State Perturbation Theory Based on a Density Matrix Renormalization Group Reference Function, with Applications to the Chromium Dimer and a Trimer Model of Poly( p-Phenylenevinylene)." *J. Chem. Theory Comput.* **12**, 1583 (2016).

[99] S. Wouters, V. Van Speybroeck, and D. Van Neck. "DMRG-CASPT2 study of the longitudinal static second hyperpolarizability of all-trans polyenes." *J. Chem. Phys.* **145**, 054120 (2016).

[100] J. B. Schriber, K. P. Hannon, C. Li, and F. A. Evangelista. "A combined selected configuration interaction and many-body treatment of static and dynamical correlation in oligoacenes." *J. Chem. Theory Comput.* **14**, 6295 (2018).

[101] K. F. Freed. "Theoretical foundations of purely semiempirical quantum chemistry." *J. Chem. Phys.* **60**, 1765 (1974).

[102] A. R. Welden, A. A. Rusakov, and D. Zgid. "Exploring connections between statistical mechanics and Green's functions for realistic systems: Temperature dependent electronic entropy and internal energy from a self-consistent second-order Green's function." *J. Chem. Phys.* **145**, 204106 (2016).

[103] A. F. White and G. K.-L. Chan. "A Time-Dependent Formulation of Coupled-Cluster Theory for Many-Fermion Systems at Finite Temperature." *J. Chem. Theory Comput.* **14**, 5690 (2018).

[104] G. Harsha, T. M. Henderson, and G. E. Scuseria. "Thermofield theory for finite-temperature coupled cluster." *J. Chem. Theory Comput.* **15**, 6127 (2019).

[105] G. D. Purvis III and R. J. Bartlett. "A full coupled-cluster singles and doubles model: The inclusion of disconnected triples." *J. Chem. Phys.* **76**, 1910 (1982).

[106] K. Raghavachari, G. W. Trucks, J. A. Pople, and M. Head-Gordon. "A fifth-order perturbation comparison of electron correlation theories." *Chem. Phys. Lett.* **157**, 479 (1989).

[107] P. Piecuch and M. Włoch. "Renormalized coupled-cluster methods exploiting left eigenstates of the similarity-transformed Hamiltonian." *J. Chem. Phys.* **123**, 224105 (2005).

[108] F. Colmenero and C. Valdemoro. "Approximating q-order reduced density matrices in terms of the lower-order ones. II. Applications." *Phys. Rev. A* **47**, 979 (1993).

[109] H. Nakatsuji and K. Yasuda. "Direct determination of the quantum-mechanical density matrix using the density equation." *Phys. Rev. Lett.* **76**, 1039 (1996).

[110] D. A. Mazziotti. "Contracted Schrödinger equation: Determining quantum energies and two-particle density matrices without wave functions." *Phys. Rev. A* **57**, 4219 (1998).

[111] D. A. Mazziotti. "Two-electron reduced density matrix as the basic variable in many-electron quantum chemistry and physics." *Chem. Rev.* **112**, 244 (2011).

[112] J. Fosso-Tande, T.-S. Nguyen, G. Gidofalvi, and A. E. DePrince III. "Large-scale variational two-electron reduced-density-matrix-driven complete active space self-consistent field methods." *J. Chem. Theory Comput.* **12**, 2260 (2016).

[113] F. A. Evangelista and N. H. Stair. "Github repository: https://github.com/evangelistalab/hydrogen-models-data." (2020).

[114] N. C. Handy. "Multi-root configuration interaction calculations." *Chem. Phys. Lett.* **74**, 280 (1980).

[115] S. Wouters and D. Van Neck. "The density matrix renormalization group for ab initio quantum chemistry." *Eur. Phys. J. D* **68**, 272 (2014).

[116] Ö. Legeza, J. Röder, and B. Hess. "Controlling the accuracy of the density-matrix renormalization-group method: The dynamical block state selection approach." *Phys. Rev. B* **67**, 125114 (2003).

[117] G. Moritz, B. A. Hess, and M. Reiher. "Convergence behavior of the density-matrix renormalization group algorithm for optimized orbital orderings." *J. Chem. Phys.* **122**, 024107 (2005).

[118] O. Legeza and J. Sólyom. "Optimizing the density-matrix renormalization group method using quantum information entropy." *Phys. Rev. B* **68**, 195116 (2003).

[119] J. Rissler, R. M. Noack, and S. R. White. "Measuring orbital interaction using quantum information theory." *Chem. Phys.* **323**, 519 (2006).

[120] P.-O. Löwdin. "Correlation Problem in Many-Electron Quantum Mechanics I. Review of Different Approaches and Discussion of Some Current Ideas." *Adv. Chem. Phys.* **2**, 207 (1958).

[121] O. Sinanoglu and D. Fu-Tai Tuan. "Quantum Theory of Atoms and Molecules." *Annu. Rev. Phys. Chem.* **15**, 251 (1964).

[122] R. J. Bartlett and J. F. Stanton. "Reviews in Computational Chemistry: Applications of Post-Hartree—Fock Methods: A Tutorial." 65–169. Wiley Online Library (1994).

[123] T. J. Lee and P. R. Taylor. "A diagnostic for determining the quality of single-reference electron correlation methods." *Int. J. Quantum Chem.* **36**, 199 (1989).

[124] I. M. B. Nielsen and C. L. Janssen. "Double-substitution-based diagnostics for coupled-cluster and Møller–Plesset perturbation theory." *Chem. Phys. Lett.* **310**, 568 (1999).

[125] A. V. Luzanov and O. V. Prezhdo. "Irreducible charge density matrices for analysis of many-electron wave functions." *Int. J. Quantum Chem.* **102**, 582 (2005).

[126] Z. Huang, H. Wang, and S. Kais. "Entanglement and electron correlation in quantum chemistry calculations." *J. Mod. Opt.* **53**, 2543 (2006).

[127] T. Juhász and D. A. Mazziotti. "The cumulant two-particle reduced density matrix as a measure of electron correlation and entanglement." *J. Chem. Phys.* **125**, 174105 (2006).

[128] A. V. Luzanov and O. Prezhdo. "High-order entropy measures and spin-free quantum entanglement for molecular problems." *Mol. Phys.* **105**, 2879 (2007).

[129] D. R. Alcoba, R. C. Bochicchio, L. Lain, and A. Torre. "On the measure of electron correlation and entanglement in quantum chemistry based on the cumulant of the second-order reduced density matrix." *J. Chem. Phys.* **133**, 144104 (2010).

[130] R. C. Bochicchio. "On spin density and hole distribution relations: valence and free valence." *J. Mol. Struc.-Theochem.* **429**, 229 (1998). ISSN 0166-1280.

[131] L. Lain, A. Torre, D. R. Alcoba, and R. C. Bochicchio. "A decomposition of the number of effectively unpaired electrons and its physical meaning." *Chem. Phys. Lett.* **476**, 101 (2009). ISSN 0009-2614.

[132] D. R. Alcoba, R. C. Bochicchio, L. Lain, and A. Torre. "On the definition of the effectively unpaired electron density matrix: A similarity measure approach." *Chem. Phys. Lett.* **429**, 286 (2006). ISSN 0009-2614.

[133] J. Pipek and P. G. Mezey. "A fast intrinsic localization procedure applicable for abinitio and semiempirical linear combination of atomic orbital wave functions." *J. Chem. Phys.* **90**, 4916 (1989).

[134] C. A. Jiménez-Hoyos, R. Rodríguez-Guzmán, and G. E. Scuseria. "Polyradical Character and Spin Frustration in Fullerene Molecules: An Ab Initio Non-Collinear Hartree–Fock Study." *J. Phys. Chem. A* **118**, 9925 (2014). ISSN 1520-5215.

[135] K. Boguslawski and P. Tecmer. "Orbital entanglement in quantum chemistry." *Int. J. Quantum Chem.* **115**, 1289 (2015).

[136] K. Boguslawski, P. Tecmer, G. Barcza, Ö. Legeza, and M. Reiher. "Orbital Entanglement in Bond-Formation Processes." *J. Chem. Theory Comput.* **9**, 2959 (2013).

[137] C. J. Stein and M. Reiher. "Automated identification of relevant frontier orbitals for chemical compounds and processes." *Chimia* **71**, 170 (2017).

[138] E. Fertitta, B. Paulus, G. Barcza, and Ö. Legeza. "Investigation of metal–insulator-like transition through the ab initio density matrix renormalization group approach." *Phys. Rev. B* **90**, 245129 (2014).

[139] V. Murg, F. Verstraete, R. Schneider, P. R. Nagy, and O. Legeza. "Tree tensor network state with variable tensor order: An efficient multireference method for strongly correlated systems." *J. Chem. Theory Comput.* **11**, 1027 (2015).

[140] R. M. Parrish, L. A. Burns, D. G. Smith, A. C. Simmonett, A. E. DePrince III, E. G. Hohenstein, U. Bozkaya, A. Y. Sokolov, R. Di Remigio, R. M. Richard, *et al.*. "Psi4 1.1: An open-source electronic structure program emphasizing automation, advanced libraries, and interoperability." *J. Chem. Theory Comput.* **13**, 3185 (2017).

[141] D. G. Smith, L. A. Burns, A. C. Simmonett, R. M. Parrish, M. C. Schieber, R. Galvelis, P. Kraus, H. Kruse, R. Di Remigio, A. Alenaizan, *et al.*. "Psi4 1.4: Open-source software for high-throughput quantum chemistry." *J. Chem. Phys.* **152**, 184108 (2020).

[142] W. J. Hehre, R. F. Stewart, and J. A. Pople. "Self-Consistent Molecular-Orbital Methods. I. Use of Gaussian Expansions of Slater-Type Atomic Orbitals." *J. Chem. Phys.* **51**, 2657 (1969).

[143] G. M. Barca, C. Bertoni, L. Carrington, D. Datta, N. De Silva, J. E. Deustua, D. G. Fedorov, J. R. Gour, A. O. Gunina, E. Guidez, *et al.*. "Recent developments in the general atomic and molecular electronic structure system." *J. Chem. Phys.* **152**, 154102 (2020).

[144] F. A. Evangelista. "Forte: an open source plugin for strongly correlated electronic systems." (2020).

[145] S. Wouters, W. Poelmans, P. W. Ayers, and D. Van Neck. "CheMPS2: A free open-source spin-adapted implementation of the density matrix renormalization group for ab initio quantum chemistry." *Comput. Phys. Commun.* **185**, 1501 (2014).

[146] G. Moritz and M. Reiher. "Construction of environment states in quantum-chemical density-matrix renormalization group calculations." *J. Chem. Phys.* **124**, 034103 (2006).

[147] T. Yanai, Y. Kurashige, E. Neuscamman, and G. K.-L. Chan. "Multireference quantum chemistry through a joint density matrix renormalization group and canonical transformation theory." *J. Chem. Phys.* **132**, 024105 (2010).

[148] G. Barcza, Ö. Legeza, K. H. Marti, and M. Reiher. "Quantum-information analysis of electronic states of different molecular structures." *Phys. Rev. A* **83**, 012508 (2011).

[149] K. Boguslawski, P. Tecmer, Ö. Legeza, and M. Reiher. "Entanglement Measures for Single- and Multireference Correlation Effects." *J. Phys. Chem. Let.* **3**, 3129 (2012).

[150] M. L. Baker, G. A. Timco, S. Piligkos, J. S. Mathieson, H. Mutka, F. Tuna, P. Kozłowski, M. Antkowiak, T. Guidi, T. Gupta, *et al.*. "A classification of spin frustration in molecular magnets from a physical study of large odd-numbered-metal, odd electron rings." *Proc. Natl. Acad. Sci. U.S.A* **109**, 19113 (2012).

[151] P. A. Limacher, P. W. Ayers, P. A. Johnson, S. De Baerdemacker, D. Van Neck, and P. Bultinck. "A new mean-field method suitable for strongly correlated electrons: Computationally facile antisymmetric products of nonorthogonal geminals." *J. Chem. Theory Comput.* **9**, 1394 (2013).

[152] I. W. Bulik, T. M. Henderson, and G. E. Scuseria. "Can single-reference coupled cluster theory describe static correlation?" *J. Chem. Theory Comput.* **11**, 3171 (2015).

[153] M. B. Hastings. "Lieb-Schultz-Mattis in higher dimensions." *Phys. Rev. B* **69**, 104431 (2004).

[154] E. M. Stoudenmire and S. R. White. "Studying two-dimensional systems with the density matrix renormalization group." *Annu. Rev. Condens. Matter Phys.* **3**, 111 (2012).

[155] F. Verstraete and J. I. Cirac. "Renormalization algorithms for quantum-many body systems in two and higher dimensions." *e-print arXiv:0407066 [cond-mat.str-el]* (2004).

[156] G. Vidal. "Entanglement renormalization." *Phys. Rev. Lett.* **99**, 220405 (2007).

[157] R. J. Needs, M. D. Towler, N. D. Drummond, and P. L. Ríos. "Continuum variational and diffusion quantum Monte Carlo calculations." *J. Phys.: Condens. Matter* **22**, 023201 (2009).

[158] M. Motta and S. Zhang. "Ab initio computations of molecular systems by the auxiliary-field quantum Monte Carlo method." *Wiley Interdiscip. Rev. Comput. Mol. Sci.* **8**, 1364 (2018).

[159] D. S. Abrams and S. Lloyd. "Simulation of Many-Body Fermi Systems on a Universal Quantum Computer." *Phys. Rev. Lett.* **79**, 2586 (1997).

[160] D. S. Abrams and S. Lloyd. "Quantum algorithm providing exponential speed increase for finding eigenvalues and eigenvectors." *Phys. Rev. Lett.* **83**, 5162 (1999).

[161] R. Babbush, N. Wiebe, J. R. McClean, J. McClain, H. Neven, and G. K.-L. Chan. "Low-depth quantum simulation of materials." *Phys. Rev. X* **8**, 011044 (2018).

[162] J. R. McClean, F. M. Faulstich, Q. Zhu, B. O'Gorman, Y. Qiu, S. R. White, R. Babbush, and L. Lin. "Discontinuous Galerkin discretization for quantum simulation of chemistry." *e-print arXiv:1909.00028 [quant-ph]* (2019).

# Chapter 3

# A quantum Krylov algorithm for strongly correlated electrons



## 3.1 Introduction

Solving the electronic many-body Schrödinger equation for systems that display strong correlation effects is a major challenge in physics and quantum chemistry.[1] Quantum computation[2] offers a potential solution to the exponential scaling of the Hilbert space dimension with particle number. Recent advances in quantum hardware design, including an early demonstrations of quantum speedup,[3] have motivated the development of new quantum algorithms that can be executed on so called noisy intermediate-scale quantum (NISQ) devices, with less than 100 qubits and shallow circuits.[4]

Algorithms based on quantum phase estimation (QPE),[5,6] were the first proposed to compute the ground state energies of fermionic many-body systems.[7] QPE was later applied to molecular problems[8] and has been implemented on a photonic quantum device.[9] Though QPE is well suited for Hamiltonian simulation on large-scale fault-tolerant quantum hardware, its application in the NISQ era presents several challenges due to the poor gate fidelity and the limited coherence time of devices available in the foreseeable fu-

ture.[10,11] As a result, hybrid quantum-classical algorithms requiring shallower circuits, such as the variational quantum eigensolver (VQE)[12,13] and the quantum approximate optimization algorithm (QAOA)[14] have recently received more attention.

In the VQE scheme, a complex trial wave function is optimized via an algorithm that subdivides the work between a classical and quantum computer. In this approach, the variational minimization of the energy is driven by a classical algorithm, while measurement of the energy and gradients is deployed to a quantum computer. VQE was originally implemented with the unitary coupled cluster (UCC)[15–20] ansatz truncated to single and double excitations.[12,13,21–24] More recently, several groups have studied alternative ansätze, including mean-field references,[25] UCC with general singles and doubles,[26] hardware-efficient parameterizations,[27] resource-efficient qubit-space UCC with 2-qubit entanglers,[28,29] general UCC with adaptively selected unitaries,[30] and linear-depth fermionic Gaussian reference states.[31] Efforts have also been made to extend the VQE algorithm to compute excited states[32–37] and approaches that combine variational methods and phase estimation have been suggested.[38,39]

Notwithstanding the significant impact of VQE schemes, they have two principal drawbacks. Firstly, VQE methods require measurement of the energy or energy gradients with respect to the variational parameters at each step of the optimization process. This results in a significant number of queries of the optimization algorithm to the quantum device. Secondly, the optimization process in VQE is challenging due to the high nonlinearity of the energy (considered as a function of the parameters), intrinsic accuracy limitation because of the inexactness of the ansatz[40] and stochastic errors that result from finite measurement and loss of fidelity.[41] As a consequence, the optimization process may be slow to convergence and may reach a local minimum instead of the true ground state.

A third and emerging family of methods, which we refer to as Quantum Subspace Diagonalization (QSD) schemes, diagonalize the Hamiltonian in a general nonorthogonal basis of many-body states.[32,33,42–46] There is a long tradition of using such a strategy in

quantum chemistry.[47–52] A natural way to extend it to quantum computing is to construct a basis of states and measure the corresponding matrix elements with a quantum device, and later solve the associated generalized eigenvalue problem via a classical computer.[32] Compared to a fully classical approach, QSD schemes can take advantage of the ability of quantum computers to store arbitrarily complex states.

QSD methods mainly differ in the way the many-body basis is generated. The quantum subspace expansion (QSE) method of McClean and co-workers, diagonalizes the Hamiltonian in the basis of states $\hat{a}_i^\dagger \hat{a}_j |\Psi\rangle$, where $\Psi$ is a reference state prepared via VQE.[32,33,42] Matrix element of the Hamiltonian in this basis are obtained by measuring the three- and four-body density matrices. QSD approaches are particularly advantageous if the many-body basis is constructed as a Krylov space[43] and does not require extensive parameter optimization. This is the case for the Quantum Lanczos (QLanczos) algorithm,[43] where the Hamiltonian is diagonalized in a basis of correlated states generated by imaginary-time propagation.[53] This basis is obtained from a single reference state by sampling at regular intervals in imaginary time. In QLanczos, the imaginary-time propagator is written as a unitary operation times a normalization factor, and a linear approximation is employed to construct this representation. For each step in the imaginary-time propagation, a linear system of equations must be solved for classically, requiring the measurement of the entries of a matrix and a vector. Recently, a quantum equation-of-motion (QEOM) approach that employs a QSD schema for computing excited states was also explored.[46]

Despite their potential, QSD methods suffer from a series of practical issues, which are the focus of this work. The generalized eigenvalue problem associated with a given nonorthogonal basis requires the efficient evaluation of off-diagonal matrix elements of the form $\langle \psi_\alpha | \hat{O} | \psi_\beta \rangle$. While in the case of QSE and QLanczos these matrix elements are easily computed,[32,43] in the general case their evaluation is more involved.[44,45] Another important issue is the linear dependency of the basis generated in a QSD procedure. This issue introduces numerical instabilities in the generalized eigenvalue problem and is potentially

amplified by poor gate fidelity and measurement errors. Bases generated by variational optimization[44] and real[45] or imaginary[43] time propagation are all plagued (to various degrees) by linear dependencies.

In this work we formulate a QSD algorithm that addresses the two problems described above. Firstly, we describe an efficient approach to evaluate the off-diagonal matrix element required in QSD methods, with a cost that is essentially identical to that of computing a diagonal matrix element. Secondly, to mitigate the linear dependency problem we consider a multireference approach in which the Krylov space is constructed from an initial set of orthogonal reference states. These references are selected via a scheme that exploits quantum measurement to identify the most important determinants in a simple trial wave function. The resulting multireference selected quantum Krylov (MRSQK) method is combined with basis generation via real-time propagation[43,45] and benchmarked on a series of problems involving strongly correlated electronic states.

While finalizing our manuscript, two papers appeared in preprint which are similar in spirit to our work. Parrish and McMahon[45] developed a quantum filter diagonalization (QFD) formalism in which a basis of many-body states is generated via an approximate real-time dynamics. QFD was inspired by classical filter diagonalization[54–57] as well as quantum time grid methods.[58–61] In both our work and that of Parrish and McMahon, the many-body basis is generated from a set of guess states. QFD, for example, was applied to a 8-qubit *ab initio* exciton model in which the guess states were comprised of the ground state and all single exciton states.[45] Our work may be viewed as a variant of QFD with selected references; however, a main difference is that in our approach the references are determined in an automated fashion using quantum measurement to determine important states. QFD and MRSQK also employ the same strategy for computing off-diagonal matrix elements (a modified Hadamard test).[62] In this work we provide detailed quantum circuits to evaluate these quantities and show that the cost of this procedure is nearly identical to that of computing the more trivial diagonal matrix elements. Our work also has some

overlap with a paper by Huggins *et al.*[44] in which they propose a non-orthgonal VQE (NOVQE) scheme. In the NOVQE approach, the Krylov basis is generated from a set of non-orthogonal VQE states, namely $k$-fold products of unitary paired coupled cluster with generalized single and double excitations ($k$-UpCCGSD) employing a single Slater determinant reference.[63] Due to the variational optimization of each element of the many-body basis, the Krylov space generated in the NOVQE method converges to the ground state, which is likely to require a smaller number of basis states. In the NOVQE scheme, the authors propose to compute off-diagonal matrix elements via an algorithm that avoids controlled unitary operations, at the expense of requiring twice the number of qubits used for the Hadamard test.

## 3.2 Theory

Consider a molecular Hamiltonian mapped to a set of qubits ($\hat{H}$)

$$\hat{H} = E_0 + \sum_{\ell} h_\ell \hat{V}_\ell \tag{3.1}$$

where $E_0$ is a scalar term, the index $\ell$ runs over all the terms in the Hamiltonian, $h_\ell$ is a matrix element, and $\hat{V}_\ell$ is the corresponding operator. Each operator $\hat{V}_\ell$ in $\hat{H}$ is a tensor product of $N_\ell$ Pauli operators (a Pauli string) that act on distinct qubits, $\hat{V}_\ell = \bigotimes_{k=1}^{N_\ell} \sigma_{l_k}^{(j_k)}$, where $l_k \in \{X, Y, Z\}$ labels the Pauli operator type and $j_k$ indicates the qubit upon which said operator is applied.

To define the MRSQK method, we start by introducing a $d$-dimensional basis of reference states, $\mathscr{M}_0 = \{\Phi_I\}$, where each $\Phi_I$ is a linear combination of Slater determinants ($\phi_\mu$) with well defined spin and spatial symmetry

$$|\Phi_I\rangle = \sum_{\mu} d_{\mu I} \left|\phi_\mu\right\rangle \tag{3.2}$$

From this basis, we generate a nonorthogonal Krylov[64,65] space $\mathscr{K}_s(\mathscr{M}_0, \hat{U}_n) = \{\psi_\alpha, \alpha = 1, \ldots, N\}$ by repeated application of a family of unitary operators $\hat{U}_n$ (with $n = 0, 1, \ldots, s$)

to all the elements of $\mathscr{M}_0$. A generic element $\psi_I^{(n)} \in \mathscr{K}$ is given by the action of $\hat{U}_n$ on $\Phi_I$.

$$|\psi_\alpha\rangle \equiv \left|\psi_I^{(n)}\right\rangle = \hat{U}_n |\Phi_I\rangle \tag{3.3}$$

For convenience, we use the collective index $\alpha = (I,n)$ to identify an element of the basis. The resulting Krylov space has dimension $N = d(s+1)$.

In MRSQK, a general state is written as a linear combination of the basis $\{\psi_\alpha\}$ as

$$|\Psi\rangle = \sum_\alpha c_\alpha |\psi_\alpha\rangle = \sum_{I=1}^{d}\sum_{n=0}^{s} c_I^{(n)} \hat{U}_n |\Phi_I\rangle \tag{3.4}$$

Variational minimization of the energy of the state $\Psi$ leads to the following generalized eigenvalue problem

$$\mathbf{Hc} = \mathbf{Sc}E, \tag{3.5}$$

where the elements of the overlap matrix (**S**) and Hamiltonian (**H**) are given by

$$S_{\alpha\beta} = \langle\psi_\alpha|\psi_\beta\rangle = \langle\Phi_I|\hat{U}_m^\dagger \hat{U}_n|\Phi_J\rangle, \tag{3.6}$$

$$H_{\alpha\beta} = \langle\psi_\alpha|\hat{H}|\psi_\beta\rangle = \langle\Phi_I|\hat{U}_m^\dagger \hat{H} \hat{U}_n|\Phi_J\rangle \tag{3.7}$$

The formalism outlined above lends itself to a large number of quantum algorithms, depending on: i) how the basis $\mathscr{M}_0$ is selected, ii) the particular choice of $\hat{U}_n$, and iii) the quantum circuits used to evaluate **S** and **H**. In the following we describe the combination that defines our multireference selected quantum Krylov approach and detail the efficient algorithm used to evaluate off-diagonal overlap and Hamiltonian matrix elements and our selection approach to generate the basis of references.

### 3.2.1 Choice of the unitary operators

In choosing the family of unitary operators $\hat{U}_n$ there are two primary criteria we aim to satisfy: i) that it generates a basis that well describes the eigenstates of $\hat{H}$ and ii) that the corresponding quantum circuit is inexpensive to evaluate. These requirements give considerable freedom, and a natural choice is a family of operators based on real-time

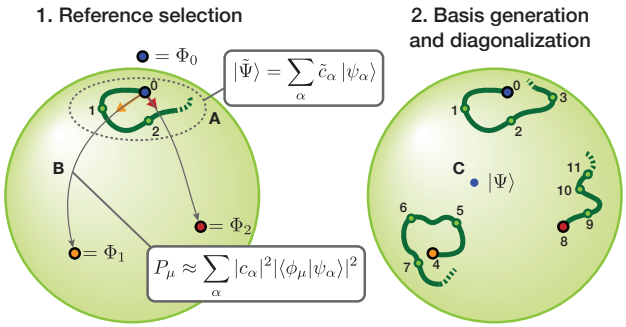


Figure 3.1: Schematic illustration of the multireference selected quantum Krylov (MRSQK) algorithm. (A) An approximate real-time dynamics using a single Slater determinant reference ($\Phi_0$) is used to generate a trial state ($\tilde{\Psi}$). (B) Measurements of the determinants that comprise the trial state are used to determine the probability of hopping ($P_\mu$) to other determinants. This information is employed to build two new reference states, $\Phi_1$ and $\Phi_2$. (C) Finally, three real-time evolutions starting from the references ($\Phi_0, \Phi_1, \Phi_2$) generate a set of 12 Krylov states $\psi_\alpha$, which are used to diagonalize the Hamiltonian and obtain the energy of the state $\Psi$.

evolution, $\hat{U}_n = \exp\left(-it_n\hat{H}\right)$, where $t_n = n\Delta t$ and $\Delta t$ is a fixed time step.

In fact, it is possible to show that for small $\Delta t$, the basis of states $\mathscr{K}_s(\Phi_I, \hat{U}_n)$ generated by real-time evolution spans a classical Krylov space. Consider a linear combination of the elements of $\mathscr{K}_s(\Phi_I, \hat{U}_n)$ and expand the exponential into a Taylor series keeping terms up to order $(\Delta t)^s$

$$\begin{aligned}
|\Psi\rangle &= \sum_{n=0}^{s} c_I^{(n)} e^{-in\Delta t\hat{H}} |\Phi_I\rangle \\
&= \sum_{k=0}^{s} \left( \sum_{n=0}^{s} \frac{(-in\Delta t)^k}{k!} c_I^{(n)} \right) \hat{H}^k |\Phi_I\rangle + \mathscr{O}(\Delta t^{s+1}) \\
&= \sum_{k=0}^{s} \left( \sum_{n=0}^{s} M_{kn} c_I^{(n)} \right) \hat{H}^k |\Phi_I\rangle + \mathscr{O}(\Delta t^{s+1})
\end{aligned} \tag{3.8}$$

The square matrix $\mathbf{M}$ is invertible, and therefore, the coefficients $c_I^{(n)}$ may be chosen to represent any combination of the classical Krylov basis $\{\hat{H}^k |\Phi_I\rangle\}$ with $k = 0, \ldots, s$, up to higher-order terms. This analysis shows that working with small time steps should be advantageous, as the quantum Krylov basis would reproduce the classical one. Indeed, this is what we find in numerical experiments. In practice, however, small time steps make the overlap matrix [Eq. (3.6)] nearly singular, which consequently reduces the numerical

stability of the generalized eigenvalue problem. In MRSQK this issue is ameliorated by the use of multiple references that are required to be orthogonal.

To realize the MRSQK method on a quantum computer, a quantum circuit is required that can approximate the time-evolution operator. The analysis presented above, suggests that it is important that any approximation to the real-time evolution operator must be sufficiently accurate. Otherwise the approximate quantum Krylov basis will likely not span the classical Krylov basis of the exact Hamiltonian, and consequently slow down the convergence of the method. To approximate the real-time evolution one may follow standard approaches like the Trotter-Suzuki decomposition[66,67] or employ a truncated Taylor series.[68] In this work we employ the former methodology, and consider the $m$-Trotter number (step) approximation of non-commuting operators $\hat{A}$ and $\hat{B}$ given by

$$e^{\hat{A}+\hat{B}} \approx \left(e^{\frac{\hat{A}}{m}} e^{\frac{\hat{B}}{m}}\right)^m \tag{3.9}$$

which is exact in the limit of $m \to \infty$. When applied to the real-time propagator this corresponds to the product

$$\hat{U}_n = \left(\prod_\ell \hat{U}_{n,\ell}(t_n/m)\right)^m = \left(\prod_\ell \exp\left(-it_n h_\ell/m\hat{V}_\ell\right)\right)^m \tag{3.10}$$

As shown in section 4.3, low Trotter number approximations ($m = 1,2$) yield large errors in the computation of the ground state electronic energy.

### 3.2.2 Efficient evaluation of off-diagonal matrix elements

To efficiently measure the overlap and Hamiltonian matrix elements [Eqs. 3.6 and 3.7], we augment the circuit used to build the basis with an ancillary qubit and construct the state $\frac{1}{\sqrt{2}}(|\psi_\alpha\rangle \otimes |0\rangle + |\psi_\beta\rangle \otimes |1\rangle)$, and then obtain $\langle\psi_\alpha|\psi_\beta\rangle$ by measuring the expectation value of the operator $2\sigma_+ = \sigma_X + i\sigma_Y$ on the ancilla qubit.[69] To produce the state $|\psi_\alpha\rangle$ we introduce the unitary operator $\hat{U}_\alpha$ defined as

$$\hat{U}_\alpha = \hat{U}_n \hat{U}_I \tag{3.11}$$

where $\hat{U}_I$ generates the reference state $|\Phi_I\rangle$ from the zero state $|\bar{0}\rangle = \bigotimes |0\rangle$. The circuit to measure off-diagonal matrix elements is shown in Fig. 3.2. We note that the use of a modified Hadamard test to measure off-diagonal matrix elements employed in this work and in Ref. 45, and the modified SWAP test used in Ref. 44, are particularly advantageous when the unitary operator $\hat{U}_\alpha$ cannot be expanded as a small sum of polynomials of Pauli operators (which is the case for real-time dynamics). In the case of a Hadamard test, this advantage comes at the cost of using controlled versions of $\hat{U}_\alpha$, and consequently, deeper quantum circuits and the use of an ancilla qubit. When the operator $\hat{U}_\alpha$ can be written as a small sum of Pauli strings, e.g., in the case of single excitations out of a VQE reference, then it is more efficient to compute off-diagonal matrix elements by averaging over all the Pauli terms of the Hamiltonian and the excitation operators that compose the Krylov subspace, as is done in the original QSE approach.[32]

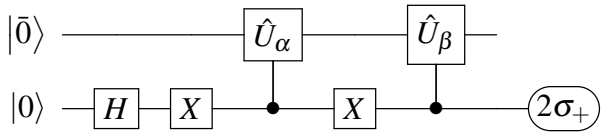


Figure 3.2: General circuit for measuring non-hermitian operators of the form $\langle\bar{0}|\hat{U}_\alpha^\dagger\hat{U}_\beta|\bar{0}\rangle$. In this circuit, the final measurement corresponds to separate measurements of $X$ and $Y$ and the evaluation of the expectation value of $2\sigma_+ = X + iY = 2|0\rangle\langle 1|$.

For $\hat{U}_n$ constructed out of exponentials of Pauli strings a crucial simplification may be employed that allows the efficient construction of the state $\frac{1}{\sqrt{2}}(|\psi_\alpha\rangle \otimes |0\rangle + |\psi_\beta\rangle \otimes |1\rangle)$.[70] First, we start by representing the product of Pauli operators in each of terms $\hat{V}_\ell$ as a unitarily-transformed Pauli string consisting of operators in the $Z$ basis

$$\hat{V}_\ell = \bigotimes_{k=1}^{N_\ell} \sigma_{l_k}^{(j_k)} = \mathscr{H}_\ell \bigotimes_{k=1}^{N_\ell} \sigma_Z^{(j_k)} \mathscr{H}_\ell \tag{3.12}$$

where $\mathscr{H}_\ell$ is a product of single qubit gates that transform each $\sigma_{l_k}^{(j_k)}$ to $\sigma_Z^{(j_k)}$.[71] Consequently, each term in $\hat{U}_{n,\ell} = \exp\left(-it_n h_\ell \hat{V}_\ell\right)$ can be written as

$$\hat{U}_{n,\ell} = \mathscr{H}_\ell \left(e^{-it_n h_\ell \bigotimes_{k=1}^{N_\ell} \sigma_Z^{(j_k)}}\right) \mathscr{H}_\ell = \tilde{U}_{n,\ell} R_{z_{N_\ell}}(2t_n h_\ell) \tilde{U}_{n,\ell} \tag{3.13}$$

where in the second step we have used a well-known representation of the exponential of Pauli strings composed of CNOT gates (collected in $\tilde{U}_{n,\ell}$) and a Z rotation on the $N_\ell$ qubit ($R_{z_{N_\ell}}$).[69,71] Using the following operator identity involving the controlled versions of generic unitary operators $\hat{A}$ and $\hat{B}$ (c-$\hat{A}$ and c-$\hat{B}$, see Fig. 3.3).

$$(\text{c-}\hat{B}^\dagger)(\text{c-}\hat{A})(\text{c-}\hat{B}) = \hat{B}^\dagger(\text{c-}\hat{A})\hat{B} \tag{3.14}$$

We can rewrite the controlled unitary evolution operator (c-$\hat{U}_{n,\ell}$) required to evaluate overlaps as

$$\text{c-}\hat{U}_{n,\ell} = \tilde{U}^\dagger_{n,\ell}[\text{c-}R_{z_{N_\ell}}(2\theta_n)]\tilde{U}_{n,\ell} \tag{3.15}$$

which requires only one extra controlled operation c-$R_{z_{N_\ell}}(2\theta_n)$, where $\theta_n = t_n h_\ell$, at the center of the circuit. Controlled unitaries evaluated in this way require at most $2N_\ell$ single qubit gates, $2N_\ell$ CNOT gates, and a controlled single-qubit gate.

Next, we discuss the the implementation of the unitary that prepares reference states from $|\bar{0}\rangle$ ($\hat{U}_I$). When $\Phi_I$ is a single Slater determinant $\hat{U}_I$ is a product of $X$ gates. For multideterminantal references, one can apply the linear combination of unitaries (LCU) algorithm,[72] or follow the procedure outlined by Tubman *et al.*[73] This approach requires only one ancilla qubit and $\mathcal{O}(nL)$ one- or two-qubit gates, where $n$ is the number of qubits and $L$ the number of determinants in a particular reference Alternatively, one may target references that are composed of a single configuration state functions[74,75] or two electron geminals.[76]

It is easy to generalize these circuits to controlled versions; however, one may pay the penalty of increasing the number of two-qubit gates (after factoring three qubit control gates into two-qubit ones). This suggests that the references $\Phi_I$ should be chosen to be compact multideterminantal wave functions, e.g., either single determinants or a small linear combinations of determinants.

Evaluation of the Hamiltonian matrix elements $H_{\alpha\beta} = \sum_\ell h_\ell \langle\psi_\alpha|\hat{V}_\ell|\psi_\beta\rangle$ proceeds in an analogous way by computing each term $\langle\psi_\alpha|\hat{V}_\ell|\psi_\beta\rangle$ individually. The circuit employed

is analogous to the one in Fig. 3.2 with the operator $\hat{U}_\beta$ by replaced by $\hat{V}_\ell \hat{U}_\beta$. Since each term $\hat{V}_\ell$ contains only product of one qubit operators, the corresponding controlled operator contains at most two-qubit operators. The evaluation of $\mathbf{S}$ and $\mathbf{H}$ lends itself to a high degree of parallelism. As in VQE methods, evaluation of a single matrix element of $\mathbf{H}$ may be parallelized over terms in the Hamiltonian. In addition, in the MRSQK, one may parallelize over the $N(N-1)/2$ unique pairs of Krylov states $\psi_\alpha/\psi_\beta$. Note that techniques used to ameliorate finite measurement errors in VQE[77–81] approaches can also be applied to MRSQK.

### 3.2.3 Reference selection

A third important aspect of the MRSQK algorithm is the procedure to select the reference configurations. Our approach exploits quantum measurement to identify a set of configurations starting from a trial MRSQK wave function. Specifically, we first form and diagonalize the Hamiltonian in the Krylov space $\mathscr{K}_s(\Phi_0, \hat{U}_n)$, where $\Phi_0$ is a single determinant (e.g., a closed-shell Hartree–Fock determinant). The resulting trial wave function $\tilde{\Psi} = \sum_\alpha \psi_\alpha \tilde{c}_\alpha$ is used to construct a list of potential important determinants. Since the probability of measuring a determinant $\phi_\mu$ is equal to $P_\mu = |\langle \phi_\mu | \tilde{\Psi} \rangle|^2$, one can in principle form the state $\tilde{\Psi}$ on a quantum computer and directly measure the determinantal composition, which in the Jordan–Wigner mapping amounts to measuring the expectation value of $Z$ for all wave function qubits. In practice, we approximate $P_\mu$ by measuring each element of the Krylov basis and estimating the total probability as a weighted sum over references

=

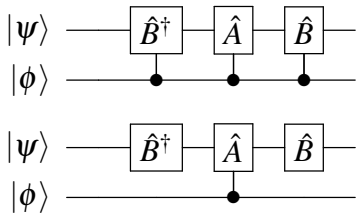


Figure 3.3: Circuit identity used to simplify the controlled version of $\hat{U}_{n,\ell}$ [Eq. (3.14)]. $\psi$ is a multi-qubit register used to encode a quantum state and the last qubit is an ancilla.

via

$$P_\mu = |\sum_\alpha \langle \phi_\mu | \psi_\alpha \rangle c_\alpha|^2 \approx \sum_\alpha |\langle \phi_\mu | \psi_\alpha \rangle|^2 |c_\alpha|^2 \tag{3.16}$$

Measurements are accumulated until we form a list of determinants of length equal to a small multiple of the number of references we aim to select (e.g., $2d$). In principle only a small number of measurements are required because the values of $P_\mu$ need only be qualitatively correct such that the determinants can be sorted. It should be noted, however, that using Eq. (5.39) as an importance criterion can lead to the overestimation of the importance of certain determinants due to neglected sign cancellation. A comparison of the the approximate sampling based on Eq. (5.39) and the exact weight of determinants in the MRSQK wave function shows that the former method is sufficient to identify the most important determinants (see Tab. S1 in the Supplemental Information). Alternatively, $\Psi$ could be directly represented on a quantum computer via the linear combination of unitaries (LCU) algorithm,[72] so that determinants would be sampled directly with their correct probabilities.

Once formed, the list of potentially important determinants is augmented to guarantee that all spin arrangements of open-shell determinants are included. Next, we diagonalize the Hamiltonian in this small determinant basis. At this stage we identify references in the following way: closed-shell determinants are considered individually, while open-shell determinants with the same spin occupation pattern are grouped together and their weight summed. Lastly, we select $d-1$ largest weighted references beyond the Hartree–Fock state. References composed of open-shell determinants are normalized to one using the determinant coefficients from the small classical CI. This procedure generates very compact reference states that can be used with the algorithm for computing off-diagonal matrix elements discussed in section 3.2.2. It is worth noting that the above procedure could also be generalized in such a way that important references are generated by an iterative algorithm that starts from a single-determinant state. An adaptive strategy like this reduces the bias introduced by selecting a starting Slater determinant reference and may be advantageous if some of the important references are generated with low weights from a single-determinant

state.

### 3.2.4 Analysis of computational cost

The quantum computational cost of the MRSQK algorithm is dominated by the application of the Trotterized Hamiltonian circuits $\hat{U}_n$. The depth of these circuits scales at worst $\mathcal{O}(mK^4)$ where $m$ is the trotter number and $K$ is the number of molecular orbitals. At the minimal Trotter number level $(m = 1)$, the maximum circuit depth for MRSQK is comparable to that of UCC with generalized singles and doubles (employng the same Trotter number), and far shallower than QPE. More importantly, the circuit depth of MRSQK is independent of size of the Krylov basis one wishes to generate, allowing for a flexible trade off-between quantum and classical cost (for a desired level of accuracy). For example, in the NISQ device era, one may avoid larger circuit depths with MRSQK by employing a modest Trotter number, but still achieve a high degree of accuracy by building a larger Krylov space that will be diagonalized classically. In this way MRSQK has both the advantage of selected CI to exploit wave function sparsity and the classical compression afforded by its quantum computational subroutines. This flexibility is a feature that distinguishes MRSQK from other QSD methods.

## 3.3 Computational details

The MRSQK method was implemented using both an exact second quantization formalism and a quantum computer simulator using the open-source package QFORTE.[82] All calculations used restricted Hartree–Fock (RHF) orbitals generated with PSI4[83] using a minimal (STO-6G)[84] basis. Molecular Hamiltonians for the hydrogen and $BeH_2$ systems were translated to a qubit representation via the Jordan–Wigner transformation as implemented in OPENFERMION[85] with default term ordering. For all calculations, references in MRSQK were selected using initial QK calculations with $s_0 = 2$ evolutions of the Hartree–Fock determinant and a time step of $\Delta t = 0.25$ a.u. Parameters such as the time time step

($\Delta t$), and number of evolutions per reference ($s$) used in MRSQK were chosen based on energy accuracy and numerical stability. We also note that we take the Trotter approximation with $m = 100$ as a good approximation to the infinite $m$ limit for the potential energy curves we plot. Adaptive derivative-assembled pseudo-Trotter ansatz variational quantum eigensolver (ADAPT-VQE)[30] calculations were performed with a in-house code provided by N. Mayhall.

## 3.4 Numerical studies and discussion

We benchmark the performance and comparative numerical stability of the MRSQK algorithm with linear chains of six and eight hydrogen atoms, two canonical models for one-dimensional materials with correlation strength modulated by bond length.[86–88] We utilize point-group symmetry, which results in a determinant space comprised of 200 and 2468 determinants for $H_6$ and $H_8$, respectively. We first consider $H_6$ at a site-site distance of 1.50 Å, which exhibits strong electron correlation, as indicated by the large correlation

Table 3.1: Ground-state energies (in $E_h$) of $H_6$ and $H_8$ at a site-site distance of 1.5 Å using exact time-evolution. Energy and overlap condition number $k(\mathbf{S})$ results are given for a single determinant (QK) using $N$ Krylov basis states and $\Delta t = 0.5$. MRSQK results are given for $N = d(s+1)$ Krylov basis states using three steps ($s = 3$) and $\Delta t = 0.5$ a.u. With $N$ greater than 12 states, the condition number for QK does not grow larger than $10^{18}$. This is likely a result of limitations of double precision arithmetic.

| $N$ | $E_{QK}$ | $k(\mathbf{S}_{QK})$ | $E_{MRSQK}$ | $k(\mathbf{S}_{MRSQK})$ |
|---|---|---|---|---|
| | | $H_6$ ($r_{HH}$ = 1.5 Å) | | |
| 4 | −3.015510 | $3.29\times10^{5}$ | −3.015510 | $3.29\times10^{5}$ |
| 8 | −3.019768 | $3.60\times10^{11}$ | −3.019301 | $4.86\times10^{5}$ |
| 12 | −3.020172 | $1.61\times10^{17}$ | −3.019696 | $9.39\times10^{5}$ |
| 16 | −3.020192 | $3.19\times10^{17}$ | −3.019835 | $5.68\times10^{6}$ |
| 20 | −3.020198 | $3.86\times10^{17}$ | −3.019929 | $6.23\times10^{6}$ |
| FCI | −3.020198 | | | |
| | | $H_8$ ($r_{HH}$ = 1.5 Å) | | |
| 4 | −4.017108 | $1.19\times10^{5}$ | −4.017108 | $1.19\times10^{5}$ |
| 8 | −4.026563 | $1.39\times10^{10}$ | −4.024268 | $1.50\times10^{5}$ |
| 12 | −4.028000 | $5.11\times10^{14}$ | −4.025894 | $2.00\times10^{5}$ |
| 16 | −4.028096 | $1.33\times10^{17}$ | −4.026042 | $2.51\times10^{5}$ |
| 20 | – | – | −4.026387 | $4.27\times10^{5}$ |
| 24 | – | – | −4.026457 | $4.44\times10^{5}$ |
| FCI | −4.028152 | | | |

energy ($E_{\text{corr}} = -0.24681\ E_{\text{h}}$) and the small weight of the Hartree–Fock determinant in the FCI expansion ($|C_{\text{HF}}|^2 = 0.634$).

In Tab. 3.1 we show a comparison of the energy and overlap matrix condition number for the single reference version of quantum Krylov (QK), taking only the HF determinant as a reference, and MRSQK as a function of the total number of basis states. For $H_6$ we observe that in both the single and multireference cases, convergence to chemical accuracy (error less than 1 kcal mol$^{-1}$ = 1.594 m$E_{\text{h}}$) is achieved with only 8 parameters, an order of magnitude smaller than the size of FCI space. For the case $N = 12$, MRSQK identifies the following three references

$$\begin{aligned}
|\Phi_0\rangle &= |220200\rangle \\
|\Phi_1\rangle &= |200220\rangle \\
|\Phi_2\rangle &= -0.302\,|2\uparrow\uparrow\downarrow\downarrow 0\rangle - 0.302\,|2\downarrow\downarrow\uparrow\uparrow 0\rangle \\
&\quad + 0.275\,|2\uparrow\downarrow\uparrow\downarrow 0\rangle + 0.577\,|2\uparrow\downarrow\downarrow\uparrow 0\rangle \\
&\quad + 0.577\,|2\downarrow\uparrow\uparrow\downarrow 0\rangle + 0.275\,|2\downarrow\uparrow\downarrow\uparrow 0\rangle
\end{aligned} \tag{3.17}$$

where the orbitals are ordered according to ($1a_g$, $2a_g$, $3a_g$, $1b_{1u}$, $2b_{1u}$, $3b_{1u}$) in the $D_{2h}$ point group. These references are comprised of two closed-shell and six open-shell determinants. If we perform a computation with a set of references consisting of eight individual (uncontracted) determinants, the resulting Krylov space has dimension 32 and the corresponding energy is $-3.019797\ E_{\text{h}}$, which is only 0.1 m$E_{\text{h}}$ lower than the contracted result ($-3.019696$). Turning to $H_8$, we find that the single-reference QK energy converges to chemical accuracy with only 12 parameters, two orders of magnitude fewer than FCI. For the same example, the MRSQK energy error is 1.06 kcal mol$^{-1}$ with 24 parameters, only slightly higher than chemical accuracy.

The linear dependency of the basis for $H_6$ and $H_8$—as measured by the condition number of the overlap matrix [$k(\mathbf{S})$]—is significantly more pronounced in the single reference QK than the MRSQK version. In the case of $H_6$, even with a small Krylov basis (8 ele-

ments), QK is potentially ill-conditioned [$k(\mathbf{S}) = 3.60 \times 10^{11}$]. In the case of 12 (or more) states, the QK eigenvalue problem is strongly ill-conditioned [$k(\mathbf{S}) = 1.16 \times 10^{17}$], while MRSQK displays only a modest condition number, [$k(\mathbf{S}) = 9.39 \times 10^{5}$]. Importantly, QK becomes ill-conditioned before reaching chemical accuracy, whereas MRSQK does not, highlighting the importance of multireference approach for practical applications.

Table 3.2: Ground-state energies (in $E_\mathrm{h}$) of $H_6$ at a bond distance of 1.5 Å. MRSQK results are given for $N = d(s+1)$ Krylov basis states using three steps ($s = 3$) and $\Delta t = 0.5$ a.u. The quantity $m$ indicates the Trotter number. For each value of $N$, selected configuration interaction (sCI) results were obtained using $N$ determinants with the largest absolute coefficient in the FCI wave function. ADAPT-VQE results show the energy with $N$ cluster amplitudes selected from the pool of spin-adapted generalized singles/doubles.

| $N$ | $E^{(m=\infty)}_{\mathrm{MRSQK}}$ | $E^{(m=8)}_{\mathrm{MRSQK}}$ | $E^{(m=4)}_{\mathrm{MRSQK}}$ | $E^{(m=2)}_{\mathrm{MRSQK}}$ | $E^{(m=1)}_{\mathrm{MRSQK}}$ | $E_{\mathrm{sCI}}$ | $E_{\mathrm{ADAPT-VQE}}$ |
|---|---|---|---|---|---|---|---|
| 4 | −3.015510 | −3.014138 | −3.009948 | −2.998858 | −2.982186 | −2.845002 | −2.906724 |
| 8 | −3.019301 | −3.018341 | −3.015872 | −3.010035 | −3.001195 | −2.909404 | −2.983042 |
| 12 | −3.019696 | −3.018808 | −3.016940 | −3.013425 | −3.008661 | −2.926337 | −2.995691 |
| 16 | −3.019835 | −3.018888 | −3.017173 | −3.014253 | −3.010543 | −2.954587 | −3.002345 |
| 20 | −3.019929 | −3.019054 | −3.017614 | −3.015311 | −3.011663 | −2.961772 | −3.008847 |
| FCI | −3.020198 | | | | | | |

Next, we assess the errors introduced by approximating the real-time dynamics with a Trotter approximation. Table 3.2 shows the performance of MRSQK using various levels of Trotter approximation for $H_6$ at a bond distance of 1.5 Å. While using exact time evolution affords the fastest energy convergence with respect to number of Krylov basis states, we find that chemical accuracy can still be achieved using a Trotterized exponential. For example, using a Trotter number $m = 8$, MRSQK gives an error of only 1.1 m$E_\mathrm{h}$ with a basis of 20 Krylov states. In Table 3.2 we also show a comparison of MRSQK with selected configuration interaction (sCI) and the adaptive derivative-assembled pseudo-Trotter ansatz variational quantum eigensolver (ADAPT-VQE).[30] For any Trotter number, MRSQK converges significantly faster than sCI and the ADAPT-VQE method. For example, even with the smallest Trotter number ($m = 1$) MRSQK with 20 Krylov states gives an error of 8.5 m$E_\mathrm{h}$, while a sCI wave function with 20 determinants yields an error of 58.4 m$E_\mathrm{h}$ (see Table (3.2) for details of the determinant selection). In comparison, an ADAPT-VQE wave function with 20 parameters yields an error of 11.4 m$E_\mathrm{h}$. These results demonstrate the ability of

MRSQK to parameterize strongly correlated states efficiently using a small fraction of the variational degrees of freedom.

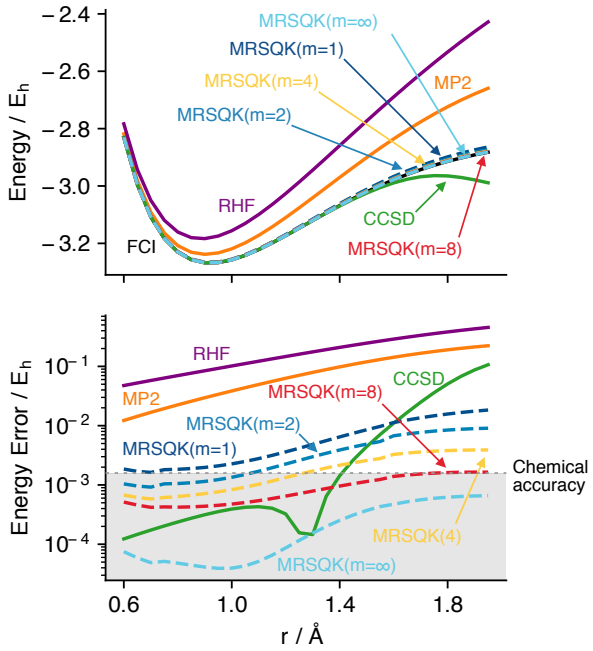


Figure 3.4: Potential energy curve (top) and error (bottom) for symmetric dissociation of linear $H_6$ in a STO-6G basis. MRSQK computations use $\Delta t = 0.5$ a.u., three time steps ($s = 3$), and five references ($d = 5$) corresponding to 20 Krylov basis states. The number of Trotter steps ($m$) is indicated in parentheses, while those from exact time evolution are labeled ($m = \infty$).

To illustrate the ability of MRSQK to determine accurate ground-state potential energy surfaces (PES) in the presence of strong correlation, we examine the dissociation of the $H_6$ chain and linear $BeH_2$. Figure 3.4 show the energy and error with respect to FCI for $H_6$, for restricted Hartree–Fock (RHF), second-order Møller–Plesset perturbation theory (MP2), coupled cluster with singles and doubles (CCSD),[89] and MRSQK with a Krylov basis of 20 states ($s = 3$, $d = 5$). With the onset of strong electron correlation, single-reference methods (RHF, MP2, CCSD) fail to capture the the correct qualitative features of the PEC. For example, CCSD produces very accurate results near the equilibrium geometry; however, it dips significantly below the FCI energy for bond distances greater than 1.5 Å. In

contrast, MRSQK far outperforms CCSD even with the lowest Trotter number ($m = 1$) and chemically accurate MRSQK results are obtained with $m = 8$.

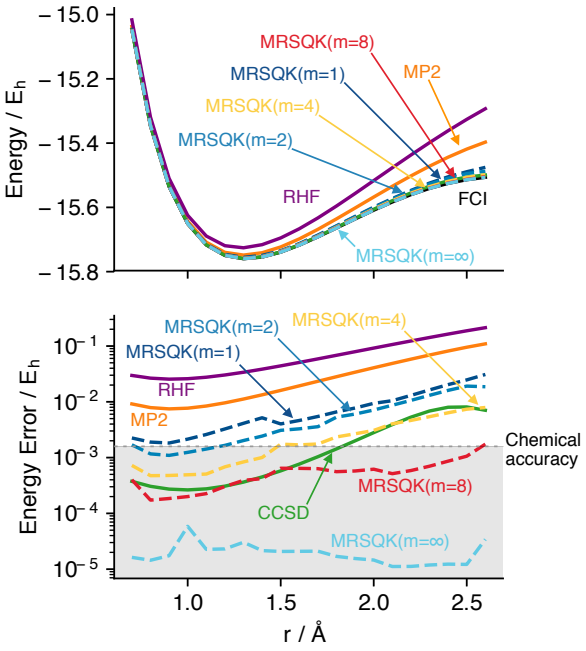


Figure 3.5: Potential energy curve (top) and error (bottom) for symmetric dissociation of linear $BeH_2$ in a STO-6G basis. MRSQK computations use $\Delta t = 2$ a.u., four time steps ($s = 4$), and six references ($d = 6$) corresponding to 30 Krylov basis states. The number of Trotter steps ($m$) is indicated in parentheses, while those from exact time evolution are labeled ($m = \infty$).

In Figure 3.5 we report the potential energy curve for the symmetric dissociation of linear $BeH_2$. For this problem, the size of the determinant space is 169. Like $H_6$, $BeH_2$ is a challenging problem for single-reference methods, although CCSD shows smaller errors (less than 10 m$E_h$) throughout the entire curve. MRSQK computations on $BeH_2$ employed 30 Krylov states generated by a space of six references and four time steps ($s = 4$). For this problem, we found that using a larger time step provides more accurate results and therefore, we report results using $\Delta t = 2$ a.u. In the case of no Trotter approximation ($m = \infty$), the MRSQK error is less than 0.1 m$E_h$ across the entire potential energy curve. The approximate MRSQK scheme based on four Trotter steps is already comparable in accuracy

to CCSD, while using $m = 8$ the error falls within chemical accuracy. By analyzing the error plot in the bottom half of Fig. 3.5, we see that there are small discontinuities in the curve due to the selection of a different set of reference states. This problem, however, is common to all selected CI methodologies,[90–94] as well as ADAPT-VQE. These discontinuities may be removed by employing references built from a fixed set of determinants.

## 3.5 Conclusions

In summary, the multireference selected quantum Krylov is a new quantum subspace diagonalization algorithm for solving the electronic Schrödinger equation on NISQ devices. MRSQK diagonalizes the Hamiltonian in a basis of many-body states generated by real-time evolution of a set of orthogonal reference states. This approach has two major advantages: (i) it requires no variational optimization of classical parameters, (ii) it avoids the linear dependency problem that may plague other QSD methods. Benchmark computations on $H_6$, $H_8$, and $BeH_2$ show that MRSQK with exact time-propagation converges rapidly to the exact energy using a number of Krylov states that is a small fraction of the full determinant space. When the real-time propagator is approximated via a Trotter decomposition, modest Trotter numbers $m = 4, 8$ are sufficient to ensure that truncation errors yield chemically accurate potential energy curves. We also report a comparison of the convergence of the energy of $H_6$ for MRSQK, selected configuration interaction (sCI), and the state-of-the-art ADAPT-VQE algorithm. In comparing sCI and MRSQK, the significantly faster convergence of the latter method indicates that the Krylov basis efficiently captures the important multideterminantal features of the wave function. The comparison with ADAPT-VQE shows that MRSQK can achieve a compact representation of the wave function competitive even with an adaptive strategy that aims to minimize the number of unitary rotations.

Together, these advantages make MRSQK a promising tool for treating strongly correlated electronic systems with quantum computation. However, there are several aspects

of the MRSQK that deserve more consideration. The current reference selection strategy may produce different sets of references as the molecular geometry is changed, which in turn causes small discontinuities in potential energy curves. Selection procedures that, e.g., identify references from a small fixed set of orbitals could be used to address this issues. In this work, we have selected fixed values for the time steps $t_n$. Schemes in which the time steps are treated as variational parameters may be able to represent states with a fewer number of Krylov states and are worth exploring. Another important aspect is improving the approximation to the real-time dynamics. Our results indicate that low Trotter number approximations ($m = 1, 2$) commonly used in other context introduce errors that are too large. It would be desirable to explore the implementation of real-time dynamics via alternative methods, e.g. truncated Taylor series.[68] An interesting alternative is to follow the strategy of Ref. 95, which employs an unphysical dynamics generated by a simple function of the Hamiltonian. This dynamics still spans the classical Krylov space and may be implemented with the same number of gates as a single Trotter number approximation.

# Bibliography

[1] R. B. Laughlin and D. Pines. "The theory of everything." *Proc. Nat. Acad. Sci. U.S.A.* **97**, 28 (2000).

[2] R. P. Feynman. "Simulating physics with computers." *Int. J. Theor. Phys.* **21**, 467 (1982).

[3] F. Arute, K. Arya, R. Babbush, D. Bacon, J. C. Bardin, R. Barends, R. Biswas, S. Boixo, F. G. S. L. Brandão, D. A. Buell, B. Burkett, Y. Chen, Z. Chen, B. Chiaro, R. Collins, W. Courtney, A. Dunsworth, E. Farhi, B. Foxen, A. Fowler, C. Gidney, M. Giustina, R. Graff, K. Guerin, S. Habegger, M. P. Harrigan, M. J. Hartmann, A. Ho, M. Hoffmann, T. Huang, T. S. Humble, S. V. Isakov, E. Jeffrey, Z. Jiang, D. Kafri, K. Kechedzhi, J. Kelly, P. V. Klimov, S. Knysh, A. Korotkov, F. Kostritsa, D. Landhuis, M. Lindmark, E. Lucero, D. Lyakh, S. Mandrà, J. R. McClean, M. McEwen, A. Megrant, X. Mi, K. Michielsen, M. Mohseni, J. Mutus, O. Naaman, M. Neeley, C. Neill, M. Y. Niu, E. Ostby, A. Petukhov, J. C. Platt, C. Quintana, E. G. Rieffel, P. Roushan, N. C. Rubin, D. Sank, K. J. Satzinger, V. Smelyanskiy, K. J. Sung, M. D. Trevithick, A. Vainsencher, B. Villalonga, T. White, Z. J. Yao, P. Yeh, A. Zalcman, H. Neven, and J. M. Martinis. "Quantum supremacy using a programmable superconducting processor." *Nature* **574**, 505 (2019).

[4] J. Preskill. "Quantum Computing in the NISQ era and beyond." *Quantum* **2**, 79 (2018).

[5] D. S. Abrams and S. Lloyd. "Simulation of Many-Body Fermi Systems on a Universal Quantum Computer." *Phys. Rev. Lett.* **79**, 2586 (1997).

[6] D. Abrams and S. Lloyd. "Quantum algorithm providing exponential speed increase for finding eigenvalues and eigenvectors." *Phys. Rev. Lett.* **83**, 5162 (1999).

[7] G. Ortiz, J. E. Gubernatis, E. Knill, and R. Laflamme. "Quantum algorithms for fermionic simulations." *Phys. Rev. A* **64**, 022319 (2001).

[8] A. Aspuru-Guzik, A. D. Dutoi, P. J. Love, and M. Head-Gordon. "Simulated quantum computation of molecular energies." *Science* **309**, 1704 (2005).

[9] B. P. Lanyon, J. D. Whitfield, G. G. Gillett, M. E. Goggin, M. P. Almeida, I. Kassal, J. D. Biamonte, M. Mohseni, B. J. Powell, M. Barbieri, A. Aspuru-Guzik, and A. G. White. "Towards quantum chemistry on a quantum computer." *Nat. Chem.* **2**, 106 (2010). ISSN 1755-4349.

[10] S. McArdle, S. Endo, A. Aspuru-Guzik, S. Benjamin, and X. Yuan. "Quantum computational chemistry." e-print arXiv:1808.10402v2 [quant-ph] (2018).

[11] Y. Cao, J. Romero, J. P. Olson, M. Degroote, P. D. Johnson, M. Kieferová, I. D. Kivlichan, T. Menke, B. Peropadre, N. P. D. Sawaya, S. Sim, L. Veis, and A. Aspuru-Guzik. "Quantum Chemistry in the Age of Quantum Computing." *Chem. Rev.* **119**, 10856 (2019).

[12] A. Peruzzo, J. McClean, P. Shadbolt, M.-H. Yung, X.-Q. Zhou, P. J. Love, A. Aspuru-Guzik, and J. L. O'Brien. "A variational eigenvalue solver on a photonic quantum processor." *Nat. Commun.* **5**, 4213 (2014). ISSN 2041-1723.

[13] M. H. Yung, J. Casanova, A. Mezzacapo, J. McClean, L. Lamata, A. Aspuru-Guzik, and E. Solano. "From transistor to trapped-ion computers for quantum chemistry." *Sci. Rep.* **4**, 3589 (2014).

[14] E. Farhi, J. Goldstone, and S. Gutmann. "A Quantum Approximate Optimization Algorithm." e-print arXiv:1411.4028v1 [quant-ph] (2014).

[15] W. Kutzelnigg. "Pair correlation theories." In I. Henry F Schaefer, editor, "Methods of electronic structure theory," 129–188. Springer US, Boston, MA (1977).

[16] P. G. Szalay, M. Nooijen, and R. J. Bartlett. "Alternative Ansatz in Single Reference Coupled-Cluster Theory .III. A Critical Analysis of Different Methods." *J. Chem. Phys.* **103**, 281 (1995).

[17] A. G. Taube and R. J. Bartlett. "New perspectives on unitary coupled-cluster theory." *Int. J. Quantum Chem.* **106**, 3393 (2006).

[18] B. Cooper and P. J. Knowles. "Benchmark studies of variational, unitary and extended coupled cluster methods." *J. Chem. Phys.* **133**, 234102 (2010).

[19] F. A. Evangelista. "Alternative single-reference coupled cluster approaches for multireference problems: The simpler, the better." *J. Chem. Phys.* **134**, 224102 (2011).

[20] G. Harsha, T. Shiozaki, and G. E. Scuseria. "On the difference between variational and unitary coupled cluster theories." *J. Chem. Phys.* **148**, 044107 (2018).

[21] J. R. McClean, J. Romero, R. Babbush, and A. Aspuru-Guzik. "The theory of variational hybrid quantum-classical algorithms." *New J Phys* **18**, 023023 (2016).

[22] P. J. J. O'Malley, R. Babbush, I. D. Kivlichan, J. Romero, J. R. McClean, R. Barends, J. Kelly, P. Roushan, A. Tranter, N. Ding, B. Campbell, Y. Chen, Z. Chen, B. Chiaro, A. Dunsworth, A. G. Fowler, E. Jeffrey, E. Lucero, A. Megrant, J. Y. Mutus, M. Neeley, C. Neill, C. Quintana, D. Sank, A. Vainsencher, J. Wenner, T. C. White, P. V. Coveney, P. J. Love, H. Neven, A. Aspuru-Guzik, and J. M. Martinis. "Scalable Quantum Simulation of Molecular Energies." *Phys. Rev. X* **6**, 031007 (2016).

[23] J. Romero, R. Babbush, J. R. McClean, C. Hempel, P. J. Love, and A. Aspuru-Guzik. "Strategies for quantum computing molecular energies using the unitary coupled cluster ansatz." *Quantum Sci. Technol.* **4**, 014008 (2019).

[24] P. K. Barkoutsos, J. F. Gonthier, I. Sokolov, N. Moll, G. Salis, A. Fuhrer, M. Ganzhorn, D. J. Egger, M. Troyer, A. Mezzacapo, S. Filipp, and I. Tavernelli. "Quantum algorithms for electronic structure calculations: particle/hole Hamiltonian and optimized wavefunction expansions." *Phys. Rev. A* **98**, 022322 (2018).

[25] I. G. Ryabinkin, S. N. Genin, and A. F. Izmaylov. "Constrained Variational Quantum Eigensolver: Quantum Computer Search Engine in the Fock Space." *J. Chem. Theory Comput.* **15**, 249 (2018).

[26] D. Wecker, M. B. Hastings, and M. Troyer. "Progress towards practical quantum variational algorithms." *Phys. Rev. A* **92**, 042303 (2015).

[27] A. Kandala, A. Mezzacapo, K. Temme, M. Takita, M. Brink, J. M. Chow, and J. M. Gambetta. "Hardware-efficient variational quantum eigensolver for small molecules and quantum magnets." *Nature* **549**, 242 (2017).

[28] I. G. Ryabinkin, T.-C. Yen, S. N. Genin, and A. F. Izmaylov. "Qubit Coupled Cluster Method: A Systematic Approach to Quantum Chemistry on a Quantum Computer." *J. Chem. Theory Comput.* **14**, 6317 (2018).

[29] I. G. Ryabinkin and S. N. Genin. "Iterative qubit coupled cluster method: A systematic approach to the full-CI limit in quantum chemistry calculations on NISQ devices." e-print arXiv:1906.11192v1 [quant-ph] (2019).

[30] H. R. Grimsley, S. E. Economou, E. Barnes, and N. J. Mayhall. "An adaptive variational algorithm for exact molecular simulations on a quantum computer." *Nat Comms* **10**, 1 (2019).

[31] P.-L. Dallaire-Demers, J. Romero, L. Veis, S. Sim, and A. Aspuru-Guzik. "Low-depth circuit ansatz for preparing correlated fermionic states on a quantum computer." *Quantum Sci. Technol.* **4**, 045005 (2019).

[32] J. R. McClean, M. E. Kimchi-Schwartz, J. Carter, and W. A. de Jong. "Hybrid quantum-classical hierarchy for mitigation of decoherence and determination of excited states." *Phys. Rev. A* **95**, 042308 (2017).

[33] J. I. Colless, V. V. Ramasesh, D. Dahlen, M. S. Blok, M. E. Kimchi-Schwartz, J. R. McClean, J. Carter, W. A. de Jong, and I. Siddiqi. "Computation of Molecular Spectra on a Quantum Processor with an Error-Resilient Algorithm." *Phys. Rev. X* **8**, 011021 (2018).

[34] O. Higgott, D. Wang, and S. Brierley. "Variational Quantum Computation of Excited States." *Quantum* **3**, 156 (2019).

[35] K. M. Nakanishi, K. Mitarai, and K. Fujii. "Subspace-search variational quantum eigensolver for excited states." e-print arXiv:1810.09434v2 [quant-ph] (2018).

[36] P. Jouzdani, M. Kostuk, and S. Bringuier. "A Method of Determining Excited-States for Quantum Computation." e-print arXiv:1908.05238v1 [quant-ph] (2019).

[37] R. M. Parrish, E. G. Hohenstein, P. L. McMahon, and T. J. Martinez. "Quantum Computation of Electronic Transitions Using a Variational Quantum Eigensolver." *Phys. Rev. Lett.* **122**, 230401 (2019).

[38] R. Santagati, J. Wang, A. A. Gentile, S. Paesani, N. Wiebe, J. R. McClean, S. Morley-Short, P. J. Shadbolt, D. Bonneau, J. W. Silverstone, D. P. Tew, X. Zhou, J. L. O'Brien, and M. G. Thompson. "Witnessing eigenstates for quantum simulation of Hamiltonian spectra." *Sci. Adv.* **4**, eaap9646 (2018).

[39] D. Wang, O. Higgott, and S. Brierley. "Accelerated Variational Quantum Eigensolver." *Phys. Rev. Lett.* **122**, 140504 (2019).

[40] F. A. Evangelista, G. K. Chan, and G. E. Scuseria. "Exact Parameterization of Fermionic Wave Functions via Unitary Coupled Cluster Theory." e-print arXiv:1910.10130 [physics.chem-ph] (2019).

[41] P. K. Barkoutsos, G. Nannicini, A. Robert, I. Tavernelli, and S. Woerner. "Improving Variational Quantum Optimization using CVaR." e-print arXiv:1907.04769v1 [quant-ph] (2019).

[42] T. Takeshita, N. C. Rubin, Z. Jiang, E. Lee, R. Babbush, and J. R. McClean. "Increasing the representation accuracy of quantum simulations of chemistry without extra quantum resources." e-print arXiv:1902.10679v2 [quant-ph] (2019).

[43] M. Motta, C. Sun, A. T. K. Tan, M. J O'Rourke, E. Ye, A. J. Minnich, F. G. S. L. Brandao, and G. K.-L. Chan. "Determining eigenstates and thermal states on a quantum computer using quantum imaginary time evolution." *Nat. Phys.* **21**, 1 (2019).

[44] W. J. Huggins, J. Lee, U. Baek, B. O'Gorman, and K. B. Whaley. "Non-Orthogonal Variational Quantum Eigensolver." e-print arXiv:1909.09114v1 [quant-ph] (2019).

[45] R. M. Parrish and P. L. McMahon. "Quantum Filter Diagonalization: Quantum Eigendecomposition without Full Quantum Phase Estimation." e-print arXiv:1909.08925v1 [quant-ph] (2019).

[46] P. J. Ollitrault, A. Kandala, C.-F. Chen, P. K. Barkoutsos, A. Mezzacapo, M. Pistoia, S. Sheldon, S. Woerner, J. Gambetta, and I. Tavernelli. "Quantum equation of motion for computing molecular excitation energies on a noisy quantum processor." *arXiv preprint arXiv:1910.12890* (2019).

[47] P. O. Löwdin. "On the non-orthogonality problem connected with the use of atomic wave functions in the theory of molecules and crystals." *J. Chem. Phys.* **18**, 365 (1950).

[48] H. F. King, R. E. Stanton, H. Kim, R. E. Wyatt, and R. G. Parr. "Corresponding Orbitals and the Nonorthogonality Problem in Molecular Quantum Mechanics." *J. Chem. Phys.* **47**, 1936 (1967).

[49] L. Noodleman. "Valence bond description of antiferromagnetic coupling in transition metal dimers." *J. Chem. Phys.* **74**, 5737 (1981).

[50] A. F. Voter and W. A. Goddard III. "The generalized resonating valence bond method: Barrier heights in the HF + D and HCl + D exchange reactions." *J. Chem. Phys.* **75**, 3638 (1981).

[51] P.-Å. Malmqvist. "Calculation of transition density matrices by nonunitary orbital transformations." *Int. J. Quantum Chem.* **30**, 479 (1986).

[52] H. Koch and E. Dalgaard. "Linear superposition of optimized nonorthogonal Slater determinants for singlet-states." *Chem. Phys. Lett.* **212**, 193 (1993).

[53] S. McArdle, T. Jones, S. Endo, Y. Li, S. C. Benjamin, and X. Yuan. "Variational ansatz-based quantum simulation of imaginary time evolution." *npj Quantum Inf* **5**, 1 (2019).

[54] D. Neuhauser. "Bound state eigenfunctions from wave packets: Time $\rightarrow$ energy resolution." *J. Chem. Phys.* **93**, 2611 (1990).

[55] D. Neuhauser. "Circumventing the Heisenberg principle: A rigorous demonstration of filter-diagonalization on a LiCN model." *J. Chem. Phys.* **100**, 5076 (1994).

[56] M. R. Wall and D. Neuhauser. "Extraction, through filter-diagonalization, of general quantum eigenvalues or classical normal mode frequencies from a small number of residues or a short-time segment of a signal. I. Theory and application to a quantum-dynamics model." *J. Chem. Phys.* **102**, 8011 (1995).

[57] V. A. Mandelshtam and H. S. Taylor. "A low-storage filter diagonalization method for quantum eigenenergy calculation or for spectral analysis of time signals." *J. Chem. Phys.* **106**, 5085 (1997).

[58] R. Somma, G. Ortiz, J. E. Gubernatis, E. Knill, and R. Laflamme. "Simulating physical phenomena by quantum networks." *Phys. Rev. A* **65**, 042323 (2002).

[59] T. E. O'Brien, B. Tarasinski, and B. Terhal. "Quantum phase estimation of multiple eigenvalues for small-scale (noisy) experiments." *New J. Phys.* (2019).

[60] O. Kyriienko. "Quantum inverse iteration algorithm for near-term quantum devices." e-print arXiv:1901.09988 [quant-ph] (2019).

[61] R. D. Somma. "Quantum eigenvalue estimation via time series analysis." e-print arXiv:1907.11748 [quant-ph] (2019).

[62] D. Aharonov, V. Jones, and Z. Landau. "A Polynomial Quantum Algorithm for Approximating the Jones Polynomial." *Algorithmica* **55**, 395 (2008).

[63] J. Lee, W. J. Huggins, M. Head-Gordon, and K. B. Whaley. "Generalized Unitary Coupled Cluster Wave functions for Quantum Computation." *J. Chem. Theory Comput.* **15**, 311 (2018).

[64] Y. Saad. *Iterative Methods for Sparse Linear Systems*. Society for Industrial and Applied Mathematics, second edition (2003).

[65] F. Furche, B. T. Krull, B. D. Nguyen, and J. Kwon. "Accelerating molecular property calculations with nonorthonormal Krylov space methods." *J. Chem. Phys.* **144**, 174105 (2016).

[66] M. Suzuki. "On the convergence of exponential operators—the Zassenhaus formula, BCH formula and systematic approximants." *Commun. Math. Phys.* **57**, 193 (1977).

[67] S. Lloyd. "Universal Quantum Simulators." *Science* **273**, 1073 (1996).

[68] D. W. Berry, A. M. Childs, R. Cleve, R. Kothari, and R. D. Somma. "Simulating Hamiltonian Dynamics with a Truncated Taylor Series." *Phys. Rev. Lett.* **114**, 29 (2015).

[69] R. Somma, G. Ortiz, E. Knill, and J. Gubernatis. "Quantum simulations of physics problems." *Int. J. Quantum Inf.* **1**, 189 (2003).

[70] M. B. Hastings, D. Wecker, B. Bauer, and M. Troyer. "Improving Quantum Algorithms for Quantum Chemistry." *Quantum Inf. Comput.* **15**, 1 (2015).

[71] J. T. Seeley, M. J. Richard, and P. J. Love. "The Bravyi-Kitaev transformation for quantum computation of electronic structure." *J. Chem. Phys.* **137**, 224109 (2012).

[72] A. M. Childs and N. Wiebe. "Hamiltonian Simulation Using Linear Combinations of Unitary Operations." *Quantum Inf. Comput.* **12**, 901 (2012).

[73] N. M. Tubman, C. Mejuto-Zaera, J. M. Epstein, D. Hait, D. S. Levine, W. Huggins, Z. Jiang, J. R. McClean, R. Babbush, and M. Head-Gordon. "Postponing the orthogonality catastrophe: efficient state preparation for electronic structure simulations on quantum devices." e-print arXiv:1809.05523 [quant-ph] (2018).

[74] K. Sugisaki, S. Yamamoto, S. Nakazawa, K. Toyota, K. Sato, D. Shiomi, and T. Takui. "Quantum chemistry on quantum computers: A polynomial-time quantum algorithm for constructing the wave functions of open-shell molecules." *J. Phys. Chem. A* **120**, 6459 (2016).

[75] K. Sugisaki, S. Yamamoto, S. Nakazawa, K. Toyota, K. Sato, D. Shiomi, and T. Takui. "Open shell electronic state calculations on quantum computers: A quantum circuit for the preparation of configuration state functions based on Serber construction." *Chem. Phys. Lett. X* **1**, 100002 (2019).

[76] K. Sugisaki, S. Nakazawa, K. Toyota, K. Sato, D. Shiomi, and T. Takui. "Quantum Chemistry on Quantum Computers: A Method for Preparation of Multiconfigurational Wave Functions on Quantum Computers without Performing Post-Hartree–Fock Calculations." *ACS Cent. Sci.* **5**, 167 (2019).

[77] A. F. Izmaylov, T.-C. Yen, and I. G. Ryabinkin. "Revising the measurement process in the variational quantum eigensolver: is it possible to reduce the number of separately measured operators?" *Chem. Sci.* **10**, 3746 (2019).

[78] A. F. Izmaylov, T.-C. Yen, R. A. Lang, and V. Verteletskyi. "Unitary partitioning approach to the measurement problem in the variational quantum eigensolver method." e-print arXiv:1907.09040 [quant-ph] (2019).

[79] P. Gokhale, O. Angiuli, Y. Ding, K. Gui, T. Tomesh, M. Suchara, M. Martonosi, and F. T. Chong. "Minimizing state preparations in variational quantum eigensolver by partitioning into commuting families." e-print arXiv:1907.13623 [quant-ph] (2019).

[80] A. Zhao, A. Tranter, W. M. Kirby, S. F. Ung, A. Miyake, and P. Love. "Measurement reduction in variational quantum algorithms." e-print arXiv:1908.08067 [quant-ph] (2019).

[81] P. Gokhale and F. T. Chong. "$\mathcal{O}(N^3)$ Measurement Cost for Variational Quantum Eigensolver on Molecular Hamiltonians." e-print arXiv:1908.11857 [quant-ph] (2019).

[82] N. H. Stair, R. Huang, N. He, and F. A. Evangelista. "QFORTE: A quantum computer simulator and algorithms library for molecular electronic structure."

[83] R. M. Parrish, L. A. Burns, D. G. Smith, A. C. Simmonett, A. E. DePrince III, E. G. Hohenstein, U. Bozkaya, A. Y. Sokolov, R. Di Remigio, and R. M. Richard. "Psi4 1.1: An open-source electronic structure program emphasizing automation, advanced libraries, and interoperability." *J. Chem. Theory Comput.* **13**, 3185 (2017).

[84] W. J. Hehre, R. F. Stewart, and J. A. Pople. "Self-Consistent Molecular-Orbital Methods. I. Use of Gaussian Expansions of Slater-Type Atomic Orbitals." *J. Chem. Phys.* **51** (1969).

[85] J. R. McClean, K. J. Sung, I. D. Kivlichan, Y. Cao, C. Dai, E. S. Fried, C. Gidney, B. Gimby, P. Gokhale, T. Häner, T. Hardikar, O. Higgott, C. Huang, J. Izaac, Z. Jiang, X. Liu, S. McArdle, M. Neeley, T. O'Brien, B. O'Gorman, I. Ozfidan, M. D. Radin, J. Romero, N. Rubin, N. P. D. Sawaya, K. Setia, S. Sim, D. S. Steiger, M. Steudtner, Q. Sun, W. Sun, D. Wang, F. Zhang, and R. Babbush. "OpenFermion: The Electronic Structure Package for Quantum Computers." e-print arXiv:1710.07629v5 [quant-ph] (2017).

[86] M. Motta, D. M. Ceperley, G. K.-L. Chan, J. A. Gomez, E. Gull, S. Guo, C. A. Jiménez-Hoyos, T. N. Lan, J. Li, and F. Ma. "Towards the solution of the many-electron problem in real materials: equation of state of the hydrogen chain with state-of-the-art many-body methods." *Phys. Rev. X* **7**, 031059 (2017).

[87] A. V. Sinitskiy, L. Greenman, and D. A. Mazziotti. "Strong correlation in hydrogen chains and lattices using the variational two-electron reduced density matrix method." *J. Chem. Phys.* **133**, 014104 (2010).

[88] L. Stella, C. Attaccalite, S. Sorella, and A. Rubio. "Strong electronic correlation in the hydrogen chain: A variational Monte Carlo study." *Phys. Rev. B* **84**, 245117 (2011).

[89] I. Shavitt and R. J. Bartlett. *Many-body methods in chemistry and physics: MBPT and coupled-cluster theory*. Cambridge university press (2009).

[90] B. Huron, J. P. Malrieu, and P. Rancurel. "Iterative perturbation calculations of ground and excited state energies from multiconfigurational zeroth-order wavefunctions." *J. Chem. Phys.* **58**, 5745 (1973).

[91] J. B. Schriber and F. A. Evangelista. "Communication: An adaptive configuration interaction approach for strongly correlated electrons with tunable accuracy." *J. Chem. Phys.* **144**, 161106 (2016).

[92] A. A. Holmes, N. M. Tubman, and C. J. Umrigar. "Heat-Bath Configuration Interaction: An Efficient Selected Configuration Interaction Algorithm Inspired by Heat-Bath Sampling." *J. Chem. Theory and Comput.* **12**, 3674 (2016).

[93] N. M. Tubman, J. Lee, T. Y. Takeshita, M. Head-Gordon, and K. B. Whaley. "A deterministic alternative to the full configuration interaction quantum Monte Carlo method." *J. Chem. Phys.* **145**, 044112 (2016).

[94] Y. Garniron, A. Scemama, P.-F. Loos, and M. Caffarel. "Hybrid stochastic-deterministic calculation of the second-order perturbative contribution of multireference perturbation theory." *J. Chem. Phys.* **147**, 034101 (2017).

[95] D. Poulin, A. Kitaev, D. S. Steiger, M. B. Hastings, and M. Troyer. "Quantum Algorithm for Spectral Measurement with a Lower Gate Count." *Phys. Rev. Lett.* **121**, 010501 (2018).

# Chapter 4

# Simulating many-body systems with a projective quantum eigensolver

## 4.1 Introduction

Efficient quantum algorithms for determining the ground and excited states of many-body systems are of fundamental interest to chemistry, condensed matter physics, and materials science.[1–4] The ability of quantum devices to represent $N$-body states with qubits scaling linearly in $N$ make them particularly appealing for representing highly entangled states, as is common in systems with strongly correlated electrons. Therefore, quantum (and hybrid quantum-classical) algorithms offer an alternative to methods such as the density matrix renormalization group[5] (DMRG), selected configuration interaction[6,7] (SCI), determinant-based Monte-Carlo,[8] variants of coupled-cluster (CC) theory[9,10] amenable to treating strong correlation,[11–14] and multireference CC (MRCC) methods.[15–20] Although these classical algorithms can accurately predicted energies and properties of certain classes of strongly correlated systems, they still have high-order polynomial or exponential cost in the general case.

Since Feynman's proposal to use a controlled quantum system to carry out simulations,[21] significant algorithmic and experimental advances have been made. The earliest demonstrations of quantum simulation for small molecules[2] utilized the quantum phase estimation algorithm[22–24] with Suzuki–Trotter decomposed time evolution[25,26] of an adi-

abatically prepared trial state. It is believed that some combination of these techniques will permit the efficient simulation[27–30] of certain classes of Hamiltonians,[31] but that they may require deep circuits with high fidelity, a requirement incompatible with current noisy intermediate-scale quantum (NISQ) devices.[32] Several low-depth quantum-classical hybrid algorithms have been developed for NISQ hardware. These algorithms prepare and measure properties of many-body states on a quantum device, but they store and optimize the parameters that define such states on a classical computer. The variational quantum eigensolver (VQE) approach[33–36] has been used in several landmark experiments, demonstrating quantum calculations on non-trivial molecular systems.[3,37–41] In VQE, the ground state is approximated by a normalized trial state $\left|\tilde{\Psi}\right\rangle = \hat{U}(\mathbf{t})\left|\Phi_0\right\rangle$, in which the unitary operator $\hat{U}(\mathbf{t})$ depends on the parameter vector $\mathbf{t}$ and $\Phi_0$ is (usually) an unentangled reference state. The VQE energy ($E_{\mathrm{VQE}}$) is then obtained by minimization of the trial state energy expectation value as

$$E_{\mathrm{VQE}} = \min_{\mathbf{t}} \left\langle \Phi_0 \right| \hat{U}^{\dagger}(\mathbf{t}) \hat{H} \hat{U}(\mathbf{t}) \left| \Phi_0 \right\rangle . \tag{4.1}$$

The VQE scheme employs an optimization algorithm running on a classical computer to minimize the energy expectation value, with all inputs (energy/gradients) being evaluated with the help of a quantum computer. An important advantage of VQE over classical many-body methods is the ability to use trial states that cannot be represented efficiently on a classical computer. VQE was initially implemented with an exponential operator ansatz inspired by unitary coupled-cluster (UCC) theory,[42–48] but has more recently been extended to hardware-efficient[3] and qubit-space[49] UCC variants as well. We exclusively use the abbreviation UCC to refer to unitary coupled-cluster theory, and not unrestricted formulations of conventional coupled-cluster methods,[50] which historically share this abbreviation. Other promising hybrid approaches include quantum imaginary time evolution,[51,52] and quantum subspace diagonalization techniques.[51,53–56]

Despite the indisputable importance of VQE in the field of quantum simulation, there are a few drawbacks that make its practical application challenging to large-scale prob-

lems. One such issue is the slow convergence of VQE due to noise in the measured energy and gradients, and the large-scale nonlinear nature of the optimization problem. These issues are compounded by the sizable number of total measurements needed for operator averaging.[57] Another challenge is the potentially large number of classical parameters and resulting circuit depth necessary to predict sufficiently accurate energies. These two problems are likely exacerbated in systems with strongly correlated electrons.

Progress addressing these deficiencies of VQE has been made on several fronts. For example, grouping commuting Pauli operators,[3,35,58–60] utilizing integral factorization strategies,[61] and employing alternative bases[29,62] have been shown to reduce the number of measurements needed for operator averaging. Concurrently, computationally feasible approaches for measuring analytical gradients with quantum devices using the parameter-shift rule,[63] or its recent lower-cost variant,[64] have allowed gradient-based VQE to become potentially realizable on NISQ hardware. Other advances, of particular importance to this work, include VQE ansätze constructed iteratively, as done in the adaptive derivative-assembled pseudo-Trotterized VQE[36] (ADAPT-VQE) and the iterative qubit coupled-cluster[65] (iQCC) methods. The primary advantage of ADAPT-VQE and iQCC is their ability to produce compact ansätze that result in fewer classical parameters, and shallower quantum circuits than those from UCC truncated to a given particle-hole rank. However, these advantages come at the cost of a greater number of energy and gradient evaluations for optimizing and selecting new unitary operators. Investigating more efficient ways to select important operators is an ongoing area of research.[66,67]

In this work, we present an alternative to VQE for optimizing the amplitudes of a factorized form of the UCC ansatz (often referred to as Trotterized[35] or quantum[68] UCC), given by a product of exponential operators rather than the exponential of a sum of operators. We refer to this ansatz as disentangled UCC (UCC)—a terminology borrowed from the field of Lie theory—to reflect the fact that it is not an approximation of UCC.[69] Inspired by the projective approach used in classical coupled-cluster theory,[10,15] we pro-

pose an alternative trial state optimization algorithm that we deem the projective quantum eigensolver (PQE). PQE does not rely on variational minimization and therefore does not require evaluation of the energy gradients. Instead, PQE requires only the evaluation of residuals, that is, projections of the Schrödinger equations onto a linearly independent basis. As shown in this paper, residuals may be easily measured on NISQ devices with similar or fewer measurements than analytical gradients, and require quantum circuits that contain only one additional exponential term. We also propose a new selection scheme for identifying important operators based on the residual vector. This selected variant of PQE (SPQE) requires no pre-defined operator pool and employs only a small number of measurements to identify important operators. To demonstrate the practical advantages of PQE, we perform a comparison of VQE and PQE using a fixed UCC ansatz for several molecular systems in the regime of weak and strong correlation, also considering the effect of stochastic noise. Finally, we compare SPQE against the ADAPT-VQE approach, selected configuration interaction, and the density matrix renormalization group.

## 4.2 Theory

### 4.2.1 The projective quantum eigensolver approach

In this work, we propose to obtain the ground state of a general many-body system using a projective approach. Like in VQE, we approximate the ground state using a trial state $\left|\tilde{\Psi}(\mathbf{t})\right\rangle = \hat{U}(\mathbf{t})\left|\Phi_0\right\rangle$. After inserting the definition of the trial state in the Schrödinger equation and left-multiplying by $\hat{U}^\dagger(\mathbf{t})$, we obtain the condition

$$\hat{U}^\dagger(\mathbf{t})\hat{H}\hat{U}(\mathbf{t})\left|\Phi_0\right\rangle = E\left|\Phi_0\right\rangle. \tag{4.2}$$

Projection onto the reference state $\Phi_0$ yields the PQE energy ($E_{\mathrm{PQE}}$)

$$E_{\mathrm{PQE}}(\mathbf{t}) = \left\langle\Phi_0\right|\hat{U}^\dagger(\mathbf{t})\hat{H}\hat{U}(\mathbf{t})\left|\Phi_0\right\rangle, \tag{4.3}$$

a quantity that is still an upper bound to the exact ground state energy. Projections onto the complete set of orthonormal many-body basis functions complementary to $\Phi_0$, here denoted as $Q = \{\Phi_\mu\}$, yields a set of residual conditions

$$r_\mu(\mathbf{t}) \equiv \left\langle \Phi_\mu \right| \hat{U}^\dagger(\mathbf{t}) \hat{H} \hat{U}(\mathbf{t}) \left| \Phi_0 \right\rangle = 0 \quad \forall \Phi_\mu \in Q, \tag{4.4}$$

where $r_\mu$ is an element of the residual vector and $\mu$ runs over all elements of the many-body basis. Eqs. (4.3) and (5.20) form a system of nonlinear equations in the parameter vector $\mathbf{t}$, that may be solved via a classical iterative solver. For an approximate ansatz with number of parameters less than the dimension of the $Q$ space, Eq. (5.20) can be enforced only for a subset of the residuals. Then, the complete projection space $Q$ can be partitioned into two sets: i) $R$, the space of basis functions $\Phi_\mu$ for which $r_\mu = 0$ is enforced, and ii) $S = Q \setminus R$ the complementary space for which $r_\mu$ may not be null.

Figure 4.1 illustrates the connection between the PQE residual condition and the uncertainty in the ground-state energy estimated via Eq. (4.3). By the Gershgorin circle theorem, the difference between the exact ($E$) and the PQE ($E_{\mathrm{PQE}}$) ground-state energy, $|E_{\mathrm{PQE}} - E|$, is bound by the radius $\rho = \sum_{\mu \neq 0} |r_\mu|$, where $\mu$ runs over the entire many-body basis, excluding the reference determinant. Therefore, when the residual is null ($\rho = 0$), the PQE energy is exact. When the PQE equation is satisfied only by a subset of the many-body basis—as in the case of an approximate trial state—the error $|E_{\mathrm{PQE}} - E|$ is bound by the sum of the absolute value of the residual elements $|r_\nu|$ with $\Phi_\nu \in S$, for which the PQE equation is not satisfied.

Note that the residual condition [Eq. (5.20)] is satisfied by any eigenstate, and the Gershgorin circle theorem error bound applies also to excited states. A potential disadvantage is that PQE could converge on an excited state (an issue we did not experience in this study). However, this feature could be used to formulate excited state algorithms based on PQE, which use the residual condition as a criterion for convergence and do not require costly measurement of the variance, as is commonly done in VQE.[35]

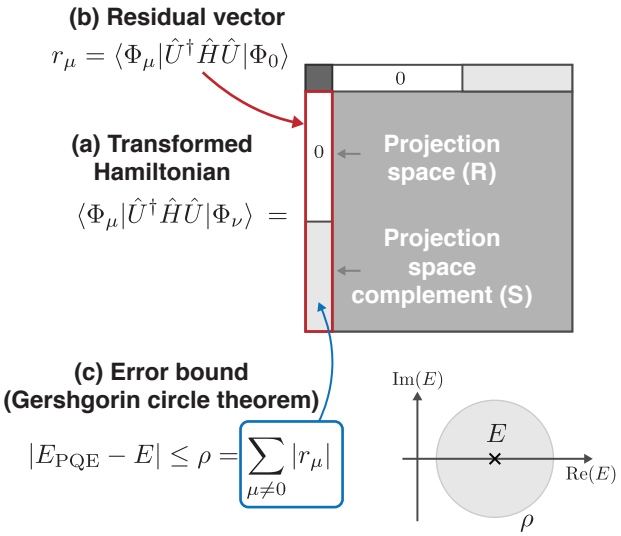


Figure 4.1: Connection between the norm of the PQE residual and the energy error via the Gershgorin circle theorem. (a) Structure of the transformed Hamiltonian in the basis of orthogonal states $\{\Phi_\mu\}$. (b) The residual vector is the first column of the transformed Hamiltonian matrix (first element excluded). (c) The difference between the approximate ground-state PQE energy ($E_{\mathrm{PQE}}$) and the exact eigenvalue ($E$) is bound by the radius $\rho$, which is equal to the 1-norm of the residual vector. The part of $r_\mu$ that corresponds to states in the projection manifold $R$ is null for the PQE solution, while elements involving projections on the space $S = Q \setminus R$ is generally nonzero and determines the value of $\rho$.

The PQE is a general approach, however, in the following, we will focus on its applications to interacting fermions using a disentangled (factorized) form of the unitary coupled-cluster ansatz. We assume that our system is described by the general two-body Hamiltonian

$$\hat{H} = \sum_{pq} h_{pq}\hat{a}_p^\dagger\hat{a}_q + \frac{1}{4}\sum_{pqrs} v_{pqrs}\hat{a}_p^\dagger\hat{a}_q^\dagger\hat{a}_s\hat{a}_r, \tag{4.5}$$

where $\hat{a}_p$ ($\hat{a}_q^\dagger$) is a fermionic annihilation (creation) operator, while $h_{pq}$ and $v_{pqrs}$ are one-electron and antisymmetrized two-electron integrals, respectively.[70]

### 4.2.2 Traditional and disentangled unitary coupled-cluster ansätze

In UCC, the reference state is an easily-prepared single determinant $|\Phi_0\rangle = |\psi_1\psi_2\cdots\rangle$ specified by the occupied spin orbitals $\{\psi_i\}$. A UCC unitary is parameterized using a pool of anti-Hermitian operators $\mathscr{P} = \{\hat{\kappa}_\mu : \mu = 1,\ldots,N_{\mathrm{op}}^{\mathrm{pool}}\}$. A generic anti-Hermitian operator $\hat{\kappa}_\mu = \hat{\tau}_\mu - \hat{\tau}_\mu^\dagger$ is defined in terms of the particle-hole excitation operators $\hat{\tau}_\mu \equiv \hat{\tau}_{ij\cdots}^{ab\cdots} =$

$\hat{a}_a^\dagger \hat{a}_b^\dagger \cdots \hat{a}_j \hat{a}_i$. Note that we have re-interpreted $\mu$ as the multi-index $\mu \equiv ((i,j,..),(a,b,..))$ of unique excitations from hole/occupied ($\psi_i \psi_j \cdots$) to particle/unoccupied ($\psi_a \psi_b \cdots$) spin orbitals. Using this parameterization, when a cluster operator $\hat{\kappa}_\mu$ acts on the reference, it generates elements of the many-body basis (excited determinants) of the form

$$\left|\Phi_\mu\right\rangle = \hat{\kappa}_\mu \left|\Phi_0\right\rangle = \left|\Phi_{ij\cdots}^{ab\cdots}\right\rangle, \tag{4.6}$$

and since in the case of a UCC (or dUCC) ansatz there is a 1-to-1 correspondence between operators and determinants, we may label them with the same index. Note that this operator basis satisfies the orthonormality condition $\langle\Phi_0| \hat{\kappa}_\mu^\dagger \hat{\kappa}_\nu |\Phi_0\rangle = \left\langle \Phi_\mu | \Phi_\nu \right| \left. \Phi_\mu | \Phi_\nu \right\rangle = \delta_{\mu\nu}$.

In traditional UCC,[42–46] the wave function is generated by an exponential operator

$$\hat{U}(\mathbf{t}) = e^{\hat{\sigma}} = e^{\sum_\mu t_\mu \hat{\kappa}_\mu}, \tag{4.7}$$

assuming the cluster amplitudes $t_\mu$ are real. In principle it is possible to construct a circuit that exactly implements the action of the UCC operator defined in Eq. (4.7), but in practice it is common to use a unitary with a simpler, and shallower, circuit. This is frequently accomplished using a factorized (disentangled) form of the UCC ansatz

$$\hat{U}(\mathbf{t}) = \prod_\mu e^{t_\mu \hat{\kappa}_\mu}. \tag{4.8}$$

Because the operators $\hat{\kappa}_\mu$ do not commute, an ansatz of the disentangled form is uniquely defined by an *ordered* set (or subset) of operators $\mathscr{A} = (\hat{\kappa}_{\mu_i} : i = 1, \ldots, N_{\text{op}})$ built from the operator pool $\mathscr{P}$. The operators in $\mathscr{A}$ are then used to form an ordered product of exponential unitaries

$$\hat{U}(\mathbf{t}) = e^{t_{\mu_1} \hat{\kappa}_{\mu_1}} e^{t_{\mu_2} \hat{\kappa}_{\mu_2}} \cdots e^{t_{\mu_{N_{\text{op}}}} \hat{\kappa}_{\mu_{N_{\text{op}}}}}, \tag{4.9}$$

where $t_{\mu_i}$ is the amplitude corresponding to the operator $\hat{\kappa}_{\mu_i}$.

The disentangled UCC ansatz may be viewed as a first-order Suzuki–Trotter approximation to UCC; however, it was recently shown[69] that this ansatz is substantially different

from the one used in conventional UCC [Eq. (4.7)] as discussed in the electronic structure literature.[42–46] An arbitrary quantum state can always be represented in the form of Eq. (4.9) using particle-hole excitation/de-excitation operators.[69] However, even when a full operator pool (containing up to $N$-body particle/hole excitations) is considered, only certain operator orderings $\mathscr{A}$ can represent any quantum state. Nevertheless, orderings that do not satisfy this condition can exactly represent states that are close to the reference. In this work we assume that all operators appear at most once in $\mathscr{A}$, but the more general case in which $\mathscr{A}$ contains repetitions has also been considered in other contexts.[36,71]

For PQE formulated using a UCC or dUCC trial state, it is possible to show (see Appendix 4.5.1) that for an exact ansatz the residual condition [Eq. (5.20)] and the VQE energy stationarity condition ($\partial E_{\mathrm{VQE}}/\partial t_\mu = 0$) are equivalent. However, for an approximate ansatz we find that the gradient of the PQE energy contains a contribution due to the nonzero residual elements corresponding to the subspace $S$:

$$\frac{\partial E_{\mathrm{PQE}}(\mathbf{t})}{\partial t_\mu} = 2\,\mathrm{Re} \sum_{\Phi_\nu \in S} r_\nu^* \langle \Phi_\nu | \hat{U}^\dagger(\mathbf{t}) \frac{\partial \hat{U}(\mathbf{t})}{\partial t_\mu} |\Phi_0\rangle \,. \tag{4.10}$$

Suppose that $R$ is chosen to be the space of single and double excitations and $S$ its complement. Then this result shows that even if $r_\mu = 0$ for all singles and doubles, the gradient of $E_{\mathrm{PQE}}$ with respect to singles and doubles may not be zero because residuals $r_\nu$ corresponding to triple and higher excitations and the term $\langle \Phi_0 | \hat{U}^\dagger(\mathbf{t}) \partial \hat{U}(\mathbf{t})/\partial t_\mu |\Phi_\nu\rangle$ are generally not null. Therefore, PQE and VQE energies obtained from approximate ansätze will be different.

We note that the combination of PQE and dUCC produces energies that are additive for non-interacting fragments (size consistent) when using a localized basis. This property follows from the fact that dUCC excitation operators for non-interacting fragments act only on orbitals localized on each fragment, and therefore, commute. Consequently, the dUCC wave function is multiplicatively separable (as long as the order of the operators within a fragment is preserved). We have verified numerically that dUCC with singles and doubles

trial states optimized with PQE energy are size consistent by performing calculations on $H_4$ + $H_2$ separated at a 1000 Å and verified to within numerical convergence ($10^{-10}$ $E_h$) that the energy is additive in the fragments.

### 4.2.3 Numerical solution of the UCC-PQE amplitude equation

To realize the PQE scheme on a quantum computer, the reference state, the Hamiltonian, and the unitary must be represented in a qubit basis via a fermionic mapping. After such a transformation, the Hamiltonian is a sum of the form $\hat{H} = \sum_\ell h_\ell \hat{O}_\ell$, where $h_\ell$ is an electron integral multiplied by a coefficient and $\hat{O}_\ell = \prod_i \hat{\sigma}_{j_{\ell_i}}^{q_{\ell_i}}$ is a unique product of $\hat{\sigma}_x$, $\hat{\sigma}_y$, or $\hat{\sigma}_z$ Pauli operators acting on qubits $q_{\ell_i}$. Similarly, each term in the unitary $\exp\left(t_\mu \hat{\kappa}_\mu\right)$ may be implemented using a combination of one- and two-qubit operators following standard approaches.[33–35]

To solve the PQE equations we measure the residuals corresponding to the operators contained in $\mathscr{A}$ on a quantum computer and update the parameter vector using a simple quasi-Newton iteration approach

$$t_\mu^{(n+1)} = t_\mu^{(n)} + \frac{r_\mu^{(n)}}{\Delta_\mu}, \tag{4.11}$$

where the superscript "$(n)$" indicates the amplitude at iteration $n$. The quantities $\Delta_\mu$ are standard Møller–Plesset denominators $\Delta_\mu \equiv \Delta_{ij\ldots}^{ab\cdots} = \varepsilon_i + \varepsilon_j + \ldots - \varepsilon_a - \varepsilon_b \ldots$ where $\varepsilon_i$ are Hartree–Fock orbital energies. This update equation is derived in Appendix 4.5.2 using Newton's method and taking the leading contributions to the Jacobian to be the diagonal elements of the Fock operator.[72] It is further assumed that the amplitudes are small, so that the Jacobian can be approximated by terms linear in the operators $\hat{\kappa}_\mu$ and issues with non-commuting operators are avoided. Therefore, convergence of this quasi-Newton scheme is not mathematically guaranteed if one or more amplitudes are large.

We found it useful to improve numerical stability and speed up convergence of the PQE equations, to combine amplitude updates via Eq. (5.23) with the direct inversion of

the iterative subspace (DIIS) convergence accelerator algorithm.[73]

It is important to note that the current formulation of PQE is compatible with any ansatz such that the metric matrix

$$S_{\mu_i\mu_j} = \langle\Phi_0|\,\hat{\kappa}^\dagger_{\mu_i}\hat{\kappa}_{\mu_j}\,|\Phi_0\rangle\,, \quad \forall\hat{\kappa}_{\mu_i},\hat{\kappa}_{\mu_j}\in\mathscr{A} \tag{4.12}$$

is the identity. In more general cases (e.g., when $S_{\mu_i\mu_j}$ is non-diagonal or singular), the PQE formalism requires a generalization of the amplitude update equations or the use of residual norm minimization instead of Eq. (5.20). These variants of PQE would allow one to consider ansätze that contain repeated operators in $\mathscr{A}$, employ general many-body operators, or a basis of qubit operators. These extensions go beyond the scope of this work and will be considered in future studies.

There are two advantages to the combination of the PQE and UCC described above. Firstly, as we will show in the following subsection, one element of the residual vector ($r_\mu$) can be evaluated with essentially the same resources required to measure the energy in VQE. Secondly, the magnitude of the residuals provides an indication of the importance of an excitation operator $\hat{\kappa}_\mu$, which in turn may be used to define a selection procedure to form the sequence of unitiaries that enter in $\hat{U}(\mathbf{t})$. The next two subsections describe these two points in detail.

### 4.2.4 Efficient measurement of the residual elements

For a trial state built from the ordered pool $\mathscr{A}$, the number of the residual elements that must be measured is equal to the size of the pool $|\mathscr{A}|$. The PQE residuals can be expressed as the off-diagonal matrix elements of the operator $\bar{H} = \hat{U}^\dagger(\mathbf{t})\hat{H}\hat{U}(\mathbf{t})$ as $r_\mu = \langle\Phi_\mu|\,\bar{H}\,|\Phi_0\rangle$ (we use this notation throughout the paper, but we note that we never explicitly form the operator $\bar{H}$ on a classical computer). Then, in principle, the residuals can be measured on a quantum computer using a variant of the Hadamard test,[74] but we have found an ancilla-free procedure in which these matrix elements are computed by measuring diagonal quantities.

Acting on the reference with the operator $e^{\theta\hat{\kappa}_\mu}$ yields the state

$$\left|\Omega_\mu(\theta)\right\rangle = e^{\theta\hat{\kappa}_\mu}\left|\Phi_0\right\rangle = \cos(\theta)\left|\Phi_0\right\rangle + \sin(\theta)\left|\Phi_\mu\right\rangle, \tag{4.13}$$

noting that the above expression is valid because $\hat{\kappa}_\mu\left|\Phi_0\right\rangle = \left|\Phi_\mu\right\rangle$ and $\hat{\kappa}_\mu^2\left|\Phi_0\right\rangle = -\left|\Phi_0\right\rangle$ (see also[47,48]). Taking the expectation value of the similarity transformed Hamiltonian with respect to $\Omega_\mu(\theta)$ using $\theta = \pi/4$, and using the fact that the wave function is real, leads to the following equation for the residual elements

$$r_\mu = \left\langle\Omega_\mu(\pi/4)\right|\bar{H}\left|\Omega_\mu(\pi/4)\right\rangle - \frac{1}{2}E_\mu - \frac{1}{2}E_0, \tag{4.14}$$

where $E_0 = \left\langle\Phi_0\right|\bar{H}\left|\Phi_0\right\rangle$ and $E_\mu = \left\langle\Phi_\mu\right|\bar{H}\left|\Phi_\mu\right\rangle$. All of these quantities are expectation values of $\bar{H}$ with respect to reference states that are easily generated with short quantum circuits. The evaluation of the exact residual via Eq. (4.14) has a cost similar to the evaluation of exact gradients in VQE via the shift rule.[63,64]

### 4.2.5 Efficient operator selection

In this section, we generalize the PQE method to utilize a flexible dUCC ansatz built iteratively using a full operator pool. As shown in the case of VQE,[36,65] significantly more compact and flexible approximations may be achieved if the operators that define the unitary are selected according to an importance criterion. To formulate a selected version of the PQE approach, we propose to combine information about the residual with a cumulative importance criterion. Since the residuals $r_\mu$ are zero if the trial state is an exact eigenstate of the Hamiltonian, we propose to estimate the importance of the operators $\hat{\kappa}_\mu$ using the magnitude of the residual ($|r_\mu|$). However, instead of evaluating the importance of all the operators in the pool via operator averaging (like in gradient-based selection schemes[36,65]), we propose to sample a quantum state whose probability amplitudes encode the importance of *all* operators up to rank $N$.

Suppose that we have determined a unitary $\hat{U}$ that satisfies the residual condition $r_\mu = 0$

for all $\hat{\kappa}_\mu$ in the current ordered set $\mathscr{A}$. In our approach we prepare a (normalized) quantum state of the form $|\tilde{r}\rangle = \tilde{r}_0 |\Phi_0\rangle + \sum_\mu \tilde{r}_\mu |\Phi_\mu\rangle$, where the quantities $\tilde{r}_\mu$ are approximately proportional to the residuals $r_\mu$. When the state $|\tilde{r}\rangle$ is represented in a qubit basis, there is a one-to-one mapping between elements of the computational basis and the states $\Phi_\mu$. Therefore, a measurement of the state $|\tilde{r}\rangle$ in the qubit basis will yield one of the states $\Phi_\mu$ with probability $P_\mu = |\tilde{r}_\mu|^2$. Repeated measurement of the state $|\tilde{r}\rangle$ provides a way to approximately determine the elements of the residual $r_\mu$ with the largest magnitude, and the corresponding operators $\hat{\kappa}_\mu$ that should be included in the unitary. When this strategy is combined with an efficient way to prepare the state $|\tilde{r}\rangle$, it is much more cost effective than evaluating all the elements of $r_\mu$ not included in $\mathscr{A}$ via operator averaging [Eq. (4.14)].

Construction of the state $|\tilde{r}\rangle$ would require one to apply the Hamiltonian, which is not a unitary operator. Therefore, we evaluate $\tilde{r}$ using the unitary operator $e^{-i\Delta t\hat{H}} = 1 - i\Delta t\hat{H} + \mathscr{O}(\Delta t^2)$ instead of $\hat{H}$. By choosing a small time step, we can ensure that the nonlinear terms and errors due to the approximate implementation of $e^{-i\Delta t\hat{H}}$ (e.g., via Trotterization) do not affect the residual to leading order in $\Delta t$. The residual state can then be defined as

$$\begin{aligned} |\tilde{r}\rangle &= \hat{U}^\dagger e^{i\Delta t\hat{H}} \hat{U} |\Phi_0\rangle \\ &= (1 + i\Delta t \hat{U}^\dagger \hat{H} \hat{U}) |\Phi_0\rangle + \mathscr{O}(\Delta t^2), \end{aligned} \tag{4.15}$$

The time-evolution operator may be approximated via Trotterization[25,26] in combination with low-rank representations of the Hamiltonian.[75] With a sufficiently large number of measurements $M$ of the state $|\tilde{r}\rangle$, we may approximate the values of the (normalized) squared residuals as

$$\left\|\tilde{r}_\mu\right\| \approx \frac{N_\mu}{M}, \tag{4.16}$$

where $N_\mu$ is the number of times the state $|\Phi_\mu\rangle$ is measured. Encoding the residual in a single quantum state allows us to efficiently sample the *entire* operator pool without the need to generate and store individual elements of the residual vector in memory. This distinctive feature makes it possible to employ SPQE with a full operator pool that includes

particle-hole excitation/de-excitation operators of arbitrary order.

To select important operators, we adopt a cumulative threshold approach that allows us to add a batch of operators at a time. Our goal is to iteratively construct a unitary that contains the fewest operators. This is realized in SPQE with a selection procedure that adds the operators with the largest value of $\tilde{r}_\mu$ to $\mathscr{A}$ (as motivated by the Gershgorin circle theorem bounds discussed in Sec. 4.2.1), and excludes all other operators in such a way that sum of their residuals squared is less than a threshold $\Omega^2$. Specifically, we enforce that

$$\sum_{\hat{\kappa}_\mu \notin \mathscr{A}}^{\text{excluded}} \left\| r_\mu \right\| \approx \sum_{\hat{\kappa}_\mu \notin \mathscr{A}}^{\text{excluded}} \frac{\left\| \tilde{r}_\mu \right\|}{\Delta t^2} \leq \Omega^2, \tag{4.17}$$

where we have used the fact that $|\tilde{r}_\mu| \approx \Delta t |r_\mu|$. In practice, we sort the operators in ascending order according to $\left\| \tilde{r}_\mu \right\|$, and starting from the first element, we discard operators until Eq. (5.26) is satisfied. The remaining operators are appended to the end of $\mathscr{A}$ in order of decreasing $\left\| \tilde{r}_\mu \right\|$. The resulting operator ordering is consistent with the following renormalization transformation of the Hamiltonian

$$\begin{aligned} \hat{H} &\to e^{-t_{\mu_1} \hat{\kappa}_{\mu_1}} \hat{H} e^{t_{\mu_1}} = \bar{H}_1 \\ &\to e^{-t_{\mu_2} \hat{\kappa}_{\mu_2}} \bar{H}_1 e^{t_{\mu_2} \hat{\kappa}_{\mu_2}} = \bar{H}_2 \\ &\to \cdots \end{aligned} \tag{4.18}$$

which begins with the largest many-body rotation and gradually continues with smaller ones. Note that this ordering is the reverse of the one used in ADAPT-VQE and iQCC, where operators with the largest gradient are applied first to the reference. In applications of SPQE, we found that our operator ordering is more numerically robust and accurate than its reverse. This selection procedure is easily integrated in the PQE algorithm by performing a series of computations with increasingly larger ordered sets. When no new operators are added to $\mathscr{A}$, the computation is considered converged, and the final operator set satisfies Eq. (5.26). The details of the selected PQE algorithm are discussed in Sec. 4.2.6.

Throughout this work, we ignore errors that arise from finite measurement of the approximate residual $|\tilde{r}\rangle$. However, since operator selection only requires an approximate

determination of the residual magnitudes, it is not necessary to perform a large number of measurements. Indeed, in Appendix 4.5.5, we discuss a simple strategy based on sampling $|\tilde{r}\rangle$ a fixed number of times that can reproduce the results presented here.

### 4.2.6 Outline of the selected PQE algorithm

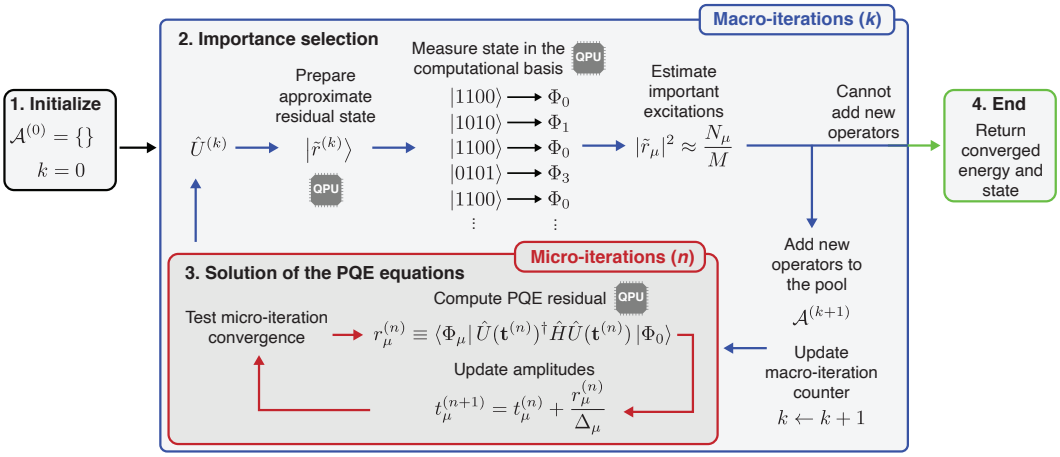


Figure 4.2: Outline of the adaptive PQE algorithm. Steps labeled "QPU" indicate parts of the algorithm that run on a quantum processing unit.

The combination of the PQE approach with the selection procedure described in Sec. 4.2.5 leads to a very efficient flexible ansatz quantum algorithm, which we refer to as selected PQE (SPQE). Finding the optimal selected PQE solution requires the simultaneous solution of the residual conditions and the selection of important excitation operators. To realize this scheme, we employ a procedure that alternates micro-iterations to converge the residual equations (for the current ordered operator set) with macro-iterations that perform importance selection of new operators. This procedure is illustrated in Fig. 4.2 and consists of the following steps:

1. **Initialization**. The user provides the occupation numbers that define the reference state $\Phi_0$. The procedure starts at macro-iteration number $k = 0$ with an empty operator set ($\mathscr{A}^{(0)} = \{\}$).

2. **Importance selection**. At macro-iteration $k$, perform $M$ measurements in the com-

putational basis for the the state $\left|\tilde{r}^{(k)}\right\rangle = \hat{U}^{(k)\dagger} e^{i\Delta t \hat{H}} \hat{U}^{(k)} |\Phi_0\rangle$. The number of times the state $\Phi_\mu$ is measured is accumulated in the variable $N_\mu$. These numbers are converted to estimates of the square residuals via Eq. (5.25), which are in turn used to select important excitations not included in the current pool $\mathscr{A}_k$. The current operator set $\mathscr{A}_k$ and all the new selected operators are included in the new set $\mathscr{A}_{k+1}$. When forming this new ordered set, we append the new operators—sorted in decreasing value of the approximate squared residual—to $\mathscr{A}_k$. If the sum in Eq. (5.26) over *all* approximate residuals is less than the threshold $\Omega^2$, such that no new operators are added, then return the final energy.

3. **Solution of the PQE equations**. Using the new set $\mathscr{A}_{k+1}$, solve the PQE equations via quasi-Newton micro-iterations. These micro-iterations alternate the evaluation of the residuals [Eq. (5.20)] and the amplitude update [Eq. (5.23)]. The micro-iterations are considered converged when the norm of the residual vector $\|\mathbf{r}\|$ is less than a user specified threshold $\omega_r$. Once converged, this step produces a new set of amplitudes [$\mathbf{t}^{(k+1)}$] and the corresponding unitary [$\hat{U}^{(k+1)}$], as well as the updated energy [$E^{(k+1)}$]. Increase the macro-iteration number by one ($k \leftarrow k+1$) and go to Step 2.

All VQE and PQE methodologies were implemented in a development branch of the open source package QFORTE , and utilize its state–vector simulator. All VQE calculations use a micro-iteration convergence threshold $\omega_g = 10^{-5}\ E_\mathrm{h}$ for the gradient norm $\|\mathbf{g}\|$ and all PQE calculations use a micro-iteration threshold $\omega_r = 10^{-5}\ E_\mathrm{h}$ for the residual norm $\|\mathbf{r}\|$. Note that when the $\hat{\kappa}_\mu$ operators are mapped to a qubit basis they can be expressed as a sum of Pauli operator strings that commute,[76] and therefore, a single operator $e^{t_\mu \hat{\kappa}_\mu}$ can be implemented exactly as a product of exponentials without invoking the Trotter approximation.

## 4.3 Results and Discussion

### 4.3.1 Comparison of PQE and VQE with a disentangled UCC ansatz

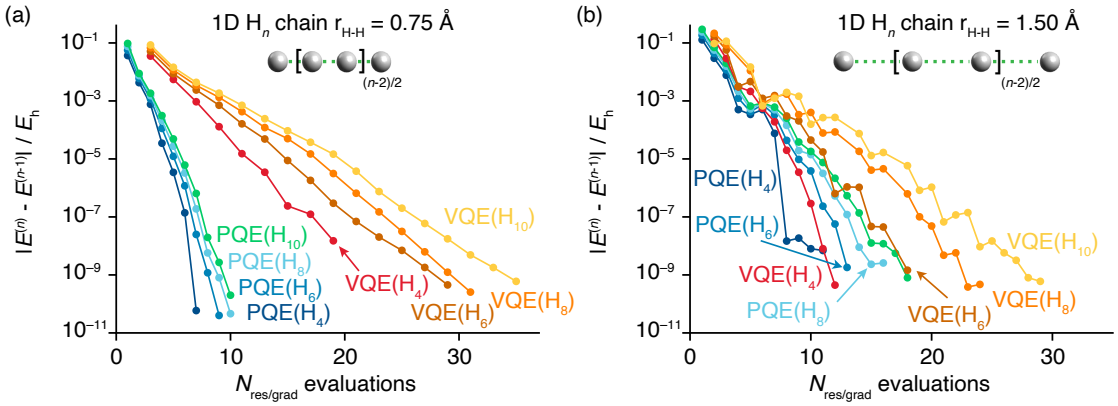


Figure 4.3: dUCCSD energy convergence for linear $H_4$–$H_{10}$ chains in a STO-6G basis at (a) $r_{H-H} = 0.75$ Å, and (b) $r_{H-H} = 1.50$ Å. $|E^{(n)} - E^{(n-1)}|$ is the absolute value of the energy change between subsequent iterations. Both plots compare PQE vs. VQE convergence with respect to number of residual (for PQE) or gradient (for VQE) evaluations ($N_{\text{res/grad}}$).

Our initial goal is to compare the performance of PQE and VQE using a unitary coupled-cluster trial state truncated at a given particle-hole excitation level. We test these two methods on a family of linear hydrogen chains (with identical nearest-neighbor distance) ranging from four to ten atoms, both near their equilibrium geometries ($r_{\text{H-H}} = 0.75$ Å) and stretched geometries ($r_{\text{H-H}} = 1.5$ Å). Hydrogen models such as these have been studied experimentally with VQE[77] and have recently been used as a benchmark for both quantum[36,55] and classical[78–80] algorithms.

Figure 4.3 shows the energy convergence of PQE and VQE using a disentangled UCC ansatz with singles and doubles (dUCCSD). All calculations employed restricted Hartree-Fock (RHF) orbitals from the quantum chemistry package PSI4,[81] and Pauli-operator Hamiltonians obtained via the Jordan–Wigner transformation implemented in QFORTE.[82] To achieve optimal performance for both VQE and PQE, we employ the Broyden–Fletcher–Goldfarb–Shannon (BFGS) algorithm[83–86] (as implemented in the SCIPY[87] scientific computing library) with analytical gradients for VQE, and DIIS[73] to

accelerate amplitude convergence of PQE. These computations use the same operator ordering for both approaches, with all amplitudes initialized to zero. The ordering of the operators $e^{t_{\mu_i}\hat{\kappa}_{\mu_i}}$ entering Eq. (4.9) is defined by the binary representation of the corresponding determinants $\left|\Phi_{\mu_i}\right\rangle = \hat{\tau}_{\mu_i}\left|\Phi_0\right\rangle$ in the occupation number representation. Because the disentangled UCCSD state cannot exactly parameterize an eigenstate of the Hamiltonian, the numerically converged PQE and VQE energies are not identical. Nevertheless, for all the cases we examined the converged PQE and VQE energies differ by less than $10^{-6}\ E_\mathrm{h}$.

Near the equilibrium geometry, we find that the PQE energy converges significantly faster than the VQE energy with number of residual vs. gradient evaluations, respectively. For example, to converge the near-equilibrium $H_{10}$ energy to $10^{-6}\ E_\mathrm{h}$, PQE requires only seven residual evaluations, while VQE requires approximately 23 gradient evaluations. In the case of VQE, we also observe that the number of required gradient evaluations grows with system size, with $H_{10}$ taking twice as many gradient vector evaluations than $H_4$ to converge. On the contrary, PQE computations converge with similar speed for all equilibrium hydrogen systems. Plots of the energy change vs. the norm of the residual/gradient vector show similar trends and are reported in Appendix 4.5.3.

At the stretched geometry, strong correlation effects cause the disentangled UCCSD trial state to perform more poorly with both PQE and VQE, yielding energy errors that range from 1.39 m$E_\mathrm{h}$ (for $H_4$) to 13.59 m$E_\mathrm{h}$ (for $H_{10}$). We see that PQE converges slightly more slowly in the stronger correlation regime, with stretched $H_{10}$ requiring 13 residual evaluations (instead of seven) to converge the energy to $10^{-6}\ E_\mathrm{h}$. However, PQE always converges faster than VQE, with the latter requiring 19 gradient-vector evaluations to converge stretched $H_{10}$ to the same accuracy level. We also find similar trends in PQE and VQE convergence for $BeH_2$, for which convergence data can be found in Appendix 4.5.3.

In summary, this initial set of results suggests that for a given trial state, optimization via PQE is faster than VQE and less dependent on the number of parameters to optimize.

We expect this to be the case also for VQE based on numerical gradients or gradient-free optimization methods, since these two variants are known to be slower compared to the the BFGS approach adopted here.[76]

### 4.3.2 Effect of stochastic errors on the convergence of PQE and VQE

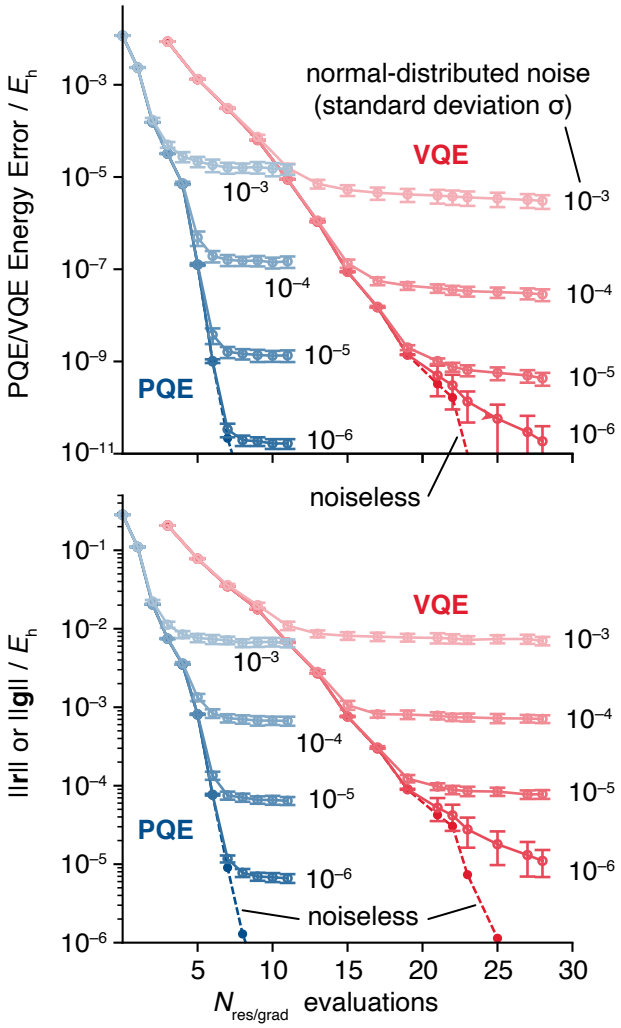


Figure 4.4: Energy and residual/gradient norm ($\|\mathbf{r}\|$)/($\|\mathbf{g}\|$) convergence of dUCCSDTQ wave functions optimized with PQE/VQE with various amounts of stochastic noise added to the residuals/gradients. Energy error is relative to FCI. $\sigma$ controls the degree of noise and is the standard deviation of the normal distribution, centered at the exact residual/gradient value, from which all residuals/gradients used in the calculations are randomly sampled [see Eq. (4.19)]. Values at each PQE/VQE iteration are averages over 50 runs on $H_4$ at $r_{H-H} = 1.0$ Å. Error bars denote one standard deviation.

The results presented in the previous section assumed error-free quantum gates and arbitrarily precise measurements. However, in practice calculations performed on NISQ hardware are affected by decoherence errors, poor gate fidelity, readout errors, and loss of precision due to insufficient measurements. These sources of error will lead to incorrect gradients and residuals that are then passed to a classical optimizer. Therefore, it is interesting to compare the resilience of PQE and VQE procedures when the residuals and gradients are affected by stochastic errors.

To model the presence of errors, we modify the PQE procedure by adding to the residual vector a stochastic error sampled from a Gaussian distribution with standard deviation $\sigma$ [$\mathcal{N}(0,\sigma^2)$]

$$r_\mu^{\text{measured}} = r_\mu + \mathcal{N}(0,\sigma^2). \tag{4.19}$$

For VQE, we similarly add stochastic noise to the exact energy gradients. Using Eq. (4.19) as a noise model mainly emulates errors that arise from finite measurement. Because the inexact residuals $r_\mu^{\text{measured}}$ are used to update the cluster amplitudes via Eq. (5.23), this noise model also gives rise to control errors, or errors that refer to the difference between the unitiaries for noiseless updated amplitudes $\hat{U}(\mathbf{t})$ and noisy updated amplitudes $\hat{U}(\mathbf{t}+\Delta\mathbf{t})$. Control errors due to finite measurement have been modeled this way in previous studies[76] and will always propagate through optimization on physical hardware. We note, however, that using Eq. (4.19) exclusively as a noise model is insufficient to capture more nuanced or device-specific errors such as decoherence. We tested the performance of PQE and VQE under noise by performing a batch of 50 computations on the linear $H_4$ molecule with nearest-neighbor distance set to 1.0 Å. We use the disentangled UCC ansatz with up to quadruple excitations, which spans the full operator set for this system.

Figure 4.4 shows a comparison of PQE and VQE optimized with various levels of noise, controlled by the magnitude of $\sigma$ in Eq. (4.19). We find that for all values of $\sigma > 0$, the energy convergence of PQE is essentially identical to that of noiseless PQE until some point, after which the energy error hovers around a finite error. Similar behavior can be seen

for convergence of the residual vector. We find that VQE has similar characteristics to PQE in the presence of noise, but that it is able to achieve slightly more accurate energies for a given $\sigma$ value. For a given level of noise, however, VQE generally requires two to three times the number of gradient evaluations as the number of residual evaluations required by PQE. An important aspect of this comparison is that for a given value of $\sigma$ both the residual and gradient vectors yield comparable asymptotic errors in PQE and VQE, respectively. Conversely, PQE and VQE computations of the comparable energy accuracy require similar precision in the measurement of the residual and gradient vectors. In Appendix 4.5.4 we use this result to estimate the relative cost of PQE and VQE via a formal analysis.

### 4.3.3 Selected PQE based on a full dUCC operator pool

Here we compare the results of selected PQE (SPQE) with an arbitrary order particle-hole operator pool, and ADAPT-VQE, which unless otherwise noted, uses a generalized singles and doubles pool (containing operators of the form $\hat{a}_p^\dagger \hat{a}_q$ and $\hat{a}_p^\dagger \hat{a}_q^\dagger \hat{a}_s \hat{a}_r$, where the indices $p,q,r,s$ run over all spin orbitals). To test these methods, we compute the energy as a function of bond distances for: 1) the symmetric dissociation of the linear $BeH_2$ molecule and 2) the symmetric dissociation of a chain of six hydrogen atoms. In both cases, as the bond length increases there is a corresponding build up of strong correlation effects. For each system, we report two sets of results for SPQE using the cumulative threshold $\Omega = 10^{-1}$ and $10^{-2}$ $E_\mathrm{h}$, and two sets of ADAPT-VQE results with gradient threshold $10^{-1}$ and $10^{-3}$ $E_\mathrm{h}$ ($\varepsilon_1$ and $\varepsilon_3$ in the original notation used by the authors). Since we later compare these methods to classical approaches formulated in a determinant basis, we do not employ a pool of spin-adapted operators.

The dissociation curve of $BeH_2$ shown in Fig. 4.5 (a) demonstrates that both SPQE and ADAPT-VQE are able to achieve significantly smaller energy errors than dUCCSD, while using only 10–20 more parameters. Although the two approaches employ different selection schemes, the ADAPT-VQE($\varepsilon_3$) and SPQE($\Omega = 10^{-2}$) approaches produce compact

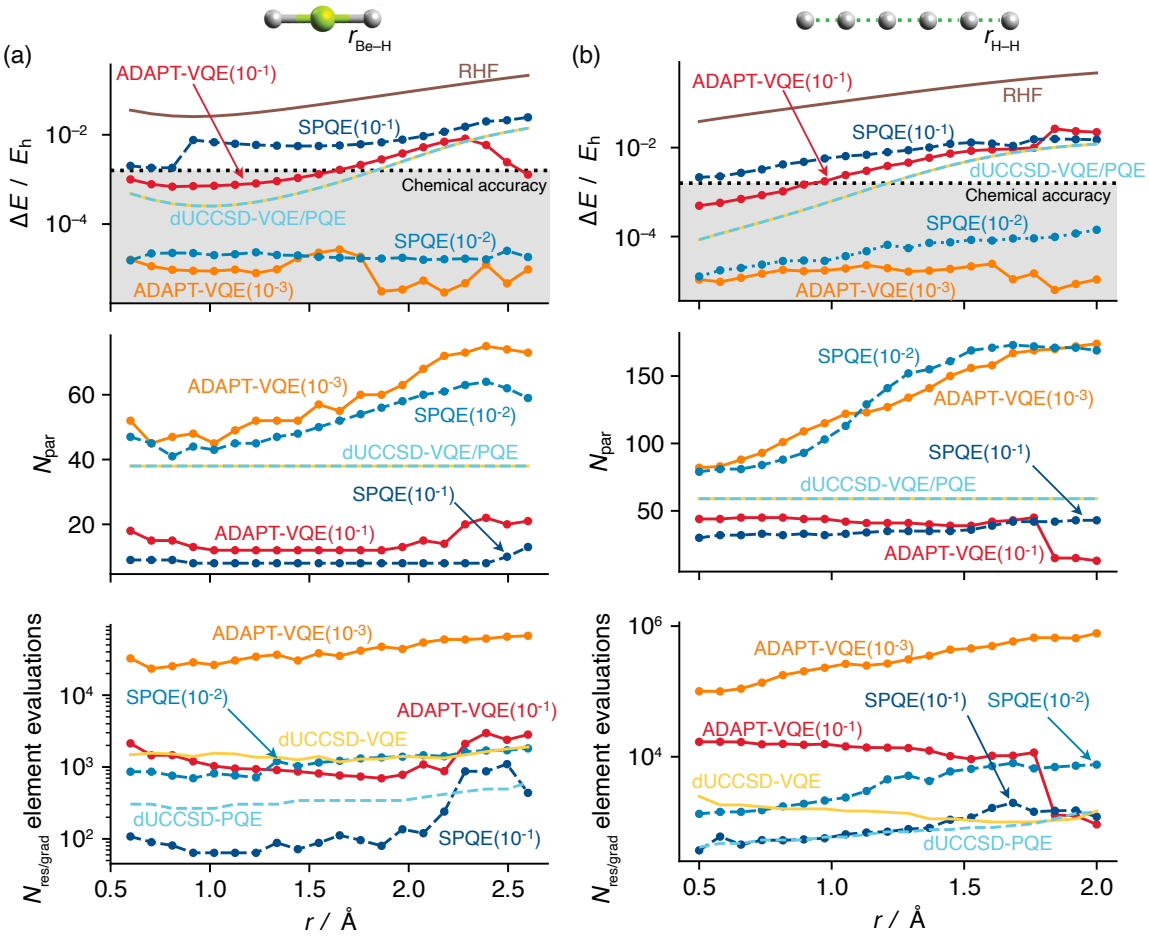


Figure 4.5: Ground state potential energy curve for the symmetric dissociation of (a) $BeH_2$ and (b) $H_6$ computed using a minimal (STO-6G) basis. The energy error relative to FCI (top), number of classical parameters used (middle), and number of individual elements of the gradient (for VQE) or residual (for PQE) evaluated (bottom) are given as a function of the Be–H and H–H bond length. Here, ADAPT-VQE uses a generalized singles and doubles operator pool and is optimized with the BFGS algorithm, and gradient convergence thresholds $10^{-1}$ ($\varepsilon_1$) and $10^{-3}$ ($\varepsilon_3$). SPQE results use macro-iteration convergence thresholds $\Omega = 10^{-1}$ and $10^{-2}$. The top plots also show the energy error corresponding to chemical accuracy, here defined as 1 kcal/mol $\approx$ 1.59 m$E_h$.

trial states with a similar number of classical parameters and comparable errors. The same trends are seen in symmetric dissociation curve of $H_6$, which is shown in Fig. 4.5 (b). However, for this system we find that achieving sub-m$E_h$ accuracy—particularly with the onset of strongly correlation at $r_{H-H}$ values greater than 1.5 Å, requires a number of parameters that approaches the size of the full Hilbert space (200) for both ADAPT-VQE and SPQE. The need to saturate Hilbert space to accurately describe $H_6$ is likely due to how small

this example is, and it speaks more to the ability of the trial states to produced compact representations rather than the performance of these algorithms in optimizing such ansätze.

The most noticeable difference between SPQE and ADAPT-VQE can be seen in the bottom panel of Fig. 4.5 (a)-(b): for trial states with comparable number of parameters, SPQE requires significantly fewer residual element evaluations than gradient element evaluations in ADAPT-VQE. For example, at a Be–H bond distance of 1.65 Å, both methods produce very similar energy errors using almost the same number of parameters, but ADAPT-VQE($\varepsilon_3$) requires the evaluation of 35155 elements of the gradient, whereas SPQE($\Omega = 10^{-2}$) requires only 1220 elements of the residual. Importantly, we note that the bottom panels of Fig. 4.5 exclusively count the number of elements of the gradient or residual required by the optimization, and do not include the additional measurements required for operator selection.

Table 4.1: Ground state of $H_6$ computed using a minimal (STO-6G) basis with RHF orbital convergence threshold of $10^{-10}$ $E_h$. Comparison of SPQE with threshold $\Omega$ and ADAPT-VQE using the same number of parameters as SPQE. ADAPT-VQE results are computed for both a generalized singles and doubles operator pool (GSD) and a particle hole singles and doubles pool (SD). The properties reported are the energy error with respect to FCI [$\Delta E$, in $E_h$ ], the number of classical parameters used [$N_{par}$], the number of parameters corresponding to three-body or higher excitations [$N_{T+}$], the number of CNOT gates used in the unitary [$N_{CNOT}$] (not optimized), and the total number of residual or gradient element evaluations [$N_{res}$ or $N_{grad}$]. $r$ denotes the H-H nearest neighbor distance in Ångstrom.

| | SPQE ($\Omega = 10^{-1}$ $E_h$) | | | | | ADAPT-VQE-GSD | | | | ADAPT-VQE-SD | | | |
|---|---|---|---|---|---|---|---|---|---|---|---|---|---|
| $r$ | $\Delta E$ | $N_{par}$ | $N_{T+}$ | $N_{CNOT}$ | $N_{res}$ | $\Delta E$ | $N_{par}$ | $N_{CNOT}$ | $N_{grad}$ | $\Delta E$ | $N_{par}$ | $N_{CNOT}$ | $N_{grad}$ |
| 0.50 | 0.002153 | 30 | 0 | 2400 | 339 | 0.002152 | 30 | 2400 | 8378 | 0.002152 | 30 | 2400 | 8378 |
| 1.00 | 0.006050 | 32 | 0 | 2720 | 503 | 0.005872 | 32 | 2720 | 8399 | 0.005872 | 32 | 2720 | 8399 |
| 1.50 | 0.012487 | 36 | 0 | 2944 | 1103 | 0.011176 | 36 | 3040 | 8046 | 0.011176 | 36 | 3040 | 8046 |
| 2.00 | 0.015066 | 43 | 8 | 20272 | 1087 | 0.011204 | 43 | 3560 | 15176 | 0.010350 | 43 | 3312 | 12592 |
| | SPQE ($\Omega = 10^{-2}$ $E_h$) | | | | | ADAPT-VQE-GSD | | | | ADAPT-VQE-SD | | | |
| $r$ | $\Delta E$ | $N_{par}$ | $N_{T+}$ | $N_{CNOT}$ | $N_{res}$ | $\Delta E$ | $N_{par}$ | $N_{CNOT}$ | $N_{grad}$ | $\Delta E$ | $N_{par}$ | $N_{CNOT}$ | $N_{grad}$ |
| 0.50 | 0.000013 | 79 | 24 | 15568 | 1127 | 0.000012 | 79 | 6608 | 87506 | 0.000085 | 79 | 4608 | 29707 |
| 1.00 | 0.000031 | 105 | 46 | 33232 | 2076 | 0.000033 | 105 | 9244 | 166119 | 0.000064 | 105 | 8128 | 388182 |
| 1.50 | 0.000079 | 166 | 111 | 166032 | 6074 | 0.000004 | 166 | 14528 | 566143 | 0.000028 | 166 | 12576 | 1437917 |
| 2.00 | 0.000141 | 169 | 114 | 226768 | 9537 | 0.000018 | 169 | 14776 | 719390 | 0.000096 | 169 | 12944 | 1312127 |

Since ADAPT-VQE and SPQE select new operators from their pools using different importance criteria, it is not possible to perform a direct comparison of their performance using fixed thresholds. To facilitate this comparison, in Table 4.1 we report SPQE results

using two values of $\Omega$ ($10^{-1}$ and $10^{-2}$ $E_\mathrm{h}$) together with ADAPT-VQE results obtained using an ansatz with the same number of parameters as SPQE. We include ADAPT-VQE results obtained using both a generalized singles and doubles operator pool (GSD), and a particle-hole singles and doubles pool (SD). The results in Tab. 4.1 obtained with $\Omega = 10^{-1}$ $E_\mathrm{h}$ show SPQE and the two variants of ADAPT-VQE to perform equally well at all bond distances. The second set of results obtained with a tighter threshold ($\Omega = 10^{-2}$) show similar performance of the methods at short bond lengths, with two notable exceptions. First, at $r_{\mathrm{H-H}} = 2.0$ Å ADAPT-VQE-GSD yields more accurate results than ADAPT-VQE-SD and SPQE. At this point, the SPQE ansatz contains 55 singles and doubles, and 114 operators of higher rank, yielding an error of about 0.14 m$E_\mathrm{h}$, while ADAPT-VQE-GSD is an order of magnitudes more accurate. Second, also at $r_{\mathrm{H-H}} = 2.0$ Å, SPQE uses only 9537 residual element evaluations, while ADAPT-VQE requires 719390 (GSD) and 1312127 (SD) gradient element evaluations. The evaluation of fewer residual elements in SQPE will correspond to approximately the same savings in total number of measurements (see Appendix 4.5.4).

A final important aspect to compare between SPQE and ADAPT-VQE is the number of native CNOT gates, which we consider as a proxy for circuit depth. Tab. 4.1 reports the number of CNOT gates for the converged trial states. These numbers overestimate the actual gate count since they ignore optimizations such as the cancellation of Jordan–Wigner strings,[88] especially for three- and higher-body operators. We see that at the larger threshold values ($\Omega = 10^{-1}$ for SPQE and $\varepsilon_1 = 10^{-1}$ for ADAPT) the number of CNOTs for all three approaches are relatively similar, and are generally within a factor of 2 of one another. However, at tighter thresholds the SPQE circuit contains significantly more CNOT gates than the one for ADAPT-VQE. For example, $r_{\mathrm{H-H}} = 2.0$ Å), 114 of the 169 operators used in SPQE are three-body or higher, while ADAPT-SD and ADAPT-GSD of course only contain only up to two-body operators. Consequently, the SPQE($\Omega = 10^{-2}$) circuit contains more CNOT gates (226768) than ADAPT-VQE-GSD (14776). As discussed in

Appendix 4.5.4, this large difference in CNOT count is due to the growth in cost to implement the exponential of $n$-body second-quantized operators as a function of $n$ (and the lack of circuit optimization). Nevertheless, it is important to note that the systems studied here are not large enough to draw definitive conclusions about the relative performance of SPQE and ADAPT-VQE. For example, the pool of generalized singles and doubles (GSD) for $H_6$ contains 870 operators, a number significantly larger than the size of the full Hilbert space (200). This scenario is unlike most systems of interest, where the number of generalized singles and doubles is much less than the number of particle-hole operators. Unfortunately, our attempts to compare numbers for systems larger than $BeH_2$ and $H_6$ were unsuccessful due to the high computational cost of simulating ADAPT-VQE.

A second aspect we investigate, is the ability of the selected PQE approach to compactly represent wave functions for systems displaying strong correlation effects, were many-body methods commonly fail due to the breakdown of the mean-field approximation. We compare the performance of SPQE with ACI and DMRG using data generated in our recent benchmark study of hydrogen systems.[80] In this work, we characterize the resource requirements of a computational method $X$ with the *accuracy volume* ($\mathscr{V}_X$), defined as the smallest number of parameters necessary to achieve a given energy error per electron (here taken to be $10^{-4}$ $E_h$/electron). We consider three $H_{10}$ model systems: a one dimensional (1D) linear chain, a two dimensional (2D) triangular lattice and a three dimensional (3D) close-packed pyramid. Using a minimal STO-6G basis and a 1 qubit to 1 spin-orbital mapping, the 1D, 2D, and 3D $H_{10}$ models are represented with $2^{20}$ computational basis states, but are restricted to 31752 and 15912, and 15912 determinants, respectively, after accounting for spin and Abelian point–group symmetries.

Figure 4.6 (a) displays the SPQE, ACI, and DMRG energy error as a function of classical variational parameters for the 1D $H_{10}$ system at a stretched bond length of $r_{H-H} =$ 1.50 Å. DMRG, which is ideally suited to simulate gapped 1D systems, affords the most compact wave function for the 1D chain, with an accuracy volume of only 176 variational

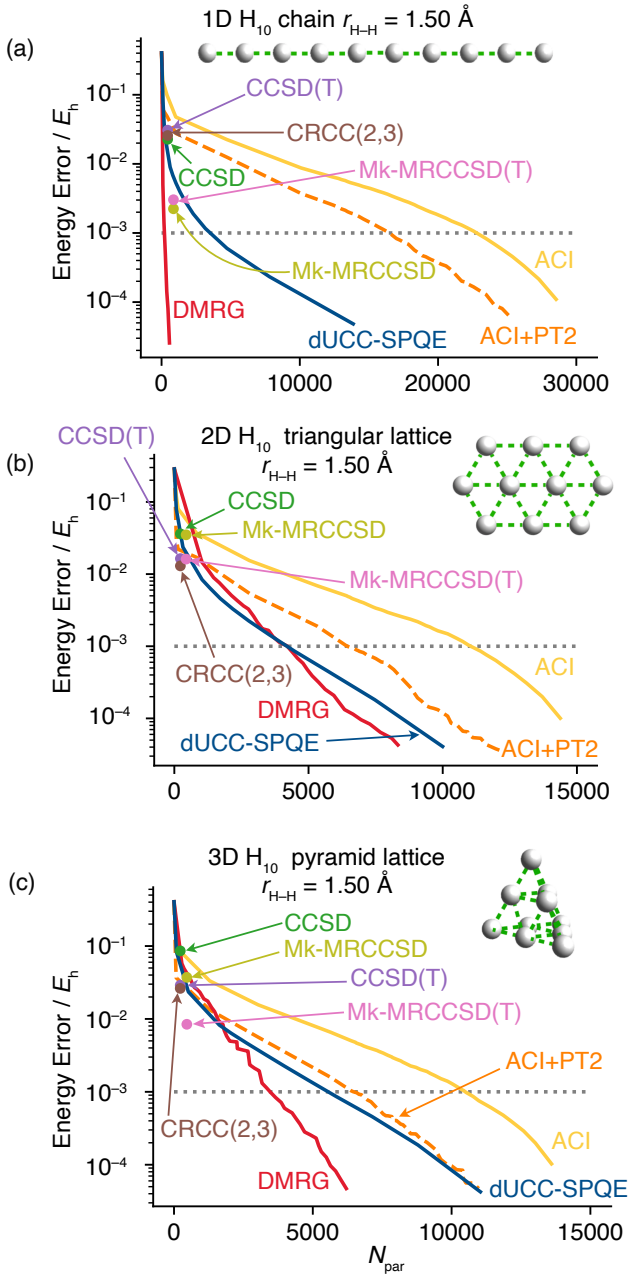


Figure 4.6: Results for the 1D, 2D, and 3D $H_{10}$ models use a STO-6G basis at $r_{\mathrm{H-H}} = 1.50$ Å. Singlet ground state energy errors relative to FCI as a function of number of variational parameters $N_{\mathrm{par}}$ for dUCC-SPQE, ACI, and DMRG. Unsigned energy errors for methods with fixed number of parameters (taken to be the number of cluster amplitudes) are shown by colored dots. Energy errors ACI with a second order perturbative correction (ACI+PT2) are also shown by orange dotted lines. For ACI+PT2, CCSD(T), CRCC(2,3), and Mk-MRCCSD(T) we only count the number of nonperturbative amplitudes. The accuracy volume threshold [0.1 m$E_{\mathrm{h}}$ per electron] is plotted as a grey dotted line.

parameters ($\mathscr{V}^{\mathrm{1D}}_{\mathrm{DMRG}} = 176$). The SPQE exponential ansatz is less compact than the DMRG matrix product state, with an accuracy volume $\mathscr{V}^{\mathrm{1D}}_{\mathrm{SPQE}} = 3510$ parameters. We observe that the ACI wave function—a linear ansatz built by selecting the determinants with the largest energy contributions—gives the least compact representation, such that $\mathscr{V}^{\mathrm{1D}}_{\mathrm{ACI}} = 22989$ at the same level of accuracy. When the ACI energy is augmented with a second-order perturbative correction—which accounts for determinants excluded from the wave-function expansion—a more compact ansatz is sufficient to achieve an energy error of $10^{-3}$ $E_{\mathrm{h}}$. This suggests that it might be valuable to formulate a classical perturbative correction to the SPQE energy to help capture even more correlation energy.

Results for the 2D $H_{10}$ lattice [Fig. 4.6 (b)] show that SPQE yields a more compact representation than DMRG or ACI until an energy error of approximately 1 m$E_{\mathrm{h}}$. For the 2D system the accuracy volume follows the order SPQE (4193) $\approx$ DMRG (4218) $<$ ACI (11122). We see however, that at energy errors less than 1 m$E_{\mathrm{h}}$ DMRG still affords the most compact representation for the 2D system. Finally, for the 3D $H_{10}$ pyramid lattice shown in Fig. 4.6 (c), we find that DMRG yields the most compact representation ($\mathscr{V}^{\mathrm{3D}}_{\mathrm{DMRG}} = 3549$), but not nearly by the same margin as for the 1D system. Again, we see that SPQE has a significantly more compact wave function than ACI such that $\mathscr{V}^{\mathrm{3D}}_{\mathrm{SPQE}} = 5544$ and $\mathscr{V}^{\mathrm{3D}}_{\mathrm{ACI}} = 10519$. While further investigation of larger strongly–correlated systems will be necessary, it is encouraging to see that SPQE performs similarly to or better than two state-of-the-art classical methodologies when applied to the 2D and 3D $H_{10}$ systems.

We have also included in Fig. 4.6 energy errors, with respect to the number of cluster amplitudes, for several classical coupled-cluster variants. Specifically we have included benchmark results from Ref.[80] for CC with singles and doubles excitations[89] (CCSD), CCSD with perturbative triples[90] [CCSD(T)], and the completely renormalized CC with perturbative triples[12] [CRCC(2,3)]. These CC methods are (generally) more computationally affordable than the other methods. In the 2D and 3D systems, CCSD performs comparably to dUCC-SQPE (with the same number of parameters), while CCSD(T) and

CRCC(2,3) produce more accurate energies. However, all coupled-cluster energies are more than 10 m$E_\mathrm{h}$ off from the FCI energy. Fig. 4.6 also reports results computed using Mukherjee MRCC with singles and doubles (Mk-MRCCSD)[91,92] and Mk-MRCCSD augmented with perturbative triples [Mk-MRCCSD(T)][93] using an active space containing the highest occupied and lowest unoccupied Hartree–Fock orbitals. The Mk-MRCC results improve upon single-reference coupled-cluster methods at the cost of doubling the number of cluster amplitudes. The Mk-MRCC methods are particularly accurate for the 1D system, where they produce errors of the order of 2–3 m$E_\mathrm{h}$. Despite the improvement shown by the multireference CC methods, it is important to note that these methods have a computational cost that scales exponentially with the number of active space determinants.

## 4.4 Conclusions

In this work, we present a new NISQ-friendly algorithm—the projective quantum eigensolver (PQE)—to compute the ground state of a many-body problem using disentangled (factorized) unitary coupled-cluster trial states. The PQE approach consists of a nonlinear optimization problem whose solution requires the evaluation of projections of the Schrödinger equation onto a many-body basis (residual vector) but still gives energies that are a variational upper bound to the ground state energy. We show how to efficiently evaluate the residual vector via measurement of simple expectation values, with a cost that is twice that of an energy evaluation (per element). For small molecular systems, we find that PQE and VQE with a fixed dUCCSD trial state converge to nearly identical energies; however, the number of residual evaluations required by PQE is smaller than that of the gradient evaluations needed by VQE. PQE shows similar resiliency as VQE and still converges more rapidly in the presence of stochastic noise.

To treat strongly correlated electrons, we introduce a selected variant of PQE in which the trial state is constructed iteratively by adding batches of important operators. The resulting SPQE algorithm can construct efficient unitary circuits like ADAPT-VQE, but

it requires orders of magnitude fewer residual element evaluations than gradient element evaluations for the latter. In SPQE, the selection of new operators is done according to the magnitude of the elements of the residual vector and is performed by sampling a quantum state that directly encodes in its probability amplitudes the importance of the entire operator pool. Because the selection cost in SQPE is not affected by the size of the operator pool, the unitary can include operators of rank up to the total number of particles.

Finally, we compare the energy convergence with the number of parameters for 1D, 2D, and 3D $H_{10}$ lattices using SPQE and two classical methods well suited to treat strong electronic correlation: the adaptive configuration interaction and the density matrix renormalization group. Given a target accuracy of up to approximately 1 m$E_h$, we find that SPQE produces significantly more compact trial states for the 2D system than ACI and is comparable to DMRG. However, DMRG affords the most compact wave function parameterization in 1D, for accuracies below 1 m$E_h$ in 2D, and by a much smaller margin, in 3D. Taken together, PQE and SPQE are very promising tools for studying many-body systems both in the strong and weak correlation regimes using NISQ hardware.

In summary, the PQE approach is a viable and more economical alternative to variational quantum algorithms. In its current formulation, PQE can be applied to any trial state generated by exponentiating a set of linearly independent operators with identity metric matrix, as it is the case for disentangled unitary coupled-cluster ansätze. For these trial states, any existing implementation of VQE could be easily extended to PQE, leveraging existing techniques to reduce the number of measurements and exploiting symmetries.[59,60,94] Interesting extensions of PQE include a generalization to unitaries that may contain repeated operators, that use generalized excitations/de-excitations pools, and hardware-efficient ansätze. In particular, a promising research direction is the formulation of a selected PQE using a basis of general one- and two-body operators, which could yield trial states with lower circuit depth than the current formulation. Within the greater ecosystem of quantum algorithms, PQE could be used to determine initial guess amplitudes for subsequent opti-

mization via VQE. Additionally, similarly to VQE, PQE can be used as an alternative to adiabatic approaches to prepare initial states for quantum phase estimation. Although we only explore applications of PQE for quantum many-body simulation, the framework outlined by Eqs. (4.3) and (5.20) can be used to solve a variety of eigenvalue problems. With appropriate modifications, for example, PQE could be employed to diagonalize covariance matrices (after quantum encoding[95,96]) for use in machine learning or data-analysis. Moreover, because there is no requirement that the PQE (or SPQE) trial states have low-entanglement, PQE could be used as an alternative to methods such as quantum principle analysis,[96] or variational quantum state diagonalization.[97] Most importantly, the most immediate impact of PQE could be speeding up quantum computations on current or near-term devices.

## 4.5 Appendix

### 4.5.1 Gradient of the PQE energy

In this section, we derive an expression for the PQE energy gradient. This result permits us to establish the equivalence of PQE and VQE for an exact UCC or dUCC ansatz, and to characterize the gradient when PQE is used to optimize approximate trial states. Consider the PQE energy expression using a UCC [Eq. (4.7)] or dUCC [Eq. (4.9)] ansatz $E_{\mathrm{PQE}}(\mathbf{t}) = \langle\Phi_0|\hat{U}^\dagger(\mathbf{t})\hat{H}\hat{U}(\mathbf{t})|\Phi_0\rangle$. The derivative of $E_{\mathrm{PQE}}(\mathbf{t})$ with respect to the parameter $t_\mu$ is given by

$$\begin{aligned}\frac{\partial E_{\mathrm{PQE}}(\mathbf{t})}{\partial t_\mu} &= 2\,\mathrm{Re}\,\langle\Phi_0|\hat{U}^\dagger(\mathbf{t})\hat{H}\frac{\partial\hat{U}(\mathbf{t})}{\partial t_\mu}|\Phi_0\rangle \\ &= 2\,\mathrm{Re}\,\langle\Phi_0|\bar{H}\hat{U}^\dagger(\mathbf{t})\frac{\partial\hat{U}(\mathbf{t})}{\partial t_\mu}|\Phi_0\rangle\,,\end{aligned} \tag{4.20}$$

where we have inserted the identity $\hat{U}^\dagger(\mathbf{t})\hat{U}(\mathbf{t}) = 1$ to rewrite this expression in terms of $\bar{H}$.

Next, we consider the resolution of the identity

$$1 = |\Phi_0\rangle\langle\Phi_0| + \sum_{\Phi_\mu \in R} |\Phi_\mu\rangle\langle\Phi_\mu| + \sum_{\Phi_\nu \in S} |\Phi_\nu\rangle\langle\Phi_\nu|, \tag{4.21}$$

where $R$ is the set of determinants for which the residual condition $r_\mu = 0$ is enforced, while $S$ contains those determinants for which $r_\nu$ may not be equal to zero. After inserting this resolution of the identity into Eq. (4.20) between $\bar{H}$ and $\hat{U}^\dagger(\mathbf{t})$ and simplifying the resulting expression, we may express the gradient as

$$\begin{aligned}\frac{\partial E_{\mathrm{PQE}}(\mathbf{t})}{\partial t_\mu} = 2E_{\mathrm{PQE}}\,\mathrm{Re}\,\langle\Phi_0|\hat{U}^\dagger(\mathbf{t})\frac{\partial \hat{U}(\mathbf{t})}{\partial t_\mu}|\Phi_0\rangle \\ + 2\,\mathrm{Re}\sum_{\Phi_\mu\in R} r_\mu^*\langle\Phi_\mu|\hat{U}^\dagger(\mathbf{t})\frac{\partial \hat{U}(\mathbf{t})}{\partial t_\mu}|\Phi_0\rangle \\ + 2\,\mathrm{Re}\sum_{\Phi_\nu\in S} r_\nu^*\langle\Phi_\nu|\hat{U}^\dagger(\mathbf{t})\frac{\partial \hat{U}(\mathbf{t})}{\partial t_\mu}|\Phi_0\rangle.\end{aligned} \tag{4.22}$$

The first term in this expression is null since from $\langle\Phi_0|\hat{U}^\dagger(\mathbf{t})\hat{U}(\mathbf{t})|\Phi_0\rangle = 1$ we can show that the coefficient that multiplies the energy is null:

$$\frac{\partial\langle\Phi_0|\hat{U}^\dagger(\mathbf{t})\hat{U}(\mathbf{t})|\Phi_0\rangle}{\partial t_\mu} = 2\,\mathrm{Re}\,\langle\Phi_0|\hat{U}^\dagger(\mathbf{t})\frac{\partial \hat{U}(\mathbf{t})}{\partial t_\mu}|\Phi_0\rangle = 0. \tag{4.23}$$

The second term in Eq. (4.22) is null due to the residual condition. Applying these two simplifications we arrive at the gradient expression [Eq. (4.10)] reported in Sec. 4.2.2, containing only the last term of Eq. (4.22). The term $\langle\Phi_\nu|\hat{U}^\dagger(\mathbf{t})\frac{\partial\hat{U}(\mathbf{t})}{\partial t_\mu}|\Phi_0\rangle$ that multiplies the residual is generally non-null for both the UCC and dUCC ansätze. In the case of dUCC, the term corresponding to the derivative with respect to $i$-th amplitude $t_{\mu_i}$, is given by:

$$\langle\Phi_\nu|\hat{U}^\dagger(\mathbf{t})\frac{\partial\hat{U}(\mathbf{t})}{\partial t_{\mu_i}}|\Phi_0\rangle = \langle\Phi_\nu|e^{-t_{\mu_{N_{\mathrm{op}}}}\hat{\kappa}_{\mu_{N_{\mathrm{op}}}}}\cdots e^{-t_{\mu_{i+1}}\hat{\kappa}_{\mu_{i+1}}}\hat{\kappa}_{\mu_i}e^{t_{\mu_{i+1}}\hat{\kappa}_{\mu_{i+1}}}\cdots e^{t_{\mu_{N_{\mathrm{op}}}}\hat{\kappa}_{\mu_{N_{\mathrm{op}}}}}|\Phi_0\rangle. \tag{4.24}$$

The states to the left and right of the operator $\hat{\kappa}_{\mu_i}$ are general many-body states that potentially span the entire Hilbert space, and therefore, this quantity is generally non-null. For completeness, we also report the same expression for the case of traditional UCC, which

may be obtained using the derivative of the exponential map:

$$\langle \Phi_\nu | \hat{U}^\dagger(\mathbf{t}) \frac{\partial \hat{U}(\mathbf{t})}{\partial t_{\mu_i}} | \Phi_0 \rangle = \int_0^1 dx \, \langle \Phi_\nu | e^{(x-1)\hat{\sigma}} \hat{\kappa}_{\mu_i} e^{(1-x)\hat{\sigma}} | \Phi_0 \rangle \,. \tag{4.25}$$

### 4.5.2 Derivation of the UCC-PQE update equations

In this section, we provide a derivation of the amplitude update equation [Eq. (5.23)] based on a quasi-Newton method for solving general nonlinear equations. To find update equations that relate new amplitudes ($\mathbf{t}^{(n+1)}$) to the previous set ($\mathbf{t}^{(n)}$), we expand the residual equation [Eq. (5.20)] as a Taylor series centered around the current amplitude vector displaced by an amount $\Delta\mathbf{t}^{(n+1)} = \mathbf{t}^{(n+1)} - \mathbf{t}^{(n)}$

$$\begin{aligned} r_\mu(\mathbf{t}^{(n+1)}) &= r_\mu(\mathbf{t}^{(n)} + \Delta\mathbf{t}^{(n+1)}) \\ &= r_\mu(\mathbf{t}^{(n)}) + \sum_\nu J_{\mu\nu}(\mathbf{t}^{(n)}) \Delta t_\nu^{(n+1)} + \ldots, \end{aligned} \tag{4.26}$$

where $J$ is the Jacobian matrix, defined as $J_{\mu\nu}(\mathbf{t}) = \partial r_\mu(\mathbf{t}) / \partial t_\nu$. To avoid computing and inverting the Jacobian, we seek a diagonal approximation to $J$. We first note that for both the conventional UCC and the UCC ansätze, the similarity transformed Hamiltonian expanded up to linear terms is of the form

$$\hat{U}^\dagger(\mathbf{t}) \hat{H} \hat{U}(\mathbf{t}) = \hat{H} + \sum_i t_{\mu_i} [\hat{H}, \hat{\kappa}_{\mu_i}] + \mathscr{O}(|\mathbf{t}|^2). \tag{4.27}$$

We now invoke the Møller–Plesset partitioning of the Hamiltonian and assume that the spin orbitals are canonical (i.e., they diagonalize the Hartree–Fock operator), allowing us to write $\hat{H} = \hat{F}^{(0)} + \hat{V}^{(1)}$, where $\hat{F}^{(0)} = \sum_p \varepsilon_p \hat{a}_p^\dagger \hat{a}_p$ is a zeroth-order diagonal one-body operator, and $\hat{V}^{(1)}$ is a first-order operator that contains two-body terms. Approximating the Jacobian with with the first two terms of Eq. (4.27) and retaining only the zeroth-order contributions, we obtain the following diagonal approximation

$$J_{\mu\nu}(\mathbf{t}) = \left\langle \Phi_\mu \right| [\hat{F}^{(0)}, \hat{\kappa}_\nu] \left| \Phi_0 \right\rangle = -\Delta_\mu \delta_{\mu\nu}, \tag{4.28}$$

where $\Delta_\mu = \varepsilon_i + \varepsilon_j + \ldots - \varepsilon_a - \varepsilon_b \ldots$ is a standard Møller–Plesset denominator corresponding to the excitation operator $\hat{\kappa}_\mu = \hat{a}_a^\dagger \hat{a}_b^\dagger \cdots \hat{a}_j \hat{a}_i - \text{h.c.}$. Inserting the diagonal Jacobian in the expanded residual we obtain

$$r_\mu(\mathbf{t}^{(n+1)}) = r_\mu(\mathbf{t}^{(n)}) - \Delta_\mu \Delta t_\mu^{(n+1)}, \tag{4.29}$$

which when solved for $r_\mu(\mathbf{t}^{(n+1)}) = 0$ yields the update equation [Eq. (5.23)].

### 4.5.3 Additional numerical comparison of PQE and VQE

Here we provide additional numerical comparison for PQE and VQE. Table 4.2 shows numerics for ground state energy convergence of $BeH_2$ using dUCCSD-PQE and dUCCSD-VQE. Figure 4.7 shows the energy converge of various hydrogen chain systems with respect to the norm of the residual vector (for PQE) and gradient vector (for VQE). For both Tab. 4.2 and Fig. 4.7 trends similar to those seen in Fig. 4.3 are observed.

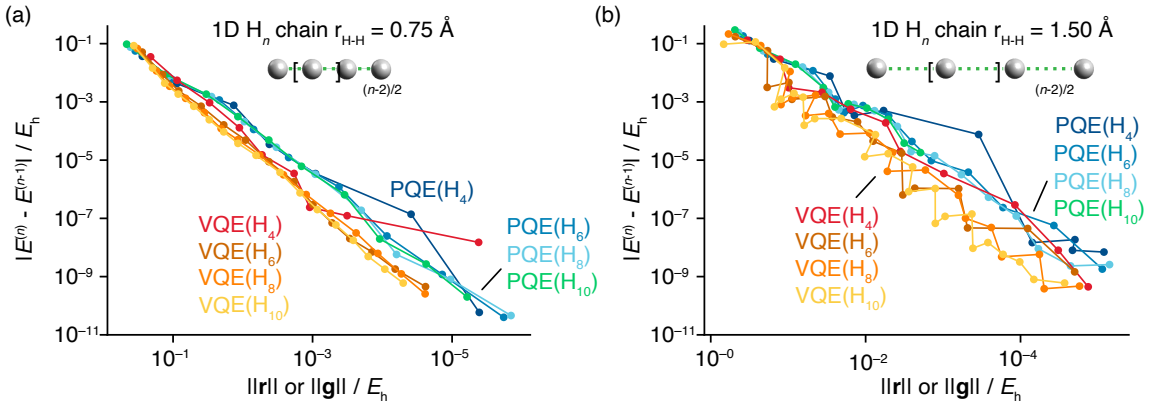


Figure 4.7: dUCCSD energy convergence for linear $H_4$–$H_{10}$ chains in a STO-6G basis at (a) $r_{H-H} = 0.75$ Å, and (b) $r_{H-H} = 1.50$ Å. $|E^{(n)} - E^{(n-1)}|$ is the absolute value of the energy change between subsequent iterations. Both plots compare PQE vs VQE convergence with respect to norm of the residual-vector (for PQE) or the norm of the gradient-vector (for VQE).

### 4.5.4 Formal comparison of PQE and VQE

We begin by assuming the case of a fixed ansatz, and since in this case state preparation costs are the same, our analysis focuses on how many measurements are necessary to

Table 4.2: Comparison of the convergence of the ground state energy of $BeH_2$ computed with PQE and VQE using a disentangled UCCSD trial state. For a method $X$ = PQE or VQE, this table reports the total energy ($E_X$, in $E_h$), the energy change from the previous to the current iteration ($E_X^{(n)} - E_X^{(n-1)}$), the number of residual/gradient evaluations ($N_X^{\cdot}$), and the norm of the residual/gradient ($\|\cdot\|$). The FCI energies at 1.0 and 2.0 Å are $-15.65068726$ and $-15.60861964$ $E_h$, respectively. All calculations use a STO-6G basis.

| Iteration | $E_{PQE}$ | $E_{PQE}^{(n)} - E_{PQE}^{(n-1)}$ | $N_{PQE}^{r-eval}$ | $\|\mathbf{r}_{PQE}\|$ | $E_{VQE}$ | $E_{VQE}^{(n)} - E_{VQE}^{(n-1)}$ | $N_{VQE}^{g-eval}$ | $\|\mathbf{g}_{VQE}\|$ |
|---|---|---|---|---|---|---|---|---|
| | | | | $BeH_2$ ($r_{Be-H}$ = 1.0 Å) UCCSD | | | | |
| 1 | −15.6480381687 | −0.0233010440 | 1 | 0.2184453066 | −15.6448482964 | −0.0201111716 | 3 | 0.3114581416 |
| 2 | −15.6500971948 | −0.0020590260 | 2 | 0.0613327467 | −15.6478816410 | −0.0030333446 | 5 | 0.1481817759 |
| 3 | −15.6504069826 | −0.0003097878 | 3 | 0.0088860708 | −15.6494462890 | −0.0015646480 | 7 | 0.1065575796 |
| 4 | −15.6504328168 | −0.0000258343 | 4 | 0.0026511924 | −15.6499421388 | −0.0004958498 | 9 | 0.0634937794 |
| 5 | −15.6504349587 | −0.0000021418 | 5 | 0.0005328227 | −15.6500470587 | −0.0001049199 | 10 | 0.0893255742 |
| 6 | −15.6504350041 | −0.0000000454 | 6 | 0.0000763318 | −15.6501955946 | −0.0001485359 | 11 | 0.0657024179 |
| 7 | −15.6504350044 | −0.0000000003 | 7 | 0.0000086198 | −15.6502874046 | −0.0000918100 | 12 | 0.0690985413 |
| 8 | | | | | −15.6503399456 | −0.0000525410 | 13 | 0.0453884569 |
| 9 | | | | | −15.6503962522 | −0.0000563066 | 14 | 0.0249260915 |
| 10 | | | | | −15.6504228495 | −0.0000265973 | 16 | 0.0137252110 |
| 11 | | | | | −15.6504302548 | −0.0000074053 | 18 | 0.0073189453 |
| 12 | | | | | −15.6504341054 | −0.0000038506 | 20 | 0.0037260965 |
| 13 | | | | | −15.6504346315 | −0.0000005261 | 22 | 0.0023579786 |
| 14 | | | | | −15.6504348973 | −0.0000002657 | 24 | 0.0014145610 |
| 15 | | | | | −15.6504349615 | −0.0000000642 | 26 | 0.0008586922 |
| 16 | | | | | −15.6504349766 | −0.0000000151 | 28 | 0.0006710048 |
| 17 | | | | | −15.6504349959 | −0.0000000193 | 29 | 0.0003518429 |
| 18 | | | | | −15.6504350027 | −0.0000000068 | 31 | 0.0001962939 |
| 19 | | | | | −15.6504350038 | −0.0000000011 | 33 | 0.0001228873 |
| 20 | | | | | −15.6504350044 | −0.0000000005 | 34 | 0.0000505365 |
| 21 | | | | | −15.6504350045 | −0.0000000001 | 36 | 0.0000433400 |
| 22 | | | | | −15.6504350047 | −0.0000000002 | 37 | 0.0000200500 |
| | | | | $BeH_2$ ($r_{Be-H}$ = 2.0 Å) UCCSD | | | | |
| 1 | −15.5888292373 | −0.0721251319 | 1 | 0.2551300809 | −15.5797540529 | −0.0630499476 | 3 | 0.7559489104 |
| 2 | −15.6022316771 | −0.0134024398 | 2 | 0.1072484292 | −15.5993381767 | −0.0195841238 | 5 | 0.2319720501 |
| 3 | −15.6055237786 | −0.0032921016 | 3 | 0.0175246100 | −15.6027545167 | −0.0034163400 | 7 | 0.1024944422 |
| 4 | −15.6056880097 | −0.0001642310 | 4 | 0.0076659595 | −15.6041840035 | −0.0014294868 | 9 | 0.1471217958 |
| 5 | −15.6057527283 | −0.0000647187 | 5 | 0.0051078803 | −15.6050561955 | −0.0008721920 | 10 | 0.0754837786 |
| 6 | −15.6058044053 | −0.0000516769 | 6 | 0.0012840244 | −15.6052847256 | −0.0002285301 | 12 | 0.0580899178 |
| 7 | −15.6058068352 | −0.0000024300 | 7 | 0.0002042506 | −15.6055945458 | −0.0003098202 | 13 | 0.0291205752 |
| 8 | −15.6058068368 | −0.0000000016 | 8 | 0.0000663613 | −15.6056501930 | −0.0000556471 | 15 | 0.0302968175 |
| 9 | −15.6058068335 | +0.0000000033 | 9 | 0.0000122091 | −15.6057330619 | −0.0000828689 | 16 | 0.0197063516 |
| 10 | −15.6058068336 | −0.0000000000 | 10 | 0.0000040077 | −15.6057681510 | −0.0000350891 | 18 | 0.0186569595 |
| 11 | | | | | −15.6058033733 | −0.0000352223 | 19 | 0.0069816557 |
| 12 | | | | | −15.6058052286 | −0.0000018553 | 21 | 0.0045627712 |
| 13 | | | | | −15.6058057676 | −0.0000005391 | 23 | 0.0036888638 |
| 14 | | | | | −15.6058065558 | −0.0000007882 | 24 | 0.0021623560 |
| 15 | | | | | −15.6058067218 | −0.0000001661 | 26 | 0.0015523193 |
| 16 | | | | | −15.6058068503 | −0.0000001285 | 27 | 0.0003628532 |
| 17 | | | | | −15.6058068547 | −0.0000000044 | 29 | 0.0002829316 |
| 18 | | | | | −15.6058068601 | −0.0000000054 | 30 | 0.0000872433 |
| 19 | | | | | −15.6058068604 | −0.0000000003 | 32 | 0.0000660842 |
| 20 | | | | | −15.6058068607 | −0.0000000002 | 33 | 0.0000166869 |

compute the gradients and residuals in the iterative optimization procedure.

The preferred approach to minimize the energy in VQE is via gradient-based algorithms. The gradient of the UCC energy with respect to a cluster amplitude $t_\mu$ is given by

$$\frac{\partial E_{VQE}(\mathbf{t})}{\partial t_\mu} = 2\,\mathrm{Re}\,\langle\Phi_0|\hat{U}^\dagger(\mathbf{t})\hat{H}\frac{\partial \hat{U}(\mathbf{t})}{\partial t_\mu}|\Phi_0\rangle \tag{4.30}$$

Equation (4.30) has the form of an off-diagonal matrix element of the Hamiltonian, and

Romero et al.[76] showed that it may be measured on a quantum device using one ancilla qubit and four time the cost of measuring the energy. With this algorithm, computing the gradient vector so that the 2-norm of the error is within precision $\bar{\varepsilon}_{\text{grad}}$ requires a total number of measurements ($m_{\text{grad}}$) that is bound by the inequality[76]

$$m_{\text{grad}} \leq 4N_{\text{par}} \frac{\left(\sum_\ell |h_\ell|\right)^2}{\bar{\varepsilon}_{\text{grad}}^2}. \tag{4.31}$$

The total number of measurements, and proportionally the runtime, required for a VQE calculation is dominated by the computation of the gradient vector and it is proportional to the number of gradient vector evaluations ($N_{\text{grad}}^{\text{VQE}}$) required to converge the energy. This implies that the total number of VQE measurements ($m_{\text{VQE}}$) is bounded approximately by

$$m_{\text{VQE}} \leq N_{\text{grad}}^{\text{VQE}} m_{\text{grad}}. \tag{4.32}$$

This estimate ignores the evaluation of the VQE energy, which has a cost inferior to that of computing one element of the gradient vector. More recently, Kottmann et al.[64] showed that the analytic gradient may be computed with a cost essentially equal to that of two energy evaluations using the so-called parameter-shift-rule.[63] This procedure avoids the use of an ancilla qubit and the number of measurements required still satisfies the bound expressed in Eq. (4.31).

In the case of PQE, the number of measurements $m_{\text{res}}$ needed to compute the residual vector with precision $\bar{\varepsilon}_{\text{res}}$ has an upper bound given by

$$m_{\text{res}} \leq 3N_{\text{par}} \frac{\left(\sum_\ell |h_\ell|\right)^2}{\bar{\varepsilon}_{\text{res}}^2}. \tag{4.33}$$

This estimate takes into account the fact that the residual can be evaluated as the sum of three terms (with different prefactors), and that $E_0$ in Eq. (4.14) only needs to be measured once. The total number of PQE measurements ($m_{\text{PQE}}$) is bounded by

$$m_{\text{PQE}} \leq N_{\text{res}}^{\text{PQE}} m_{\text{res}}, \tag{4.34}$$

where $N_{\text{res}}^{\text{PQE}}$ is the number of PQE residual vector evaluations. Assuming that the energy gradients in VQE and the residual in PQE are measured with the same precision ($\bar{\varepsilon}_{\text{grad}} \approx \bar{\varepsilon}_{\text{res}}$), we estimate that $m_{\text{res}} \approx \frac{3}{4} m_{\text{grad}}$. This result suggest that PQE should have a similar or perhaps slightly smaller cost per iteration than VQE. However, a more important factor in determining the relative performance of VQE and PQE is the number of residual/gradient evaluations required, which as shown in Sec. 4.3, favors PQE over VQE.

A detailed comparison of the adaptive variants of VQE (e.g., ADAPT-VQE) and PQE is more complex due to the significant differences in the form of the ansatz and the selection procedure used in these two methods. At iteration $k$, the ADAPT-VQE approach selects the operator $\hat{\kappa}_\mu$ with the largest absolute energy gradient. This selection scheme requires evaluating the gradient $g_\mu^{(k)}$ for all the operators in the pool

$$g_\mu^{(k)} = \left\langle \Psi^{(k)} \middle| [\hat{H}, \hat{\kappa}_\mu] \middle| \Psi^{(k)} \right\rangle . \tag{4.35}$$

Because most sub-terms of the Hamiltonian will commute with $\hat{\kappa}_\mu$, a relatively small number of $\left\langle \hat{\kappa}_\mu \hat{O}_\ell \middle| \hat{\kappa}_\mu \hat{O}_\ell \right\rangle$ and $\left\langle \hat{O}_\ell \hat{\kappa}_\mu \middle| \hat{O}_\ell \hat{\kappa}_\mu \right\rangle$ terms need to be measured. Both $\hat{H}$ and the operator pool $\{\hat{\kappa}_\mu\}$ contain of the order $N^4$ elements (assuming a pool of general one and two-body operators).

However, it has recently been pointed out[67] that if the quantity $[\hat{H}, \hat{\kappa}_\mu]$ is decomposed in terms of the reduced density matrices, then one can determine the pool gradients [Eq. (4.35)] with the evaluation of a number of Pauli terms that scales as $N^6$ (again assuming a pool of general one and two-body operators). In ADAPT-VQE this cost must then be multiplied by the number of iterations performed. It is important to note that the ADAPT-VQE macro-iteration convergence threshold $\varepsilon_\alpha = 10^{-\alpha}$ is based on the norm of the vector of pool gradients [Eq. (4.35)], such that ADAPT-VQE is considered converged when $\|\mathbf{g}_{\text{pool}}\| \leq \varepsilon_\alpha$. The number of measurements of the approximate residual vector ($|\tilde{r}\rangle$) for the purpose of selection in SPQE is a parameter of a computation. In Appendix 4.5.5, we show that a probabilistic estimate for the number of measurements required to converge

SPQE with a threshold of $\Omega$ is of the order of $(\Delta t\Omega)^{-2}$.

A trade-off of using three- and higher-body operators in SPQE is a greater circuit depth since an operator $\hat{\kappa}_{ij\cdots}^{ab\cdots}$ of many-body rank $n$ becomes a sum of $2^{2n-1}$ Pauli strings after Jordan–Wigner mapping to the qubit basis. Since all Pauli strings that are generated in this mapping commute, the unitary $\exp\left(\theta\,\hat{\kappa}_{ij\cdots}^{ab\cdots}\right)$ can be written as the product of $2^{2n-1}$ exponentials of operators containing Pauli strings of length $2n$.

To analyze the compromise between the rank of the operator pool and the compactness of the ansatz in ADAPT-VQE and SPQE we consider the example of a three-body operator $\exp\left(t\,\hat{\kappa}_{ijk}^{abc}\right)$. In ADAPT-VQE this term may be approximated using general two-body operators as

$$e^{t\,\hat{\kappa}_{ijk}^{abc}} = e^{t\,[\hat{\kappa}_{ij}^{ae},\hat{\kappa}_{ke}^{bc}]} \approx e^{t\,\hat{\kappa}_{ij}^{ae}}\, e^{t\,\hat{\kappa}_{ke}^{bc}}\, e^{-t\,\hat{\kappa}_{ij}^{ae}}\, e^{-t\,\hat{\kappa}_{ke}^{bc}}, \tag{4.36}$$

where the last term is a lowest-order Trotter approximation of the exponential of the commutator $[\hat{\kappa}_{ij}^{ae}, \hat{\kappa}_{ke}^{bc}]$ (with $e \neq a,b,c$). The last term in Eq. (4.36) is implemented as a circuit that contains four different parameters and a product of 32 exponentials of Pauli strings of length four. The same three-body excitation is represented in SPQE using a single parameter and a longer circuit as a product of 32 exponentials of Pauli strings of length six. This comparison suggests, in accordance with the results of our study, that higher-body operators are represented less efficiently with an arbitrary particle-hole operator pool than a general singles and doubles operator pool.

### 4.5.5 Reduced-cost estimation of the approximate residual in selected PQE

This appendix explores various methods to reduce the number of measurements $M$ required to compute the approximate the residuals $\tilde{r}_\mu$ used in the selected PQE method (see Sec. 4.2.5). Selection requires the identification of the elements of the approximate residual that corresponds to projections onto excited determinants. However, for small values of $\Delta t$, the state $|\tilde{r}\rangle$ is dominated by the reference determinant $\Phi_0$, and consequently,

the measurement of important missing excitations may become inefficient. In practice one

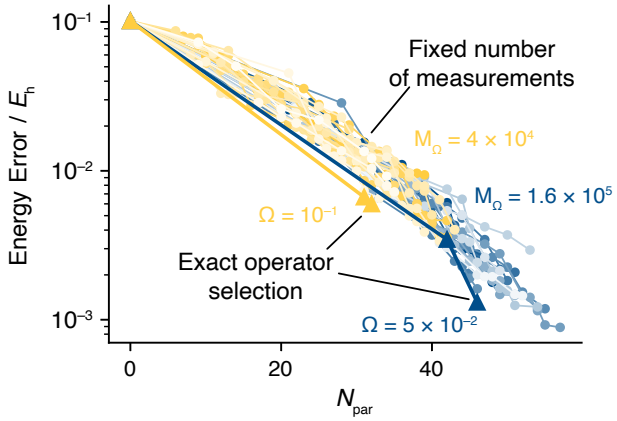


Figure 4.8: SPQE energy convergence for $H_6$ at a separation of $r_{H-H} = 1.0$ Å, with $\Delta t = 0.05$ au. Data sets with triangular markers denote exact operator selection and convergence via Eqs. (5.25) and (5.26) for $\Omega = 1.0 \times 10^{-1}$ (yellow) and $\Omega = 5.0 \times 10^{-2}$ (dark blue). Data sets with dots denote operator selection and convergence with a fixed number of measurements $M_\Omega = 4.0 \times 10^4$ (yellow) and $M_\Omega = 1.6 \times 10^5$ (dark blue) calculated via Eq. (4.37) for the corresponding $\Omega$ values.

can consider an alternative convergence criterion for SPQE based on performing a fixed number of measurements $M_\Omega$ on the state $|\tilde{r}\rangle$. In such an approach, at each iteration $k$, the operators $\hat{\kappa}_\mu$ whose corresponding determinants $|\Phi_\mu\rangle$ are measured at least once (over all $M_\Omega$ measurements) are added to $\mathscr{A}$. Because the residual magnitudes go to zero as the eigenstate is better approximated in successive $k$ iterations, it becomes increasingly unlikely that any determinants besides the reference $|\Phi_0\rangle$ will be measured. The SPQE algorithm can then be considered converged when all $M_\Omega$ measurements yield the reference state. Starting from Eqs. (5.25) and (5.26), and making the assumption that at convergence only a single determinant $\Phi_\mu$ is measured that is not the reference (i.e., $\sum_\mu N_\mu = 1$), one can use a number of measurements

$$M_\Omega = \frac{1}{\Delta t^2 \Omega^2}, \tag{4.37}$$

to probabilistically test convergence of the residual vector to within the threshold $\Omega$. In practice we find that using Eq. (4.37) works well compared to the exact threshold given in Eq. (5.26). Figure 4.8 compares the energy convergence with number of selected op-

erators/parameters using both convergence criterion corresponding to the same value of $\Omega$.

# Bibliography

[1] S. Lloyd. "Universal quantum simulators." *Science* **273**, 1073 (1996).

[2] A. Aspuru-Guzik, A. D. Dutoi, P. J. Love, and M. Head-Gordon. "Simulated quantum computation of molecular energies." *Science* **309**, 1704 (2005).

[3] A. Kandala, A. Mezzacapo, K. Temme, M. Takita, M. Brink, J. M. Chow, and J. M. Gambetta. "Hardware-efficient variational quantum eigensolver for small molecules and quantum magnets." *Nature* **549**, 242 (2017).

[4] A. Kandala, K. Temme, A. D. Córcoles, A. Mezzacapo, J. M. Chow, and J. M. Gambetta. "Error mitigation extends the computational reach of a noisy quantum processor." *Nature* **567**, 491 (2019).

[5] S. R. White. "Density matrix formulation for quantum renormalization groups." *Phys. Rev. Lett.* **69**, 2863 (1992).

[6] B. Huron, J.-P. Malrieu, and P. Rancurel. "Iterative perturbation calculations of ground and excited state energies from multiconfigurational zeroth order wavefunctions." *J. Chem. Phys.* **58**, 5745 (1973).

[7] R. J. Buenker and S. D. Peyerimhoff. "Individualized configuration selection in CI calculations with subsequent energy extrapolation." *Theor. Chim. Acta* **35**, 33 (1974). ISSN 1432-2234.

[8] G. H. Booth, A. J. W. Thom, and A. Alavi. "Fermion Monte Carlo without fixed nodes: A game of life, death, and annihilation in Slater determinant space." *J. Chem. Phys.* **131**, 054106 (2009).

[9] F. Coester and H. Kümmel. "Short-range correlations in nuclear wave functions." *Nuc. Phys.* **17**, 477 (1960).

[10] J. Čížek. "On the correlation problem in atomic and molecular systems. Calculation of wavefunction components in Ursell-type expansion using quantum-field theoretical methods." *J. Chem. Phys.* **45**, 4256 (1966).

[11] P. Piecuch, S. Zarrabian, J. Paldus, and J. Čížek. "Coupled-cluster approaches with an approximate account of triexcitations and the optimized-inner-projection technique. II. Coupled-cluster results for cyclic-polyene model systems." *Phys. Rev. B* **42**, 3351 (1990).

[12] P. Piecuch and M. Włoch. "Renormalized coupled-cluster methods exploiting left eigenstates of the similarity-transformed Hamiltonian." *J. Chem. Phys.* **123**, 224105 (2005).

[13] P. A. Limacher, P. W. Ayers, P. A. Johnson, S. De Baerdemacker, D. Van Neck, and P. Bultinck. "A new mean-field method suitable for strongly correlated electrons: Computationally facile antisymmetric products of nonorthogonal geminals." *J. Chem. Theory Comput.* **9**, 1394 (2013).

[14] I. W. Bulik, T. M. Henderson, and G. E. Scuseria. "Can single-reference coupled cluster theory describe static correlation?" *J. Chem. Theory Comput.* **11**, 3171 (2015).

[15] J. Čížek. "On the use of the cluster expansion and the technique of diagrams in calculations of correlation effects in atoms and molecules." *Adv. Chem. Phys* **14**, 35 (1969).

[16] I. Lindgren. "A coupled-cluster approach to the many-body perturbation theory for open-shell systems." *Int. J. Quantum Chem.* **14**, 33 (1978).

[17] B. Jeziorski and H. J. Monkhorst. "Coupled-cluster method for multideterminantal reference states." *Phys. Rev. A* **24**, 1668 (1981).

[18] D. I. Lyakh, M. Musiał, V. F. Lotrich, and R. J. Bartlett. "Multireference Nature of Chemistry: The Coupled-Cluster View." *Chem. Rev.* **112**, 182 (2012).

[19] A. Köhn, M. Hanauer, L. A. Mück, T.-C. Jagau, and J. Gauss. "State-specific multireference coupled-cluster theory." *Wiley Interdiscip. Rev.: Comput. Mol. Sci.* **3**, 176 (2013).

[20] F. A. Evangelista. "Perspective: Multireference coupled cluster theories of dynamical electron correlation." *J. Chem. Phys.* **149**, 030901 (2018).

[21] R. P. Feynman. "Simulating physics with computers." *Int. J. Theor. Phys* **21** (1982).

[22] A. Y. Kitaev. "Quantum measurements and the Abelian stabilizer problem." *arXiv:9511026* (1995).

[23] D. S. Abrams and S. Lloyd. "Simulation of many-body fermi systems on a universal quantum computer." *Phys. Rev. Lett.* **79**, 2586 (1997).

[24] D. S. Abrams and S. Lloyd. "Quantum algorithm providing exponential speed increase for finding eigenvalues and eigenvectors." *Phys. Rev. Lett.* **83**, 5162 (1999).

[25] H. F. Trotter. "On the product of semi-groups of operators." *Proc. Am. Math. Soc.* **10**, 545 (1959).

[26] M. Suzuki. "Improved Trotter-like formula." *Physics Letters A* **180**, 232 (1993).

[27] V. von Burg, G. H. Low, T. Häner, D. S. Steiger, M. Reiher, M. Roetteler, and M. Troyer. "Quantum computing enhanced computational catalysis." *arXiv:2007.14460* (2020).

[28] J. Lee, D. Berry, C. Gidney, W. J. Huggins, J. R. McClean, N. Wiebe, and R. Babbush. "Even more efficient quantum computations of chemistry through tensor hypercontraction." *arXiv:2011.03494* (2020).

[29] R. Babbush, N. Wiebe, J. R. McClean, J. McClain, H. Neven, and G. K.-L. Chan. "Low-depth quantum simulation of materials." *Phys. Rev. X* **8**, 011044 (2018).

[30] M. Reiher, N. Wiebe, K. M. Svore, D. Wecker, and M. Troyer. "Elucidating reaction mechanisms on quantum computers." *Proc. Natl. Acad. Sci. U.S.A* **114**, 7555 (2017).

[31] J. Kempe, A. Kitaev, and O. Regev. "The complexity of the local Hamiltonian problem." *SIAM J. Comput.* **35**, 1070 (2006).

[32] J. Preskill. "Quantum Computing in the NISQ era and beyond." *Quantum* **2**, 79 (2018).

[33] A. Peruzzo, J. R. McClean, P. Shadbolt, M.-H. Yung, X.-Q. Zhou, P. J. Love, A. Aspuru-Guzik, and J. L. O'Brien. "A variational eigenvalue solver on a photonic quantum processor." *Nat. Commun.* **5**, 4213 (2014).

[34] M.-H. Yung, J. Casanova, A. Mezzacapo, J. R. McClean, L. Lamata, A. Aspuru-Guzik, and E. Solano. "From transistor to trapped-ion computers for quantum chemistry." *Sci. Rep.* **4**, 3589 (2014).

[35] J. R. McClean, J. Romero, R. Babbush, and A. Aspuru-Guzik. "The theory of variational hybrid quantum-classical algorithms." *New J. Phys.* **18**, 023023 (2016).

[36] H. R. Grimsley, S. E. Economou, E. Barnes, and N. J. Mayhall. "An adaptive variational algorithm for exact molecular simulations on a quantum computer." *Nat. Commun.* **10**, 1 (2019).

[37] P. J. J. O'Malley, R. Babbush, I. D. Kivlichan, J. Romero, J. R. McClean, R. Barends, J. Kelly, P. Roushan, A. Tranter, N. Ding, *et al.*. "Scalable Quantum Simulation of Molecular Energies." *Phys. Rev. X* **6**, 031007 (2016).

[38] J. I. Colless, V. V. Ramasesh, D. Dahlen, M. S. Blok, M. Kimchi-Schwartz, J. R. McClean, J. Carter, W. De Jong, and I. Siddiqi. "Computation of molecular spectra on a quantum processor with an error-resilient algorithm." *Phys. Rev. X* **8**, 011021 (2018).

[39] Y. Shen, X. Zhang, S. Zhang, J.-N. Zhang, M.-H. Yung, and K. Kim. "Quantum implementation of the unitary coupled cluster for simulating molecular electronic structure." *Phys. Rev. A* **95**, 020501 (2017).

[40] C. Hempel, C. Maier, J. Romero, J. McClean, T. Monz, H. Shen, P. Jurcevic, B. P. Lanyon, P. Love, R. Babbush, *et al.*. "Quantum chemistry calculations on a trapped-ion quantum simulator." *Phys. Rev. X* **8**, 031022 (2018).

[41] Y. Nam, J.-S. Chen, N. C. Pisenti, K. Wright, C. Delaney, D. Maslov, K. R. Brown, S. Allen, J. M. Amini, J. Apisdorf, *et al.*. "Ground-state energy estimation of the water molecule on a trapped-ion quantum computer." *npj Quantum Inf.* **6**, 1 (2020).

[42] P. G. Szalay, M. Nooijen, and R. J. Bartlett. "Alternative ansätze in single reference coupled-cluster theory. III. A critical analysis of different methods." *J. Chem. Phys.* **103**, 281 (1995).

[43] A. G. Taube and R. J. Bartlett. "New perspectives on unitary coupled-cluster theory." *Int. J. Quantum Chem.* **106**, 3393 (2006).

[44] B. Cooper and P. J. Knowles. "Benchmark studies of variational, unitary and extended coupled cluster methods." *J. Chem. Phys.* **133**, 234102 (2010).

[45] F. A. Evangelista. "Alternative single-reference coupled cluster approaches for multireference problems: The simpler, the better." *J. Chem. Phys.* **134**, 224102 (2011).

[46] G. Harsha, T. Shiozaki, and G. E. Scuseria. "On the difference between variational and unitary coupled cluster theories." *J. Chem. Phys.* **148**, 044107 (2018).

[47] M.-A. Filip and A. J. W. Thom. "A stochastic approach to unitary coupled cluster." *J. Chem. Phys.* **153**, 214106 (2020).

[48] J. Chen, H.-P. Cheng, and J. K. Freericks. "Quantum-Inspired Algorithm for the Factorized Form of Unitary Coupled Cluster Theory." *J. Chem. Theory Comput.* **17**, 841 (2021).

[49] I. G. Ryabinkin, T.-C. Yen, S. N. Genin, and A. F. Izmaylov. "Qubit Coupled Cluster Method: A Systematic Approach to Quantum Chemistry on a Quantum Computer." *J. Chem. Theory Comput.* **14**, 6317 (2018).

[50] P. J. Knowles, C. Hampel, and H.-J. Werner. "Coupled cluster theory for high spin, open shell reference wave functions." *J. Chem. Phys.* **99**, 5219 (1993).

[51] M. Motta, C. Sun, A. T. Tan, M. J. O'Rourke, E. Ye, A. J. Minnich, F. G. Brandão, and G. K.-L. Chan. "Determining eigenstates and thermal states on a quantum computer using quantum imaginary time evolution." *Nat. Phys.* **16**, 1 (2019).

[52] S.-N. Sun, M. Motta, R. N. Tazhigulov, A. T. Tan, G. K.-L. Chan, and A. J. Minnich. "Quantum Computation of Finite-Temperature Static and Dynamical Properties of Spin Systems Using Quantum Imaginary Time Evolution." *Phys. Rev. X Quantum* **2**, 010317 (2021).

[53] J. R. McClean, M. E. Kimchi-Schwartz, J. Carter, and W. A. de Jong. "Hybrid quantum-classical hierarchy for mitigation of decoherence and determination of excited states." *Phys. Rev. A* **95**, 042308 (2017).

[54] R. M. Parrish and P. L. McMahon. "Quantum filter diagonalization: Quantum eigendecomposition without full quantum phase estimation." *arXiv:1909.08925* (2019).

[55] N. H. Stair, R. Huang, and F. A. Evangelista. "A Multireference Quantum Krylov Algorithm for Strongly Correlated Electrons." *J. Chem. Theory Comput.* **16**, 2236 (2020). ISSN 1549-9626.

[56] W. J. Huggins, J. Lee, U. Baek, B. O'Gorman, and K. B. Whaley. "A non-orthogonal variational quantum eigensolver." *New J. Phys.* **22**, 073009 (2020).

[57] D. Wecker, M. B. Hastings, and M. Troyer. "Progress towards practical quantum variational algorithms." *Phys. Rev. A* **92**, 042303 (2015).

[58] P. Gokhale, O. Angiuli, Y. Ding, K. Gui, T. Tomesh, M. Suchara, M. Martonosi, and F. T. Chong. "Minimizing state preparations in variational quantum eigensolver by partitioning into commuting families." *arXiv:1907.13623* (2019).

[59] T.-C. Yen, V. Verteletskyi, and A. F. Izmaylov. "Measuring all compatible operators in one series of single-qubit measurements using unitary transformations." *J. Chem. Theory Comput.* **16**, 2400 (2020).

[60] V. Verteletskyi, T.-C. Yen, and A. F. Izmaylov. "Measurement optimization in the variational quantum eigensolver using a minimum clique cover." *J. Chem. Phys.* **152**, 124114 (2020).

[61] W. J. Huggins, J. R. McClean, N. C. Rubin, Z. Jiang, N. Wiebe, K. B. Whaley, and R. Babbush. "Efficient and noise resilient measurements for quantum chemistry on near-term quantum computers." *npj Quantum Inf.* **7**, 1 (2021).

[62] J. R. McClean, F. M. Faulstich, Q. Zhu, B. O'Gorman, Y. Qiu, S. R. White, R. Babbush, and L. Lin. "Discontinuous Galerkin discretization for quantum simulation of chemistry." *New J. Phys.* **22**, 093015 (2020).

[63] M. Schuld, V. Bergholm, C. Gogolin, J. Izaac, and N. Killoran. "Evaluating analytic gradients on quantum hardware." *Phys. Rev. A* **99**, 032331 (2019).

[64] J. S. Kottmann, A. Anand, and A. Aspuru-Guzik. "A feasible approach for automatically differentiable unitary coupled-cluster on quantum computers." *arXiv:2011.05938* (2020).

[65] I. G. Ryabinkin, R. A. Lang, S. N. Genin, and A. F. Izmaylov. "Iterative Qubit Coupled Cluster approach with efficient screening of generators." *J. Chem. Theory Comput.* **16**, 1055 (2020).

[66] Z.-J. Zhang, T. H. Kyaw, J. S. Kottmann, M. Degroote, and A. Aspuru-Guzik. "Mutual information-assisted adaptive variational quantum eigensolver ansatz construction." *arXiv:2008.07553* (2020).

[67] J. Liu, Z. Li, and J. Yang. "An efficient adaptive variational quantum solver of the Schrodinger equation based on reduced density matrices." *arXiv preprint arXiv:2012.07047* (2020).

[68] P. K. Barkoutsos, J. F. Gonthier, I. Sokolov, N. Moll, G. Salis, A. Fuhrer, M. Ganzhorn, D. J. Egger, M. Troyer, A. Mezzacapo, S. Filipp, and I. Tavernelli. "Quantum algorithms for electronic structure calculations: Particle-hole Hamiltonian and optimized wave-function expansions." *Phys. Rev. A* **98**, 022322 (2018).

[69] F. A. Evangelista, G. K.-L. Chan, and G. E. Scuseria. "Exact parameterization of fermionic wave functions via unitary coupled cluster theory." *J. Chem. Phys.* **151**, 244112 (2019).

[70] T. D. Crawford and H. F. Schaefer. "An introduction to coupled cluster theory for computational chemists." *Rev. Comput. Chem.* **14**, 33 (2000).

[71] J. Lee, W. J. Huggins, M. Head-Gordon, and K. B. Whaley. "Generalized unitary coupled cluster wave functions for quantum computation." *J. Chem. Theory Comput.* **15**, 311 (2018).

[72] T. Helgaker, P. JÃÿrgensen, and J. Olsen. *Coupled-Cluster Theory*, chapter 13, 648–723. John Wiley & Sons, Ltd (2000). ISBN 9781119019572.

[73] P. Pulay. "Convergence acceleration of iterative sequences. The case of SCF iteration." *Chem. Phys. Lett.* **73**, 393 (1980).

[74] D. Aharonov, V. Jones, and Z. Landau. "A polynomial quantum algorithm for approximating the Jones polynomial." *Algorithmica* **55**, 395 (2009).

[75] D. W. Berry, C. Gidney, M. Motta, J. R. McClean, and R. Babbush. "Qubitization of arbitrary basis quantum chemistry leveraging sparsity and low rank factorization." *Quantum* **3**, 208 (2019).

[76] J. Romero, R. Babbush, J. R. McClean, C. Hempel, P. J. Love, and A. Aspuru-Guzik. "Strategies for quantum computing molecular energies using the unitary coupled cluster ansatz." *Quantum Sci. Technol.* **4**, 014008 (2019).

[77] F. Arute, K. Arya, R. Babbush, D. Bacon, J. C. Bardin, R. Barends, S. Boixo, M. Broughton, B. B. Buckley, D. A. Buell, *et al.*. "Hartree-Fock on a superconducting qubit quantum computer." *Science* **369**, 1084 (2020).

[78] M. Motta, D. M. Ceperley, G. K.-L. Chan, J. A. Gomez, E. Gull, S. Guo, C. A. Jiménez-Hoyos, T. N. Lan, J. Li, F. Ma, *et al.*. "Towards the solution of the many-electron problem in real materials: equation of state of the hydrogen chain with state-of-the-art many-body methods." *Phys. Rev. X* **7**, 031059 (2017).

[79] M. Motta, C. Genovese, F. Ma, Z.-H. Cui, R. Sawaya, G. K.-L. Chan, N. Chepiga, P. Helms, C. Jiménez-Hoyos, A. J. Millis, *et al.*. "Ground-state properties of the hydrogen chain: dimerization, insulator-to-metal transition, and magnetic phases." *Phys. Rev. X* **10**, 031058 (2020).

[80] N. H. Stair and F. A. Evangelista. "Exploring Hilbert space on a budget: Novel benchmark set and performance metric for testing electronic structure methods in the regime of strong correlation." *J. Chem. Phys.* 104108 (2020).

[81] D. G. Smith, L. A. Burns, A. C. Simmonett, R. M. Parrish, M. C. Schieber, R. Galvelis, P. Kraus, H. Kruse, R. Di Remigio, A. Alenaizan, *et al.*. "Psi4 1.4: Open-source software for high-throughput quantum chemistry." *J. Chem. Phys.* **152**, 184108 (2020).

[82] N. H. Stair and F. A. Evangelista. "QForte: A quantum computer simulator and algorithms library for molecular simulation (see https://github.com/evangelistalab/qforte and https://education.molssi.org/2020-software-fellow-posters/nick-stair)." (2020).

[83] C. G. Broyden. "The convergence of a class of double-rank minimization algorithms: 2. The new algorithm." *J. Inst. Math. Appl.* **6**, 222 (1970).

[84] R. Fletcher. "A new approach to variable metric algorithms." *Comput. J* **13**, 317 (1970).

[85] D. Goldfarb. "A family of variable-metric methods derived by variational means." *Math. Comput.* **24**, 23 (1970).

[86] D. F. Shanno. "Conditioning of quasi-Newton methods for function minimization." *Math. Comput.* **24**, 647 (1970).

[87] P. Virtanen, R. Gommers, T. E. Oliphant, M. Haberland, T. Reddy, D. Cournapeau, E. Burovski, P. Peterson, W. Weckesser, J. Bright, *et al.*. "SciPy 1.0: fundamental algorithms for scientific computing in Python." *Nat. Methods* **17**, 261 (2020).

[88] M. B. Hastings, D. Wecker, B. Bauer, and M. Troyer. "Improving Quantum Algorithms for Quantum Chemistry." *Quantum Info. Comput.* **15**, 1 (2015). ISSN 1533-7146.

[89] G. D. Purvis III and R. J. Bartlett. "A full coupled-cluster singles and doubles model: The inclusion of disconnected triples." *J. Chem. Phys.* **76**, 1910 (1982).

[90] K. Raghavachari, G. W. Trucks, J. A. Pople, and M. Head-Gordon. "A fifth-order perturbation comparison of electron correlation theories." *Chem. Phys. Lett.* **157**, 479 (1989).

[91] U. S. Mahapatra, B. Datta, and D. Mukherjee. "A size-consistent state-specific multireference coupled cluster theory: Formal developments and molecular applications." *J. Chem. Phys.* **110**, 6171 (1999).

[92] F. A. Evangelista, W. D. Allen, and H. F. Schaefer. "Coupling term derivation and general implementation of state-specific multireference coupled cluster theories." *J. Chem. Phys.* **127**, 024102 (2007).

[93] F. A. Evangelista, E. Prochnow, J. Gauss, and H. F. Schaefer. "Perturbative triples corrections in state-specific multireference coupled cluster theory." *J. Chem. Phys.* **132**, 074107 (2010).

[94] K. Setia, R. Chen, J. E. Rice, A. Mezzacapo, M. Pistoia, and J. D. Whitfield. "Reducing Qubit Requirements for Quantum Simulations Using Molecular Point Group Symmetries." *J. Chem. Theory Comput.* **16**, 6091 (2020).

[95] V. Giovannetti, S. Lloyd, and L. Maccone. "Quantum random access memory." *Phys. Rev. Lett.* **100**, 160501 (2008).

[96] S. Lloyd, M. Mohseni, and P. Rebentrost. "Quantum principal component analysis." *Nat. Phys.* **10**, 631 (2014).

[97] R. LaRose, A. Tikku, É. O'Neel-Judy, L. Cincio, and P. J. Coles. "Variational quantum state diagonalization." *npj Quantum Inf.* **5**, 1 (2019).

# Chapter 5

# QForte

## 5.1 Introduction

The past decade has seen tremendous progress in the development quantum computational hardware, facilitating early demonstrations of quantum advantage,[1] and numerous non-trivial calculations for applications ranging from quantum simulation[2–7] to constrained optimization.[8,9] These advances have concurrently inspired rapid development of numerous quantum algorithms amenable to both noisy intermediate scale quantum[10] (NISQ), and fault-tolerant devices.

In the field of quantum simulation, particularly for those algorithms designed to determine the ground and low-lying eigenstates of many-body systems, a variety of methods now exist[11,12] which vary dramatically in quantum resource requirements, often with a tradeoff between circuit depth and measurement overhead. Moreover, within the subclass of hybrid quantum-classical approaches such the as variational quantum eigensolver[13,14] (VQE), and approaches such as quantum imaginary time evolution[15] (QITE), one also considers the accuracy of the unitary ansatz as well as the classical memory and computational overhead associated with (i) the number of classical parameters utilized, (ii) the procedure used to update/augment the parameters, and (iii) the potentially large number of iterations needed to converge the the parameters (particularly in the presence of vanishing gradients[16]).

While it is almost unheard-of to publish a new method in (classical) electronic structure without a detailed numerical comparison to existing algorithms, it is far more rare to see such comparisons (with respect to some of the aforementioned resource requirements) for quantum (or hybrid) algorithms. The lack of cross comparison, however, is largely due to the lack of available software resources, as most implementations of new quantum algorithms exists only as code written by independent research groups and are often not publicly available without special request. Moreover, these independent implementations rarely give detailed numerics for the quantum and classical resource counts such as the number of classical parameters, the total number operators averaged over for determining expectation values, and the circuit depths. To help ameliorate this issue, we introduce the new open-source package QFORTE , the first black-box quantum algorithms library for molecular electronic structure.

The software ecosystem for the development of new quantum algorithms is ever-expanding. This is particularly true in the context of quantum algorithms for molecular electronic structure, because there are many complex software challenges involved in the complete pipeline that begins with specification of a molecular geometry and ends (usually) with a specified algorithm's numerical prediction of the eigenvalue(s). In order to accomplish this task, one must first install a (usually open-source) classical electronic structure package such as PYSCF or PSI4 to obtain the one ($h_{pq}$) and two-electron ($v_{pqrs}$) integrals. Next, one must utilize a package for fermionic encoding such as OPENFERMION, as well as appropriate application programming interfaces (API) such as OPENFERMION-PYSCF or OPENFERMION-PSI4, to convert the fermionic operators (such as the Hamiltonian)

$$\hat{\mathscr{H}} = \sum_{pq} h_{pq} \hat{a}_p^\dagger \hat{a}_q + \frac{1}{4} \sum_{pqrs} v_{pqrs} \hat{a}_p^\dagger \hat{a}_q^\dagger \hat{a}_s \hat{a}_r \rightarrow \hat{\mathscr{H}} = \sum_{\ell} \theta_\ell \hat{P}_\ell \tag{5.1}$$

to a so-called qubit representation given as a sum of products of Pauli operators $\hat{P}_\ell$. In order to apply quantum circuits associated with the transformed operators (such as the time

evolution unitary, or various ansatz used commonly in VQE) one is required to install one of the numerous–often industry affiliated–backend quantum-computer simulators such as IBM's QISKIT,[17] Google's CIRQ[18] or FQS,[19] Microsoft's Q#,[20] or Rigetti's PYQUILL;[21] again with the appropriate API's. In the outermost software layer exist packages such as TEQUILA[22] that serve as sandbox implantation tool which solve many of the interoperability challenges associated with interfacing the aforementioned dependancies. While flexible packages for sand-box development are undoubtably important, it is still usually left to the user to implement a desired algorithm, which is generally a non-trivial task given the diversity of quantum algorithms present in modern literature. A single-package (incorporating all of the described steps) black-box implementation of such algorithms with which one can easily specify a molecular geometry and desired quantum algorithm (as is the case for classical electronic structure packages) is highly desirable for researchers interested quickly generating comparative results.

As previously mentioned, an additional challenge to black-box implementation of quantum algorithms is their now significant level of diversity. Arguably the simplest and most well established (hybrid) algorithm is the variational quantum eigensolver[13,14] (VQE), in which (usually) the ground state is approximated by a normalized trial state $\left|\tilde{\Psi}\right\rangle = \hat{U}(\boldsymbol{\theta})\left|\Phi_0\right\rangle$, in which the circuit $\hat{U}(\boldsymbol{\theta})$ depends on the parameter vector $\boldsymbol{\theta}$ and $\Phi_0$ is (usually) an unentangled reference state. The VQE energy ($E_{\text{VQE}}$) is then obtained by minimization of the trial state energy expectation value as $E_{\text{VQE}} = \min_{\boldsymbol{\theta}} \left\langle\Phi_0\right| \hat{U}^\dagger(\boldsymbol{\theta}) \hat{\mathscr{H}} \hat{U}(\boldsymbol{\theta}) \left|\Phi_0\right\rangle$, and is repeatedly evaluated (often along with the energy gradients) in a classical optimization loop. While implementation of the base VQE structure is straight forward for toy examples, automatic generation of the ansatz circuit is in general more complicated and obviously dependent on the inspiration for ansatz (i.e. disentangled unitary coupled cluster,[3] hardware-efficient,[3] Hamiltonian variational,[23] qubit coupled cluster,[24] etc…). Moreover, many hybrid approaches such as adaptive ansatz approaches[25,26] or subspace expansion methods[27] incorporate the basic VQE schema as a subroutine and require additional imple-

mentation for determination of matrix elements to solve a generalized eigenvalue problem and/or an additional algorithmic layer to extend the ansatz. Similar implementation challenges exist for algorithms that rely on (often controlled) Hamiltonian time evolution such as quantum phase estimation[28–30] (QPE), or subspace methods like quantum filter diagonalization[31] [also known as quantum Krylov[32] (QK)]. For algorithms that measure projected quantities such as quantum imaginary time evolution[15] (QITE) and the projective quantum eigensolver[33] (PQE), one must additionally implement the (often iterative) parameter update procedure.

Our new open-source package QFORTE is an end-to-end electronic structure package for quantum algorithms, and is still capable of facilitating sand-box implementations of new algorithms, only relying on a classical electronic structure package as a dependancy. The remainder of this article is organized as follows. In Sec. 5.2 we will describe QFORTE 's key data structures and its interface to PSI4. In Sec. 5.3 will discuss each of the quantum algorithms currently implemented in QFORTE as well as some of their implementation details in terms of the key data structures.

## 5.2 Key data structures

In order to facilitate simple molecular-geometry to quantum algorithm energy functionality, QFORTE relies on several key data structures. The lowest level structures, which include QFORTE 's `Computer` (state-vector simulator) and `Circuit` class are all implemented in C++, but are exposed in Python via Pybind11.[34] Higher level data structures such as the `SystemFactory` class which interfaces QFORTE to classical electronic structure packages, and the subclasses in which the actual algorithms are implemented are all explicitly written in Python. Here we will give an overview of some of the most important data structures for QFORTE 's workflow pipeline using a now-canonical example of the $H_2$ molecule.

### 5.2.1 The state-vector simulator

An important aspect of QFORTE that distinguishes it from many other packages is its incorporation of a dedicated state-vector simulator. State vector simulators, which store a copy of the complex vector representing the quantum state on the device at all points during a calculation, are among some of the most common quantum computer simulators employed today. While many such simulators rely (mostly) on sparse tensor operations, QFORTE takes an approach that closer resembles modern FCI implementations.[35]

*The QuantumComputer class*

The backbone of the QFORTE 's state-vector simulator is the `Computer` class, which stores a complex vector `coeff_`, as well as a vector of `QubitBasis` objects (both of dimension $2^{n_{\text{qb}}}$ where $n_{\text{qb}}$ is the number of qubits). One can then apply a `Gate`, `Circuit`, or `QubitOperator` to transform the state vector by modifying `coeff_`.

An example of how to instantiate a `Computer` with four qubits and print the representation is shown in Lst. 5.1.

```
nqb = 4
qcomp = qf.Computer(nqb)
```

Listing 5.1: Initializing a QuantumComputer object.

*The QuantumGate class*

Once a `Computer` is initialized, the state can be modified by applying `Gate`s. The `Gate` class is the most fundamental building block for all quantum algorithms in QFORTE . Some of the most pertinent gates used quantum simulation are the Pauli gates ($X$, $Y$, and $Z$), the Hadamard gate $H$ (not to be confused with the Hamiltonian $\hat{\mathscr{H}}$), the controlled NOT [CNOT] gate, and the parametric z rotation gate $R_z(\theta)$. A full list of gates can be found in the QFORTE documentation.

The `Gate` class has several important attributes including a string (`label_`) which gives its identity, the integer `target_` and `control_` qubit indicies, and the matrix of complex values `gate_` that represents the operator. Instanciating a `Gate` is simple, and is done via the `gate()` member function.

List 5.2 shows how to instantiate the Pauli $\hat{X}$ gate that will target the qubit $q_4$.

```
target_idx = 4
X_4gate = qf.gate('X', target_idx)
```

Listing 5.2: Initializing a QuantumGate object.

List 5.3 shows a small example of using QFORTE 's state-vector simulator to construct the two-qubit Bell state

$$|\Psi_{\text{Bell}}\rangle = \frac{1}{\sqrt{2}}|00\rangle + \frac{1}{\sqrt{2}}|11\rangle . \tag{5.2}$$

Recall that the action of the controlled $X$ Pauli gate [with target qubit $q_0$, and control qubit $q_1$ $(cX_{0,1})$] is:

$$cX_{0,1}|00\rangle = |00\rangle \tag{5.3}$$

$$cX_{0,1}|01\rangle = |11\rangle , \tag{5.4}$$

$$cX_{0,1}|10\rangle = |10\rangle , \tag{5.5}$$

$$cX_{0,1}|11\rangle = |01\rangle . \tag{5.6}$$

Recall that the action of the Hadamrad gate $H$ is:

$$H|0\rangle = \frac{1}{\sqrt{2}}\big(|0\rangle + |1\rangle\big) \tag{5.7}$$

$$H|1\rangle = \frac{1}{\sqrt{2}}\big(|0\rangle - |1\rangle\big) \tag{5.8}$$

```
# Initialize a two-qubit QuantumComputer.
nqb = 2
qbell = qf.Computer(nqb)

# Initialize the gates needed to build the Bell state.
H_0 = qf.gate('H', 0)
cX_0_1 = qf.gate('cX', 1, 0)

# Apply the Hadamard gate.
qbell.apply_gate(H_0)

# Apply the CNOT (cX) gate.
qbell.apply_gate(cX_0_1)
```

Listing 5.3: Initializing a QuantumGate object.

*The QuantumCircuit class*

In virtually any quantum algorithm it is necessary to apply many gates sequentially. A so called quantum circuit, commonly referred to as a unitary ($\hat{U}$), is represented by a product of quantum gates, making the overall circuit itself a unitary operation. The `Circuit` class operates at one level above the `Gate` class and its primary attribute is the vector `gates_` of `Gate` objects.

Although any product of elementary gates technically constitutes a circuit, one of the most important circuit structures in quantum simulation is that which represents unitaries obtained by exponentiating a product of Pauli operators:

$$e^{i\theta_\ell \hat{P}_\ell} = \left(\prod_k^{n_\ell} \hat{V}_k^{(\ell)}\right)^\dagger \left(\prod_k^{n_\ell - 1} \text{c-}\hat{X}_{k,k+1}^{(\ell)}\right)^\dagger \hat{R}_z(2\theta_\ell) \left(\prod_k^{n_\ell - 1} \text{c-}\hat{X}_{k,k+1}^{(\ell)}\right) \left(\prod_k^{n_\ell} \hat{V}_k^{(\ell)}\right), \tag{5.9}$$

where

$$\hat{P}_\ell = \prod_k^{n_\ell} \hat{\sigma}_k^{(\ell)} \tag{5.10}$$

is a unique product of $n_\ell$ Pauli operators ($\hat{X}$, $\hat{Y}$, or $\hat{Z}$). In this case, $k = (p, [X, Y, \text{or } Z])$ is a compound index over the products in a term $\hat{P}_\ell$ and denotes the qubit ($p$) and specific Pauli gate. The transformation unitary $\hat{V}_k^{(\ell)}$ is a one qubit gate that transforms $\hat{X}$ or $\hat{Y}$ into $\hat{Z}$. An example of how one would construct such a circuit in QFORTE is shown in Lst. 5.4.

```
# Construct the desired preliminary circuit (X3 Z2 Z1 Z0)
circ = qf.Circuit()
circ.add_gate(qf.gate('Z', 0))
circ.add_gate(qf.gate('Z', 1))
circ.add_gate(qf.gate('Z', 2))
circ.add_gate(qf.gate('X', 3))
print('\n The origional unitary circuit \n',circ.str())

# Define the factor (-i theta)
theta = 0.5
factor = -1.0j * theta

# Construct the unitary for the exponential.
Uexp, phase = exponentiate_single_term(factor, circ)
print('\n The exponential unitary circuit \n',Uexp.str())
```

Listing 5.4: Constructing the circuit corresponding to $\exp\left(-i0.5\hat{X}_3\hat{Z}_2\hat{Z}_1\hat{Z}_0\right)$.

### 5.2.2 The QubitOperator and SQOperator classes

The outer-most operations class in QForte is the `QubitOperator` class. Again, mathematically speaking, a generic quantum operator $\hat{O}$ is given by a linear combination of $N_\ell$ unitaries ($\hat{U}_\ell$) as

$$\hat{O} = \sum_\ell u_\ell \hat{U}_\ell, \tag{5.11}$$

where $u_\ell$ is a complex coefficient. It is important to note that although applying a `QubitOperator` to a state is possible in QFORTE , is in general it is not a physically valid operation.

The key attribute of the `QubitOperator` class is `terms_`: a vector of pairs of the form `<complex::double, QuantumCircuit>`. Importantly, the `QubitOperator` class is used to represent objects such as the Hamiltonian $\hat{\mathscr{H}}$ or the cluster operator[36] $\hat{T}$ in QFORTE 's algorithmic implementations.

QFORTE also supports operators in the form of second quantization, that is, operators comprised of fermionic annihilation ($\hat{a}_p$) and creation ($\hat{a}_p^\dagger$) operators. The `SQOperator` class functions very similarly to the `QubitOperator` class, but utilizes a slightly different syntax. We note that second quantized operators in QFORTE always assume that the individual fermionic operators are normal ordered within a term. The second quantized operators can then be transformed to the `QubitOperator` representation (given as a linear combination of products of Pauli operators) via the Jordan-Wigner transformation.[37] Under this transformation, there is a one-to-one mapping between a spin orbital $\phi_p$ and qubit $q_p$ such that the fermionic annihilation ($\hat{a}_p$) and creation ($\hat{a}_p^\dagger$) operators are represented by

$$\hat{a}_p = \frac{1}{2}\left(\hat{X}_p + i\hat{Y}_p\right)\hat{Z}_{p-1}\ldots\hat{Z}_0, \tag{5.12}$$

and,

$$\hat{a}_p^\dagger = \frac{1}{2}\left(\hat{X}_p - i\hat{Y}_p\right)\hat{Z}_{p-1}\ldots\hat{Z}_0. \tag{5.13}$$

Listing 5.5 shows how to instantiate a `SQOperator` and transform it into a

`QubitOperator`.

```
# Initialize the second quantized operator
sq_op = qf.SQOperator()

# Construct the terms and add them to the list.
h1 = 0.5
h2 = -0.25j
sq_op.add_term(h1, [1], [2])
sq_op.add_term(h2, [4, 2], [3, 1])

# Transform to the qubit operator representation
pauli_op = sq_op.jw_transform()
```

Listing 5.5: Converting SQOperators into QuantumOperators.

### 5.2.3 The molecule class

As discussed in the introduction, the first task for implementing a quantum algorithm for molecular electronic structure is to obtain the molecular Hamiltonian in the qubit operator representation, based on a specified molecular geometry. In QFORTE this is all accomplished using the `system_factory` and `molecule` classes. To begin, as shown in Lst. 5.6, one simply imports the appropriate modules and specifies a geometry:

```
from qforte import *

# Define the reference and geometry lists.
geom = [('H', (0., 0., 0.0)), ('H', (0., 0., 0.75))]

# Instantiate the system_factory object (also populates the integrals).
factory = system_factory(build_type='psi4', mol_geometry=geom, basis='
    sto-3g')

# Get the molecule object.
H2mol = factory.get_molecule()
```

Listing 5.6: Initializing the QFORTE molecule object.

Once the molecule class has been populated the user has access to the molecular Hamiltonian both in second-quantization representation [as a `SQOperator`] and in a qubit representation [as a `QubitOperator`] resulting from the Jordan-Wigner transformation. The molecule object is a key data structure in QFORTE that is passed to all algorithms to perform a quantum computation.

## 5.3 Overview of algorithms implemented

We consider the algorithms implemented in QFORTE partitioned into several overlapping categories. The first is variational hybrid algorithms[13,14,38] in which a classical optimizer is utilized to minimize the energy expectation value. The second category is projective approaches[15,33] where projective quantities are measured on a quantum device and then used to directly update or augment a classically parameterized unitary. The third category is subspace diagonalization[15,27,31,32,39] (QSD) in which a non-orthogonal many body basis is generated from a family of unitaries, and the matrix elements of a generalized eigenvalue problem are measured on a quantum device. And finally, there are those algorithms derived from quantum phase estimation[29,30] where the eigenvalue of a time evolved state is estimated by a binary readout of a set of ancialla qubits.

Currently, QFORTE contains black-box implementations of the following algorithms: (i) variational quantum eigensolver[13,14] (VQE) and (ii) projective quantum eigensolver[33] (PQE) both with a disentangled[40] (factorized) unitary coupled cluster[41–45] (dUCC) ansatz, (iii) the adaptive derivative-assembled pseudo-trotter (ADAPT)-VQE,[25] (iv) the selected PQE[33] (SPQE), (v) a variant of quantum imaginary time evolution[15] (QITE) and its quantum Lanczos[15] (QL) extension, (vi) quantum Krylov[31,32] (QK) and (vii) its selected multireference variant[32] (MRSQK) Each of these algorithms is implemented using the key data structures described in Sec. 5.2 In the following subsections we will briefly discuss the theoretical details of each of these methodologies.

### 5.3.1 dUCC variational quantum eigensolver

In the general VQE schema, one uses a unitary circuit $\hat{U}(\boldsymbol{\theta})$ parameterized by the vector $\boldsymbol{\theta}$ to construct a trial state of the form

$$|\Psi_{\mathrm{VQE}}\rangle = \hat{U}(\boldsymbol{\theta})\,|\Phi_0\rangle \tag{5.14}$$

from an easily prepared reference state $|\Phi_0\rangle$ (such as the Hartree–Fock state). One then wishes to minimize the energy expectation value of the state

$$E(\boldsymbol{\theta}) = \langle \Phi | \hat{U}^\dagger(\boldsymbol{\theta}) \hat{\mathscr{H}} \hat{U}(\boldsymbol{\theta}) | \Phi \rangle . \tag{5.15}$$

by iteratively averaging over the expectation value of each Hamiltonian sub-terms $\langle h_\ell \hat{P}_\ell \rangle$ to determine $E(\boldsymbol{\theta})$ and employing a classical optimization algorithm to update the parameters.

In QFORTE we have implemented VQE with a disentangled (or factorized) UCC ansatz $\hat{U}_{\mathrm{dUCC}}(\mathbf{t})$. We assume reference state is an easily prepared single determinant $|\Phi_0\rangle = |\phi_1 \phi_2 \cdots\rangle$ (such as the Hartree–Fock determinant) specified by occupied spin orbitals $\{\phi_i\}$ and unoccupied (virtual) spin orbitals $\{\phi_a\}$. The operator $\hat{\tau}_\mu \equiv \hat{\tau}_{ij\ldots}^{ab\cdots} = \hat{a}_a^\dagger \hat{a}_b^\dagger \cdots \hat{a}_j \hat{a}_i$ is a particle-hole excitation operator who's action turns the reference determinant $|\Phi_0\rangle$ into the excited determinant $\left|\Phi_\mu\right\rangle$.

The dUCC ansatz is then constructed as a product of exponentiated anti-hermitian operators $\hat{\kappa}_\mu \equiv \hat{\tau}_\mu - \hat{\tau}_\mu^\dagger$ as

$$\hat{U}_{\mathrm{dUCC}}(\mathbf{t}) = \prod_\mu e^{t_\mu \hat{\kappa}_\mu}. \tag{5.16}$$

The dUCC circuit is built automatically in QFORTE by initializing a list of `SQOperators` that represent $\hat{\kappa}_\mu$, transforming to a list of `QuantumOperators` via the Jordan-Wigner transformation and constructing the circuit for the exponential each of sub-term [Eq. (5.9)].

*Adaptive VQE*

We have also implemented an adaptive variant of dUCC-VQE, namely the ADAPT-VQE approach.[25] In ADAPT-VQE, the unitary ansatz at maco-iteration $k$ is defined as

$$\hat{U}_{\mathrm{ADAPT}}^{(k)}(\mathbf{t}) = \prod_\nu^k e^{t_\nu^{(k)} \hat{\kappa}_\nu^{(k)}}, \tag{5.17}$$

where $\nu$ is likewise a compound index corresponding to operators $\hat{\kappa}_\nu$ in a pool $\mathscr{P}$ of generalized single and double excitation/de-excitation operators (although in QFORTE is possible to construct $\mathscr{P}$ in a variety of ways). The parameters $t_\nu^{(k)}$ are optimized at each macro-iteration employing the general VQE schema. New operators are determined from

the pool by computing the energy gradient

$$g_\nu = \langle \Psi_{\mathrm{VQE}} | \left[ \hat{\mathscr{H}}, \hat{\kappa}_\nu \right] | \Psi_{\mathrm{VQE}} \rangle \tag{5.18}$$

with respect to $t_\nu$ of each operator in $\mathscr{P}$ and selecting the operator with the largest gradient magnitude to place at the end of the ansatz in the next iteration.

### 5.3.2 dUCC projective quantum eigensolver

In the dUCC projective quantum eigensolver approach we likewise consider a trail state of the form $|\Psi\rangle = \hat{U}(\boldsymbol{t}) |\Phi_0\rangle$, where $\hat{U}(\boldsymbol{t})$ is also defined by Eq. (5.16). In PQE we are interested in solving Schrödinger equation for the trial-state left-multiplied by $\hat{U}^\dagger(\boldsymbol{t})$,

$$\hat{U}^\dagger(\mathbf{t}) \hat{\mathscr{H}} \hat{U}(\mathbf{t}) |\Phi_0\rangle = E |\Phi_0\rangle . \tag{5.19}$$

Rather than accomplishing this via variational minimization (as is done in VQE), PQE seeks to minimize the residual condition

$$r_\mu(\mathbf{t}) \equiv \left\langle \Phi_\mu \right| \hat{U}^\dagger(\mathbf{t}) \hat{\mathscr{H}} \hat{U}(\mathbf{t}) |\Phi_0\rangle = 0 \quad \forall \Phi_\mu \in Q, \tag{5.20}$$

where the residual $r_\mu(\boldsymbol{t})$ is given by the projection of the Schrödinger equation onto a determinant $\left|\Phi_\mu\right\rangle = \hat{\kappa}_\mu |\Phi_0\rangle$ excited from the Hartree–Fock state. In practice we only consider enforcing the residual condition for a subset $Q$ of excited determinants (such as all single and double excitations).

The residuals $r_\mu$ can be easily determined from symmetric expectation values and can therefore be measured via operator averaging on a quantum device. In this form they are given by

$$r_\mu(\boldsymbol{t}) = \left\langle \Omega_\mu \right| \hat{U}^\dagger(\mathbf{t}) \hat{\mathscr{H}} \hat{U}(\mathbf{t}) \left| \Omega_\mu \right\rangle - \frac{1}{2} \langle \Phi_0 | \hat{U}^\dagger(\mathbf{t}) \hat{\mathscr{H}} \hat{U}(\mathbf{t}) |\Phi_0\rangle - \frac{1}{2} \left\langle \Phi_\mu \right| \hat{U}^\dagger(\mathbf{t}) \hat{\mathscr{H}} \hat{U}(\mathbf{t}) \left| \Phi_\mu \right\rangle , \tag{5.21}$$

where,

$$\left|\Omega_\mu\right\rangle = e^{\frac{\pi}{4} \hat{\kappa}_\mu} |\Phi_0\rangle = \frac{1}{\sqrt{2}} |\Phi_0\rangle + \frac{1}{\sqrt{2}} \left|\Phi_\mu\right\rangle , \tag{5.22}$$

is an easily preparable (equal) superposition of $|\Phi_0\rangle$ and $\left|\Phi_\mu\right\rangle$.

One of the most important features of dUCC-PQE is that the parameter vector $\boldsymbol{t}$ can be updated using a simple quasi-Newton iteration approach

$$t_\mu^{(n+1)} = t_\mu^{(n)} + \frac{r_\mu^{(n)}}{\Delta_\mu}, \tag{5.23}$$

where the superscript "$(n)$" indicates the amplitude at iteration $n$. The quantities $\Delta_\mu$ are standard Møller–Plesset denominators $\Delta_\mu \equiv \Delta_{ij\ldots}^{ab\cdots} = \varepsilon_i + \varepsilon_j + \ldots - \varepsilon_a - \varepsilon_b \ldots$ where $\varepsilon_i$ are Hartree–Fock orbital energies.

*Selected PQE*

The selected ansatz variation of PQE (SPQE) is also implemented in QFORTE and, similarly to ADAPT, it utilizes a dUCC ansatz constructed iteratively from a (growing) set of operators $\mathscr{A}$. In brief, the selection procedure is done by construction of a normalized state $|\tilde{r}\rangle$ defined as

$$\begin{aligned} |\tilde{r}\rangle &= \hat{U}^\dagger(\boldsymbol{t}) e^{i\Delta t \hat{\mathscr{H}}} \hat{U}(\boldsymbol{t}) |\Phi_0\rangle \\ &= (1 + i\Delta t \hat{U}^\dagger(\boldsymbol{t}) \hat{\mathscr{H}} \hat{U}(\boldsymbol{t})) |\Phi_0\rangle + \mathscr{O}(\Delta t^2). \end{aligned} \tag{5.24}$$

for which the square moduli of its probability amplitudes $|C_\mu|^2 \approx |\left\langle \Phi_\mu \right| \Delta t \hat{U}^\dagger(\boldsymbol{t}) \hat{\mathscr{H}} \hat{U}(\boldsymbol{t}) |\Phi_0\rangle|^2$ are proportional to residuals $r_\mu$. In QFORTE the time step is taken as a parameter of the calculation and the Suzuki-Trotter approximation[46,47] is used for the time evolution operator. We may then approximate the values of the (normalized) squared residuals as

$$|\tilde{r}_\mu|^2 \approx \frac{N_\mu}{M}, \tag{5.25}$$

where $N_\mu$ is the number of times the state $\left|\Phi_\mu\right\rangle$ is measured from $M$ preparations of $|\tilde{r}\rangle$. A cumulative thresholding procedure is then utilized to add new operators $\hat{\kappa}_\mu$ (corresponding to $|\tilde{r}_\mu|^2$) to the ansatz, enforcing the condition

$$\sum_{\hat{\kappa}_\mu \notin \mathscr{A}}^{\text{excluded}} |r_\mu|^2 \approx \sum_{\hat{\kappa}_\mu \notin \mathscr{A}}^{\text{excluded}} \frac{|\tilde{r}_\mu|^2}{\Delta t^2} \leq \Omega^2, \tag{5.26}$$

where $\Omega$ is a user-specified convergence threshold parameter. This selection strategy is particularly appealing for strongly correlated systems because it does not require the candidate operators $\hat{\kappa}_\mu$ to be restricted to any particular excitation order.

### 5.3.3 Quantum imaginary time evolution

The quantum imaginary time evolution algorithm is based on the principle that the ground state can be found by evolving a trial state $|\Phi\rangle$ with the imaginary time evolution operator $e^{-\beta\hat{\mathscr{H}}}$ in the infinite time-step limit,

$$|\Psi_0\rangle = \lim_{\beta\to\infty} \frac{1}{\sqrt{c(\beta)}} e^{-\beta\hat{\mathscr{H}}} |\Phi\rangle ; \langle\Psi_0|\Phi\rangle \neq 0 \tag{5.27}$$

such that a factor of $1/\sqrt{c(\beta)} = 1/\sqrt{\langle\Phi| e^{-2\beta\hat{\mathscr{H}}} |\Phi\rangle}$ normalizes the evolved state. The imaginary time evolution operator is non-unitary, making it impractical for implementation on quantum computers. However, one may approximate the action of the imaginary time evolution operator with time step $\beta$ using a unitary operation of the form.

$$c(\beta)^{-1/2} e^{-\beta\hat{\mathscr{H}}} |\Phi\rangle \approx |\psi(\beta)\rangle \equiv e^{-i\beta\hat{A}} |\Phi\rangle \tag{5.28}$$

where $\hat{A}$ is Hermetian. Approximating both sides to first order and Left multiplying by $\hat{A}^\dagger$ and $\langle\Phi|$, respectively, gives

$$c(\beta)^{-1/2} \langle\Phi|\hat{A}^\dagger\hat{\mathscr{H}}|\Phi\rangle \approx -i \langle\Phi|\hat{A}^\dagger\hat{A}|\Phi\rangle \tag{5.29}$$

the principal equation of QITE. The Hermitian operator $\hat{A}$ can be written as a linear expansion of Pauli operator products $\hat{\rho}_\mu = \prod_l \hat{\sigma}_{\mu_l}^{(l)}$ such that $\hat{A} = \sum_{\mu\in\mathscr{P}} \alpha_\mu \hat{\rho}_\mu$. Here, $\mathscr{P}$ is a subset with dimension $M$ of all possible $4^{N_{\text{qb}}}$ Pauli operator products $\mathscr{Q}$, $\mu \equiv (\mu_1, \mu_2, .., \mu_{N_{\text{qb}}})$ is a multi-index describing a unique Pauli operator product, and $\mu_l \in \{I, X, Y, Z\}$. Inserting the above from of $\hat{A}$ into Eq. (5.29) gives

$$c(\beta)^{-1/2} \langle\Phi| \sum_{\mu\in\mathscr{P}} \alpha_\mu \hat{\rho}_\mu^\dagger \hat{\mathscr{H}} |\Phi\rangle \approx -i \langle\Phi| \sum_{\mu,\nu\in\mathscr{P}} \alpha_\mu \alpha_\nu \hat{\rho}_\mu^\dagger \hat{\rho}_\nu |\Phi\rangle \tag{5.30}$$

from which one seeks to solve the $M$ dimensional linear system $\mathbf{S}\boldsymbol{\alpha} = \mathbf{b}$. The elements of $\mathbf{S}$, and $\mathbf{b}$, as well as the value of $c(\beta)$ can be determined via measurement of symmetric expectation values such that

$$S_{\mu\nu} = \langle\Phi|\,\hat{\rho}_\mu^\dagger \hat{\rho}_\nu\,|\Phi\rangle \tag{5.31}$$

$$b_\mu = \frac{-i}{\sqrt{c(\beta)}}\,\langle\Phi|\,\hat{\rho}_\mu^\dagger \hat{\mathscr{H}}\,|\Phi\rangle \tag{5.32}$$

and,

$$c(\beta) \approx 1 - 2\beta\,\langle\Phi|\,\hat{\mathscr{H}}\,|\Phi\rangle \tag{5.33}$$

In QFORTE , the Pauli operator products used to populate $\mathscr{P}$ are generated automatically from a user-specified manifold of second-quantized excitations/de-excitations as all unique Jordan-Wigner transformed sub-terms containing an odd number of $\hat{Y}$ gates. We note that the QFORTE implementation of QITE differs for the "inexact QITE" described by the original authors in which a subgroup of important Pauli operators is chosen for *each* $k$-local hamiltonian term.

*Quantum Lanczos*

In quantum Lanczos, one wants utilize the QITE subroutine to determine the matrix elements $S_{mn} = \langle\psi(\beta_m)|\psi(\beta_n)\rangle$ and $H_{mn} = \langle\psi(\beta_m)|\,\hat{\mathscr{H}}\,|\psi(\beta_n)\rangle$ of a generalized eigenvalue problem $\mathbf{Hc} = \mathbf{Sc}E$, where $\beta_m = m\Delta\beta$ are different integer $m$ durations of imaginary time evolution. A convenient feature of QL is that the matrix elements can be (approximately) evaluated in terms of the normalization coefficients $c$, such that

$$S_{mn} \approx \langle\Phi|\,e^{-m\Delta\beta\hat{A}}e^{-n\Delta\beta\hat{A}}\,|\Phi\rangle = \frac{c(\beta_m)c(\beta_n)}{c^2(\beta_k)} \tag{5.34}$$

and,

$$H_{mn} \approx \langle\Phi|\,e^{-m\Delta\beta\hat{A}}|\hat{\mathscr{H}}|e^{-n\Delta\beta\hat{A}}\,|\Phi\rangle = \frac{c(\beta_m)c(\beta_n)}{c^2(\beta_k)}\,\langle\psi(\beta_k)|\hat{\mathscr{H}}|\psi(\beta_k)\rangle \tag{5.35}$$

where $2k = m + n$. This is significant without because it implies that all of the quantities needed for QL can be determined *without* ancilla qubits.

### 5.3.4 Quantum Krylov

In quantum Krylov diagonalization, a general state is written as a linear combination of the basis $\{\psi_n\}$ generated from Hamiltonian evolutions of time $t_n = n\Delta t$ as

$$|\Psi\rangle = \sum_{\alpha} c_n |\psi_n\rangle = \sum_{n=0}^{s} c_n e^{-it_n \hat{\mathscr{H}}} |\Phi\rangle . \tag{5.36}$$

In QFORTE the quantum circuit used to approximate the time evolution is likewise generated via Eq. (5.9) using the Suzuki-Trotter decomposition

$$e^{-it\hat{\mathscr{H}}} = e^{-it\sum_\ell \theta_\ell \hat{P}_\ell} \approx \left( \prod_{\ell} e^{\frac{-it\theta_\ell \hat{P}_\ell}{r}} \right)^r , \tag{5.37}$$

with $r$ Trotter steps. Variational minimization of the energy of the state $\Psi$ leads to the following generalized eigenvalue problem $\mathbf{Hc} = \mathbf{Sc}E$, where the elements of the overlap matrix ($\mathbf{S}$) and Hamiltonian ($\mathbf{H}$) are given by $S_{mn} = \langle \psi_m | \psi_n \rangle$ and $H_{mn} = \langle \psi_m | \hat{\mathscr{H}} | \psi_n \rangle$, respectively.

The quantum circuits used to evaluate $\mathbf{S}$ and $\mathbf{H}$ are implemented in QFORTE via a variant of the now-commonplace Hadamard test.[48] The basis of states $\mathscr{K}_s(\psi_n)$ generated by real-time evolution spans a classical Krylov space in the small time-step limit. In QFORTE the time step $(\Delta t)$, number of time evolutions states $(s)$, and number of Trotter steps $(r)$ are all given as user-specified values.

*Multireference selected QK*

A selected multireference variant of QK (MRSQK) is also implemented in QFORTE. The base procedure is identical to that of QK described in the above section, but several orthogonal reference states $|\Phi_I\rangle$ are included in the subspace and time evolved in order to improve numerical stability and target states with multireference character. The MRSQK wave function is thus given by

$$|\Psi\rangle = \sum_{\alpha} c_\alpha |\psi_\alpha\rangle = \sum_{I=1}^{d} \sum_{n=0}^{s} c_I^{(n)} e^{-it_n \hat{\mathscr{H}}} |\Phi_I\rangle \tag{5.38}$$

In MRSQK, a preliminary single-reference QK calculation is performed in order to determine the set of important references. The resulting single-reference QK wave function $\left|\tilde{\Psi}\right\rangle = \sum_n \tilde{c}_n \left|\psi_n\right\rangle$ is used to construct a list of determinants with importance value $P_\mu = |\langle\phi_\mu|\tilde{\Psi}\rangle|^2$, since the probability of measuring a determinant $\phi_\mu$ is equal to $P_\mu = |\langle\phi_\mu|\tilde{\Psi}\rangle|^2$. In QFORTE , the quantity $P_\mu$ is approximated by measuring each element of the Krylov basis and estimating the total probability as a weighted sum over references via

$$P_\mu = |\sum_\alpha \langle\phi_\mu|\psi_\alpha\rangle c_\alpha|^2 \approx \sum_\alpha |\langle\phi_\mu|\psi_\alpha\rangle|^2 |c_\alpha|^2. \tag{5.39}$$

Once formed, the list of the most important determinants is augmented to guarantee that all spin arrangements of open-shell determinants are included, and the $d$ most important references are used in the MRSQK subspace. The number of references ($d$), the MRSQK time step $\Delta t_{\mathrm{mr}}$, the number of time evolutions per reference $(s)$, and the parameters for the preliminary single-reference QK calculation are all specified by the user at runtime.

## 5.4 Conclusion

In this article we introduce the unique open-source software package QFORTE to aid in the development or quantum simulation algorithms for molecular electronic structure. QFORTE 's ability to facilitate black-box calculations with a wide variety of quantum algorithms using only a classical electronic structure package as a dependency makes it ideal tool for implementing and comparing quantum algorithms. Moreover, the easy-to-use data structures (implemented as C++ classes exposed in Python) allow QFORTE to function as an excellent platform for implementation of new quantum algorithms. We hope to continue implementing new algorithms and features in QFORTE so it will find wide usage with a variety of research groups and as well as its place in the already impressive cohort of open-source software for quantum simulation.

# Bibliography

[1] F. Arute, K. Arya, R. Babbush, D. Bacon, J. C. Bardin, R. Barends, R. Biswas, S. Boixo, F. G. Brandao, D. A. Buell, *et al.*. "Quantum supremacy using a programmable superconducting processor." *Nature* **574**, 505 (2019).

[2] P. J. J. O'Malley, R. Babbush, I. D. Kivlichan, J. Romero, J. R. McClean, R. Barends, J. Kelly, P. Roushan, A. Tranter, N. Ding, B. Campbell, Y. Chen, Z. Chen, B. Chiaro, A. Dunsworth, A. G. Fowler, E. Jeffrey, E. Lucero, A. Megrant, J. Y. Mutus, M. Neeley, C. Neill, C. Quintana, D. Sank, A. Vainsencher, J. Wenner, T. C. White, P. V. Coveney, P. J. Love, H. Neven, A. Aspuru-Guzik, and J. M. Martinis. "Scalable Quantum Simulation of Molecular Energies." *Phys. Rev. X* **6**, 031007 (2016).

[3] A. Kandala, A. Mezzacapo, K. Temme, M. Takita, M. Brink, J. M. Chow, and J. M. Gambetta. "Hardware-efficient variational quantum eigensolver for small molecules and quantum magnets." *Nature* **549**, 242 (2017).

[4] J. I. Colless, V. V. Ramasesh, D. Dahlen, M. S. Blok, M. Kimchi-Schwartz, J. McClean, J. Carter, W. De Jong, and I. Siddiqi. "Computation of molecular spectra on a quantum processor with an error-resilient algorithm." *Physical Review X* **8**, 011021 (2018).

[5] Y. Shen, X. Zhang, S. Zhang, J.-N. Zhang, M.-H. Yung, and K. Kim. "Quantum implementation of the unitary coupled cluster for simulating molecular electronic structure." *Physical Review A* **95**, 020501 (2017).

[6] C. Hempel, C. Maier, J. Romero, J. McClean, T. Monz, H. Shen, P. Jurcevic, B. P. Lanyon, P. Love, R. Babbush, *et al.*. "Quantum chemistry calculations on a trapped-ion quantum simulator." *Physical Review X* **8**, 031022 (2018).

[7] Y. Nam, J.-S. Chen, N. C. Pisenti, K. Wright, C. Delaney, D. Maslov, K. R. Brown, S. Allen, J. M. Amini, J. Apisdorf, *et al.*. "Ground-state energy estimation of the water molecule on a trapped-ion quantum computer." *npj Quantum Information* **6**, 1 (2020).

[8] C. Y.-Y. Lin and Y. Zhu. "Performance of QAOA on typical instances of constraint satisfaction problems with bounded degree." *arXiv preprint arXiv:1601.01744* (2016).

[9] Z. Wang, S. Hadfield, Z. Jiang, and E. G. Rieffel. "Quantum approximate optimization algorithm for maxcut: A fermionic view." *Physical Review A* **97**, 022304 (2018).

[10] J. Preskill. "Quantum Computing in the NISQ era and beyond." *Quantum* **2**, 79 (2018).

[11] S. McArdle, S. Endo, A. Aspuru-Guzik, S. C. Benjamin, and X. Yuan. "Quantum computational chemistry." *Rev. Mod. Phys.* **92**, 015003 (2020).

[12] B. Bauer, S. Bravyi, M. Motta, and G. Kin-Lic Chan. "Quantum algorithms for quantum chemistry and quantum materials science." *Chem. Rev.* **120**, 12685 (2020).

[13] A. Peruzzo, J. McClean, P. Shadbolt, M.-H. Yung, X.-Q. Zhou, P. J. Love, A. Aspuru-Guzik, and J. L. O'Brien. "A variational eigenvalue solver on a photonic quantum processor." *Nat. Commun.* **5**, 4213 (2014).

[14] J. R. McClean, J. Romero, R. Babbush, and A. Aspuru-Guzik. "The theory of variational hybrid quantum-classical algorithms." *New J. Phys.* **18**, 023023 (2016).

[15] M. Motta, C. Sun, A. T. Tan, M. J. O'Rourke, E. Ye, A. J. Minnich, F. G. Brandão, and G. K.-L. Chan. "Determining eigenstates and thermal states on a quantum computer using quantum imaginary time evolution." *Nat. Phys.* **16**, 1 (2019).

[16] J. R. McClean, S. Boixo, V. N. Smelyanskiy, R. Babbush, and H. Neven. "Barren plateaus in quantum neural network training landscapes." *Nature communications* **9**, 1 (2018).

[17] H. Abraham, I. Y. Akhalwaya, G. Aleksandrowicz, T. Alexander, G. Alexandrowics, E. Arbel, A. Asfaw, C. Azaustre, P. B. AzizNgoueya, G. Barron, *et al.*. "Qiskit: An open-source framework for quantum computing." *zenodo, https://doi. org/10.5281/zenodo* **2562111** (2019).

[18] C. Developers. "Cirq." (2021). See full list of authors on Github: https://github.com/quantumlib/Cirq/graphs/contributors.

[19] N. C. Rubin, T. Shiozaki, K. Throssell, G. K. Chan, and R. Babbush. "The Fermionic Quantum Emulator." *arXiv preprint arXiv:2104.13944* (2021).

[20] Microsoft. "The qsharp user guide - microsoft quantum." (2020).

[21] R. S. Smith, M. J. Curtis, and W. J. Zeng. "A practical quantum instruction set architecture." *arXiv preprint arXiv:1608.03355* (2016).

[22] J. S. Kottmann, S. Alperin-Lea, T. Tamayo-Mendoza, A. Cervera-Lierta, C. Lavigne, T.-C. Yen, V. Verteletskyi, P. Schleich, A. Anand, M. Degroote, *et al.*. "Tequila: A platform for rapid development of quantum algorithms." *Quantum Science and Technology* **6**, 024009 (2021).

[23] D. Wecker, M. B. Hastings, and M. Troyer. "Progress towards practical quantum variational algorithms." *Phys. Rev. A* **92**, 042303 (2015).

[24] I. G. Ryabinkin, T.-C. Yen, S. N. Genin, and A. F. Izmaylov. "Qubit Coupled Cluster Method: A Systematic Approach to Quantum Chemistry on a Quantum Computer." *J. Chem. Theory Comput.* **14**, 6317 (2018).

[25] H. R. Grimsley, S. E. Economou, E. Barnes, and N. J. Mayhall. "An adaptive variational algorithm for exact molecular simulations on a quantum computer." *Nat. Commun.* **10**, 1 (2019).

[26] I. G. Ryabinkin, R. A. Lang, S. N. Genin, and A. F. Izmaylov. "Iterative Qubit Coupled Cluster approach with efficient screening of generators." *J. Chem. Theory Comput.* **16**, 1055 (2020).

[27] J. R. McClean, M. E. Kimchi-Schwartz, J. Carter, and W. A. de Jong. "Hybrid quantum-classical hierarchy for mitigation of decoherence and determination of excited states." *Phys. Rev. A* **95**, 042308 (2017).

[28] A. Y. Kitaev. "Quantum measurements and the Abelian stabilizer problem." *e-print arXiv:9511026 [quant-ph]* (1995).

[29] D. S. Abrams and S. Lloyd. "Simulation of Many-Body Fermi Systems on a Universal Quantum Computer." *Phys. Rev. Lett.* **79**, 2586 (1997).

[30] D. S. Abrams and S. Lloyd. "Quantum algorithm providing exponential speed increase for finding eigenvalues and eigenvectors." *Phys. Rev. Lett.* **83**, 5162 (1999).

[31] R. M. Parrish and P. L. McMahon. "Quantum Filter Diagonalization: Quantum Eigendecomposition without Full Quantum Phase Estimation." *e-print arXiv:1909.08925 [quant-ph]* (2019).

[32] N. H. Stair, R. Huang, and F. A. Evangelista. "A Multireference Quantum Krylov Algorithm for Strongly Correlated Electrons." *J. Chem. Theory Comput.* **16**, 2236 (2020). ISSN 1549-9626.

[33] N. H. Stair and F. A. Evangelista. "Simulating Many-Body Systems with a Projective Quantum Eigensolver." *arXiv preprint arXiv:2102.00345* (2021).

[34] W. Jakob, J. Rhinelander, and D. Moldovan. "pybind11–Seamless operability between C++ 11 and Python." *URL: https://github. com/pybind/pybind11* (2017).

[35] P. J. Knowles and N. C. Handy. "A new determinant-based full configuration interaction method." *Chem. Phys. Lett.* **111**, 315 (1984).

[36] T. D. Crawford and H. F. Schaefer. "An introduction to coupled cluster theory for computational chemists." *Reviews in computational chemistry* **14**, 33 (2000).

[37] P. Jordan and E. P. Wigner. "über das paulische äquivalenzverbot." In "The Collected Works of Eugene Paul Wigner," 109–129. Springer (1993).

[38] M. Cerezo, A. Arrasmith, R. Babbush, S. C. Benjamin, S. Endo, K. Fujii, J. R. McClean, K. Mitarai, X. Yuan, L. Cincio, *et al.*. "Variational quantum algorithms." *arXiv preprint arXiv:2012.09265* (2020).

[39] W. J. Huggins, J. Lee, U. Baek, B. O'Gorman, and K. B. Whaley. "A non-orthogonal variational quantum eigensolver." *New Journal of Physics* (2020).

[40] F. A. Evangelista, G. K.-L. Chan, and G. E. Scuseria. "Exact parameterization of fermionic wave functions via unitary coupled cluster theory." *The Journal of Chemical Physics* **151**, 244112 (2019).

[41] P. G. Szalay, M. Nooijen, and R. J. Bartlett. "Alternative ansätze in single reference coupled-cluster theory. III. A critical analysis of different methods." *The Journal of chemical physics* **103**, 281 (1995).

[42] A. G. Taube and R. J. Bartlett. "New perspectives on unitary coupled-cluster theory." *International journal of quantum chemistry* **106**, 3393 (2006).

[43] B. Cooper and P. J. Knowles. "Benchmark studies of variational, unitary and extended coupled cluster methods." *The Journal of chemical physics* **133**, 234102 (2010).

[44] F. A. Evangelista. "Alternative single-reference coupled cluster approaches for multireference problems: The simpler, the better." *The Journal of chemical physics* **134**, 224102 (2011).

[45] G. Harsha, T. Shiozaki, and G. E. Scuseria. "On the difference between variational and unitary coupled cluster theories." *The Journal of chemical physics* **148**, 044107 (2018).

[46] H. F. Trotter. "On the product of semi-groups of operators." *Proceedings of the American Mathematical Society* **10**, 545 (1959).

[47] M. Suzuki. "Improved Trotter-like formula." *Physics Letters A* **180**, 232 (1993).

[48] D. Aharonov, V. Jones, and Z. Landau. "A polynomial quantum algorithm for approximating the Jones polynomial." *Algorithmica* **55**, 395 (2009).

# Chapter 6

# Conclusions and future directions

In this dissertation, we explore the limitations of classical algorithms for strongly correlated electronic structure problems, outline the initial development of two novel categories of quantum simulation algorithm, and discuss an novel tool for implementation of new quantum methods. The studies presented here motivate a need for algorithms capable of treating strong correlation with a tractable number of classical parameters. They also showcase suitable quantum algorithms to fulfill this need which will become increasingly viable for treatment of large-scale strong correlation as physical quantum computers come into maturity.

Our first study explores the ability of classical electronic structure methods to efficiently represent (compress) the information content of full configuration interaction (FCI) wave functions of strongly correlated systems. We introduce a benchmark set of four hydrogen model systems of different dimensionality and distinctive electronic structures: a 1D chain, a 1D ring, a 2D triangular lattice, and a 3D close-packed pyramid. To assess the ability of a computational method to produce accurate and compact wave functions, we introduce the accuracy volume, a metric that measures the number of variational parameters necessary to achieve a target energy error. Using this metric and the hydrogen models, we examine the performance of three classical deterministic methods: i) selected configuration interaction (sCI) realized both via an *a posteriori* (ap-sCI) and variational selection of the most important determinants, ii) an *a posteriori* singular value decomposition of the FCI tensor

(SVD-FCI), and iii) the matrix product state representation obtained via the density matrix renormalization group (DMRG). We find that DMRG generally gives the most efficient wave function representation for all systems, particularly in the 1D chain with a localized basis. For the 2D and 3D systems, all methods (except DMRG) perform best with a delocalized basis, and the efficiency of sCI and SVD-FCI is closer to that of DMRG. For larger analogs of the models, DMRG consistently requires the fewest parameters, but still scales exponentially in 2D and 3D systems, and the performance of SVD-FCI is essentially equivalent to that of ap-sCI.

Motivated by the findings of our first study, we then introduce a multireference quantum Krylov (MRSQK) algorithm suitable for quantum simulation of many-body problems. MRSQK is a low-cost alternative to the quantum phase estimation algorithm that generates a target state as a linear combination of non-orthogonal Krylov basis states. This basis is constructed from a set of reference states via real-time evolution avoiding the numerical optimization of parameters. An efficient algorithm for the evaluation of the off-diagonal matrix elements of the overlap and Hamiltonian matrices is discussed and a selection procedure is introduced to identify a basis of orthogonal references that ameliorates the linear dependency problem. Preliminary benchmarks on linear $H_6$, $H_8$, and $BeH_2$ indicate that MRSQK can predict the energy of these strongly correlated systems accurately using very compact Krylov bases.

In our third study we present another new hybrid quantum-classical algorithm for optimizing unitary coupled-cluster (UCC) wave functions deemed the projective quantum eigensolver (PQE), amenable to near-term noisy quantum hardware. Contrary to variational quantum algorithms, PQE optimizes a trial state using residuals (projections of the Schrödinger equation) rather than energy gradients. We show that the residuals may be evaluated by simply measuring two energy expectation values per element. We also introduce a selected variant of PQE (SPQE) that uses an adaptive ansatz built from arbitrary-order particle-hole operators and circumvents the expensive gradient-based selection pro-

cedures used in adaptive variational quantum algorithms. PQE and SPQE are tested on a set of molecular systems covering both the weak and strong correlation regimes, including hydrogen clusters with 4–10 atoms and the $BeH_2$ molecule. When employing a fixed ansatz, we find that PQE can converge UCC wave functions to essentially identical energies as variational optimization while requiring fewer computational resources. A comparison of SPQE and adaptive variational quantum algorithms shows that—for ansätze containing the same number of parameters—the two methods yield results of comparable accuracy. Finally, we show that SPQE performs similar to, and in some cases, better than selected configuration interaction and the density matrix renormalization group on 1–3 dimensional strongly correlated $H_{10}$ systems.

In the last work presented in this dissertation we introduce an novel open-source software package QFORTE. The package is a tool for development of new quantum algorithms, and facilitated the (now publicly available) implementation of the algorithms presented in the aforementioned studies. It additionally contains black-box implementations of a wide variety of quantum algorithms, requiring only a classical electronic structure package as a dependancy. QFORTE will undoubtably improve the quality of future quantum algorithmic developments by allowing researchers to easily compare new methods to existing approaches without implementing them from scratch.

While the developments presented in this dissertation represent entirely new insight and approaches for the treatment of strongly correlated fermionic systems, there is still much potential for future work following our initial directions. Firstly, investigation of the two and three dimensional systems used in our first study with more general tensor network approaches (beyond matrix product states) would provide valuable insight for construction of (potentially ultra-compact) unitary ansatz in VQE. Additionally, we envision the usage of our MRSQK algorithm for targeted treatment of excited states by augmenting the reference selection procedure, and fine-tuning of the time grid. The projective quantum eigensolver presented in our third study can likewise be extended in a number of ways such as derivation

of the amplitude update equations for repeated or generalized operators or investigation of an orthogonality-constrained variant to treat excited states. Generalization of the work presented in this dissertation has the potential to define a new state-of-the art for quantum simulation algorithms.